ROCK MASS SLOPE STABILITY ANALYSIS BASED ON TERRESTRIAL LIDAR SURVEY ON SELECTED LIMESTONE HILLS IN KINTA VALLEY, PERAK

MUHAMMAD AFIQ ARIFF BIN MOHD HELLMY

FACULTY OF SCIENCE
UNIVERSITY OF MALAYA
KUALA LUMPUR

2020

ROCK MASS SLOPE STABILITY ANALYSIS BASED ON TERRESTRIAL LIDAR SURVEY ON SELECTED LIMESTONE HILLS IN KINTA VALLEY, PERAK

MUHAMMAD AFIQ ARIFF BIN MOHD HELLMY

DISSERTATION SUBMITTED IN FULFILMENT OF THE REQUIREMENTS FOR THE DEGREE OF MASTER OF SCIENCE

DEPARTMENT OF GEOLOGY
FACULTY OF SCIENCE
DEPARTMENT OF GEOLOGY
UNIVERSITY OF MALAYA
KUALA LUMPUR

2020

UNIVERSITY OF MALAYA

ORIGINAL LITERARY WORK DECLARATION

Name of Candidate: **MUHAMMAD AFIQ ARIFF BIN MOHD HELLMY**

Matric No: **SGR 160048**

Name of Degree: **MASTER OF SCIENCE**

Title of Dissertation ("this Work"):

ROCK MASS SLOPE STABILITY ANALYSIS BASED ON TERRESTRIAL LIDAR SURVEY ON SELECTED LIMESTONE HILLS IN KINTA VALLEY, PERAK

Field of Study:

GEOHAZARD AND KARST

I do solemnly and sincerely declare that:

(1) I am the sole author/writer of this Work;
(2) This Work is original;
(3) Any use of any work in which copyright exists was done by way of fair dealing and for permitted purposes and any excerpt or extract from, or reference to or reproduction of any copyright work has been disclosed expressly and sufficiently and the title of the Work and its authorship have been acknowledged in this Work;
(4) I do not have any actual knowledge nor do I ought reasonably to know that the making of this work constitutes an infringement of any copyright work;
(5) I hereby assign all and every rights in the copyright to this Work to the University of Malaya ("UM"), who henceforth shall be owner of the copyright in this Work and that any reproduction or use in any form or by any means whatsoever is prohibited without the written consent of UM having been first had and obtained;
(6) I am fully aware that if in the course of making this work, I have infringed any copyright whether intentionally or otherwise, I may be subject to legal action or any other action as may be determined by UM.

Candidate's Signature Date:

Subscribed and solemnly declared before,

Witness's Signature Date:

Name:

Designation:

ROCK MASS SLOPE STABILITY ANALYSIS BASED ON TERRESTRIAL LIDAR SURVEY ON SELECTED LIMESTONE HILLS IN KINTA VALLEY, PERAK

ABSTRACT

The use modern mapping technology is necessary in assessing slopes and cliffs, especially in tropical countries as it is mostly inaccessible and covered with thick vegetation which restricts the conventional data collection only at the base of the cliff. Overhanging and sub-vertical characteristics of limestone hills in Kinta Valley together with highly fractured and day-lighting joints increase the possibility of rock slope failure. The main objective of this research is to assess the stability and rock mass properties of the limestone hills in Kinta Valley based on the output provided by terrestrial LiDAR and scanline survey. Terrestrial laser scanning (TLS) helps engineers and geologist to collect a high numbers of discontinuity data where it is inaccessible for manual data measurement. A total number of about 14 cliffs on 4 limestone hills were assessed. Gunung Lang and Kek Lok Tong show major potential failure trending towards east, Gunung Lanno towards southwest, Kwan Yin Tong towards west, and Gunung Cheroh with three directions of failure which are pointed towards the south, southwest and southeast direction. The integration of LiDAR method with the manual compass clinometer has become a better approach to assess the stability of limestone hills and other rock slope in the possible future.

Keywords: Limestone hills, slope stability, terrestrial laser scanning

ANALISIS KESTABILAN CERUN BATUAN BERDASARKAN SURVEI TERRESTRIAL LIDAR PADA GUNUNG BATU KAPUR YANG TERPILIH DI LEMBAH KINTA, PERAK

ABSTRAK

Penggunaan teknologi pemetaan yang moden ialah satu keperluan dalam menilai cerun dan tebing terutamanya di negara tropika kerana kebanyakan kawasannya tidak boleh diakses dan diliputi oleh tumbuhan yang tebal yang mana menghadkan pengumpulan data secara konvensional hanya pada bawah cerun sahaja. Ciri gunung batu kapur tropika yang curam dan sub-vertikal di Lembah Kinta bersama dengan retakan teruk dan satah yang mengarah keluar dari cerun meningkatkan kecenderungan kegagalan cerun batuan. Pernyataan masalah kajian ini adalah bagaimana "terrestrial LiDAR" boleh membantu survei tradisional dalam pencirian cerun. Objektif utama penyelidikan ini ialah untuk menilai kestabilan dan ciri jasad batuan gunung batu kapur di Lembah Kinta berdasarkan output yang disediakan oleh "terrestrial LiDAR" dan kaedah survei garis imbasan. Terrestrial laser scanning (TLS) membantu jurutera dan ahli geologi mengumpul data ketakselanjaran dalam bilangan yang tinggi di kawasan yang tidak dapat diakses untuk pengukuran data secara manual oleh compass klinometer. Sebanyak empat belas cerun dari empat gunung batu kapur telah dinilai. Gunung Lang dan Kek Lok Tong menunjukkan trend jatuhan kea rah timur, Gunung Lanno ke arah barat daya, Kwan Yin Tong ke arah barat dan Gunung Cheroh dengan tiga arah jatuhan iaitu barat selatan, barat daya, dan tenggara. Integrasi LiDAR dan kompas klinometer merupakan pendekatan yang baik untuk menilai kestabilan gunung batu kapur dan cerun batuan lain pada masa hadapan,

Kata kunci: Gunung batu kapur, kestabilan cerun, terrestrial laser scanning

ACKNOWLEDGEMENTS

Assalamualaikum, I would like to thank my parents Mohd Hellmy Bin Ajis and Noor Anida bte Che Amin for their love and support since the beginning of my journey until today. Without them I will not be able to get this far and may Allah bless them with happiness and success.

I would also like to express my gratitude to my supervisor, Dr Ros Fatihah binti Muhammad. Thank you, Dr, for your advice and guidance throughout the candidature. Thank you for always being patience and polite to me. Without your guidance and comments, I will not be able to finish this thesis.

My deepest appreciation to all of my friends BigNik, Frodo, Yaqzan, Kapiu, Farhan, and Syahmi. Thank you for the supports and motivation that keep me going throughout the thesis writing.

I am also very thankful for my GMT friends Faruq, Farid, Fadhil, Asraff and Afifi. Thank you for the wonderful moments we have shared especially the RHT mapping and Bukit Jelapang mapping during the fasting month. Craziest moments in my life!

My special thanks to Izzati, thanks for your lame jokes and motivational talks that you have gave to me during this journey.

TABLE OF CONTENTS

LIST OF FIGURES

LIST OF TABLES

LIST OF SYMBOLS AND ABBREVIATIONS

DGPS	:	Differential Global Positioning System
GLCS	:	Global Coordinate System
ICP	:	Iterative Closest Points
MSE	:	Mean Square Error
PRCS	:	Project Coordinate System
RMS	:	Rock Mass Strength
RTK	:	Real Time Kinematic
SMR	:	Slope Mass Rating

LIST OF APPENDICES

CHAPTER 1: INTRODUCTION

1.1 Research Background

Rock mass slope stability analysis have been used for decades in monitoring exposed rock slope to evaluate their potential hazard. The mechanical behaviour of rock masses is determined by the geometry of the slopes and the discontinuity properties. Therefore, detailed information of the discontinuity properties such as dip angle, dip direction, and spacing of the joints present within the rock mass were observed for kinematic analysis and rockfall prediction.

Traditional discontinuity measurements such as scanline survey, cell mapping, and geologic structure mapping have several major disadvantages (Priest & Hudson, 1981; Priest, 1993). Scanline measurement technique is a commonly applied and well established method. However it is time consuming and relies on a visual inspection and direct measurements by the researchers. This results in biased data based on the skill level and knowledge of the researchers concerning the rockmass discontinuity properties and resultant ratings (Lato & Vöge, 2012). This technique also directly exposes the researchers to a potential rockfall impacts during the survey. Furthermore, discontinuities on the upper part of the slope were unreachable via scanline technique.

Recent advancements in remote sensing technology through the 2000s have resulted in the widespread use of these technologies in geotechnical field and slope monitoring (Agliardi & Crosta, 2003; Guzzetti et al., 2004; Marquinez et al., 2003). 3D Terrestrial Laser Scanner (3D TLS) is one of the examples of remote sensing that has been used in slope monitoring and analysis of rock face structure (Dunning et al., 2009; Sturzenegger & Stead, 2009). 3D TLS provides more dense, rapid and safe rock mass discontinuity measurements. Discontinuities properties such as dip angle and dip direction of the

joints even at which unreachable by scanline technique can be quickly scanned and extracted from the 3D Digital Terrain Model (DTM) and Digital Elevation Model (DEM) created by 3D TLS. These data can be processed for rock slope stability analysis input.

Rock mass discontinuities studies is important key element for the stability analysis of the slopes, especially on steep sided rock slope such as in Kinta Valley limetone hills. Kinta Valley is well known for its fascinating karst landscape and steep sided limestone hills protruding from alluvial plain. Limestone hills are commonly being intersected with geological structures such as joints and fault together with the bedding planes of the limestones, these structures control the formation of karstic features and the morphology of the limestone hills in Kinta Valley (Tan, 1988). According to Simon et al. (2015), most of the limestone hills in Kinta Valley are mainly characterised by adverse structural conditions and day lighting blocks. Therefore, it is crucial to understand the discontinuity properties and the geological structures as it is the main aspect that control the stability of limestone hills.

1.2 Research Questions

Light Detection and Rangin (LiDAR) has been the principal acquisition technique for deriving virtual outcrops in the last decade (Buckley et al., 2008; Jones et al., 2009). 3D Digital Terrain Model (DTM) and Digital Elevation Model (DEM) of the actual outcrop in the field are useful in characterizing the outcrop and rockfall (Abellán et al., 2006; Rabatel et al., 2008). Usually the analysis of geological structures are performed by manual geomechanical surveys but sometimes it can be challenging due to the access steep, high and dangerous rock faces (Barbarella et al., 2015).

Terrestrial Laser Scanning (TLS) represent a useful complement to conventional field mapping and rock mass characterization (Bistacchi et al., 2011; Coggan et al., 2007; De Souza et al., 2013; Ferrero et al., 2009). However, the validity of using virtual outcrops to make predictions has been addressed by a number of workers (Gillespie et al., 2011; Gold et al., 2012). The accuracy and precision of virtual outcrops was found to be critical if geological models derived from them are to make reliable predictions and decisions (García-Sellés et al., 2011; Martín et al., 2013; Tavani et al., 2014).

Therefore, for this research, data from terrestrial LiDAR 3D model was used in the validation with the manual compass clinometer data. These data validation was done by choosing the "control surface" which represent the joints plane and bedding planes of the slope (Cawood et al., 2017). Multiple dip angle and dip direction measurements were collected on each surface by using traditional compass clinometer and the process was repeated with the terrestrial LiDAR measurements (Cawood et al., 2017). These data were then plotted as a pole on the stereonet for comparison with the control data (manual compass clinometer measurements).

According to Cawood et al., 2017, accurately reconstructed bedding planes by terrestrial LiDAR did not automatically provide accurate along strike predictions due to structurally important, data rich parts of the outcrop were not sampled. This outcome is an effect of where the discontinuity planes were partially occluded to terrestrial LiDAR camera positions (Cawood et al., 2017).

Another research question that appear is the relationship of the Kinta Valley structural trend with the trend of rockfall that occurs. According to Tan (1988) the north-south bedding planes of the limestone hills are the major structural features controlling the morphology and the stability of the cliff faces.

1.3 Objectives of Research

The main objective of this research is to evaluate the stability of the limestone hills in Kinta Valley, Ipoh based on the discontinuity plane model derived from the 3D TLS. Furthermore, the specific objectives are the following :

- To develop a rock mass discontinuity plane model from 3D TLS point cloud data
- To extract out the rock mass discontinuity properties from the 3D TLS model created for stability and kinematic analysis
- To validate 3D TLS measurements with manual scanline measurements in the field
- To relate the trend of rockfall with overall Kinta Valley structural trend

1.4 General Methodology and Thesis Structure

3D Terrestrial Laser Scanning (TLS) was carried out in order to assess the stability of the limestone hills in Kinta Valley, Perak, Malaysia. A total number of 4 limestone hills and 14 number of rock slope faces were selected for this research. Based on the point clouds data from the scanning of these limestone hills, 3D discontinuity plane model were developed for stability analysis. Furthermore, for the purpose of comparison and validation, manual field compass clinometer measurements were also conducted. These manual measurement were then being used to validate the 3D TLS measurement collected.

The thesis is divided into five chapters. This chapter (Chapter one) provide the general introduction of this research. Chapter two focusing on the relevant literature review about various conventional method of rock mass characterization and its limitations. This is followed by discussion on the theory, concepts, applications, and

limitation of 3D TLS technique. Chapter three gives the description of the study area and the details on the field procedures that were carried out in the study area. This chapter also provides detailed information on the methodology used in this research, which includes the pre-processing and post-processing od 3D TLS data. Followed by how manual data validation with the TLS data were conducted. Chapter four presents the results and discussion of this research in details. Finally, the conclusion and recommendation are summarized in chapter five.

CHAPTER 2: LITERATURE REVIEW

2.1 Introduction

Rock mass discontinuity characterization is a crucial fundamental step in the slope stability analysis, therefore review on the characterization method used in this research is presented. This includes the rock mass characterization by conventional method and its limitations, followed by the application of terrestrial laser scanning (TLS) and its limitations in discontinuity detections.

2.2 Traditional Rock Mass Discontinuity Measurements

The fundamental step in rock slope stability analysis is to absolutely understand and evaluate the rock mass discontinuity properties properly. Rock mass properties such as the joints set orientation, joints spacing, and joints roughness are all together controls the stability of the rock slope. Therefore, it is very important to accurately collect and analyze these properties in a rock mass to prevent rock failure.

Scanline measurements is one of the example of conventional rock mass characterization and still widely being used nowdays. It is conducted using established techniques developed to provide consistent results under a wide range of conditions (Priest & Hudson, 1981). Structural data such as the strike, dip direction and dip angle of discontinuities are collected by field mapping and hand held compass clinometer. In the scanline survey, discontinuity properties are collected along a line at a rock face. For example, for each of 10 meter scanline interval, discontinuity information such as dip angle and dip direction of any joints set are measured by a compass clinometer. The advantages of scanline survey is that it can provide precised information on the minor fractures and joints present on the rock face which then can be statistically analysed. In

order to characterize features of exposed rock faces on the field, the International Society of Rock Mechanics (ISRM) proposed ten parameters (ISRM & Hudson, 2007), which are the orientation, spacing, persistence, roughness, aperture, wall strength, filling, seepage, number of fractures sets, and finally the block size (Figure 3.15).

However, scanline method relies on a visual inspection and direct measurements by the evaluating operator. This results in biased data depending on the knowledge and skill level of the operator. According to (Ewan & West, 1982), error in compass measurement due to an operator may be up to 5 degree for dip angle and 10 degree for dip direction. Previous study by (Herda, 1999) has shown that deviation of strike measurement for shallow dipping discontinuities can exceed 20 degree to 30 degree even if the compass is repeatedly placed on the same spots. This add more to uncertainty.

Furthermore, there is a difficulty in gathering a large number of measurements in a short period of time due to its intensive manual operation. For example, (i) aligning and levelling the compass; (ii) determining where the compass can be put in order to obtain the true orientation of the discontinuities; (iii) taking notes in the field notebook to record measurements are time consuming (Feng et al., 2011). Moreover, especially in the tropical country with humid environment, vegetation is one of the biggest problem encountered during manual data measurement. This is because the base of some limestone hills slopes are covered with thick vegetation which restrict and make it almost impossible for manual compass clinometer data collection at the rock faces.

The uniqueness of the Kinta Valley karst lies mainly, among others, on the spectacular shape of steep sided limestone towers which protrude from the vast alluvial plain (Muhammad & Komoo, 2003). Furthermore, some of the limestone hills are characterized by deep horizontal notches located at the base of the rock slope which can

be extended up to 5-10 meter from the ground surface due to dissolution by swamp water in the past. This karst features inhibits direct contact between the operator with the rock faces thus restrict the data collection only to the part which can be accessible on the slope.

Due to several disadvantages in the traditional characterization method, various methods such digital photogrametry and image processing (Post et al., 2001), total station (Bulut & Tüdeş, 1996) and 3D terrestrial laser scanning (Feng et al., 2001; Slob et al., 2002) have emerged. These emerging new technologies allow rock mass characterization be completed without physical contact with the slope. Furthermore, it reduce errors related with human bias and increase the amount of data collected due to its wider coverage in a short time. Operator will be much safer and accessibility related problems are reduced as it can be done at a distance from the slope (Post et al., 2001). Therefore, this research focusing more on the application of 3D Terrestrial Laser Scanner in rock mass slope stability analysis.

2.3 3D Terrestrial Laser Scanning Discontinuity Measurements

2.3.1 Theory and Applications

3D Terrestrial Laser Scanning or the LiDAR technique, which stands for 'light detection and ranging', utilizes the emission and return time of highly collimated electromagnetic radiation to calculate the distance from the instrument optical centre to a reflecting target surface (Baltsavias, 1999). 3D TLS represents an especially valuable new technology for providing detailed information on exposed rock faces, which are vital in slope stability analysis (Slob et al., 2005). For some years terrestrial laser scanning has been used as an efficient tool to analyse rock face structures and monitoring movements (Eberhardt et al., 2007; Janeras et al., 2004; Lim et al., 2005;

Sturzenegger et al., 2007). Rock failure are mainly controlled by the topography, geomorphology, mechanical properties, orientation and distribution of discontinuities (Rowe et al., 2018). However, these parameters are usually difficult to gather by traditional manual surveys especially for high rock slope or slope which is inaccessible.

The principle of 3D TLS data acquisition is shown in Figure 2.1. Terrestrial laser scanner sensors send out laser pulses that get back-scattered by various object on the ground surface such as vegetation, rock faces, man-made constructions and then record the returning signal. The laser scanners use the measurement of the time of flight of the laser pulse to compute the distance and two mirror are used to orientate the laser beam in a well-defined direction. Then, the coordinate position of reflective surface in x, y, z relatively to the device can be determine by knowing the line of sight (LOS) direction and the altitude of the device (pitch, roll, and yaw).

Various researchers have shown that 3D laser scanning is a promising remote sensing technique to gather, from a safe distance, highly accurate discontinuity measurements (Feng et al., 2001; Kemeny & Post, 2003; Sturzenegger et al., 2007; Voyat et al., 2006). Especially, its wider area coverage up to several thousands meter, high precision with milimetre accuracy, easy and faster data acquisition gives a significant advantage as compared to conventional methods.

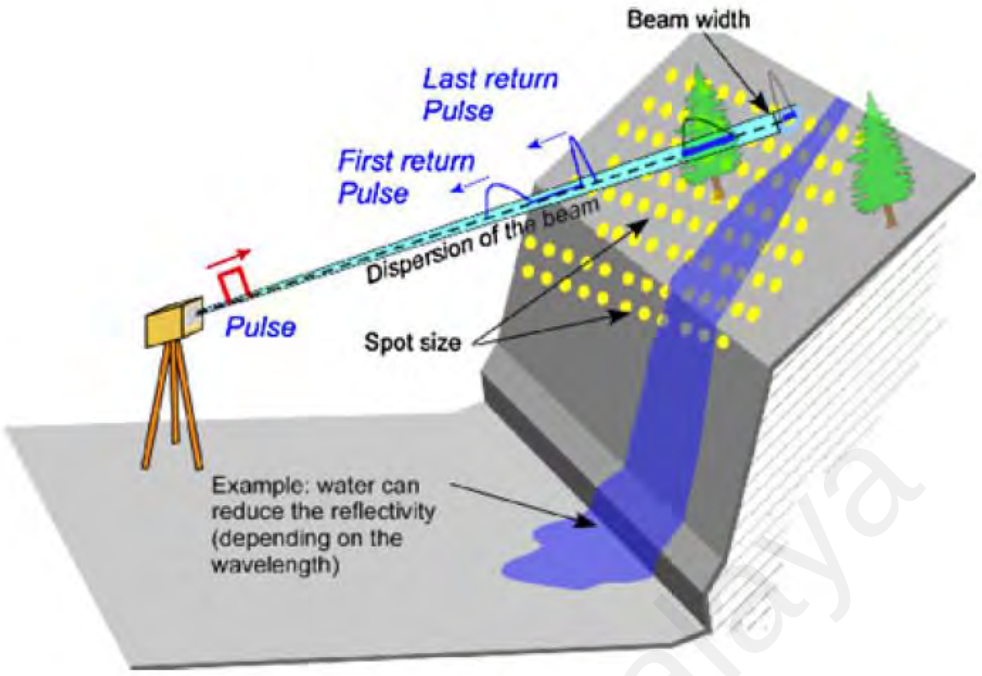

Figure 2.1: The principal of Terrestrial Laser Scanning data acquisition. Laser scanner emits pulses that scattered back to the sensor (Jaboyedoff et al., 2010).

Rock mass characterization by TLS is mainly to obtain accurate slope profile and discontinuity sets orientations. However there are several ways in characterizing the discontinuity sets in rock mass. Several studies are proposing different ways to characterize discontinuity sets, which can be mainly classified as (a) using fitting planes (Abellán et al., 2006; Fernández, 2005; Sturzenegger & Stead, 2009), (b) using TIN surfaces as indicators of the plane orientations (Slob et al., 2002). A description of the methodology employed for rockmass characterization using the commercial software Split-FX is provided in (Kemeny & Post, 2003) (c) Other techniques allow for the automatic delimination of a set of neighbourhood points characterized by the same normal vector. As a result, the calculation of the orientation of the discontinuity planes is obtained. The COLTOP technique (Derron et al., 2005; Jaboyedoff et al., 2007) permits to visualize the orientation of different discontinuity set by unique colour (Figure 2.2), which makes the approach very similar to a field data acquisition. The

extracted data permit to analyse the rock instability mechanism (Janeras et al., 2004; Oppikofer et al., 2009).

According to Feng and Röshoff (2015), in order to avoid the drawbacks of traditional measurement methods, 3D TLS method must have the following key features; (i) quickly capturing discontinuity data in the field; (ii) digitally gathering data in order to utilise computer aided processing procedure; (iii) having the ability to visually operate the data so that the operator's background knowledge and experiences can be fully used to analyse complicated events related to a jointed rock mass and then obtain the required information for rock slope applications; (iv) keeping a certain level of accuracy; (v) capturing discontinuity data remotely without physically cantacting the rock faces.

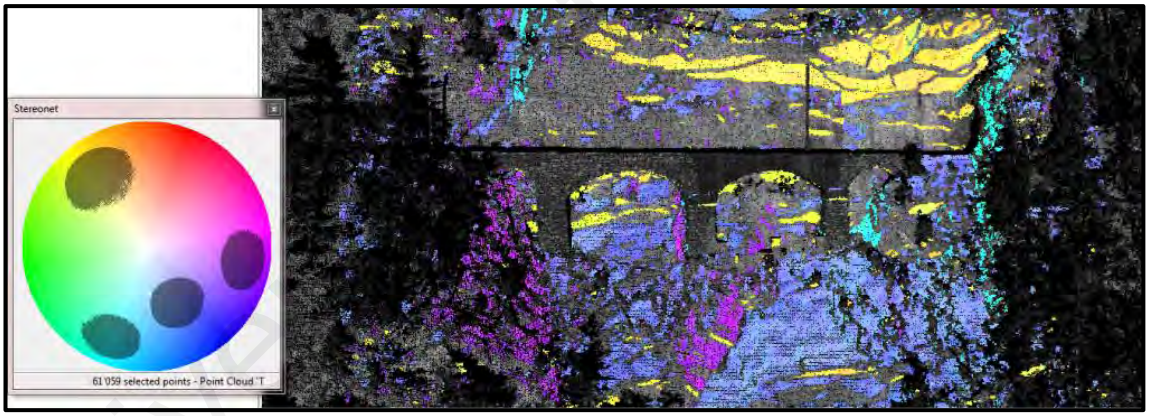

Figure 2.2: Application of COLTOP in visualizing the orientation of discontinuity by unique color. Each color represents different sets of discontinuity. Source: COLTOP manual.

2.3.2 3D Terrestrial Laser Scanning Limitations in Discontinuity Measurements

3D TLS though, give a great advancement in rock mass characterization, however have some limitations. There are four common limitations that occur during the scanning (Sturzenegger et al., 2007), which are (i) occlusion (ii) truncation (iii) censoring (iv) orientation bias.

i. Occlusion occurs when some of the rock faces is unable to be scanned due to the unfavourable position of the laser scanner which restrict the data acquisition on the rock slope discontinuity features. Occlusion also may occur due to some other rock features covering the rock face. Some of the important features on the rock slope maybe disappeared due to the effect of occlusion.

ii. Truncation occurs when the exposure of discontinuity is less than the available resolution of the 3D TLS. Features such as joints and bedding planes with low exposure make it difficult for the scanner to detect the discontinuity. Extreme weathering and dissolution on the rock slope faces such as in the tropics country may have experienced this limitation.

iii. Censoring occurs due to a surface that appears only partly on a rock face with the part of it hidden within the rock face which result to underestimation of the persistence of discontinuities.

iv. Orientation bias occurs when the scanner line of sight (LOS) is parallel to the orientation of the discontinuity (Figure 2.3 and 2.4). Frequently these daylighting discontinuities give great influence in the stability of the slope. Hence, very important information may not be considered in slope analysis if this bias occured.

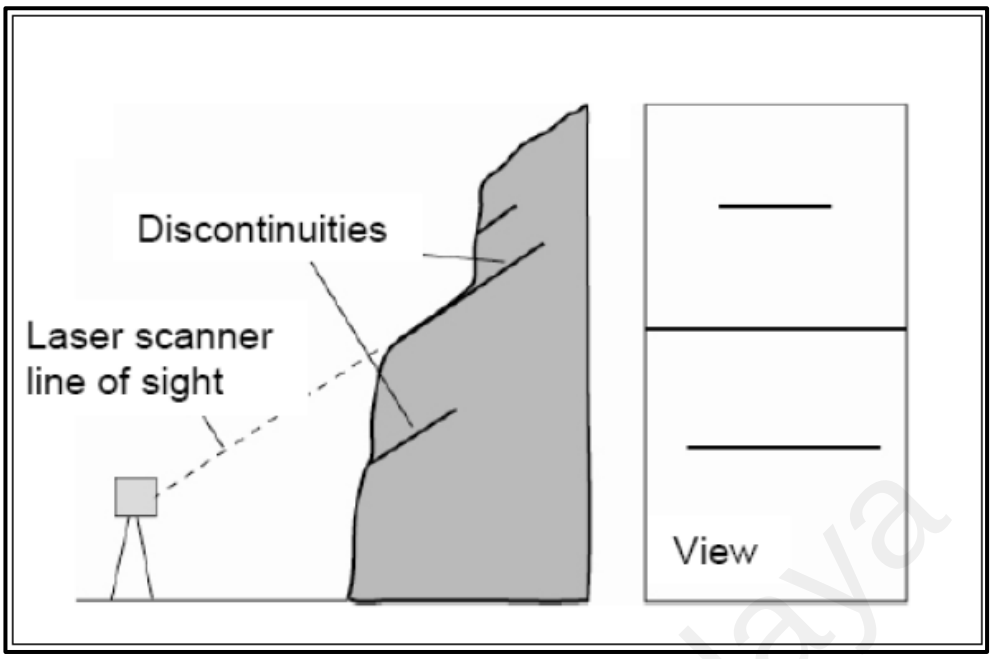

Figure 2.3: Illustration of orientation bias where the dipping discontinuities plane are parallel to the line of sight (LOS) of the scanner (Sturzenegger et al., 2007).

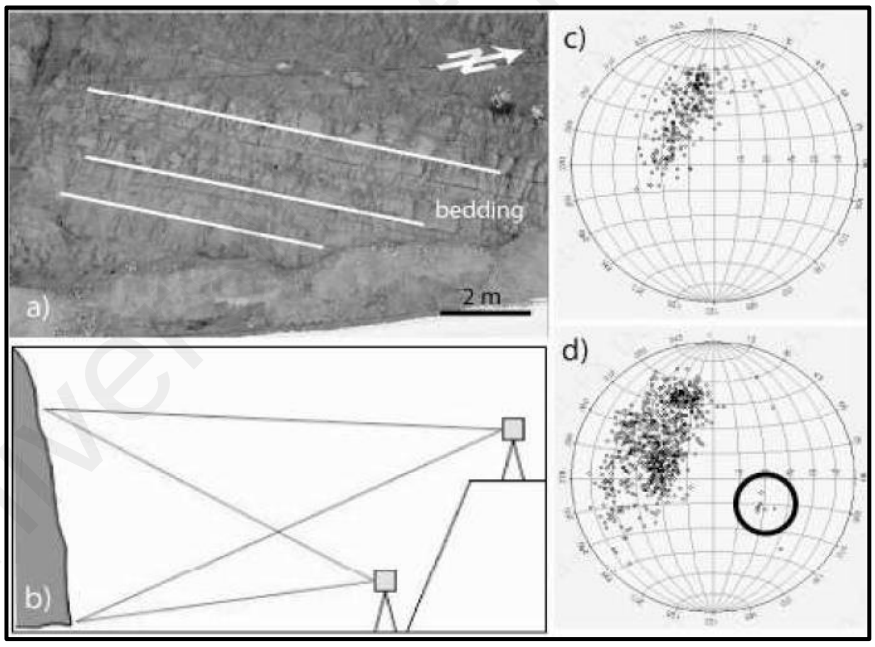

Figure 2.4: Illustration of the laser scan elevation bias. (a) Rock face showing bedding joints, (b) positions of the laser scanner at two different elevation with respect to the rock face, (c) stereonet obtained from the upper position, on which bedding joints do not appear, (d) stereonet obtained from the lower position showing poles representing the bedding joints inside the black circle (Sturzenegger et al., 2007).

Several errors should be taken into account during the processing of raw point cloud data from the scanner. Since it is involving multiple processing step which include pre-processing and post-processing, the data processing will always prone to errors. Noise and vegetation filtering are the examples of processes that can affect the quality of the data. This is because, some of the important features on the rock faces may be filtered together with the noise and removing it from the point cloud data. Therefore, filtering processes need to be done carefully. According to (Slob et al., 2005), during 3D TLS survey, the laser scan system will always be susceptible to small errors, which depend upon the 3D TLS system characteristic parameter, such as the angular accuracy, beam divergence, and range accuracy. Thus, the data chosen for analysis may also result in under-characterization and over-characterization of discontinuity properties.

2.4 Comparison between Lidar measurements and manual measurements

The application of Lidar measurements has been rapidly grown over the past decade. Comparing these two method will offer a better advantage for field data collection and analysis. A case study by Kong et al. (2020), compare the joints orientation of Lidar survey and manual survey and discovered there are differences of orientations from both method due to the roughness and waviness of discontinuity surfaces on the field.

The stability of steep slopes have also been evaluated by block analysis based on traditional surveys and laser scanner acquisitions (Ferrero et al., 2009). In his work, due to large dimensions of the slope, traditional surveys have been coupled with laser scanning technique in order to gather geo structural information remotely without direct contact to the rock mass.

An integrated methodology based on traditional field and remote surveys such as terrestrial laser scanning have also proposed by Gigli and Casagli (2013). In his work,

he integrate traditional field survey with a TLS survey to gather geomechanical parameters suggested by Barton (1978) by using Matlab tool called DiAna in order to define susceptibility scenarios affected by instability processes.

2.5 Previous Stability Analysis in Study Area

Reports on stability analysis of limestone hills in Kinta Valley have been done by many researchers recently. Several studies proposes different ways in assessing the limestone hills stability, which are by using the Rock Mass Strength (RMS) method (Simon et al., 2015) a number of seven components were used to assess the rock slope which are (a) intact rock strength (b) weathering (c) joints spacing (d) joints orientation (e) joints width (f) continuity of joints (g) outflow of groundwater. According to Simon et al. (2015), based on the seven components in the RMS system, Gunung Rapat, Gunung Datok, and Gunung Lang are classified as weak while other hills are classified as moderate.

Furthermore, other method used in assessing the limestone hills is the Slope Mass Rating (SMR) method (Lai et al., 2016). Based on his study, he suggested that the rock slopes at Gunung Lang are stable to unstable by using the SMR method (Romana, 1985) with the probability of failure ranging from 0.2 to 0.6 respectively.

There is also study on geomechanical strength of carbonate rock in Kinta Valley by using uniaxial compressive strength test, point load test, and Brazilian tensile test (Mazlan et al., 2018). Based on the test, the results revealed that the geomechanical strengths of rock material of carbonate rocks for material and discontinuities failure deteriorates approximately ½ from material failure (Mazlan et al., 2018).

Last but not least, a study of lineament density in potential evaluation of rock fall in Kinta Valley (Ghani et al., 2016). The study shows a good correlation between lineament density map and the RMS score, suggested that the slope stability in Kinta

Valley is influenced by the regional lineament density. Above all of these previous study, most of it is conducted at the base of the slope while this research apply 3D TLS to remotely assess the slopes and hopefully will help to better understand the Kinta Valley slopes and morphology in the near future.

CHAPTER 3: RESEARCH METHODOLOGY

3.1 Location of the Study Area

This research study area is located in the Kinta Valley, Perak, Malaysia. Numerous limestone hills with an average size of 1.08 km square feet and some of the hills are unnamed (Simon et al., 2015). Widespread occurence of limestone hills are shown in the map below (Figure 3.1). Due to its magnificent landscape, Kinta Valley has been declared as one of the National Geoparks in Malaysia (Leman, 2013).

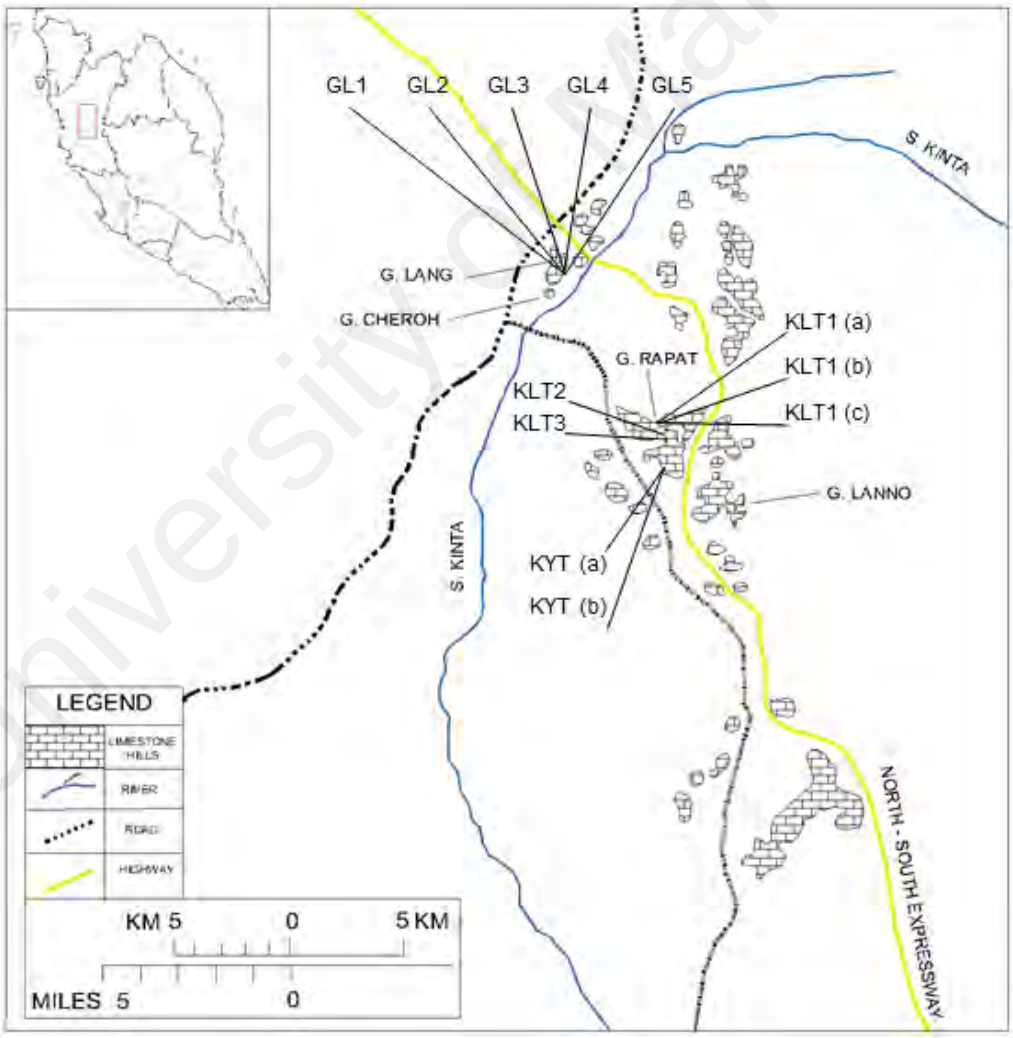

Figure 3.1: Map showing the wide spread of limestone hills in the study area.

3.2 Geomorphology of the Study Area

Tropical country like Malaysia produce unique steep sided tropical limestone towers which protruded from the alluvial plain, for example like in Kinta Valley. These unique characteristics of Kinta Valley limestone hills is made possible by various factors, namely: the humid, wet tropical climate, accelerated karstification and its location in the floodplain of Kinta (Muhammad & Komoo, 2003). Constant supply of allogenic water from the floodplain nearby the limestone hills has speed up the karstification processes. Furthermore, Kinta Valley limestone hills are mostly steep sided, with subvertical to overhanging cliffs which restricts the manual data collection only at the base of the slope. Therefore, 3D TLS is used to remotely assess the overall slope. The base of limestone hills also often can be characterize with deep horizontal notches and undercuts due to horizontal dissolution by swamp water or streams (Figure 3.4). This karst notch features was also being used as indicator for paleoclimate environment and base level changes (Muhammad & Komoo, 2003). The interior of file limestone hill mass may also be pock- marked with deep hollows or solution sinkholes or dolines, locally called "wangs" (Tan, 1988). Within the limestone hills, cave system with magnificent cave deposits, stalactite, and stalagmite are one of the major tourist attraction. Some of the well known cave in Kinta Valley are Gua Tempurung and Gua Kek Lok Tong.

3.3 Geology of the Study Area

Geologically, Kinta Valley is underlain by the Kinta Limestone which has been dated Devonian to Permian (Suntharalingam, 1968). The limestones includes several relatively thin argillaceous beds, and exceed 3000 meter in stratigraphic thickness (Ingham & Bradford, 1960). Much of the limestone is found beneath the general surface where it underlies the tin ore bearing alluvium for which the Kinta Valley was once

famous (Muhammad & Komoo, 2003). The Kinta Valley Schist occurs mainly below the Kinta Limestone though parts are found to interbed with the former (Ingham & Bradford, 1960). Furthermore, Kinta Valley also being flanked by schist and granite on the eastern and western sides of the valley (Hutchison & Tan, 2009). According to (Muhammad & Komoo, 2003) these Paleozoic rocks (limestone and schist) were intruded by the Kledang Range and Main Range Granites during the very Late Triassic.

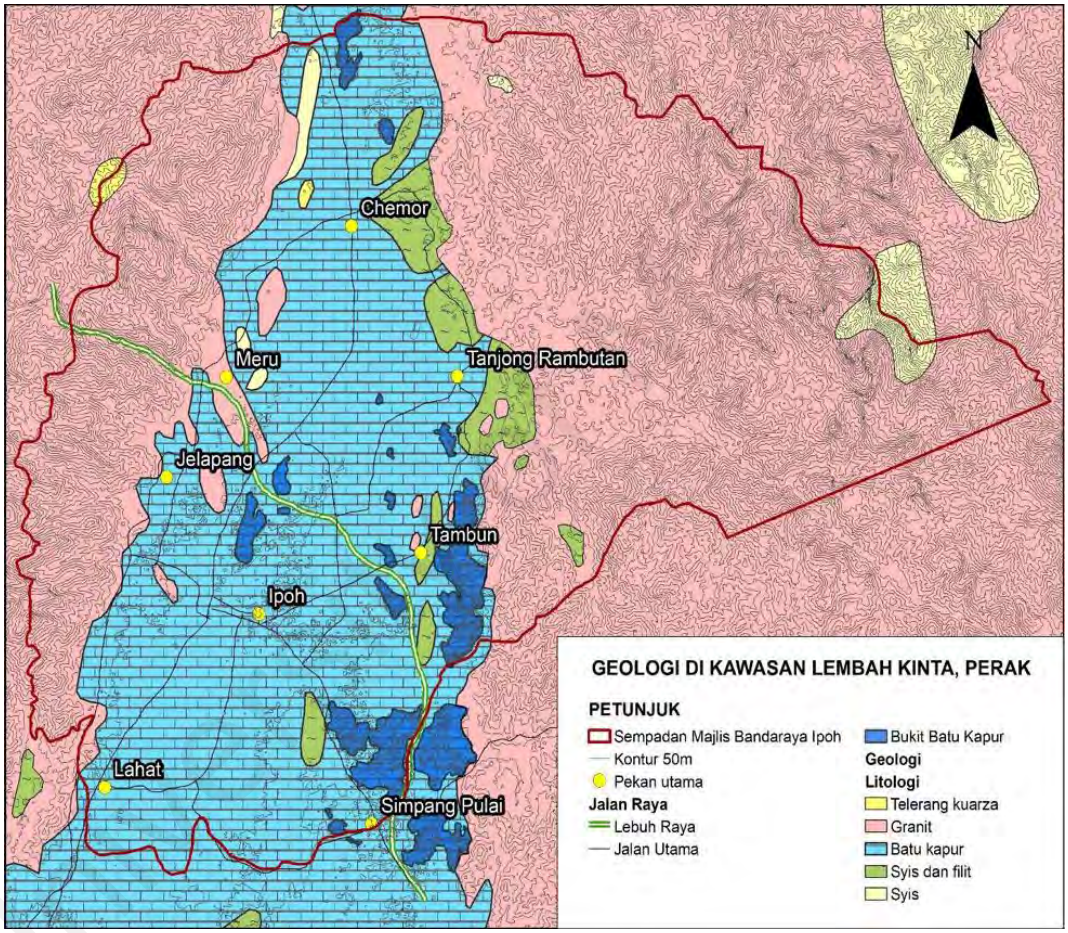

Figure 3.2: Geological map of the study area (Ismail et al., 2017).

3.4 Structural Geology of the Study Area

Kinta valley limestone hills is also characterized as massive limestone bodies which are heavily jointed and fractured. Joints and fractures are common features in the limestone bodies with two to four joint sets (Simon et al., 2015). According to Tan (1988), Kinta Valley limestone hills are actually the remnants of the limestone

formation which has been degraded or dissolved, and the collapse of the limestone cliffs contributes to the reduction in the size of the limestone hills. For example, some 40 limestone hills of various sizes have been recorded (Tan, 1988). While some limestone hills are 'massive' and spatially extensive such as Gunung Tempurung and Gunung Rapat, while others appear as slender, needle like limestone hill pinnacles, the notable example being so called Tambun Tower (Tan, 1998).

In terms of structural geology of the study area, a straight 26 km long scarp is found on the eastern flank of the Kledang Range which is suggestive of a major fault and several smaller faults have been observed at the eastern side of the Kinta Valley (Simon et al., 2015). According to (Muhammad & Djin, 2003) the trend of Kinta Valley karst structure is mainly along the 310-350^{o} with minor directions of about 030^{o}, 040^{o}, 055^{o}, 070^{o}, and 085^{o}. These trend originate from tectonic stresses and controlled the formation of certain karst features such as dolines, wangs, caves and collapse. Numerous studies on karst concluded that structure plays a major role in determining the formation of the karst features (Song, 1983). This is further supported by (Tjia, 1969) observation on positive and negative lineaments in several karst region showing that they represent fracture direction which agree with (Escher, 1931) who was of the opinion that the dolines are located at intersection of fractures. The importance of rock strike in controlling both the orientation of pinnacles long axes and the direction to the pinnacles has also been observed by (Dian, 1996) in Mt. Zebri and Llasa area, respectively in Tibet. Furthermore, a number of geologist had ascribed the formation of Kinta Valley to block faulting occuring at the contact between the granites and the metasedimentary rocks (Gobbett, 1973). Gobbett (1973) also shows that the orientation of lineaments from Main Range and Kledang Range is far from irregular but somehow shows the dominant strike of northwest with subsidiary set striking east-northeast and

he concluded that these lineations may also be observed cutting the limestone hills in the valley.

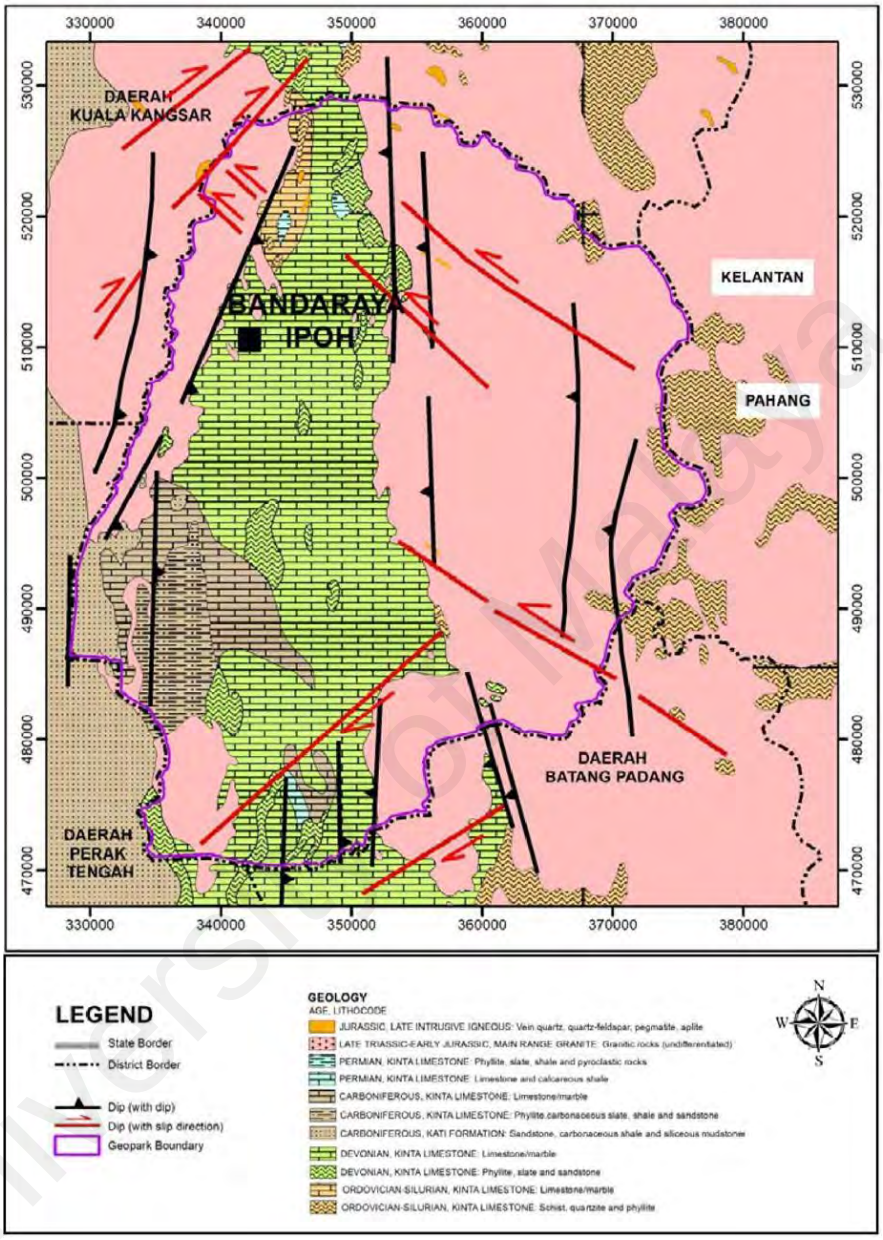

Figure 3.3: Structural geology map of the study area (Ismail et al., 2017).

Figure 3.4: Steep sided morphology of the limestone hills at Gunung Cheroh.

3.5 Field Survey

3.5.1 Scanline Measurements

Horizontal scanline survey are conducted along the rock slope faces of the limestone hills in the study area. Discontinuity readings are recorded for each of rock slope faces and being used for the validation and comparison with the 3D TLS readings. All of the joints orientation readings for each limestone hills are presented in Table 4.27, Table 4.28, and Table 4.29. Aside from joints orientations, other parameters suggested by (ISRM) were also collected, namely; spacing, persistence, and seepage of water in order to be compared with Lidar measurements. However, some of the base of limestone hills are covered with thick vegetation and highly weathered limestones which restricts manual scanline data collection. Karst features such as shelter cave and notches make it more difficult for scanline survey to be conducted. The equipment needed during measurements is compass clinometer and a measuring tape of at least 10 metre in length (Figure 3.5). Scanline length for each of the slope and the slope characteristics are presented in Table 3.1.

Table 3.1: Slope characteristic in study area.

Slope	Slope Length (m)	Slope Height (m)	Scanline Length (m)
GL1	23 m	15 m	20 m
GL2	40.5 m	30.1 m	20 m
GL3	32 m	28 m	20 m
GL4	134 m	88 m	50 m
GL5	87.5 m	58.3 m	20 m
KLT 1(a)	51.6 m	41 m	20 m
KLT 1 (b)	54.5 m	62.5 m	20 m
KLT 1 (c)	81.7 m	64.6 m	-
KLT 2	36.5 m	91.9 m	10 m
KLT 3	44.5 m	48 m	20 m
KYT (a)	160.5 m	98.6 m	-
KYT (b)	160.5 m	98.6 m	-
G Cheroh	87 m	48 m	-
G Lanno	45.3 m	49.5 m	-

Figure 3.5: Compass clinometer and measuring tape used for scanline measurement survey.

3.5.2 3D Terrestrial Laser Scanning Measurements

Terrestrial laser scanning was conducted on the limestone cliff faces starting on November 2017 untill December 2018. A total number of 4 limestone hills and 14 rock slope faces are selected for this research based on slope accessibility and safety near the man-made structure. A few of these sites are geosites within the Kinta Valley National Geopark. The cliff faces are GL1, GL2, GL3, GL4, GL5 in Gunung Lang, KLT 1 (a), KLT 1 (b), KLT 1 (c), KLT 2, KLT 3, KYT (a), KYT (b) in Gunung Rapat, G Cheroh in Gunung Cheroh and G Lanno in Gunung Lanno.

The measurement was conducted using RIEGL VZ-400 laser scanner which has a scanning capability at a maximum range up to 400 meters, however scanning at maximum range of the scanner may give rise to more error and noise. This is because at this range, the spacing between the point clouds becomes further, and resulting in loss of important features which are located between this point clouds gap. A complete digital model of each limestone hills was obtained by the terrestrial laser scanning with multiple scanning positions, depending on the length and size of the cliff surface.

3D Terrestrial laser scanning produce millions of points known as “point cloud”, which is a three dimensional (X, Y, and Z) coordinates representation of the scan object with respect to the laser scanner. Since all of the scanned objects were present in the point clouds, which includes the terrain, rock faces, and vegetation, the raw scanning data cannot be directly used for the stability analysis. Vegetation and noise need to be treated and removed from the cliff surface data leaving only point clouds data which are needed for the analysis.This filtering process was manually done by using the software RiSCAN PRO.

According to Slob et al. (2005), in order to determine the orientation parameters of the discontinuity the point cloud has to be reorient relative to the true north and ensure

that the data are levelled. Since the scanner RIEGL VZ-400 true north is not indicated in the coordinate system of the scanner, all of the scanned data were geo referenced in WGS 1984 projection. Geo-referencing process helps register the project coordinate system (PRCS) into the global coordinate system (GLCS) WGS 1984. Table 3.2 shows the details of the RIEGL VZ-400 specifications, and Figure 3.6 shows the equipment used for the scanning.

Table 3.2: RIEGL VZ-400 specification. Source: RIEGL manual.

Parameter	RIEGL VZ-400
Wavelength	Near infrared
Accuracy	5 mm
Scan Angle Range	Vertical scan of 100° (+60°/ -40°)
	Horizaontal scan of 360°
Laser Beam Divergence	0.3 mrad
Measurement rate	42 kHz at long range mode
	122 kHz at speed mode

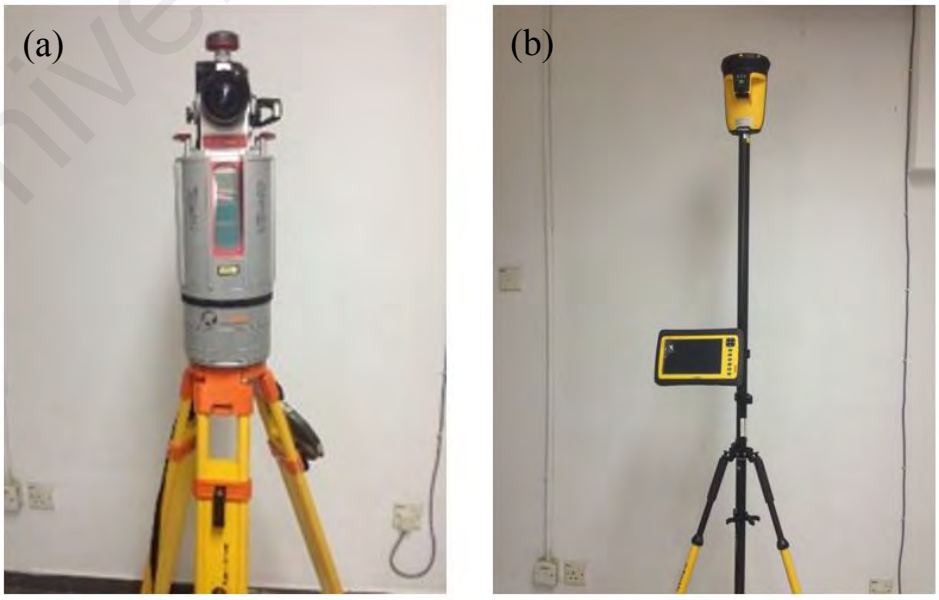

Figure 3.6: RIEGL VZ-400 laser scanner (a) and TRIMBLE GNSS receiver (b) used for scanning and georeferencing.

3.6 Methodology Workflow used for Application of TLS in Stability Analysis

The morphology workflow consists of the following steps:

- Data acquisition on the field; this was carried out by using RIEGL VZ-400 scanner which produced millions of 3D points (point clouds) and direct measurements on the field of joints orientation, joints spacing, trace length and water seepage on the rock slope faces.
- Data pre-processing; multiple pre-processing steps which consists of pre-point cloud registration, vegetation and noise filtering, and georeferencing of point cloud data.
- Data post-processing; consist of discontinuity selection using COLTOP 3D software
- Result Validation; 3D TLS measurements validation with manual measurements
- Kinematic analysis and hazard assessment.

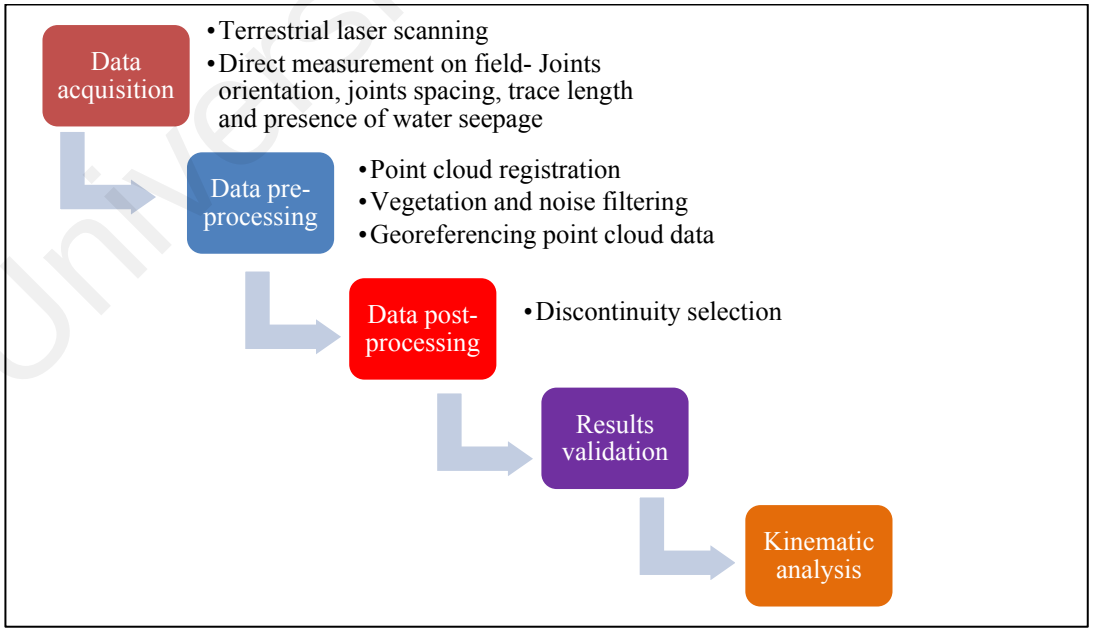

Figure 3.7: Methodology workflow.

3.7 Pre-Processing of Point Cloud Data

3.7.1 Point Cloud Registration

3D TLS surveys on the field produce up to a million of points which are called "point cloud". This point cloud is the representation of the reflected surface on the field in x, y, and z coordinates system. To produce a 3D model of the study area, raw point clouds data from the scanning need to be registered because it consists of data from multiple scanning positions (Figure 3.8). Alignment of the point cloud usually consists of a two-step process: a preliminary registration by a visual identification of homologous points and an optimization of the alignment using an Iterative Closest Points (ICP) procedure (Besl & McKay, 1992; Chen & Medioni, 1992). By using this algorithm, the distance between two points are iteratively reduced by a minimization of a mean square cost function. Alternatively, the alignment over discrete parts of the slope can be carried out using the Roto-Translation technique described by different authors (Monserrat & Crosetto, 2008; Oppikofer et al., 2009; Teza et al., 2007). The registration procedure in this study is by using the RiSCAN PRO software.

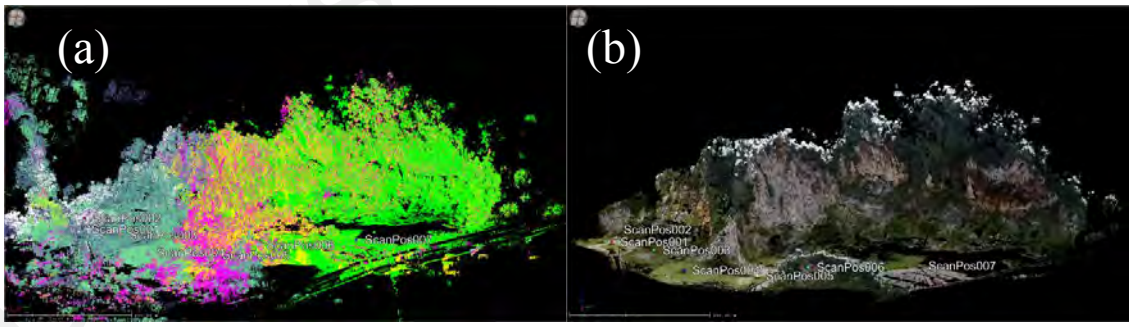

Figure 3.8: 3D TLS model of Gunung Lang slope (a) registered point cloud view with multiple colours, each of the colours belongs to single scanning positions, therefore 7 numbers of scanning positions gives 7 colours on the model (b) colorized true colour 3D TLS model of Gunung Lang slope.

3.7.2 Vegetation and Noise Filtering

Vegetation and noise filtering process are crucially needed and done carefully since it can affect the quality of the 3D model data. This is because during this process, some of the important features on the rock faces may be filtered together from the point cloud data. One of the main issue in laser scanning is the removal of the vegetation (Harding et al., 2008). Vegetation filtering can be carried out both manually and automatically. The full waveform of the laser signal from the 3D TLS makes it possible to filter vegetation automatically by using the reflectance difference. Vegetation has indeed a lower reflectance than the rock of the cliff, so a reflectance threshold has been chosen to remove most of the points corresponding to vegetation (D'Amato et al., 2015). However, not all of the vegetation can be filtered automatically by using this method. Some of the vegetation still presents especially the small-scale vegetation located on to the rock surface. In this case, manual filtering is needed.

3.7.3 Geo-Referencing of Point Cloud Data

The 3D model produced by the 3D TLS is not truly aligned according to the true north; this is because the model is registered to scanner coordinate system. In order for the model to be extracted into other processing software such as the COLTOP 3D and DIPS software, the point cloud need to be registered into the Global Coordinate System (GLCS) which then can be exported usually into ASCII format and PLY format. This can be achieved by conducting a Differential Global Positioning System (DGPS) survey on the field with Real Time Kinematic (RTK) corrections. In this survey Trimble GNSS receiver is used together with the tripod. The accuracy of the survey depends upon the quality of the control survey and the distribution of control points within the point cloud (Yiu & King, 2009).

3.8 Post-Processing of Point Cloud Data

3.8.1 Discontinuity Selection and Characterization

Registered point clouds data can be merged and manipulated to obtain rock mass properties such as the dip angle, dip direction, spacing, and trace length of the joints. Several studies proposes different ways to characterize discontinuity sets, which can be mainly classified as (a) using fitting planes (Abellán et al., 2006; Fernández, 2005; Sturzenegger & Stead, 2009), (b) using TIN surfaces as indicators of the plane orientations (Feng et al., 2001), and (c) Other techniques that allow the automatic delimitation of a set of neighbourhood points characterized by the same normal vector.

This research uses the latter technique which characterizes points by the same normal vector. The COLTOP 3D software is used to extract and characterize the properties from the 3D point cloud model. The COLTOP technique (Derron et al., 2005; Jaboyedoff et al., 2007) permits to visualize the orientation of each discontinuity set by a unique colour, which makes the approach very similar to a field data acquisition (Figure 3.9). The extracted data is used to analyse the rock instability mechanism (Janeras et al., 2004; Oppikofer et al., 2009).

Different authors have pointed out the existence of two types of biases in the determination of the orientation of discontinuities (Lato et al., 2009; Sturzenegger & Stead, 2009): (a) scale bias, when discontinuity sets are smaller than the spatial resolution (point spacing) and (b) orientation bias, when the incidence angle of a given data set influences the spatial resolution. This subsequently automatically transferred and shown in the number of poles plotted on the stereonets. To prevent this bias, manual discontinuity selection by the operating geologist is necessary in order to characterize the actual discontinuity plane while using COLTOP 3D software (Sturzenegger & Stead, 2009).

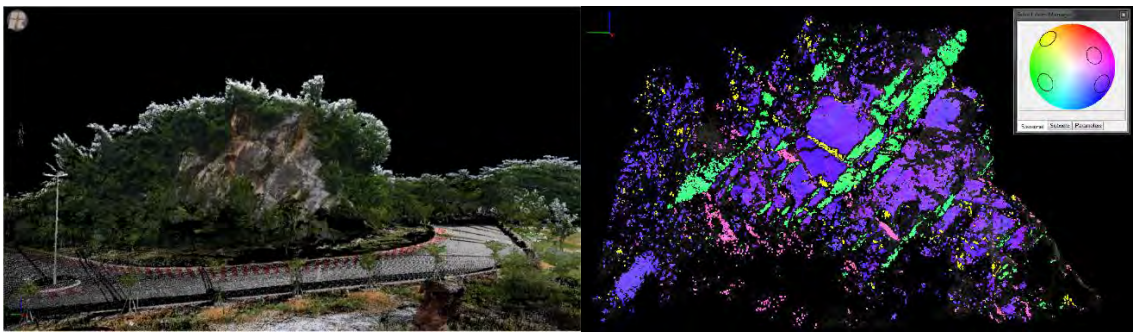

Figure 3.9: A rock slope from Gunung Lang shows (a) 3D model of the slope in true colour view (b) shows the visualization of different discontinuity sets by COLTOP 3D software which allows the discontinuity sets be presented in a unique colour according to the stereographic projection.

3.9 3D TLS Measurements Validation with Manual Measurements

Over the all of 14 number of rock slope faces, manual measurements of dip angle, dip direction, spacing, and trace length are recorded by using the scanline method. However, not all of the slopes permit manual scanline method due to site limitation such as thick vegetation covering the joints plane and the inaccessible location of the rock slope. This manual measurement is then used to make a comparison and validation with the 3D TLS measurements. This data validation is carried out according to the method suggested by (Cawood et al., 2017); on a control surface which represents the joints and bedding planes of the slope in the field. Multiple dip angle and dip direction measurements are collected on each of the control surface by using traditional compass clinometer and the same process is repeated by using the overall scan of 3D TLS on the same surface chosen. Figure 3.10 shows the example of how validation was done on GL 1 rock slope faces. These data were then plotted as a pole on the stereonet for comparison (Figure 3.11).

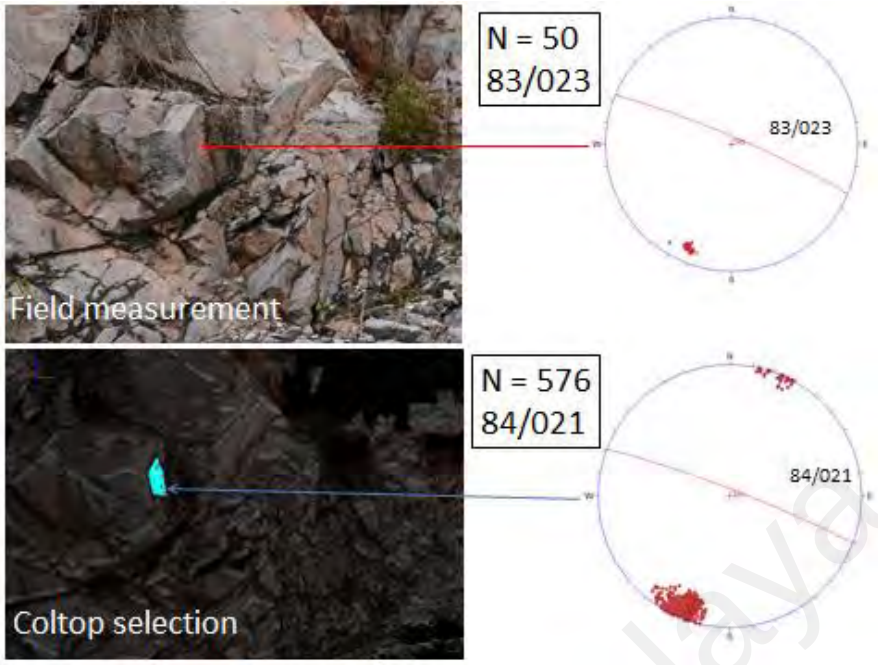

Figure 3.10: A number of 50 manual compass clinometer measurements are collected on the control surface and the same process was repeated with the 3D TLS measurements.

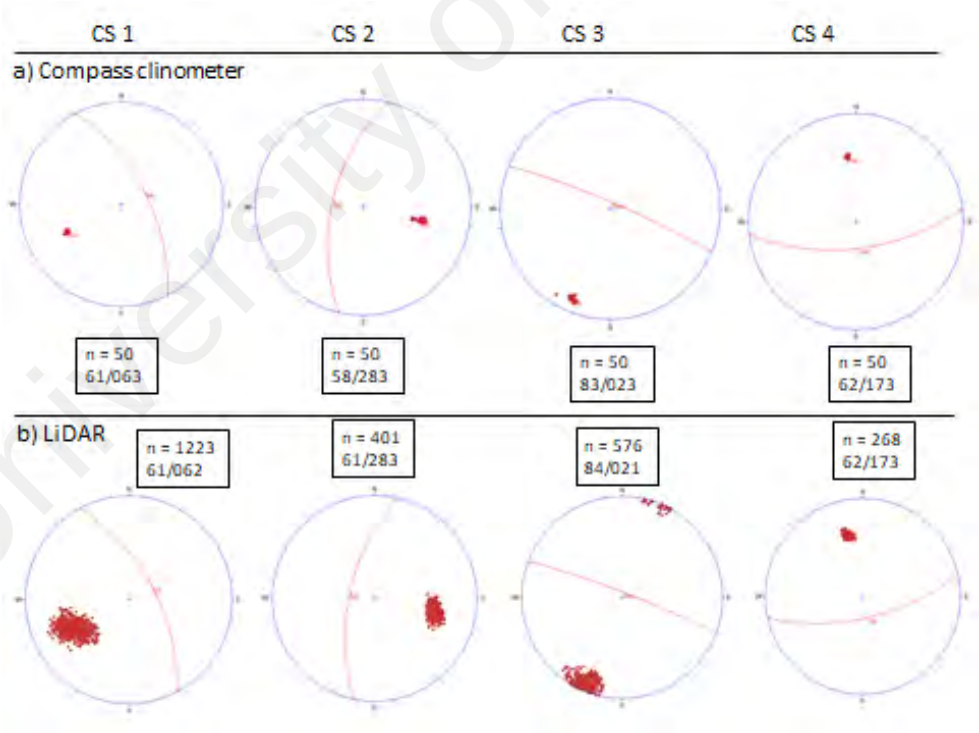

Figure 3.11: Figure shows the comparison between 3D TLS measurements with manual compass clinometer measurements on the four different control surface which was chosen on the field.

3.10 Kinematic Analysis

Kinematic analysis is a technique used to analysed the potential of various rock failures, some examples of common rock failure are the planar failure, wedge failure, and topple failure (Hoek & Bray, 1981). These failures occur due to the presence of unfavourably oriented discontinuities (Figure 3.13). The kinematic analysis is carried out using the Markland test procedure implemented in the Dips Software by Rocscience (Figure 3.14) and COLTOP 3D for discontinuity extraction (Figure 3.12). Markland tests is designed to establish the possibility of a wedge failure in which sliding takes places along the line of intersection of two planar discontinuities. The test is generally explained about the characteristics of slope failure. According to Hoek and Bray (1981), a planar failure is likely to occur when a discontinuity dips in the same direction (within 20^{o}) as the slope face, at an angle gentler than the slope angle but greater than the friction angle along the failure plane. A wedge failure may occur when the line of intersection of two discontinuities, forming the wedge-shaped block, plunges in the same direction as the slope face and the plunge angle is less than the slope angle but greater than the friction angle along the planes of failure (Hoek & Bray, 1981). A toppling failure may result when a steeply dipping discontinuity is parallel to the slope face (within 30^{o}) and dips into it (Hoek & Bray, 1981).

Figure 3.12: Rocscience DIPS software and COLTOP 3D software used for kinematic analysis.

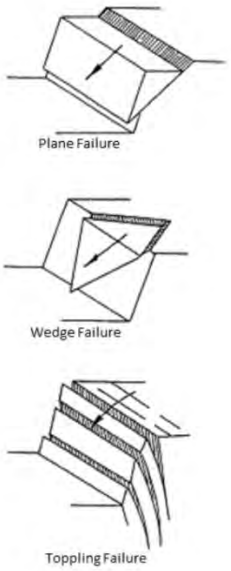

Figure 3.13: Types of rock slope failure associated with unfavorable orientation of discontinuity (Hoek & Bray, 1981).

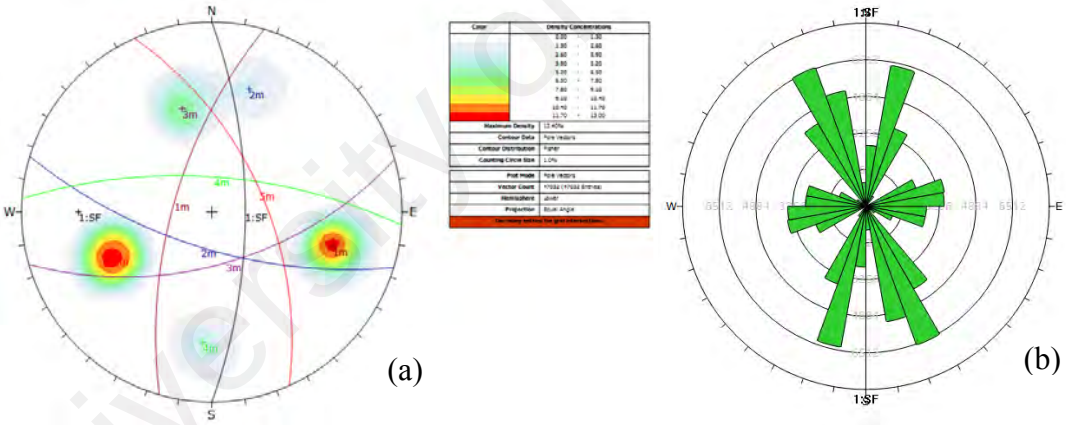

Figure 3.14: Example data from Gunung Lang Area 1 rock slope (a) Stereonet shows the poles plot and major planes plot of all discontinuity sets and (b) Rose diagram showing trend of discontinuity sets.

3.11 Integration of Lidar TLS Method with Manual Direct Measurement

Rock mass properties such as joints orientation, joints spacing, and water seepage acquired from both 3D TLS measurements and manual scanline measurements can be integrated as following:

- Joints orientation such as dip angle, and dip direction of joints can be integrated. Wide coverage of 3D TLS scanning provide more inclusive joints orientation data throughout the whole slope, while manual direct measurements by compass clinometer focusing only at the base of the slope. Integration and combination of both methods deliver a better rock mass characterization of the slope.
- Joints spacing and trace length are commonly measured by manual direct measurements, however, 3D point cloud data provided by the laser scanning permit joints spacing measurement from the tools provided by the processing software Riscan Pro. Both reading from manual and TLS are used for comparison.
- The presence of water seepage on the rock slope can also be detected by TLS and manual visual direct measurements. Multiple waveform intensity emitted by the laser scanning make it possible to distinguished between the bare rock surface with the one covered with water or soils.

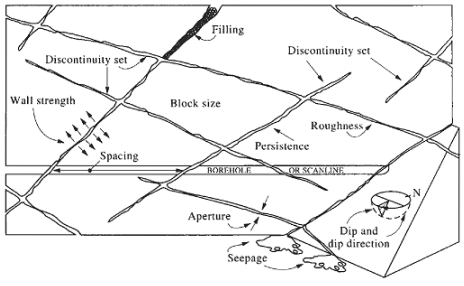

Figure 3.15: Rock mass properties of discontinuities (ISRM & Hudson, 2007).

CHAPTER 4: RESULTS AND DISCUSSION

4.1 Introduction

This chapter presents the utilization of discontinuity measurements derived from 3D TLS and scanline method in assessing the rock slope stability. Description of each rock slope such as the height, length, and exact location of the rock slopes are also presented. Finally, the relationship between the trends of potential rock failure with the structural trend in Kinta Valley are interpreted based on the combined data.

4.2 Gunung Lang Limestone Hills

Gunung Lang is well known for its recreational park that attracts many visitors from all over the country (Figure 4.1). A 3D TLS measurement is carried out with a number of seven scanning positions in order to cover all side of the hills (Figure 4.2) Gunung Lang limestone hill is approximately 100 meter high from the ground and 380 meter in slope length, a total number of 5 slopes were evaluated and labelled as GL1, GL2, GL3, GL4, and GL5 respectively (Figure 4.3). Gunung Lang limestone hill was an ex-mining area which exposed to blasting in the past. According to Simon et al. (2015), joints on the hills were noticeably clear but joint patterns were difficult to recognise due to blasting activities. The joints spacing are closely spaced and the joints dip moderately to steeply out of the slope (Simon et al., 2015)

Figure 4.1: Figure shows the location of Gunung Lang limestone hills and its well-known recreational park. Image from (Google earth).

Figure 4.2: The position of 7 scanning position in the field, 3D model derived from RiScan Pro software.

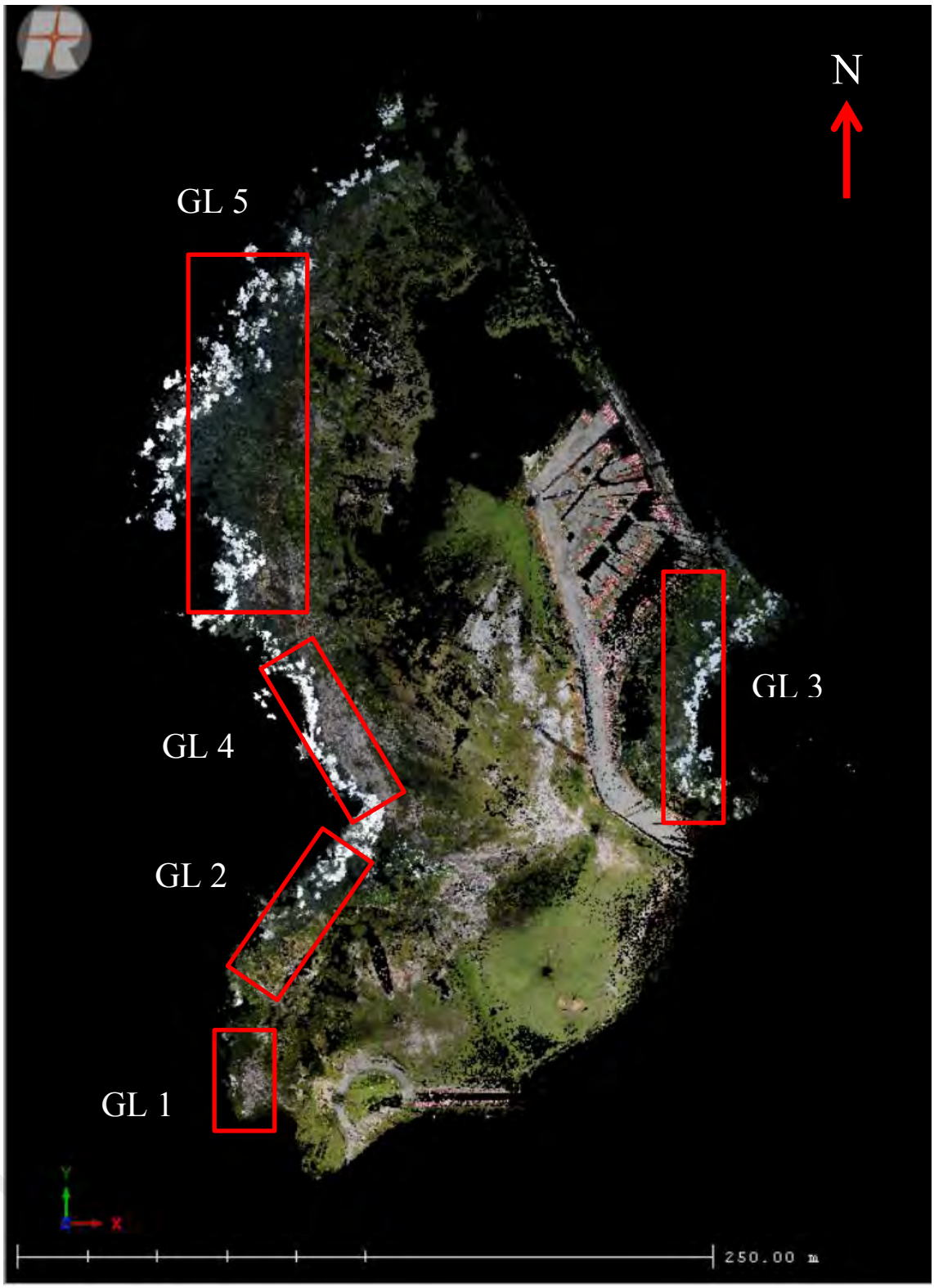

Figure 4.3: A 3D model aerial view of Gunung Lang scanning area derived from RiScan Pro software, it is divided into 5 individual slopes which are GL1, GL2, GL3, GL4, and GL5 respectively.

4.2.1 GL 1 Slope Stability Analysis

Based on the analysis and discontinuity selection from the Coltop 3D software, GL1 slope have five joint sets which are J1 (67/286), J2 (68/197), J3 (59/164), J4 (69/004), and J5 (59/066) as shown in Figure 4.4b. The entire major plane of the joint sets is plotted on the stereonet and the trend of the discontinuity orientation is presented in the rose plot (Figure 4.7). Based on the rose plot shown in the figure, most of the joint sets in the GL1 slope are trending northwest-southeast direction. Kinematic analysis has also been done at the slope. Planar, wedge, and topple failure test was conducted and all of the potential failure are shown in the stereonet in (Figure 4.8). For planar failure, joint sets J5 (59/066) favour the criteria for planar failure, and the direction of planar failure that will occur is towards east direction 090^{o}. For topple failure, based on the kinematic analysis criteria provided by the Dips software, there is no potential topple failure detected. However, based on the stereonet, discontinuity J5 (59/066) will act as a base plane for topple failure. For wedge failure, three possible wedge failure has been identified which are involving the intersection between joint sets J5 and J2, J5 and J3, and J5 and J4 respectively. Possible wedge failures that will occur are towards northeast (055^{o}), and southeast (115^{o} and 125^{o}). Scanline method survey is also conducted on the slope, dip angle, dip direction, spacing, and trace length of discontinuity are collected along the slope and are plotted in the stereonet. Figure 4.5 and 4.6 shows the slope geometry and the cross section profile along A-A' on the slope. Validation of TLS measurements and manual measurements are done such as shown in (Figure 4.9). Based on the validation from 4 control surfaces selected, Lidar measurements deviates maximum of 2^{o} degree from the control manual measurements data (Figure 4.10). Mean square error of dip angle is 2.5 and for dip direction is 1.25. Discontinuity reading from Lidar measurements and manual measurements are also being compared such as shown in Table 4.1 and Table 4.2.

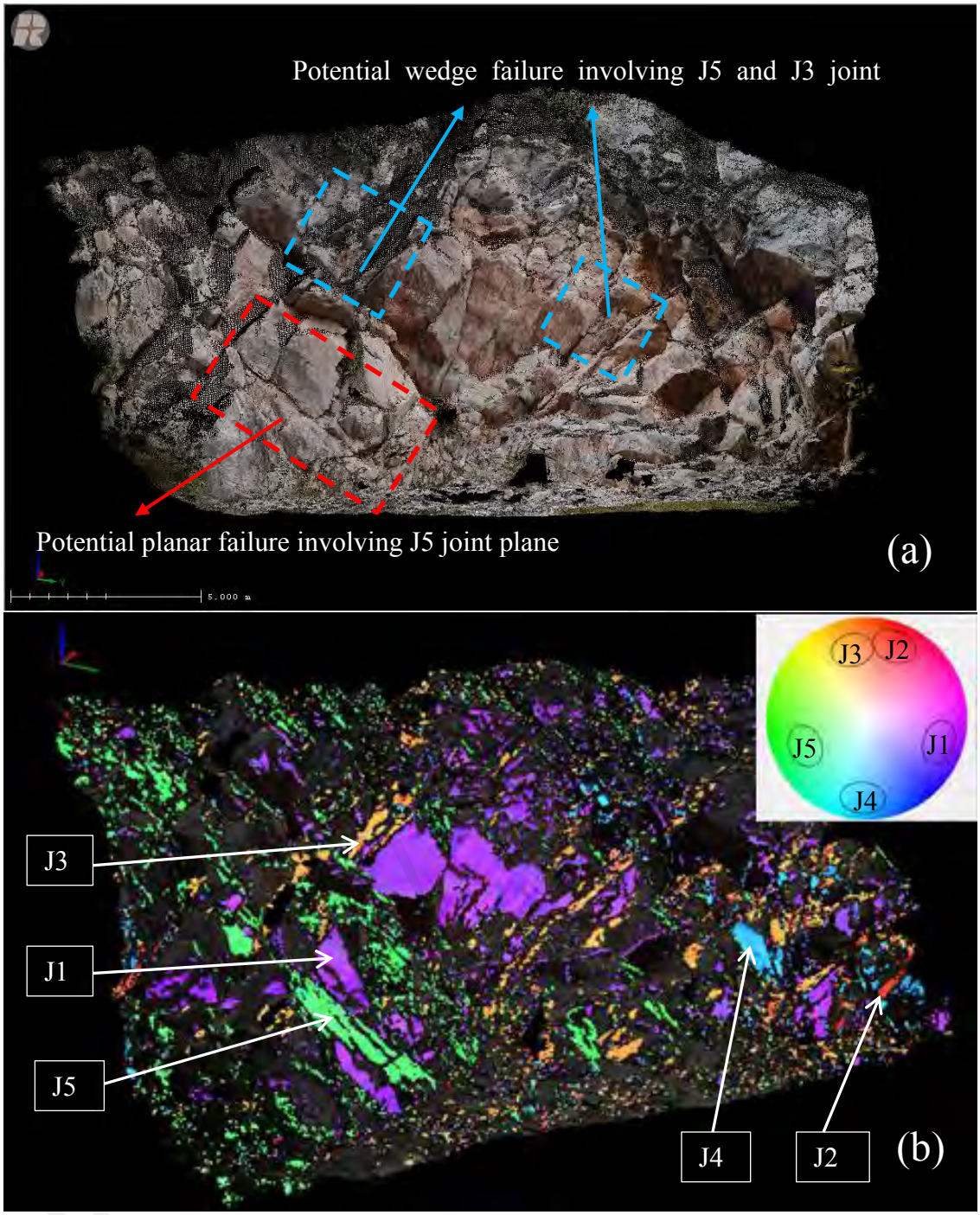

Figure 4.4: (a) True colour 3D Digital Terrain Model (DTM) of the GL1 slope, (b) Multiple joint sets presented in unique colour based on the stereographic projection, each colour represents one joint set (view from Coltop 3D). A total of 5 joint sets were identified which are J1 (67/286), J2 (68/197), J3 (59/164), J4 (69/004), and J5 (59/066). All of the data shown represents the dip angle and dip direction of the joint sets.

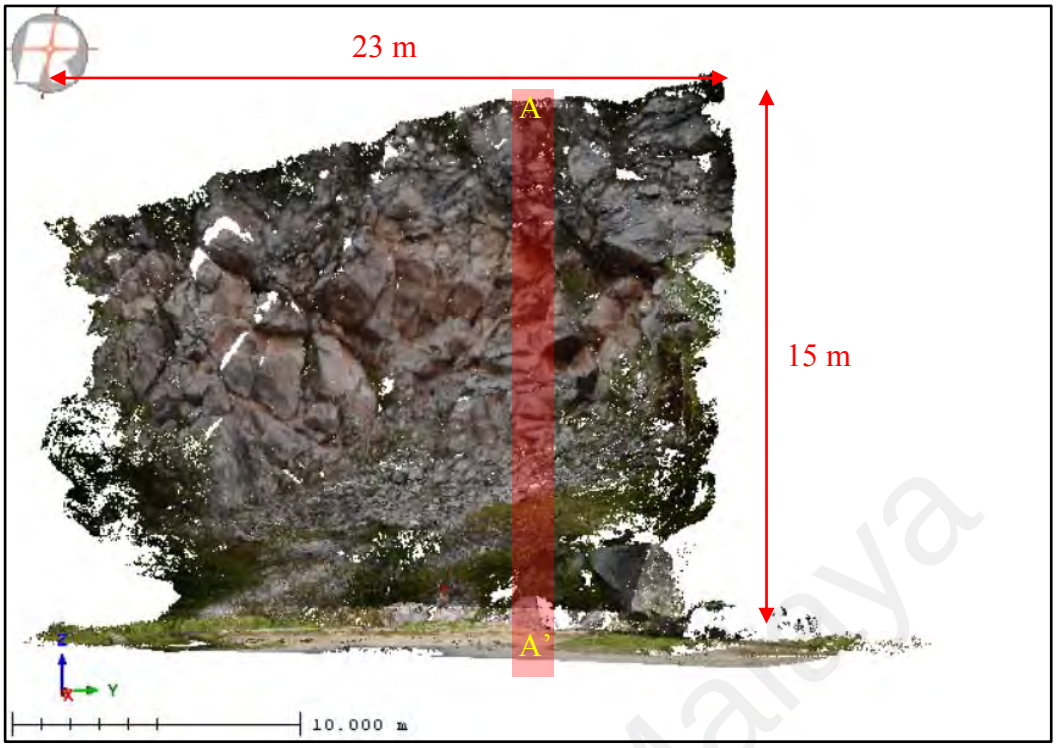

Figure 4.5: Slope geometry of GL1. Figure showing length, height and location of profile A-A' on the slope.

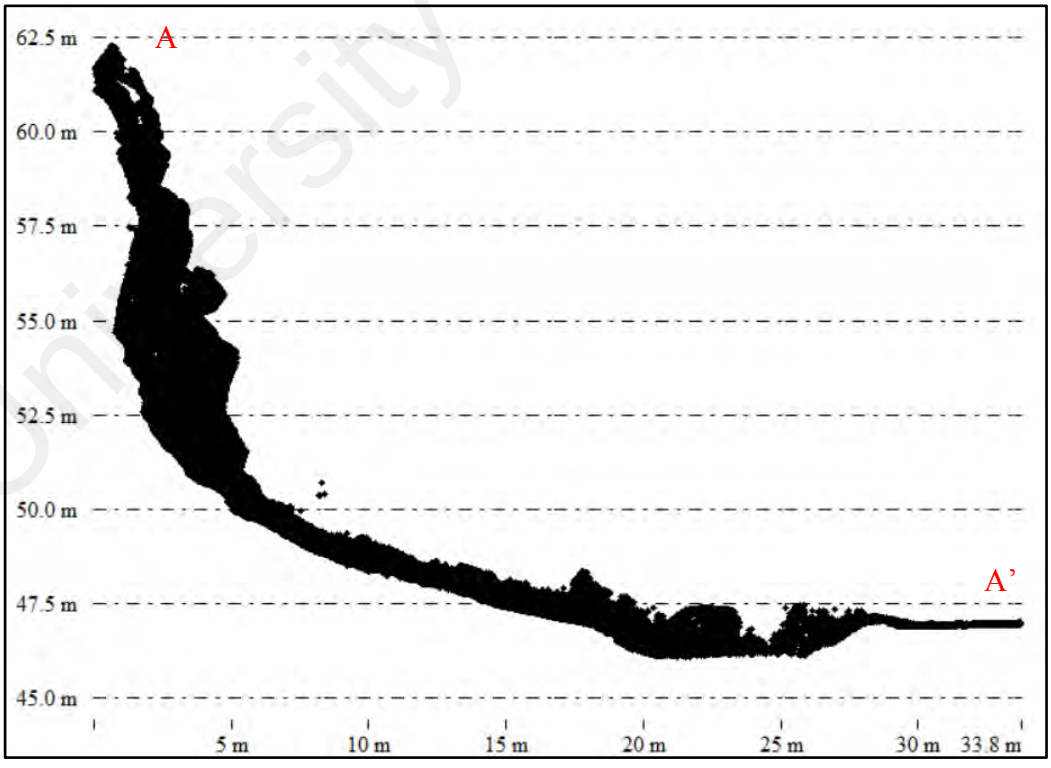

Figure 4.6: Profile A-A' of slope GL1.

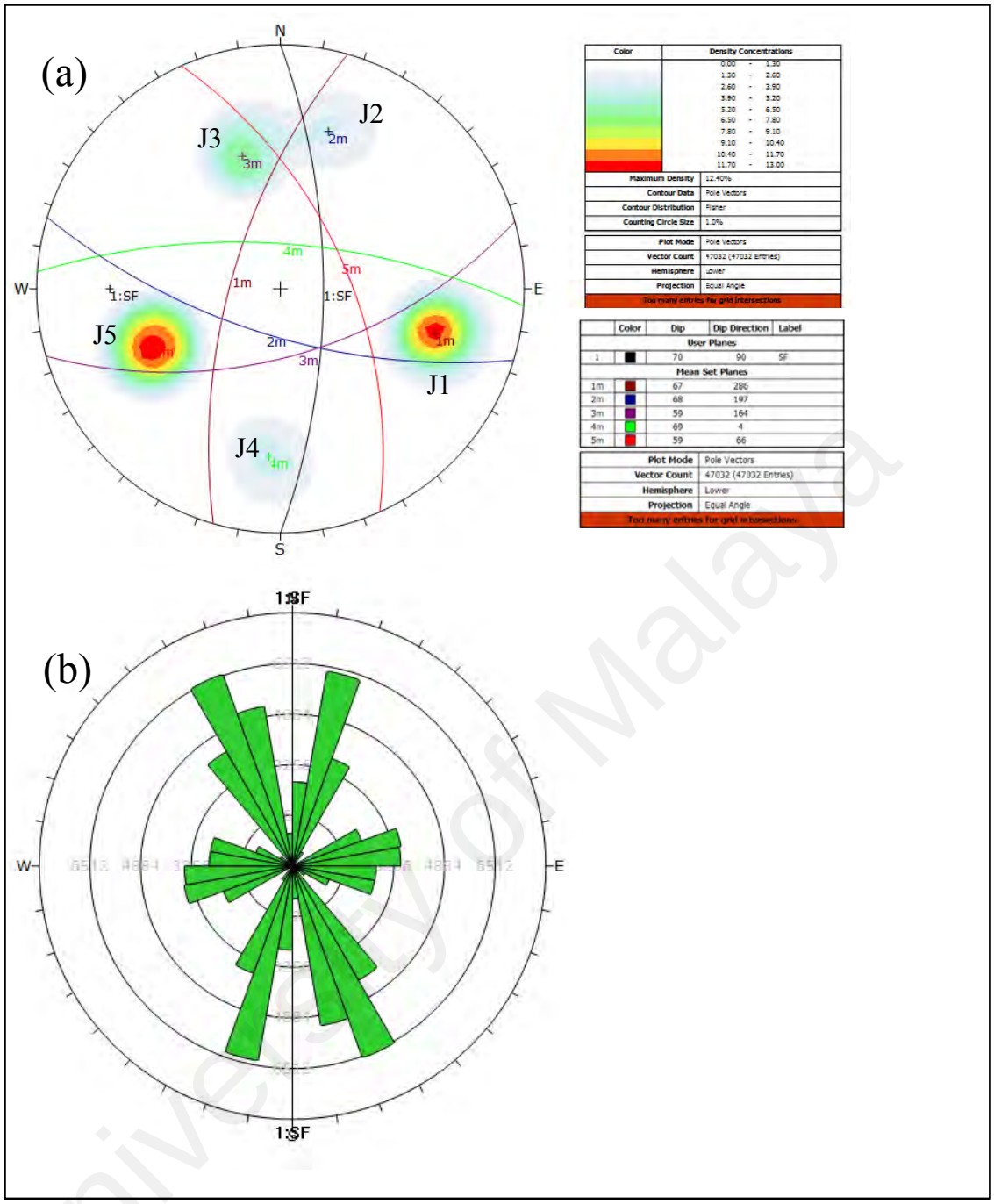

Figure 4.7: (a) Poles plot and major planes plot of all five joint sets in a stereonet (b) Rose plot showing the trend of all major joint sets and the slope face orientation in GL1 slope. Based on the rose plot, most dominant major joint sets orientation is trending northwest-southeast.

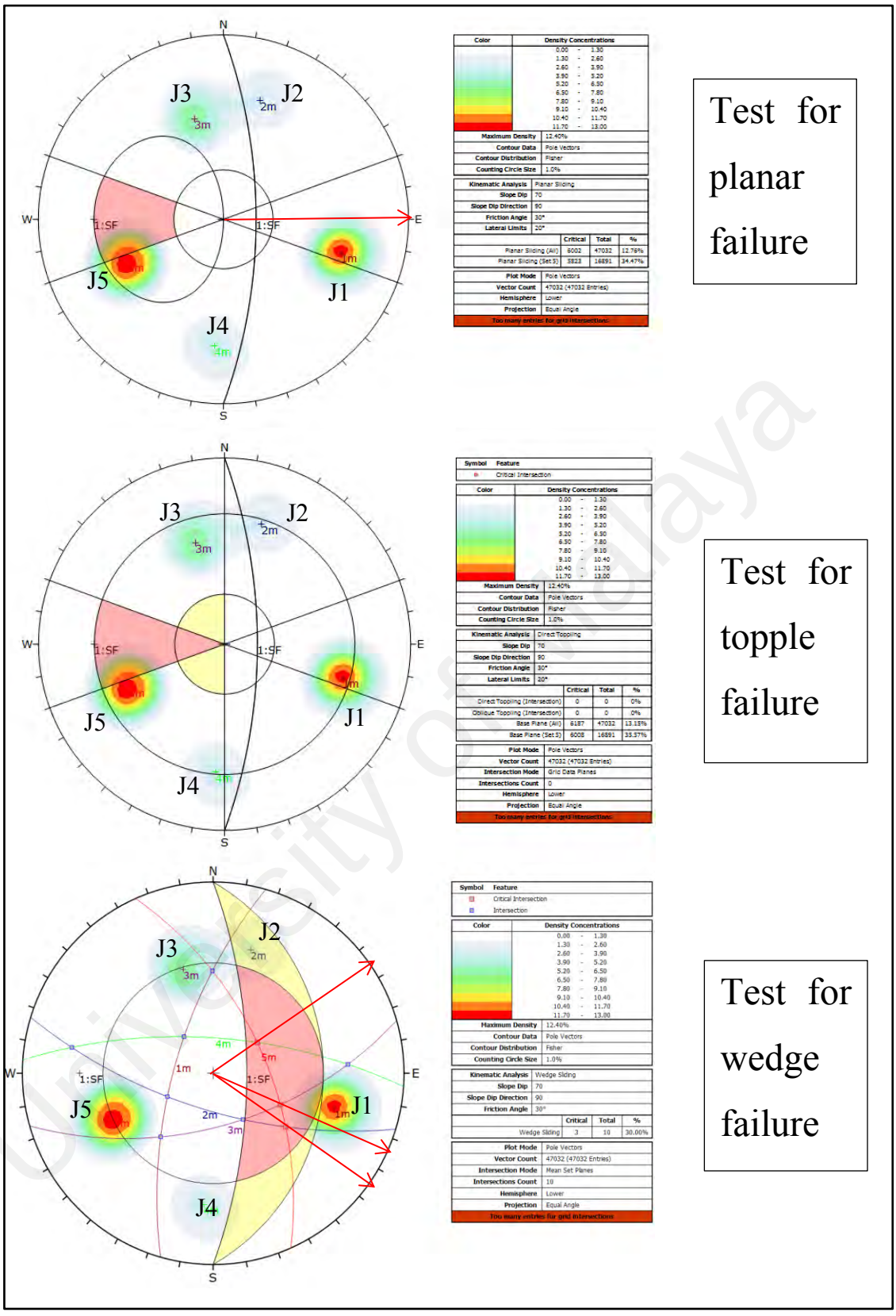

Figure 4.8: Kinematic analysis testing for planar failure, wedge failure, and topple failure in GL1 slope. Red arrows represent the direction of possible failure.

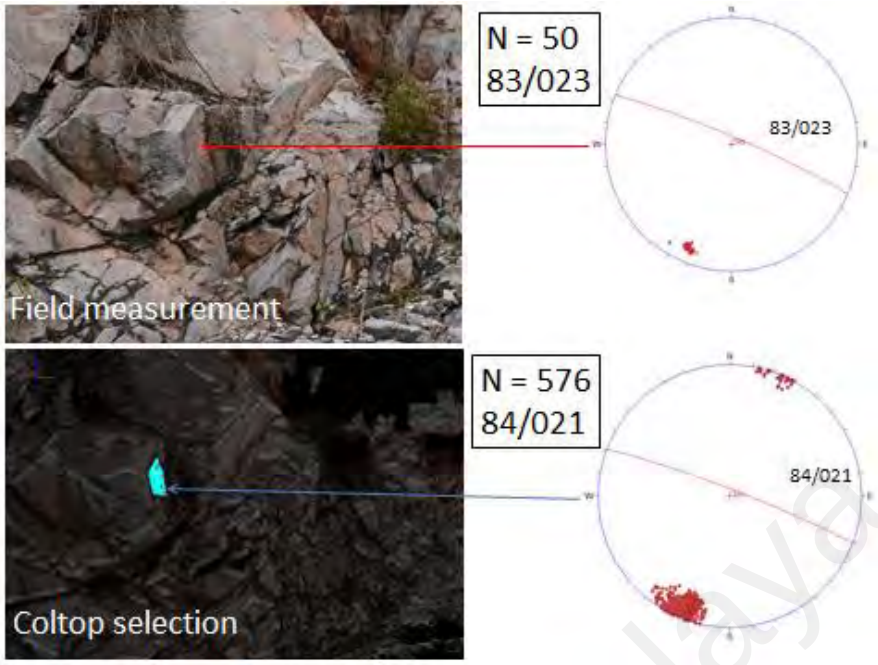

Figure 4.9: Figure shows reading collected on the same joint plane by both field measurement and lidar measurement.

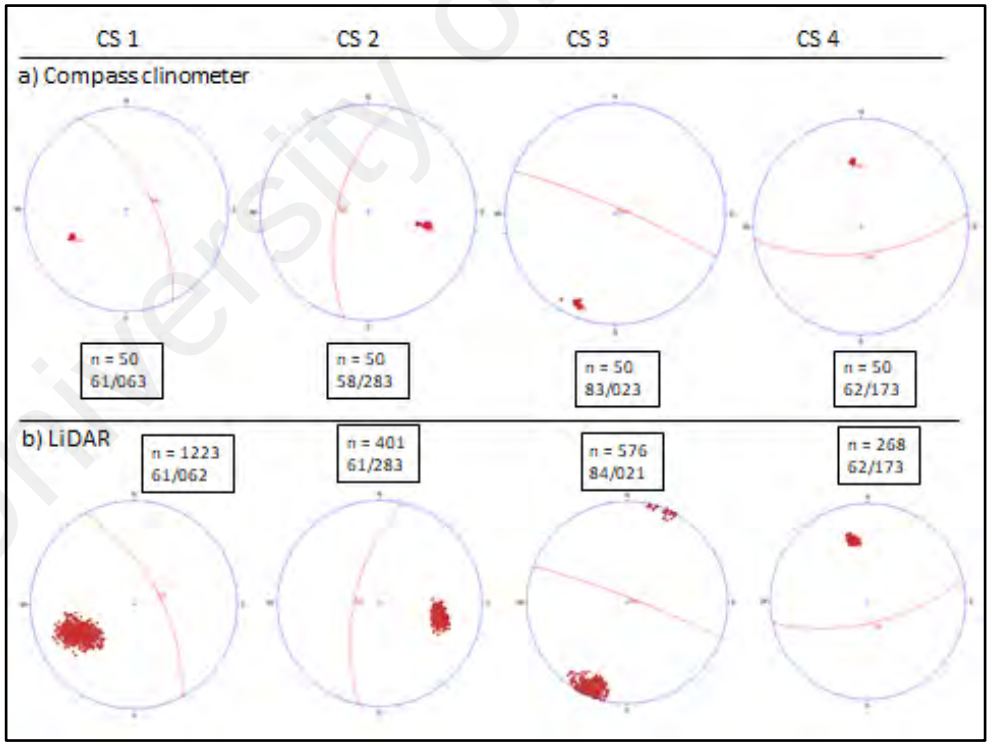

Figure 4.10: Lidar measurement validation with manual measurement at GL1 slope. Four control surfaces CS1, CS2, CS3, and CS4 which represent the joint planes were selected on the slope for validation purposes.

Figure 4.11: GL1 slope.

Table 4.1: Manual measurements at GL1.

Set	Dip Direction	Dip Angle	Joints Spacing (mm)	Trace length (m)	Seepage
J1	280	65	200-600	3-10	Dry
J2	201	70	60-200	3-10	Dry
J3	166	60	200-600	3-10	Dry
J4	005	70	200-600	3-10	Dry
J5	065	61	200-600	3-10	Dry

Table 4.2: Lidar measurements at GL1.

Set	Dip Direction	Dip Angle	Joints Spacing (mm)	Trace length (m)	Seepage
J1	286	67	200-600	3-10	Dry
J2	197	68	60-200	3-10	Dry
J3	164	59	200-600	3-10	Dry
J4	004	69	200-600	3-10	Dry
J5	066	59	200-600	3-10	Dry

4.2.2 GL 2 Slope Stability Analysis

Based on the analysis and the discontinuity selection from Coltop 3D software, GL2 slope have five joint sets which are J1 (54/291), J2 (74/164), J3 (79/196), J4 (73/085), and J5 (73/272) respectively as shown in Figure 4.12b. Major joint sets plane is plotted on the stereonet and the trend of discontinuity orientation is presented on the rose plot (Figure 4.15). According to the rose plot, most of the joint sets orientations in GL2 slope are trending northeast-southwest direction. Stability analysis test for planar, wedge, and topple failure are conducted and all of the possible failure are shown in (Figure 4.16). For planar failure, some of the J2 (74/164) poles satisfy the criteria for planar failure. The direction of planar failure that might occur is towards southeast direction (145^{o}). For topple failure, based on the kinematic analysis threshold provided by the Dips software, there is no potential topple failure will occur. However, some of the J2 (74/164) poles will act as a base plane if topple failure take place. For wedge failure, three possible wedge failures have been identified which involving the intersection between joint sets J4 and J3, J4 and J2, and J2 and J3 respectively. The directions of possible wedge failure are towards southeast direction (120^{o}, 130^{o}, 145^{o}). Slope geometry and a cross section profile along A-A' are shown in Figure 4.13 and Figure 4.14. Validation of manual and Lidar measurements are done such as shown in Figure 4.17. Based on the validation in Table 4.3, the mean square error for dip angle is 16.5, while for the dip direction is 10.8. Discontinuity reading from both survey methods are presented in Table 4.4 and Table 4.5.

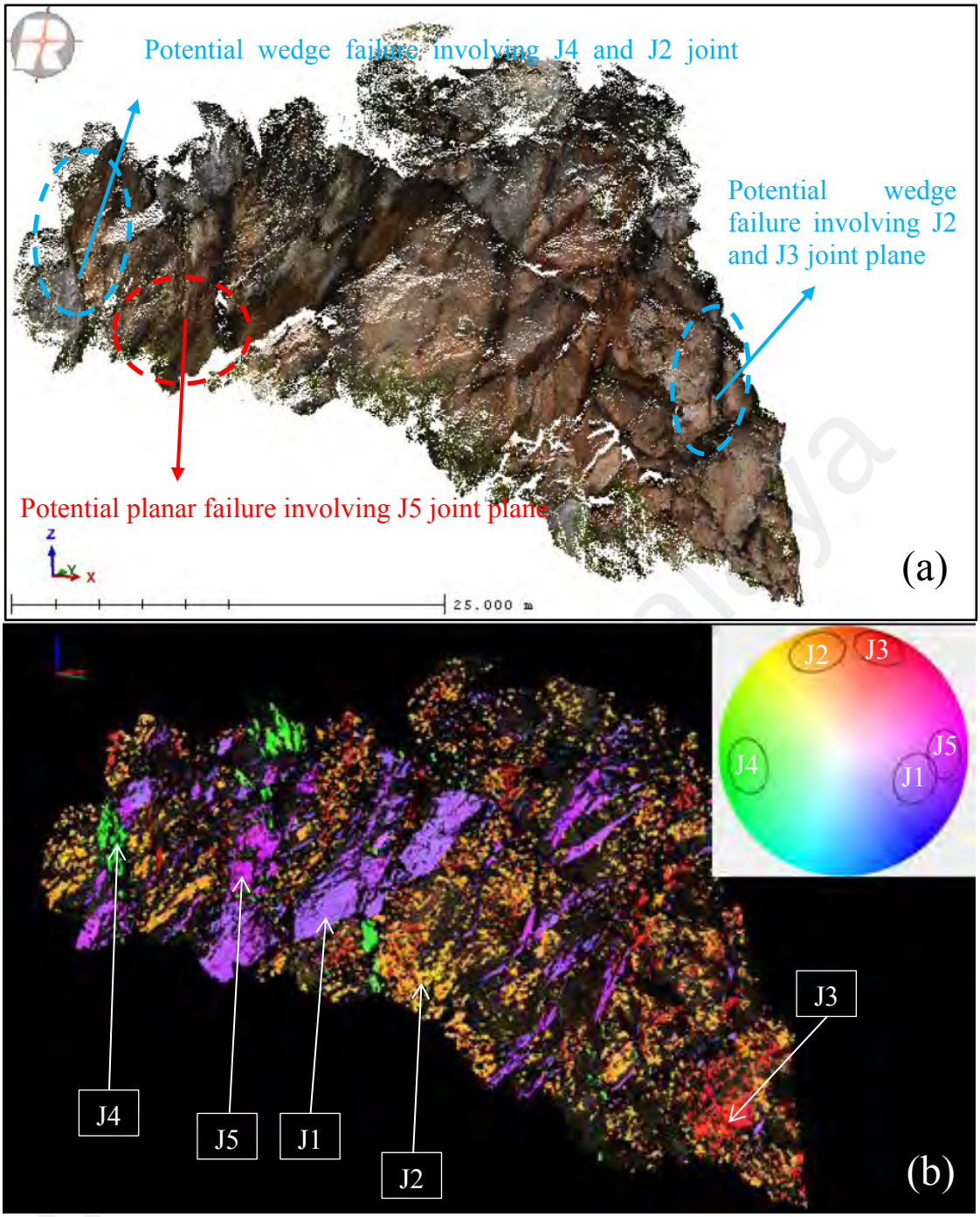

Figure 4.12: (a) True colour Digital Terrain Model (DTM) of GL2 slope (b) Multiple joint sets visualized in unique colour based on stereographic projections (view from Coltop 3D). Five joint sets were identified which are J1 (54/291), J2 (74/164), J3 (79/196), J4 (73/085), and J5 (73/272). Data collected are all in dip angle and dip directions.

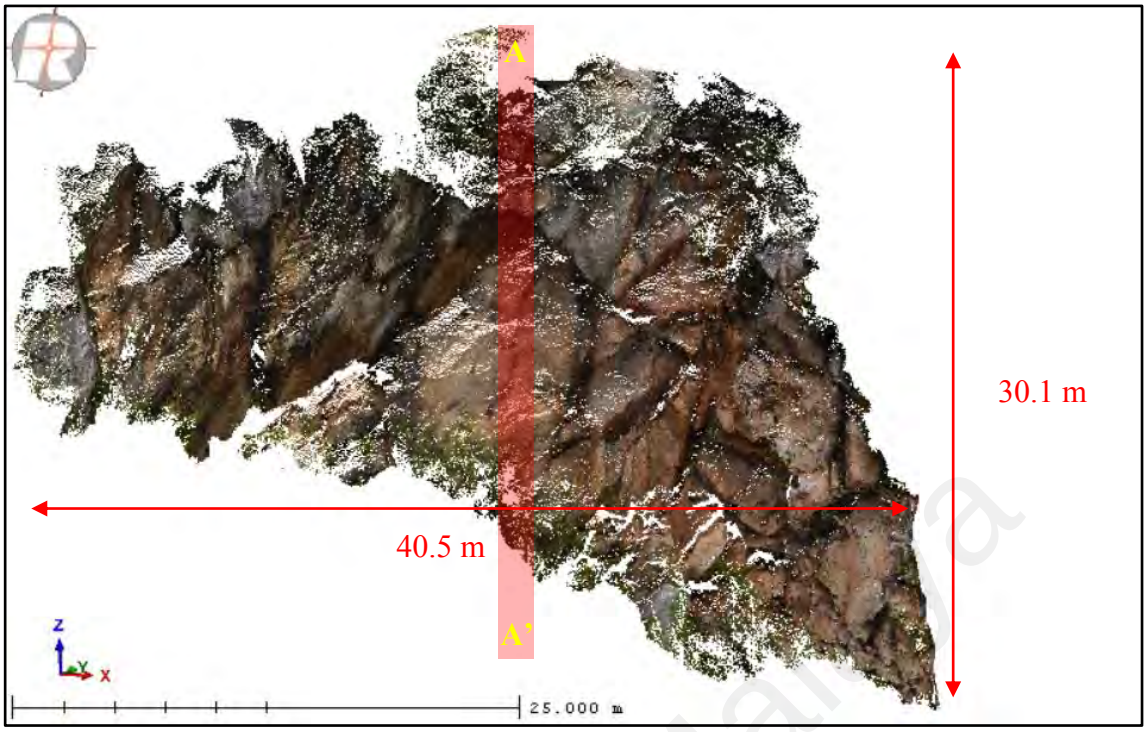

Figure 4.13: Slope geometry of GL2. Figure showing height, length and location of profile A-A' on the slope.

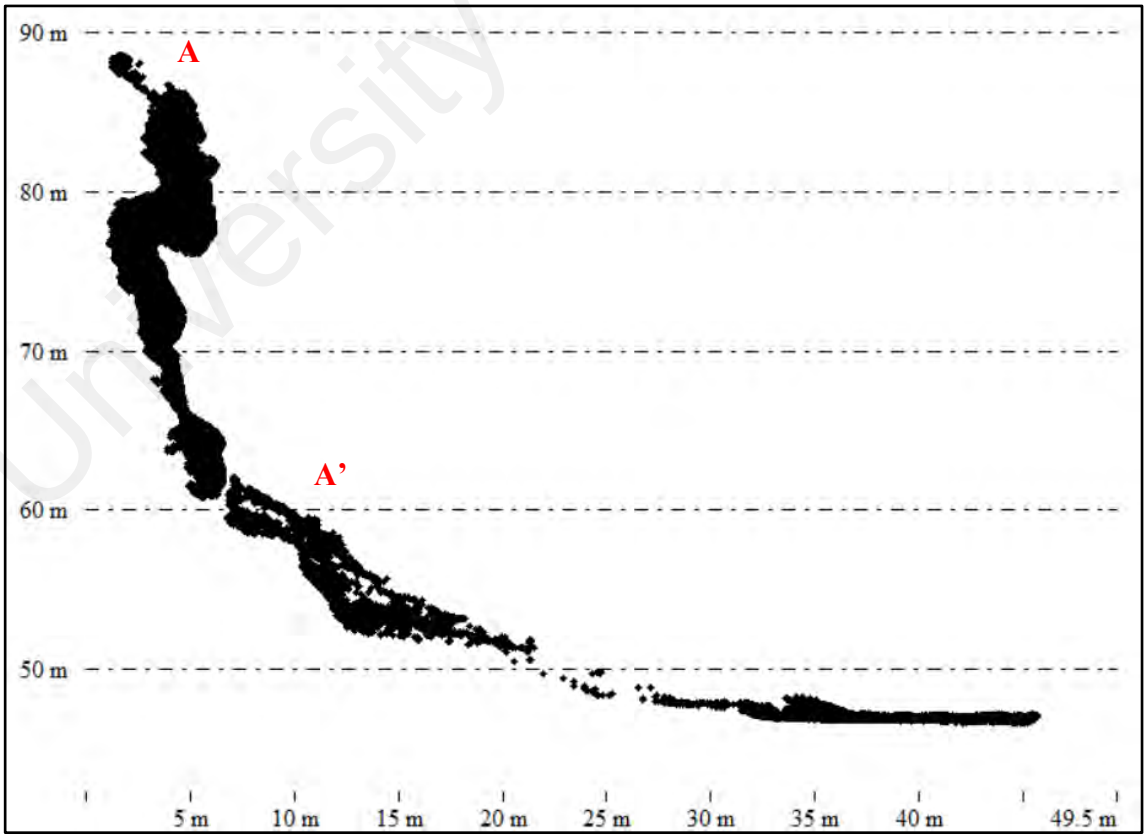

Figure 4.14: Profile A-A' of slope GL2.

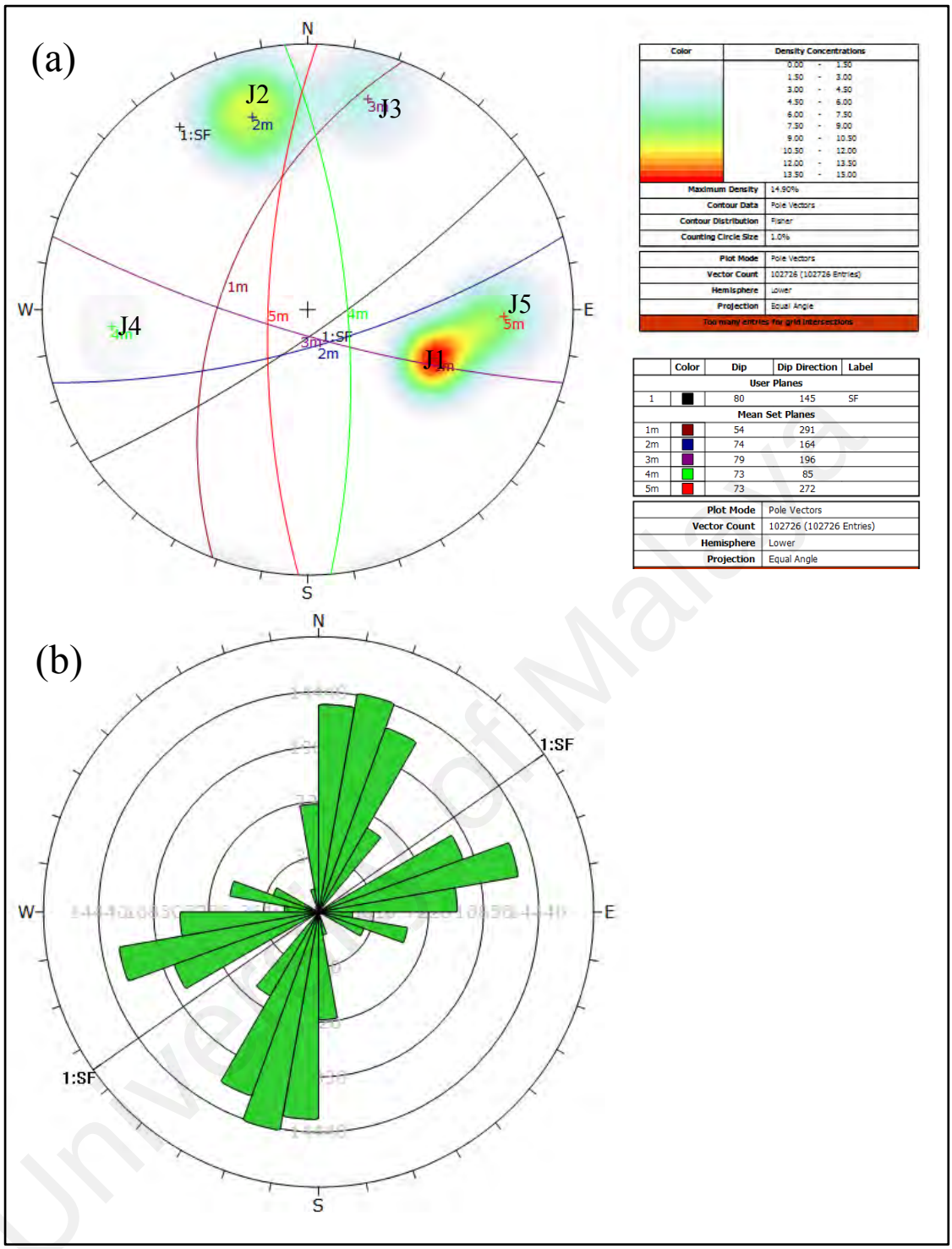

Figure 4.15: (a) Poles plot and major planes plot of all five joint sets in a stereonet (b) Rose plot showing the trend of all major joint sets and the slope face orientation in GL2 slope. Based on the rose plot, most dominant major joint sets orientation is trending NE-SW.

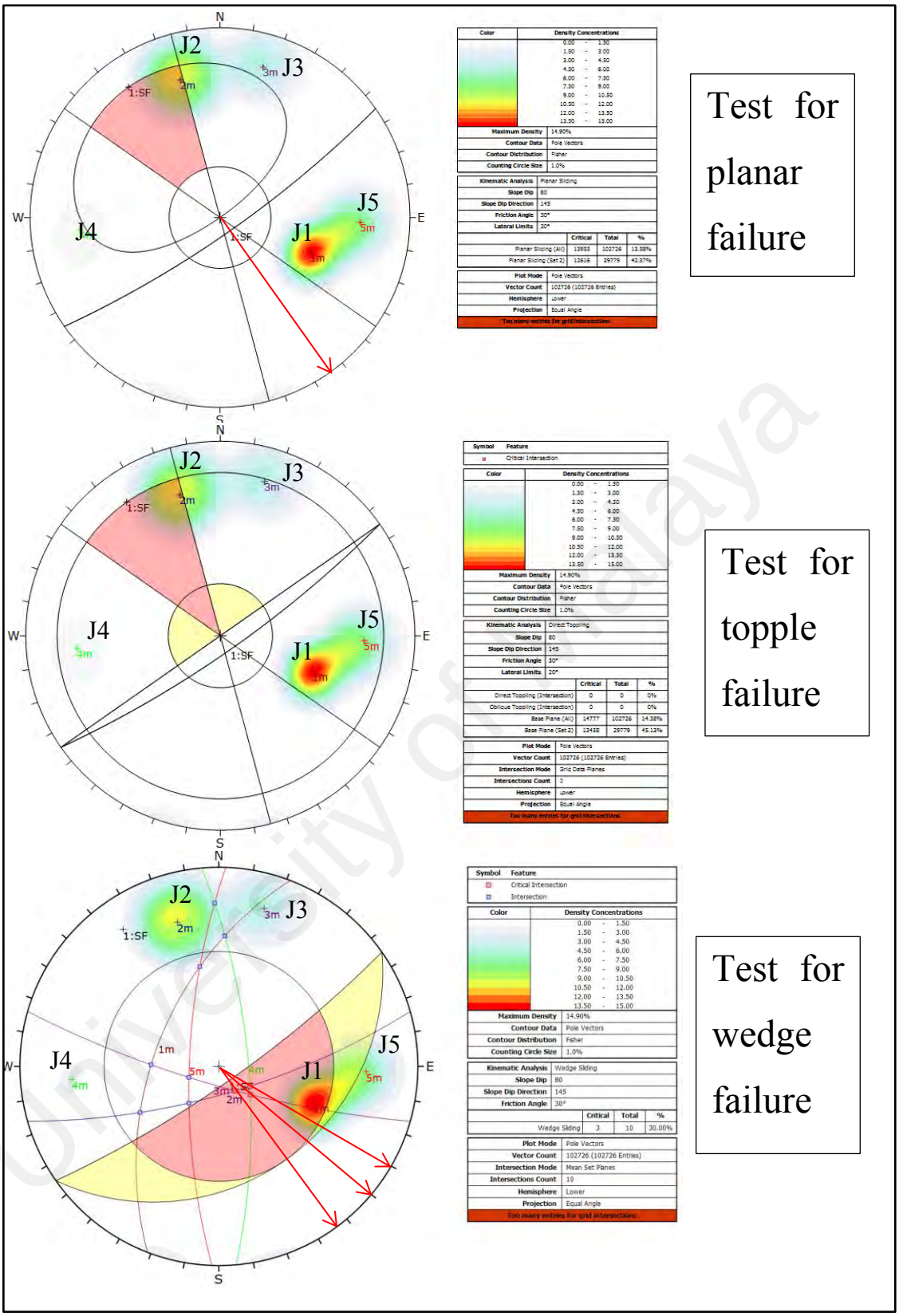

Figure 4.16: Kinematic analysis testing for planar failure, wedge failure, and topple failure in GL2 slope. Red arrows represent the direction of possible failure.

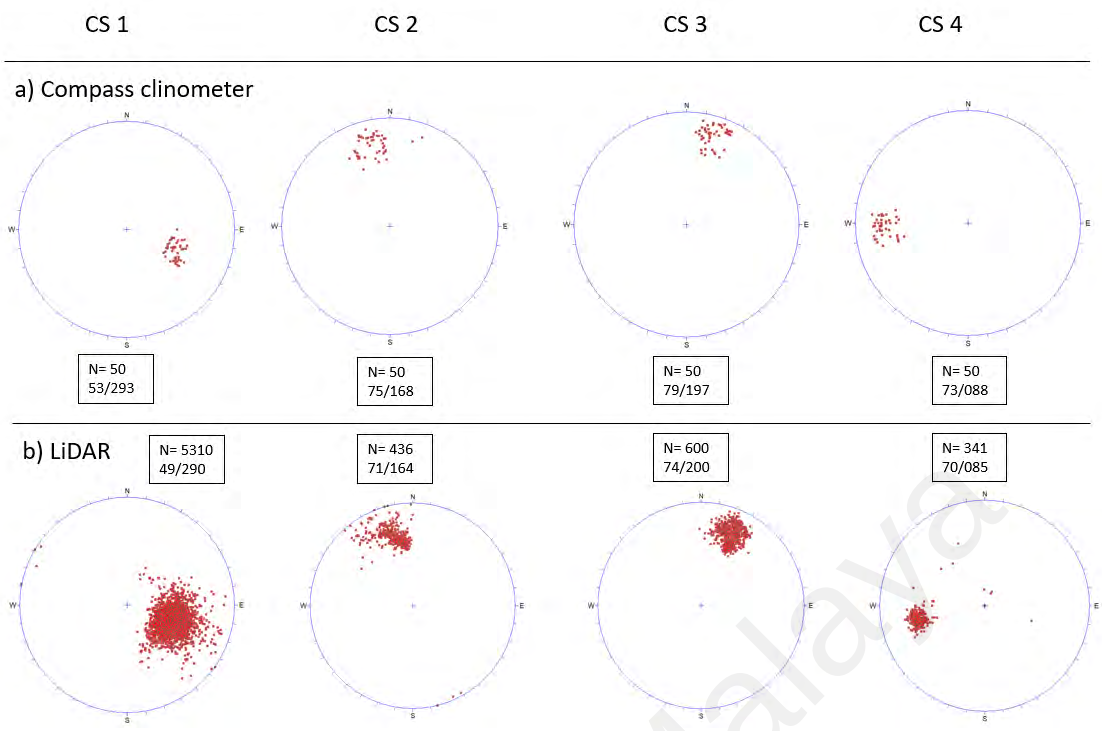

Figure 4.17: Lidar measurement validation with manual measurement at GL2 slope. Four control surfaces CS1, CS2, CS3, and CS4 which represent the joint planes were selected on the slope for validation purposes.

Table 4.3: Validation at GL 2.

Control surfaces	Compass clinometer		Lidar measurements		Mean square error	
	Dip angle	Direction	Dip angle	Direction	Dip angle	Direction
CS 1	53	293	49	290	16.5	10.8
CS 2	75	168	71	164		
CS 3	79	197	74	200		
CS 4	73	088	70	085		

Figure 4.18: GL 2 slope.

Table 4.4: Manual measurements at GL2.

Set	Dip Direction	Dip Angle	Joints Spacing (mm)	Trace length (m)	Seepage
J1	290	55	200-600	10-20	Dry
J2	166	70	200-600	3-10	Dry
J3	200	75	200-600	10-20	Dry
J4	82	75	200-600	3-10	Dry
J5	270	73	200-600	10-15	Dry

Table 4.5: Lidar measurements at GL2.

Set	Dip Direction	Dip Angle	Joints Spacing (mm)	Trace length (m)	Seepage
J1	291	54	200-600	10-20	Dry
J2	164	74	200-600	3-10	Dry
J3	196	79	200-600	10-20	Dry
J4	085	73	200-600	3-10	Dry
J5	272	73	200-600	10-20	Dry

4.2.3 GL 3 Slope Stability Analysis

Based on the analysis and discontinuity selection from the Coltop 3D software, four joint sets have been identified in slope GL 3 which are J1 (69/299), J2 (66/058), J3 (50/245), and J4 (80/137) as shown in Figure 4.19b. Major joint sets plane is plotted on the stereonet and the discontinuity orientation trend is shown in the rose plot (Figure 4.22). Based on the plot, major joint sets orientation is trending northeast-southwest with slope face orientation of (80/270). Stability analysis test for planar, wedge, and topple failure are conducted and all of the possible failure are shown in Figure 4.23. For planar failure, some of the J1 (69/299) poles satisfy the criteria for planar failure. The direction of possible planar failure is towards west direction (270^{o}). For topple failure, no poles satisfy the criteria for topple failure from the Dips software. However, J1 (69/299) poles will act as the base plane if topple failure take place. For wedge failure, three possible wedge failures have been identified which involving the intersection between joint sets of J4 and J3, J4 and J1, and J3 and J1 respectively. The direction of wedge failure is towards southwest direction (215^{o}, 220^{o}, and 235^{o}). Slope geometry and cross section profile along A-A' are shown such as in Figure 4.20 and Figure 4.21. Validation of Lidar and manual measurements are conducted such as shown in Figure 4.24. Based on the validation in Table 4.6, the mean square error (MSE) of dip angle from the validation is 9.5, while the mean square error for dip direction is 13. Discontinuity reading from lidar and manual measurements are being used for comparison such as shown in Table 4.7 and Table 4.8.

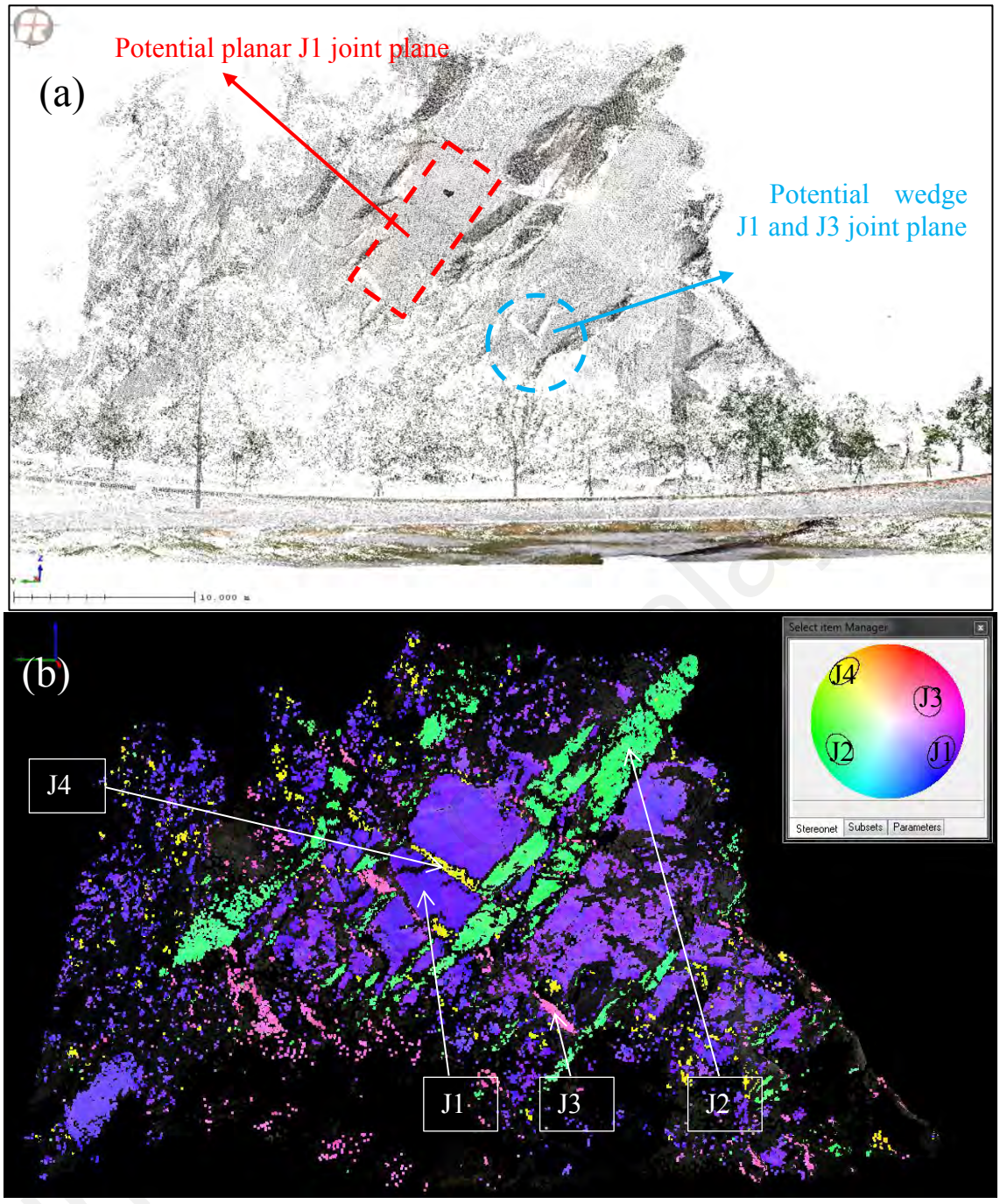

Figure 4.19: (a) Figure shows the true colour Digital Terrain Model (DTM) of the GL3 slope (b) 3D discontinuity plane model with unique colour derived from Coltop 3D. Four joint sets can be identified on the slope which are J1 (69/299), J2 (66/058), J3 (50/245), and J4 (80/137).

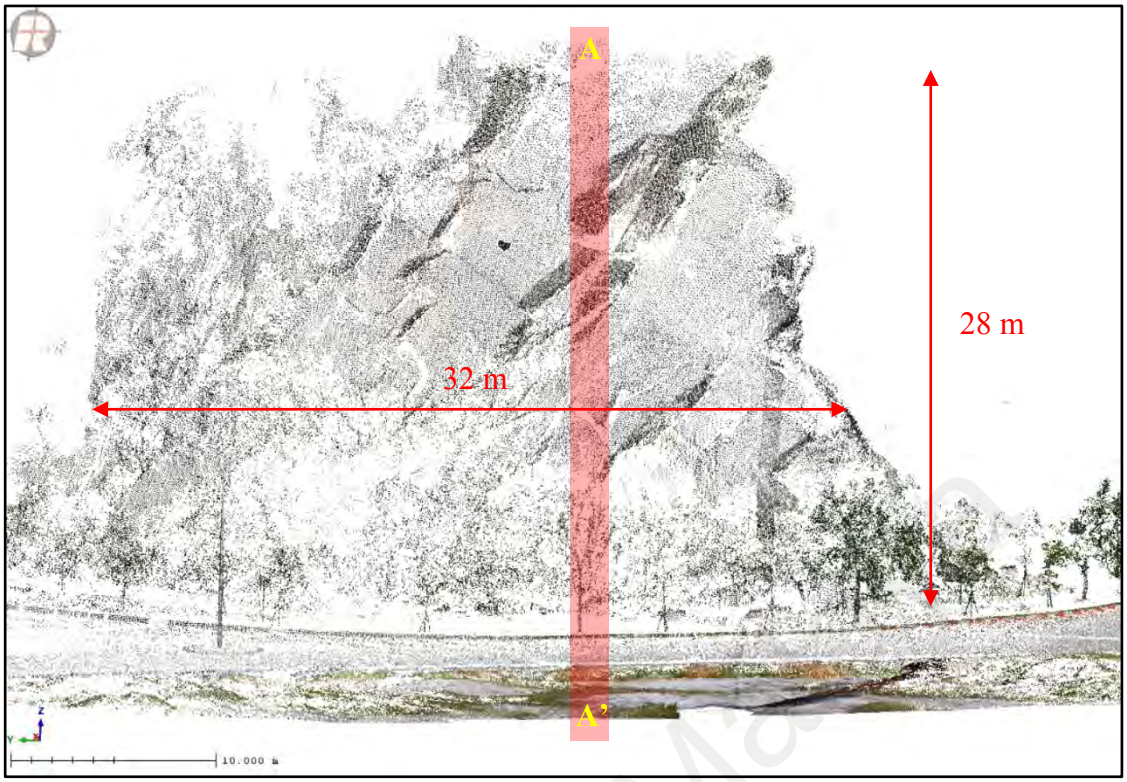

Figure 4.20: Slope geometry of slope GL3. Figure showing the height, length and location of profile A-A' on the slope.

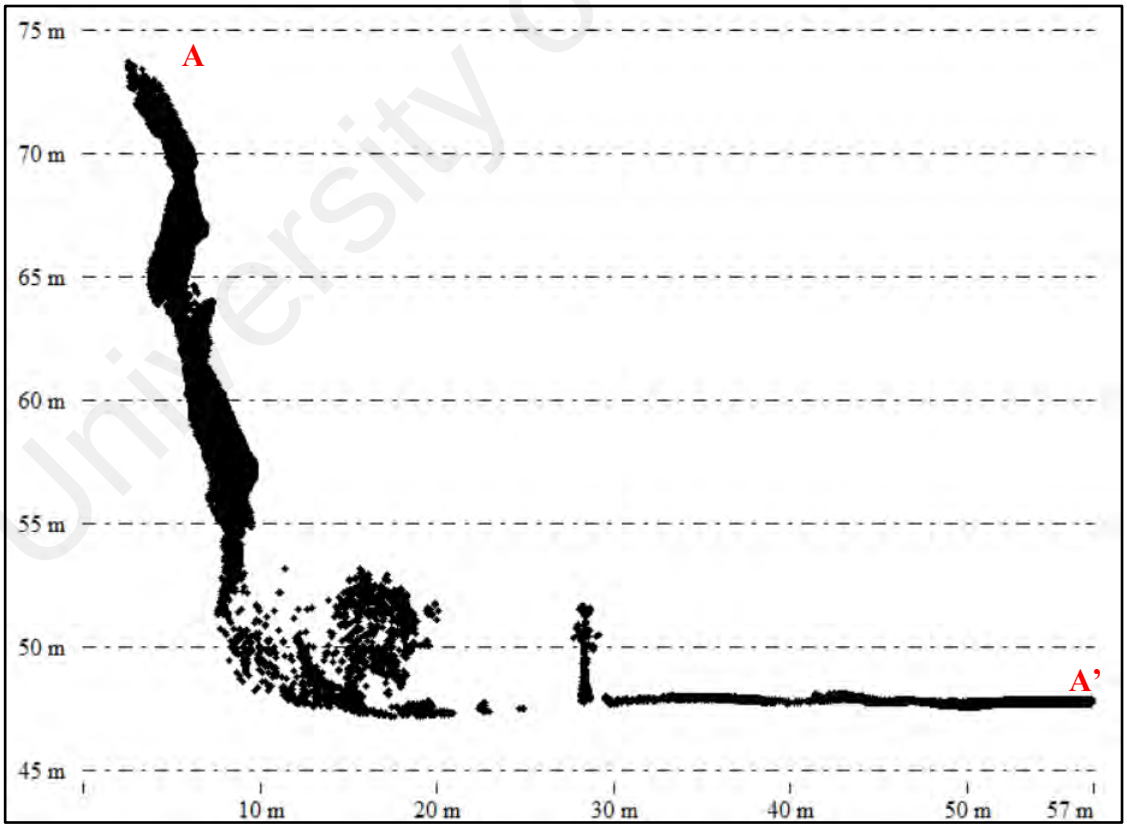

Figure 4.21: Profile A-A' of slope GL3.

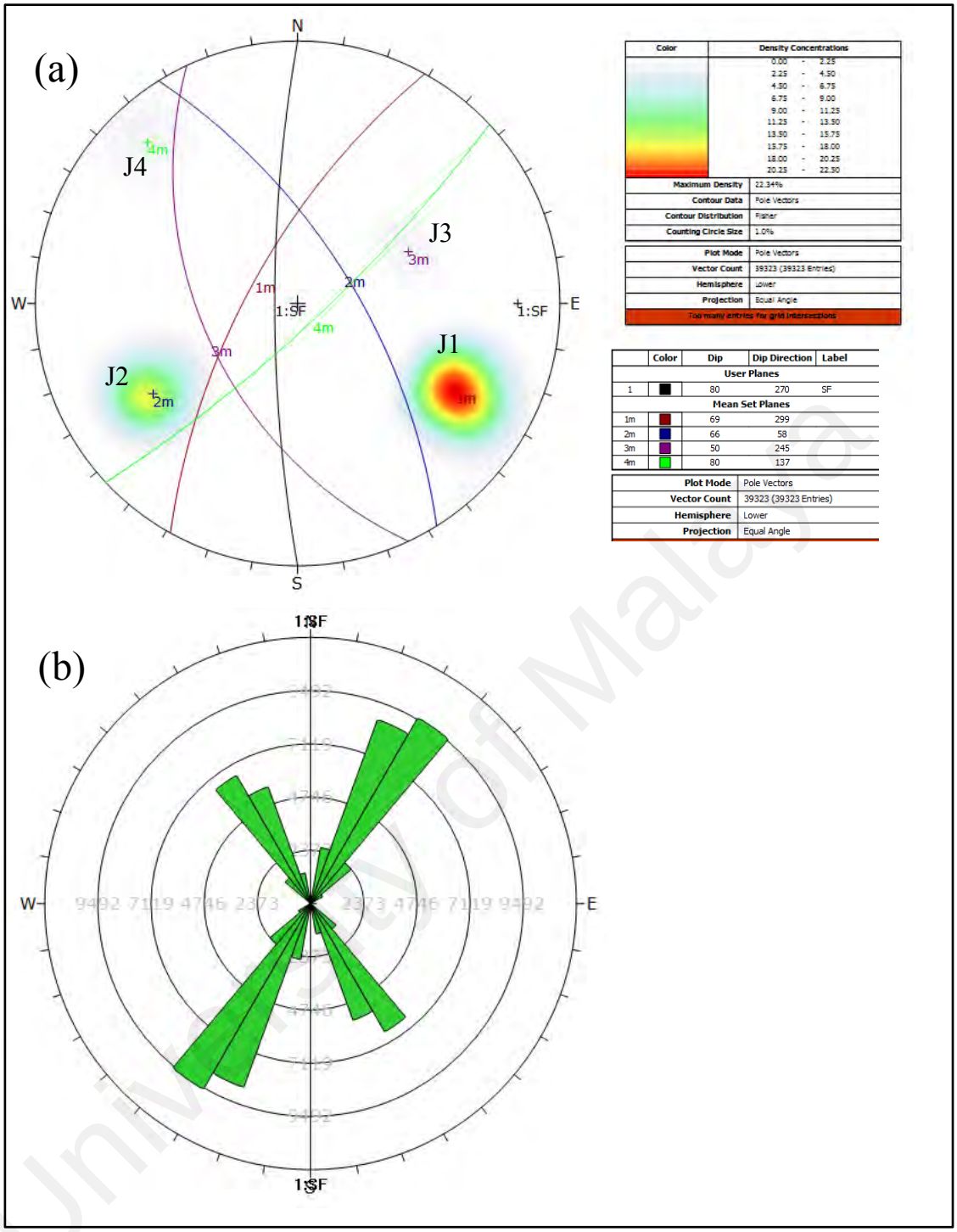

Figure 4.22: (a) Poles plot and major planes plot of all four joint sets in a stereonet (b) Rose plot showing the trend of all major joint sets and the slope face orientation in GL3 slope. Based on the rose plot, most dominant joint sets orientation is trending northeast-southwest.

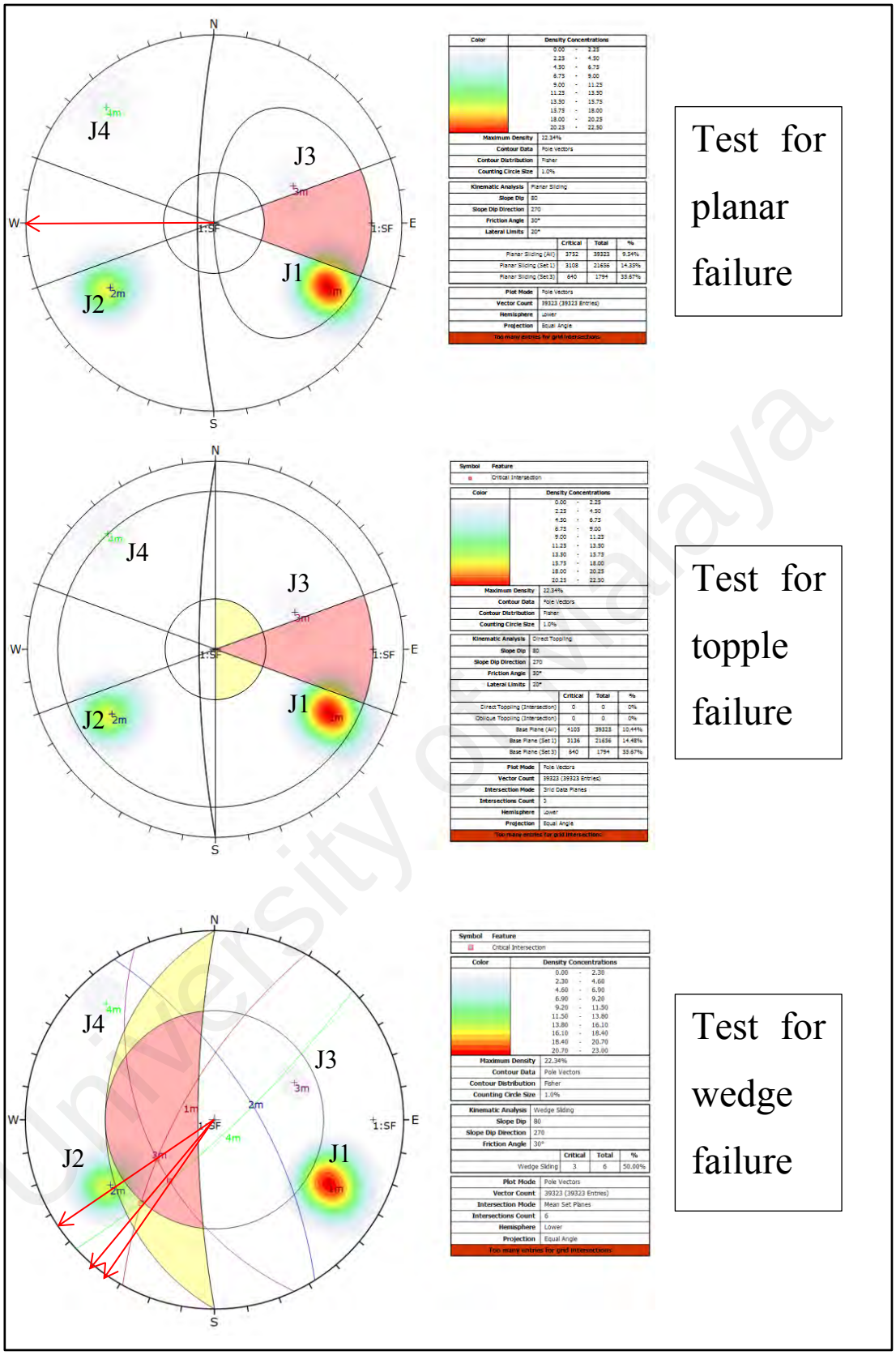

Figure 4.23: Kinematic analysis testing for planar failure, wedge failure, and topple failure in GL3 slope. Red arrows represent the direction of possible failure.

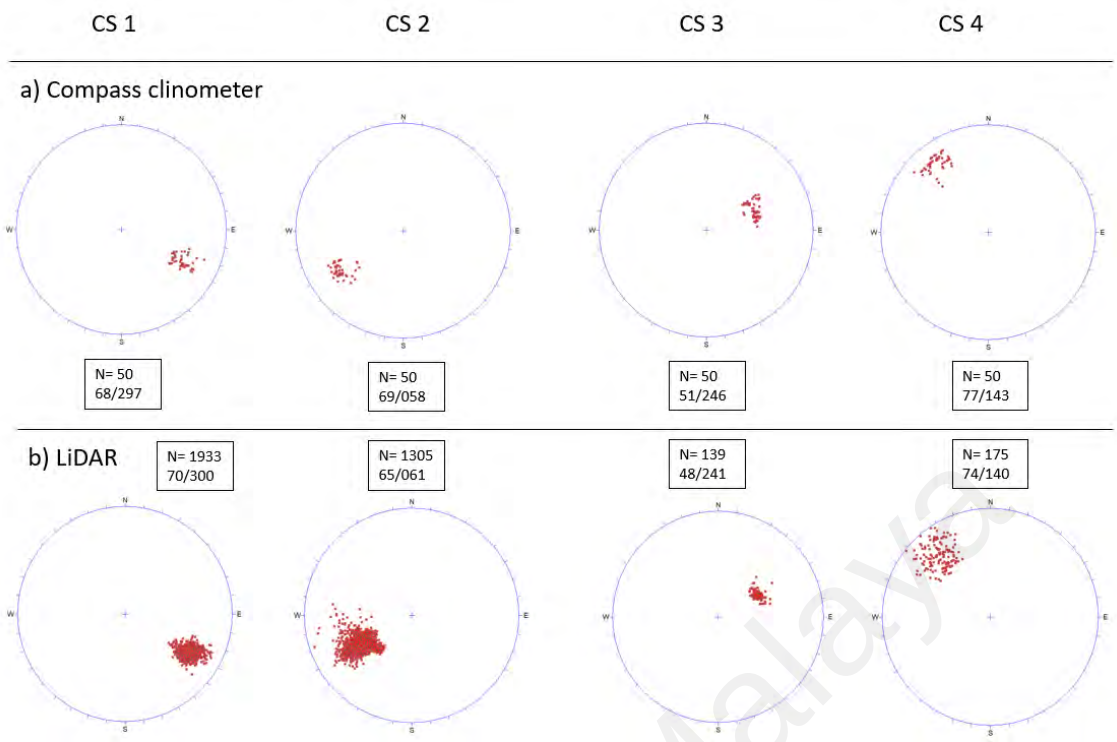

Figure 4.24: Lidar measurement validation with manual measurement at GL3 slope. Four control surfaces CS1, CS2, CS3, and CS4 which represent the joint planes were selected on the slope for validation purposes.

Table 4.6: Validation at GL 3.

Control surfaces	Compass clinometer		Lidar measurements		Mean square error	
	Dip angle	Direction	Dip angle	Direction	Dip angle	Direction
CS 1	68	297	70	300	9.5	13
CS 2	69	058	65	061		
CS 3	51	246	48	241		
CS 4	77	143	74	140		

Figure 4.25: GL3 slope.

Table 4.7: Manual measurements at GL3.

Set	Dip Direction	Dip Angle	Joints Spacing (mm)	Trace length (m)	Seepage
J1	300	71	200-600	3-10	Dry
J2	060	65	60-200	3-10	Dry
J3	243	52	60-200	3-10	Dry
J4	135	80	60-200	3-10	Dry

Table 4.8: Lidar measurements at GL3.

Set	Dip Direction	Dip Angle	Joints Spacing (mm)	Trace length (m)	Seepage
J1	299	69	200-600	3-10	Dry
J2	058	66	60-200	3-10	Dry
J3	245	50	60-200	3-10	Dry
J4	137	80	60-200	3-10	Dry

4.2.4 GL 4 Slope Stability Analysis

Based on the discontinuity selection from Coltop 3D, five family of joint sets has been identified at GL4 slope which are J1 (69/291), J2 (75/203), J3 (75/039), J4 (68/101), and J5 (74/256) respectively as shown in Figure 4.26b. Major joint sets plane is plotted in the stereonet and the orientation of discontinuity is presented in the rose plot (Figure 4.29). Based on the rose plot, major orientation of discontinuity in GL4 is trending northeast—southwest with the slope face orientation trend (80/080). Stability analysis test for planar, wedge, and topple failure are conducted and all of the possible failure are shown in Figure 4.30. For planar failure, some of J4 (68/101) satisfy the criteria for planar failure and the direction of planar failure is towards northeast direction (080^{o}). For topple failure, there is no possible topple failure detected. However, J4 (68/101) plane may act as the base plane for topple failure. For wedge failure, there is two possible wedge failure identified which involving the intersection between joint sets J4 and J3, and J4 and J2 respectively. The directions of possible wedge failure are towards northeast (085^{o}) and southeast (145^{o}) direction. Slope geometry and cross section profile from A-A' are shown such as in Figure 4.27 and Figure 4.28. Validation of Lidar and manual measurements are also done such in Figure 4.31. Based on the validation in Table 4.9, the mean square error (MSE) of the dip angle is 10.25, while for the dip direction is 11.75. Discontinuity data from both measurements are also used for comparison (Table 4.10 and Table 4.11).

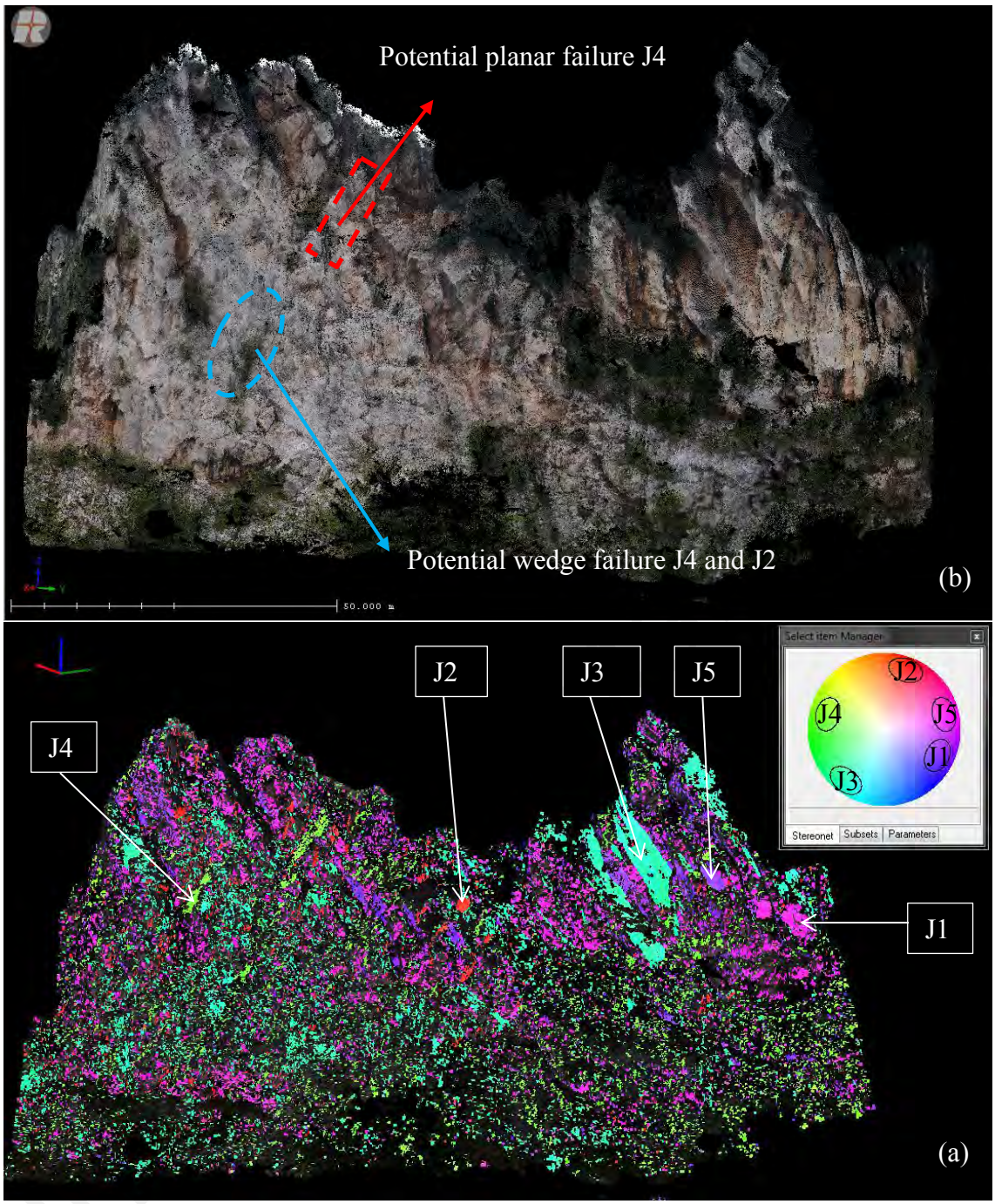

Figure 4.26: (a) True colour Digital Terrain Model (DTM) of the GL4 slope (b) 3D discontinuity model derived from Coltop 3D. The discontinuity model shows more scattered distribution of joints in this slope, this is due to previous blasting in the slope which produces more highly jointed and fractured discontinuity in the area. Discontinuity selection by Coltop 3D identify 5 family of joint sets which are J1 (69/291), J2 (75/203), J3 (75/039), J4 (68/101), and J5 (74/256) with the slope face trend (80/080).

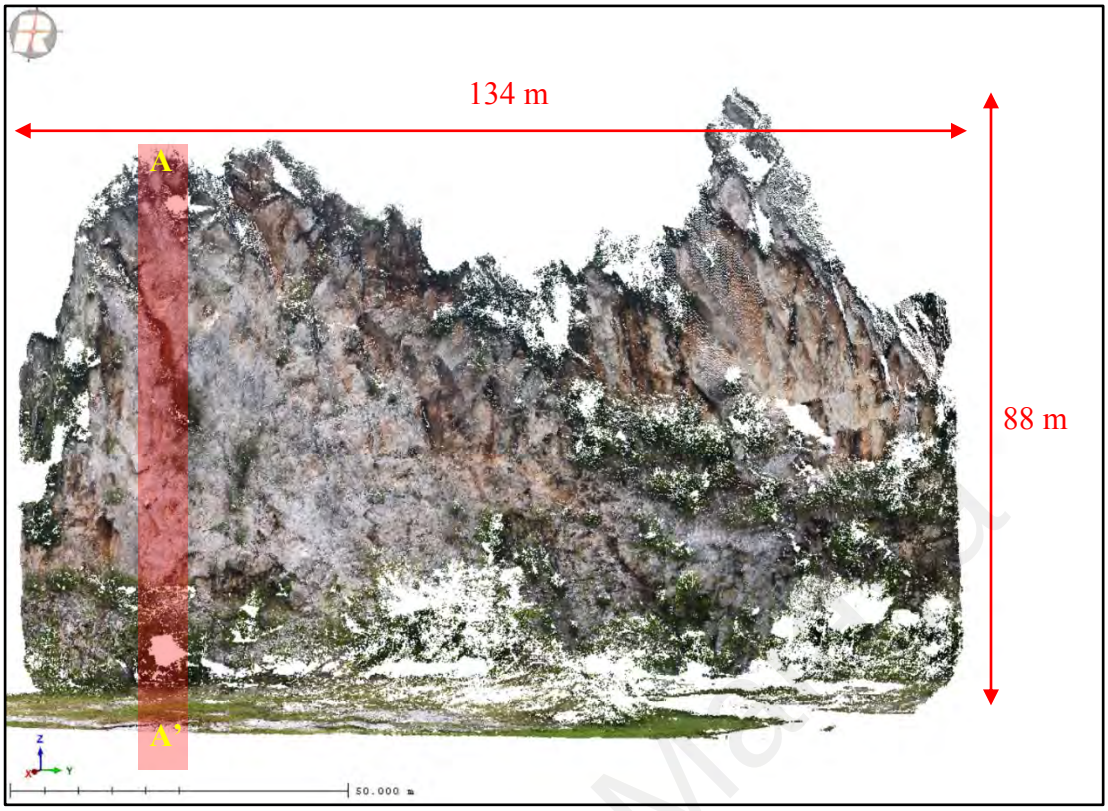

Figure 4.27: Slope geometry of GL4. Figure showing the height, length and location of profile A-A’ on the slope.

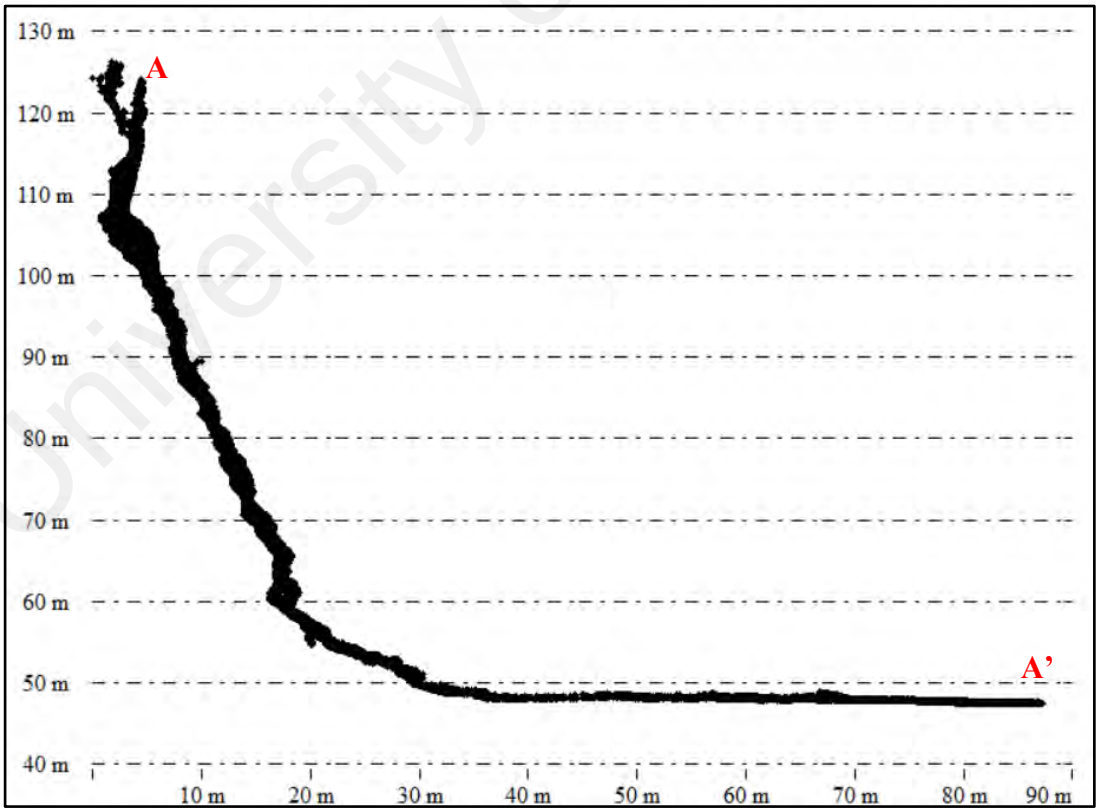

Figure 4.28: Profile A-A' of slope GL4.

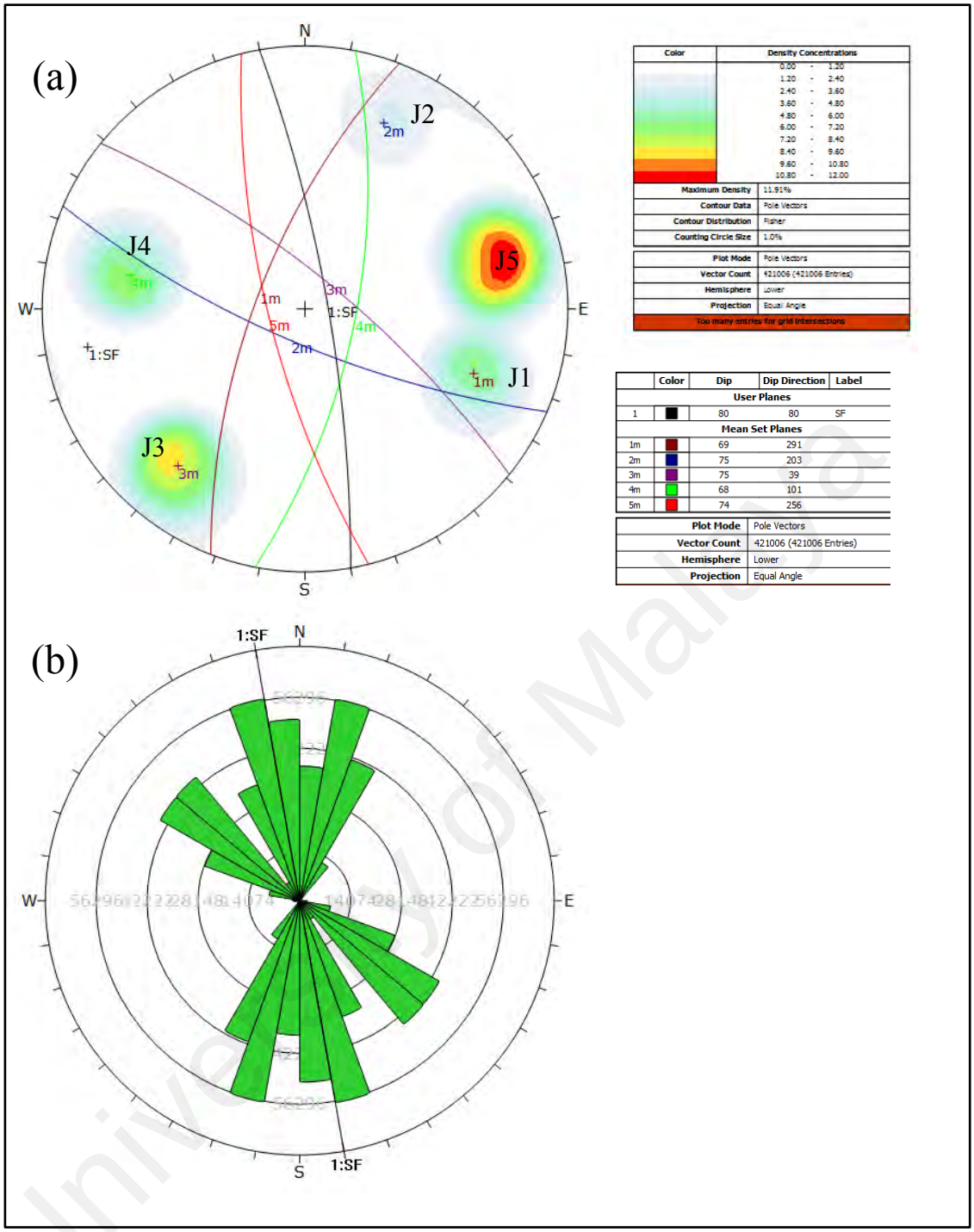

Figure 4.29: (a) Poles plot and major planes plot of all five joint sets in a stereonet (b) Rose plot showing the trend of all major joint sets and the slope face orientation in GL4 slope. Based on the rose plot, most dominant joint sets orientation is trending northwest-southeast.

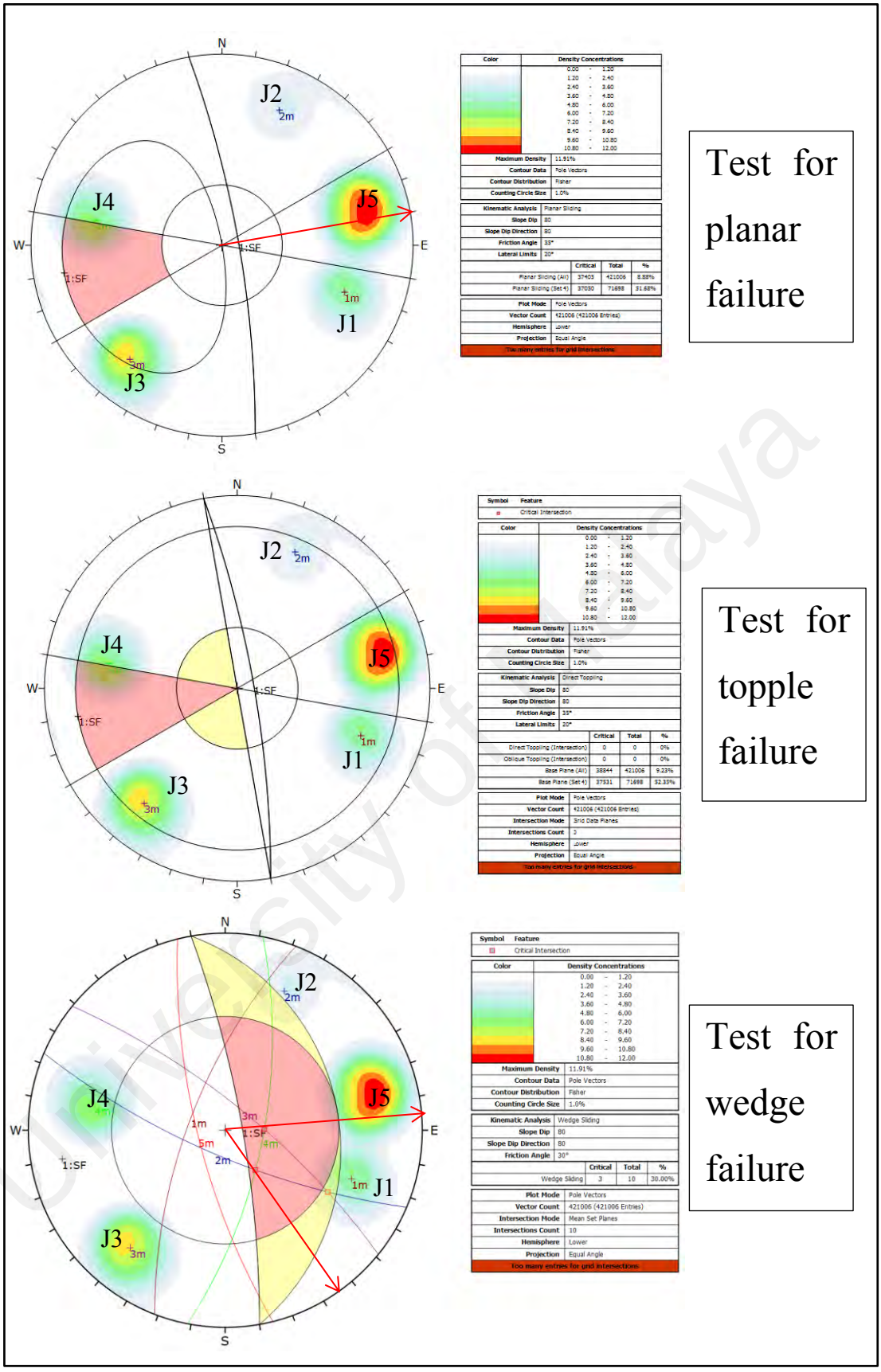

Figure 4.30: Kinematic analysis testing for planar failure, wedge failure, and topple failure in GL4 slope. Red arrows represent the direction of possible failure.

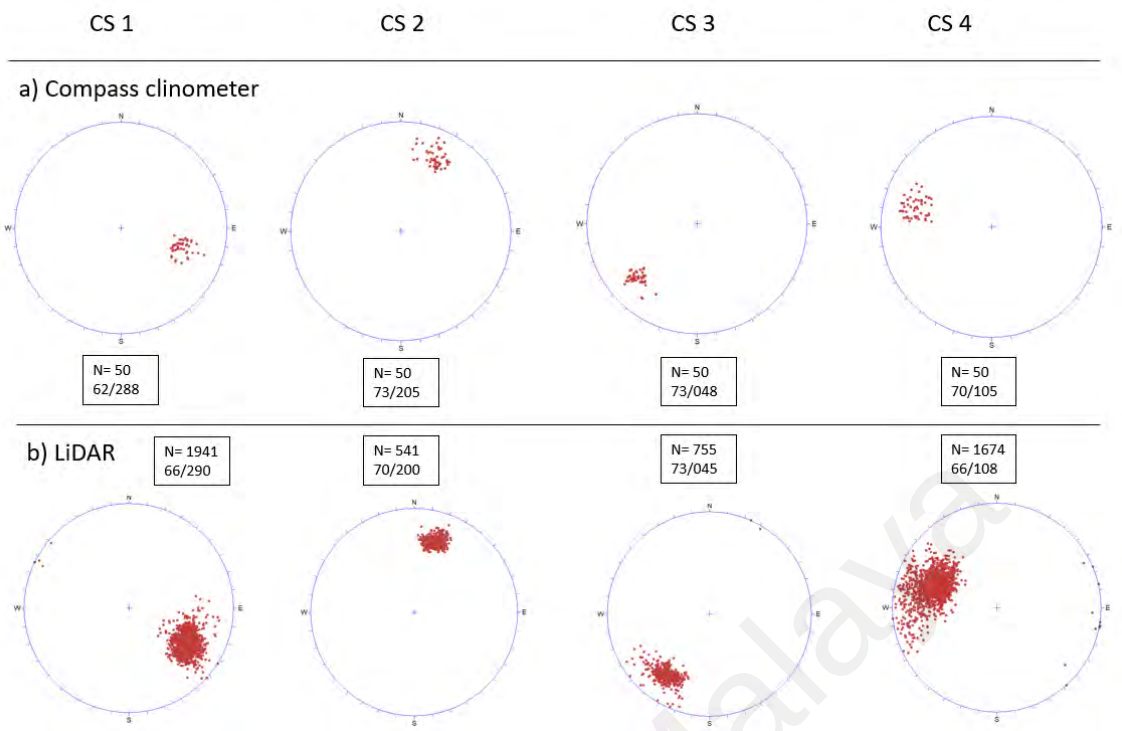

Figure 4.31: Lidar measurement validation with manual measurement at GL4 slope. Four control surfaces CS1, CS2, CS3, and CS4 which represent the joint planes were selected on the slope for validation purposes.

Table 4.9: Validation at GL 4.

Control surfaces	Compass clinometer		Lidar measurements		Mean square error	
	Dip angle	Direction	Dip angle	Direction	Dip angle	Direction
CS 1	62	288	66	290	10.25	11.75
CS 2	73	205	70	200		
CS 3	73	048	73	045		
CS 4	70	105	66	108		

Figure 4.32: GL4 slope.

Table 4.10: Manual measurements at GL4.

Set	Dip Direction	Dip Angle	Joints Spacing (mm)	Trace length (m)	Seepage
J1	295	71	60-200	3-10	Dry
J2	205	73	60-200	3-10	Dry
J3	040	75	60-200	10-20	Dry
J4	105	67	20-60	3-10	Dry
J5	255	75	20-60	>20	Dry

Table 4.11: Lidar measurements at GL4.

Set	Dip Direction	Dip Angle	Joints Spacing (mm)	Trace length (m)	Seepage
J1	291	69	60-200	3-10	Dry
J2	203	75	60-200	3-10	Dry
J3	039	75	60-200	10-20	Dry
J4	101	68	20-60	3-10	Dry
J5	256	74	20-60	>20	Dry

4.2.5 GL 5 Slope Stability Analysis

Based on the discontinuity selection from Coltop 3D, six number of joint sets has been identified which are J1 (73/310), J2 (77/163), J3 (51/141), J4 (77/084), J5 (66/280), and J6 (81/259) respectively as shown in Figure 4.33b. Major planes of the joint sets are plotted in the stereonet and the trend of discontinuity orientation is presented in the rose plot (Figure 4.36). Based on the rose plot, discontinuity orientation is trending northeast-southwest direction with the slope face trend (80/100). Stability analysis test for planar, wedge, and topple failure are conducted and all of the possible failure are shown in Figure 4.37. For planar failure, some of J4 (77/084) poles satisfy criteria for planar failure and the direction of planar failure is towards southeast (100^{o}). For topple failure, there is no possible topple detected, however some of the J4 (77/084) poles may act as the base plane for topple failure. For wedge failure, there are four possible wedge failure identified by the Dips software which involving the intersection between joint sets J3 and J2, J3 and J4, J3 and J6, and J2 and J4 respectively. The directions of possible wedge failure are towards southeast (175^{o}, 160^{o}, 120^{o}) and northeast direction (080^{o}). The slope geometry and the cross-section profile of A-A' are presented such as in Figure 4.34 and Figure 4.35. Manual and Lidar measurements are validated such as shown in Figure 4.38. Based on the validation in Table 4.12, the mean square error of the dip angle is 3.3, while for the dip direction is 14.3. The discontinuity reading from manual and Lidar measurements are also used for comparison purposes such as shown in Table 4.13 and Table 4.14.

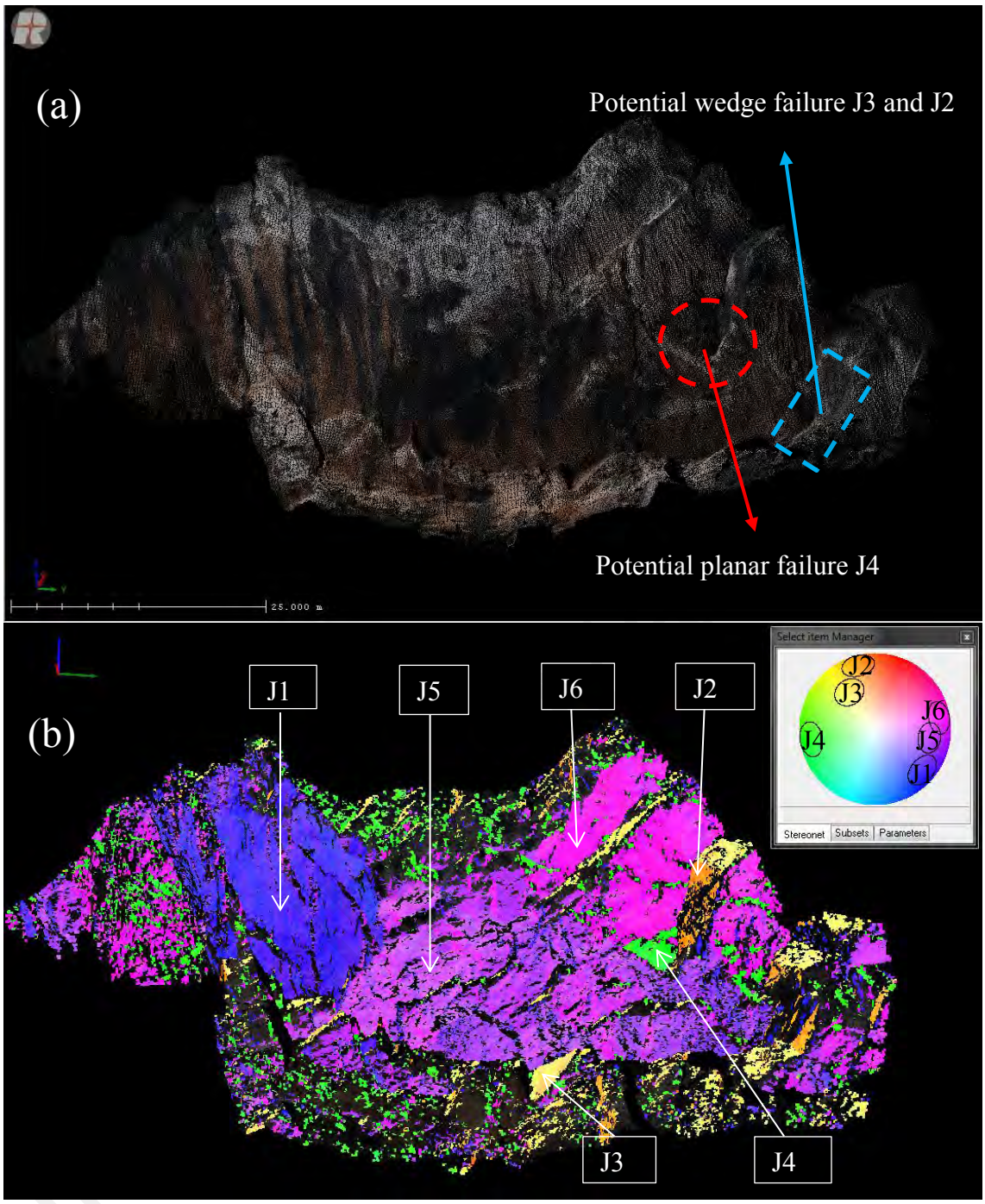

Figure 4.33: (a) True colour Digital Terrain Model (DTM) of the GL 5 slope (b) 3D discontinuity model derived from Coltop 3D, based on the model, six joint sets has been identified which are J1 (73/310), J2 (77/163), J3 (51/141), J4 (77/084), J5 (66/280), and J6 (81/259).

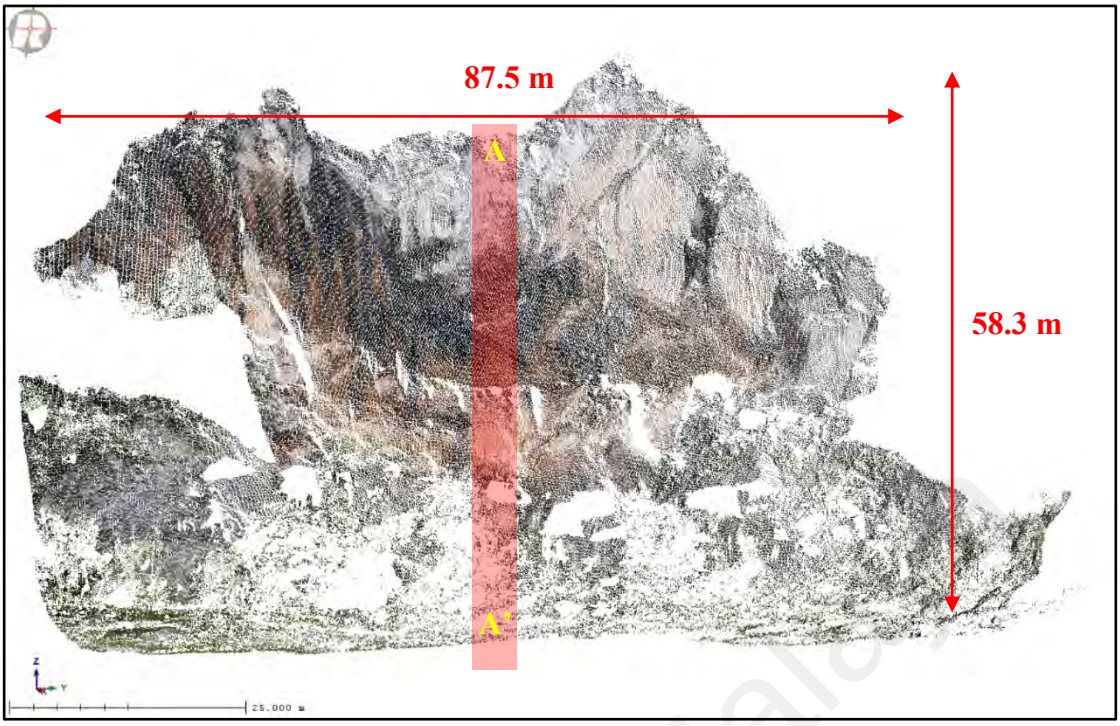

Figure 4.34: Slope geometry of GL5. Figure showing the height, length, and the location of profile A-A' on the slope.

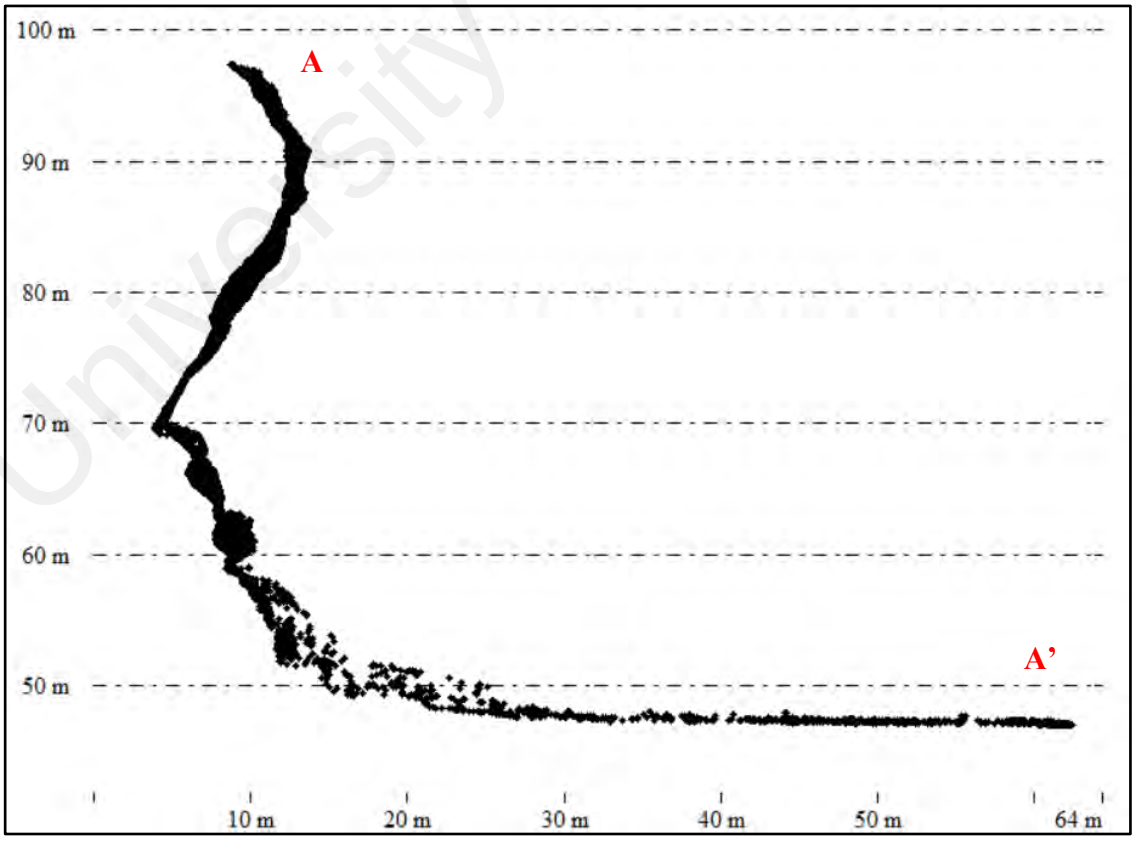

Figure 4.35: Profile A-A' on the slope of GL5.

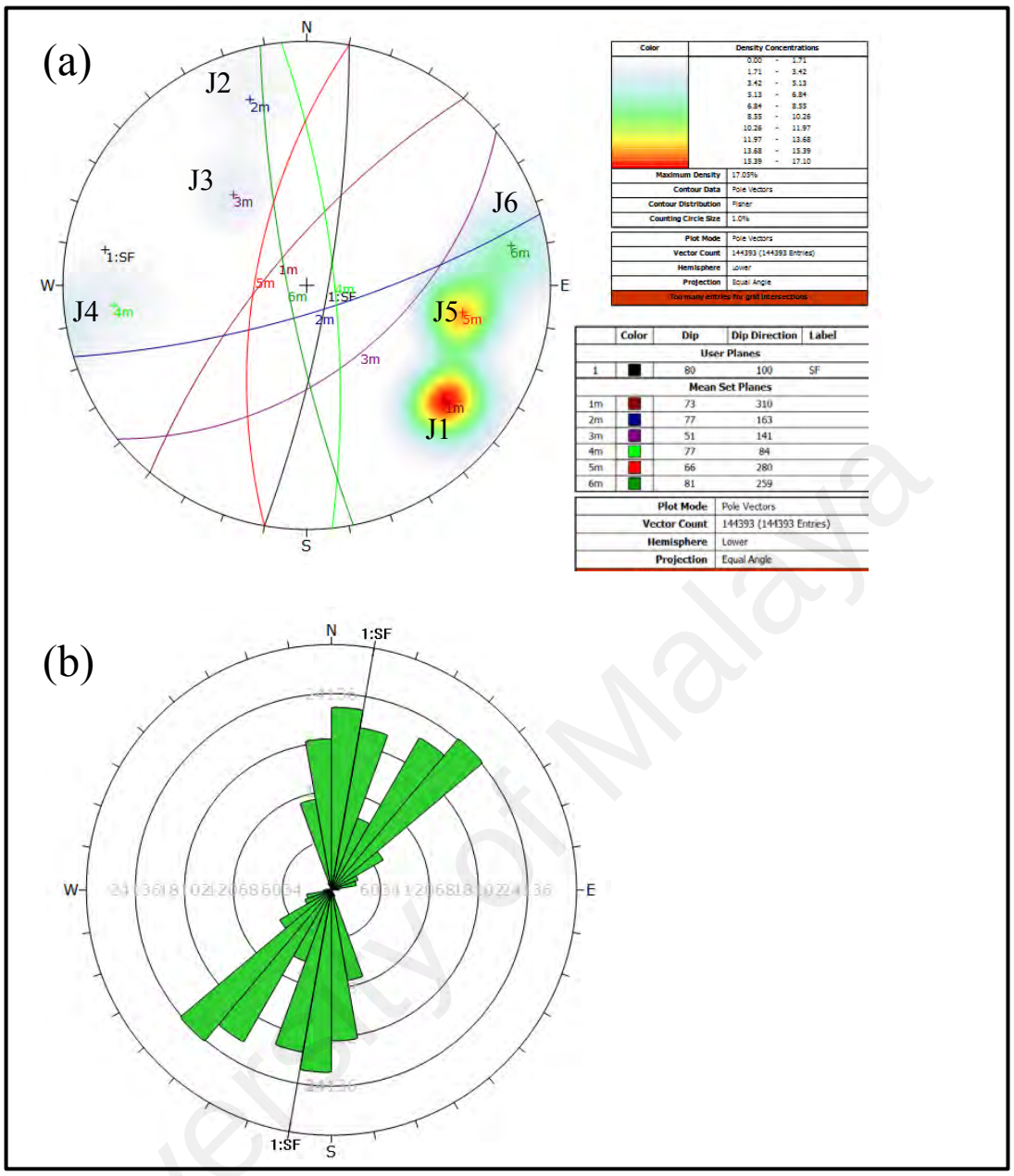

Figure 4.36: (a) Poles plot and major planes plot of all six joint sets in a stereonet (b) Rose plot showing the trend of all major joint sets and the slope face orientation in GL 5 slope. Based on the rose plot, most dominant joint sets orientation is trending northeast-southwest.

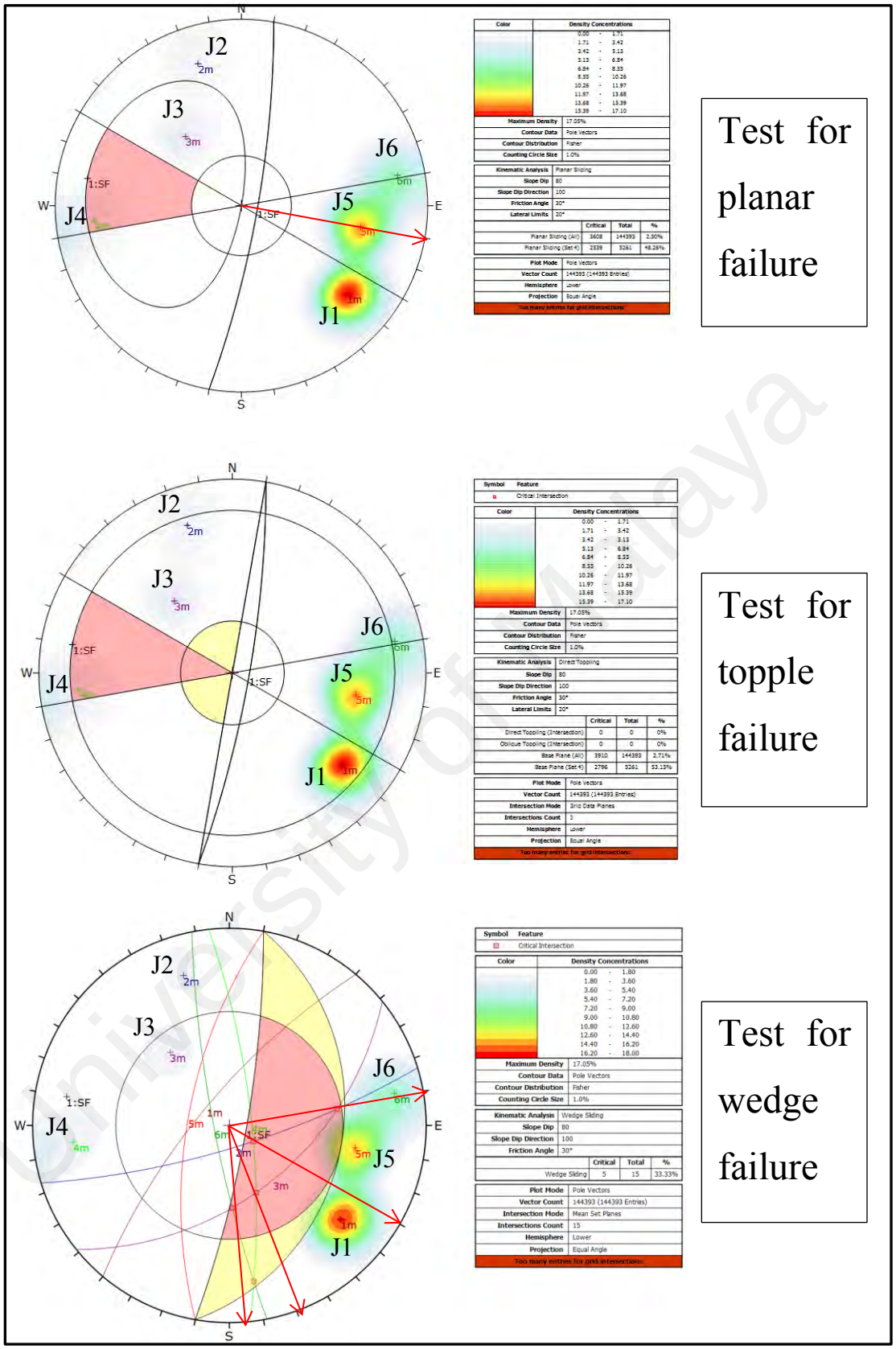

Figure 4.37: Kinematic analysis testing for planar failure, wedge failure, and topple failure in GL 5 slope. Red arrows represent the direction of possible failure.

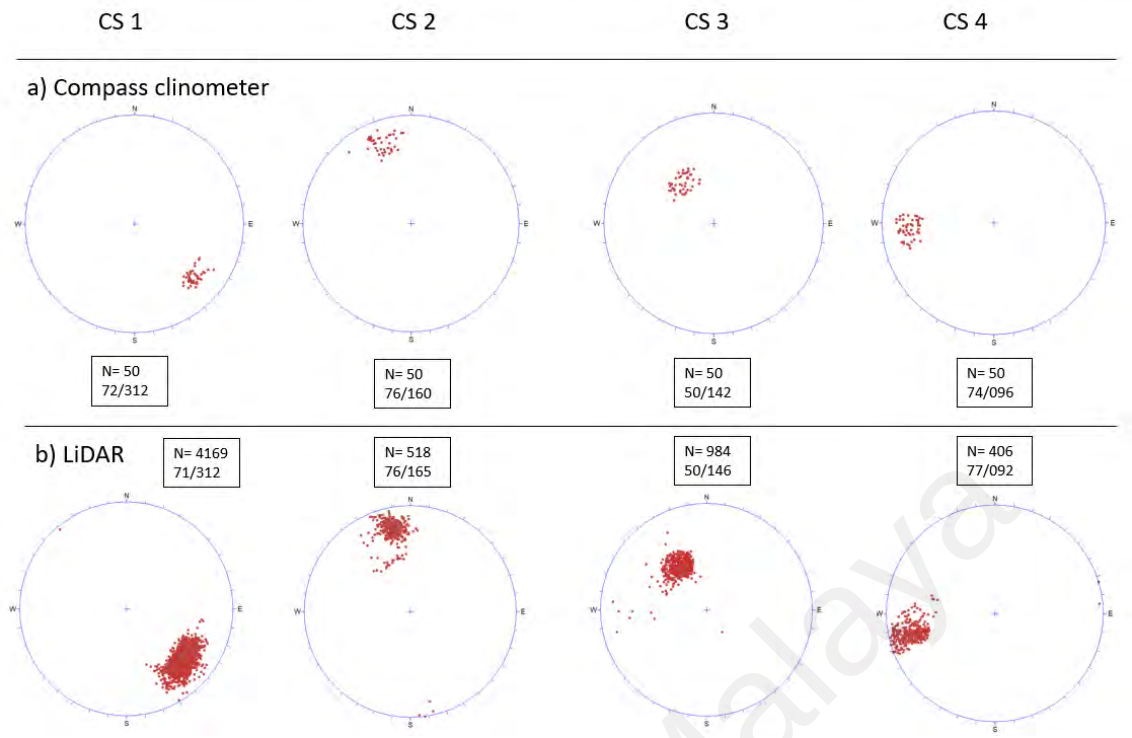

Figure 4.38: Lidar measurement validation with manual measurement at GL5 slope. Four control surfaces CS1, CS2, CS3, and CS4 which represent the joint planes were selected on the slope for validation purposes.

Table 4.12: Validation at GL 5.

Control surfaces	Compass clinometer		Lidar measurements		Mean square error	
	Dip angle	Direction	Dip angle	Direction	Dip angle	Direction
CS 1	73	312	71	312	3.3	14.3
CS 2	76	160	76	165		
CS 3	50	142	50	146		
CS 4	74	096	77	092		

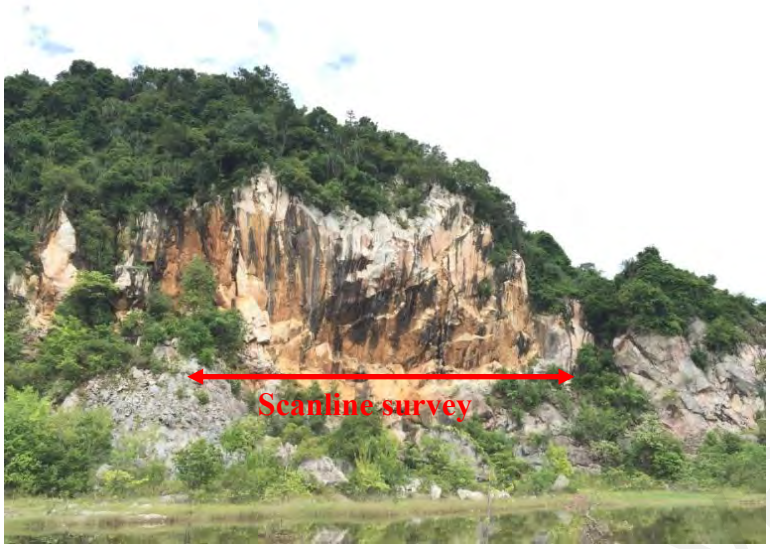

Figure 4.39: GL5 slope.

Table 4.13: Manual measurements at GL5.

Set	Dip Direction	Dip Angle	Joints Spacing (mm)	Trace length (m)	Seepage
J1	306	70	200-600	10-20	Dry
J2	165	75	200-600	3-10	Dry
J3	141	50	60-200	3-10	Dry
J4	085	76	200-600	>20	Dry
J5	279	66	200-600	>20	Dry
J6	260	80	60-200	10-20	Dry

Table 4.14: Lidar measurements at GL5.

Set	Dip Direction	Dip Angle	Joints Spacing (mm)	Trace length (m)	Seepage
J1	310	73	200-600	10-20	Dry
J2	163	77	200-600	3-10	Dry
J3	141	51	60-200	3-10	Dry
J4	084	77	200-600	>20	Dry
J5	280	66	200-600	>20	Dry
J6	259	81	60-200	10-20	Dry

4.3 Gunung Rapat Limestone Hills

Gunung Rapat is one of the famous limestone hills in the Kinta Valley, for its accessibility from Ipoh Town and beautiful karstic features. Furthermore, almost the entire cave in Gunung Rapat has been developed into a temple (Figure 4.40). Some examples of the famous temples are the Sam Poh Tong Temple, Kek Lok Tong, Kwan Yin Tong Temple, and Ling Sen Tong Temple. The stability analysis is conducted at the Kek Lok Tong Temple and Kwan Yin Tong Temple.

Figure 4.40: Google maps showing the location of Gunung Rapat Limestone Hills which is surrounded by numerous temples. Image from (google map).

4.3.1 Kek Lok Tong

Kek Lok Tong Temple is located in the Gunung Rapat Limestone Hills and is well known for its beautiful temple which situated inside the cave. Stability analysis is conducted in this area to ensure the safety of the visitor and to make one aware of any possible rock failure that might happen. (Figure 4.41) shows the location of Kek Lok Tong Temple and the slope division for the stability analysis.

Figure 4.41: Location of Kek Lok Tong Temple and the slope division KLT 1, KLT 2, and KLT 3 respectively. (Modified from google map).

KLT 1 is located near to the cave entrance, while KLT 2 and KLT 3 are situated after the cave exit. The presence of KLT 2 and KLT 3 slope is the results from the development of wang in the area. Wangs are always filled with tin-rich alluvium where they were formerly mined; ex-mining ponds were left behind (Muhammad & Komoo, 2003). KLT 1 is divided into three sections which are KLT 1 (a), KLT 1 (b), and KLT 1 (c) such as shown in (Figure 4.42b).

4.3.1.1 KLT 1 (a) Slope Stability Analysis

Based on the discontinuity selection from Coltop 3D software, three number of joint sets has been identified which are J1 (82/040), J2 (55/074), and J3 (83/251) respectively such in Figure 4.44b. Major joint sets plane is plotted in the stereonet and the trend of discontinuity orientation is presented in the rose plot such as shown in Figure 4.47. Based on the plot, the major trend of discontinuity orientation is northwest-southeast direction with the slope face trend (85/270). Stability analysis test for planar, wedge, and topple failure are conducted and all of the possible failure are shown in Figure 4.48. For planar failure, some of the poles from joint set J3 (83/251) satisfy the criteria for planar failure based on the threshold provided by Dips software. The direction of possible planar failure is towards west direction (270^{o}). For topple failure, there is no possible topple failure detected, however joint set J3 (83/251) will act as the base plane for topple failure. For wedge failure, there is one possible wedge failure has been identified which involving the intersection between joint sets J1 and J3 respectively. The direction of wedge failure is towards northwest direction (330^{o}). The slope geometry and slope cross section profile are presented such as shown in Figure 4.45 and Figure 4.46. Validation of manual and Lidar measurements are also done such as shown in Figure 4.49. Based on the validation in Table 4.15, the mean square error for the dip angle is 26.3, while for the dip direction is 15.8. The discontinuity reading from manual and Lidar measurements are also being used for comparison such as shown in Table 4.16 and Table 4.17.

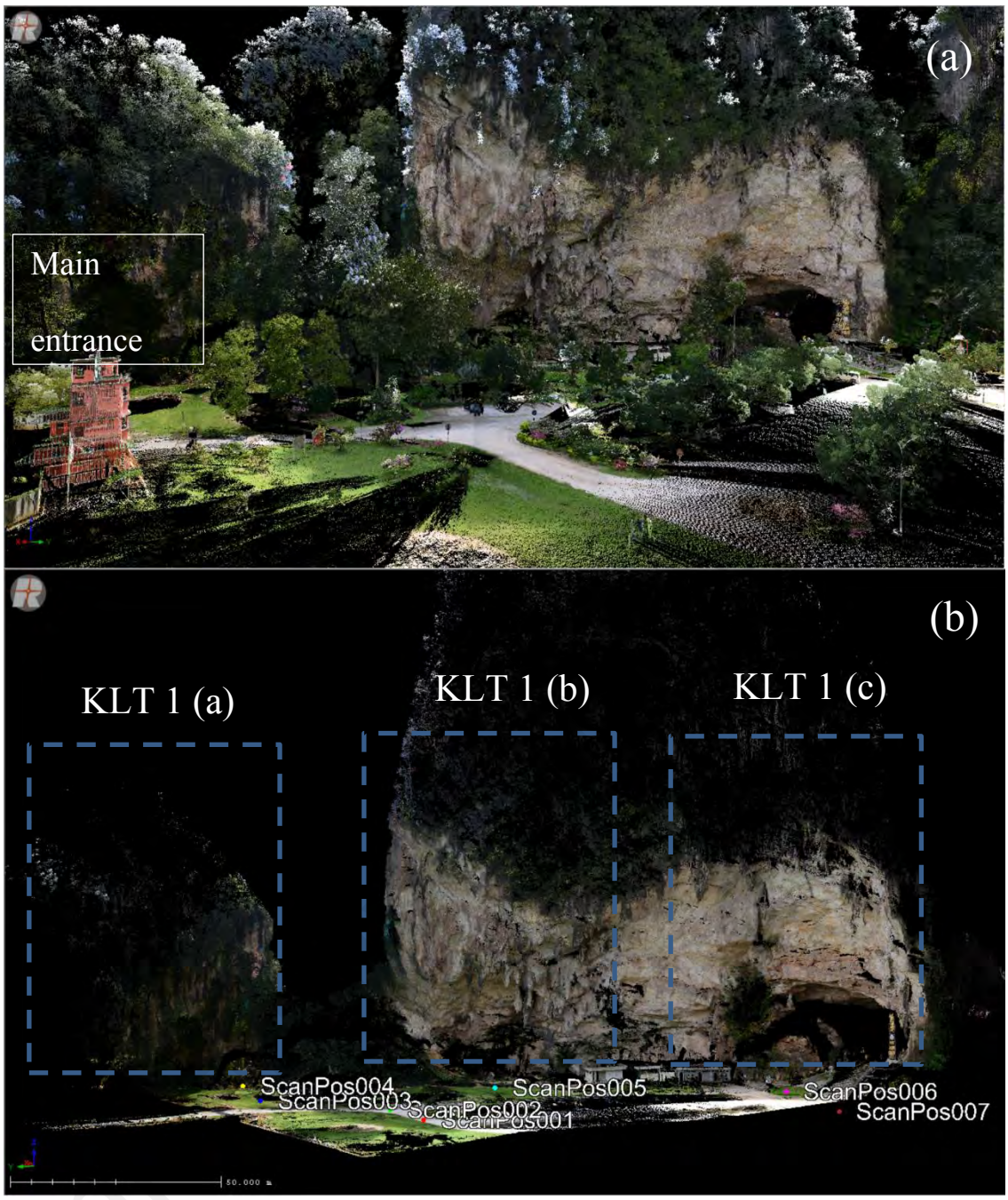

Figure 4.42: (a) True colour Digital Terrain Model (DTM) of KLT 1 slope (b) Slope division for stability analysis and the location of scanning position.

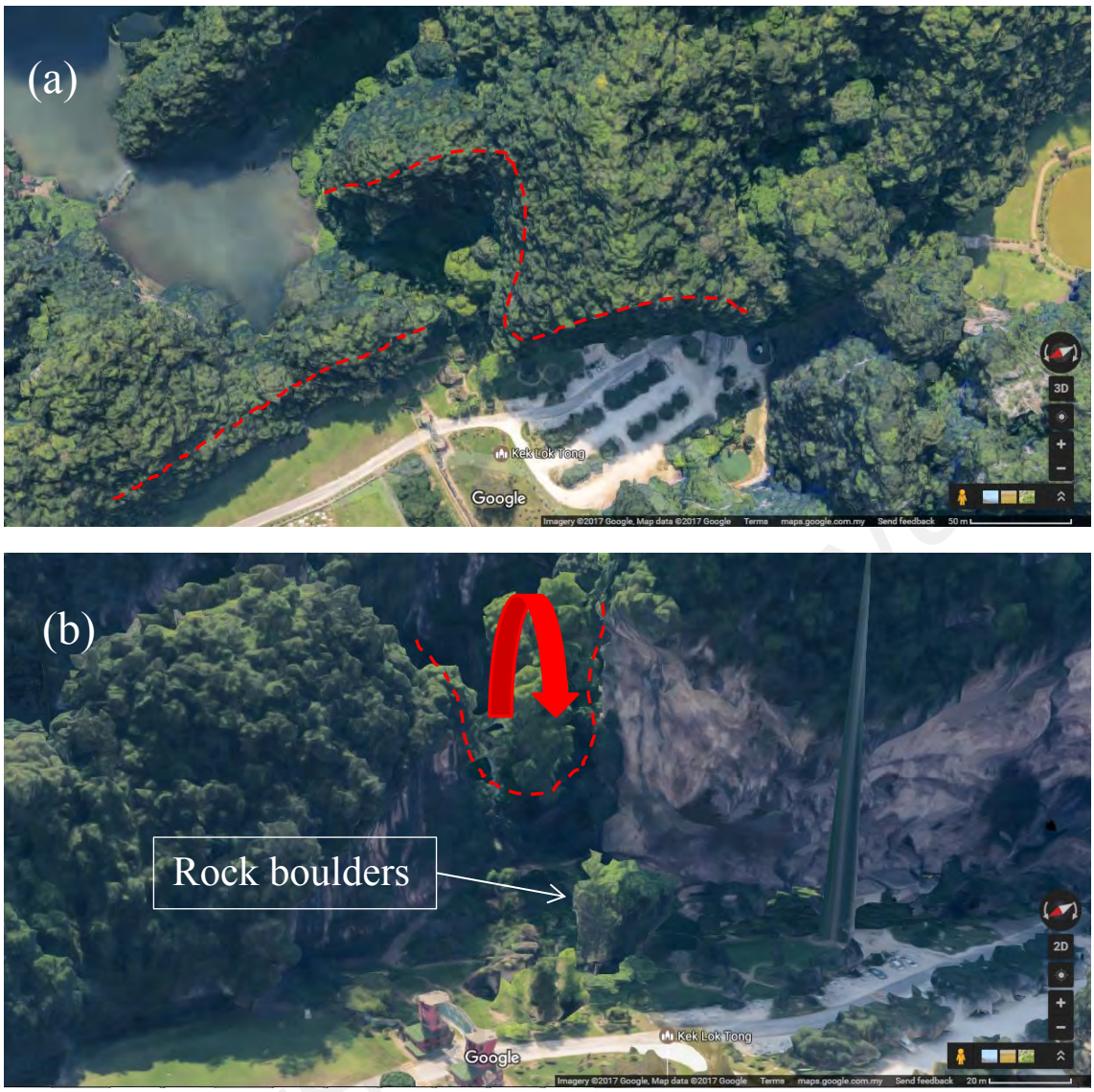

Figure 4.43: Evidence of rock failure in KLT 1 area. (a) Aerial view of KLT 1 limestone hills (b) Rock boulders at the base of the slope. Red inferred line shows the outline of slopes. (Modified from Google maps).

Based on the Figure 4.43a, top view image from google maps shows that limestone hill is discontinuous separated by the gap in between the hills. There is also an evidence of boulders and rock block at the base of the slope indicating the previous rock failure possibly topple failure in the area. This failure creates gap in between hills such as shown in Figure 4.43b.

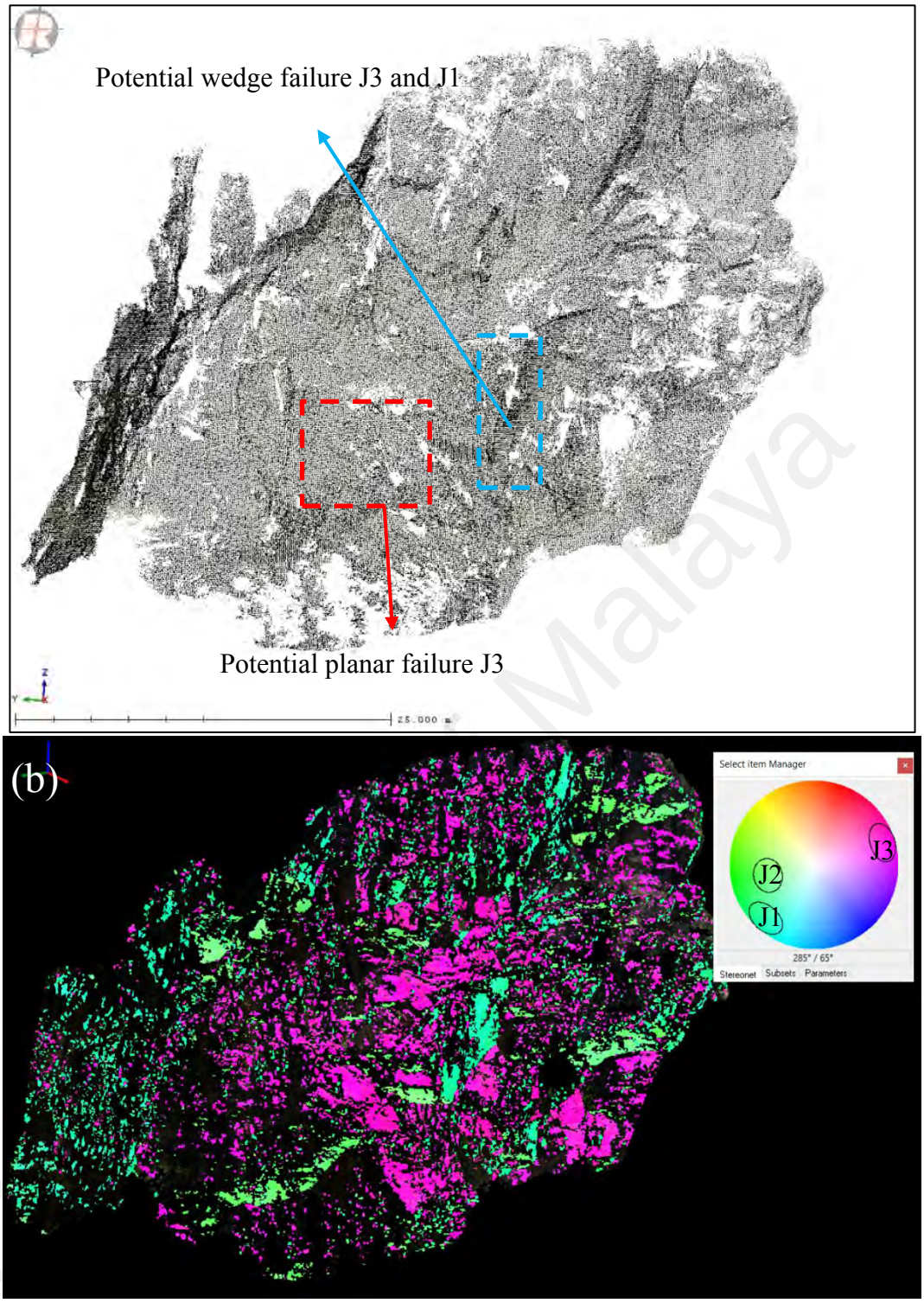

Figure 4.44: (a) Digital Terrain Model (DTM) of KLT 1(a) slope with amplitude colour (b) 3D discontinuity model derived from Coltop 3D, based on the model, three numbers of joint sets has been identified which are J1 (82/040), J2 (55/074) and J3 (83/251).

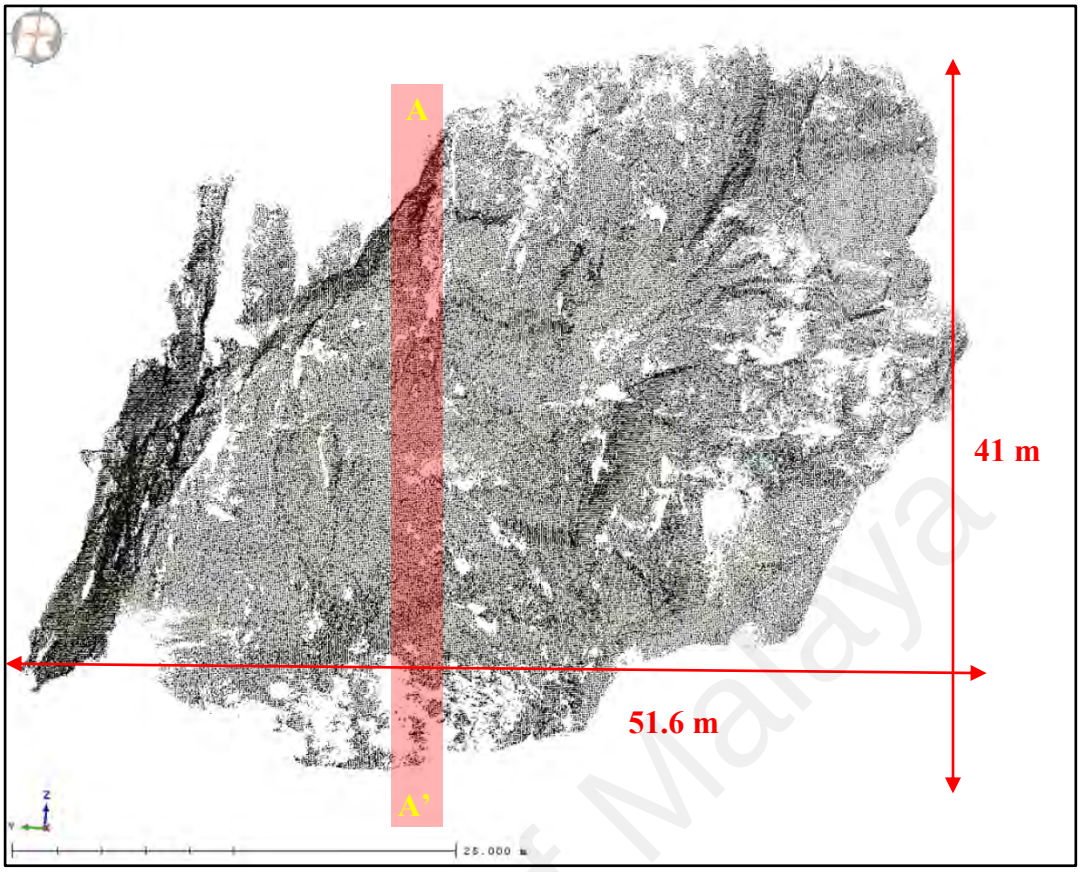

Figure 4.45: Slope geometry of KLT 1 (a). Figure showing the height, length, and the location of profile A-A' on the slope.

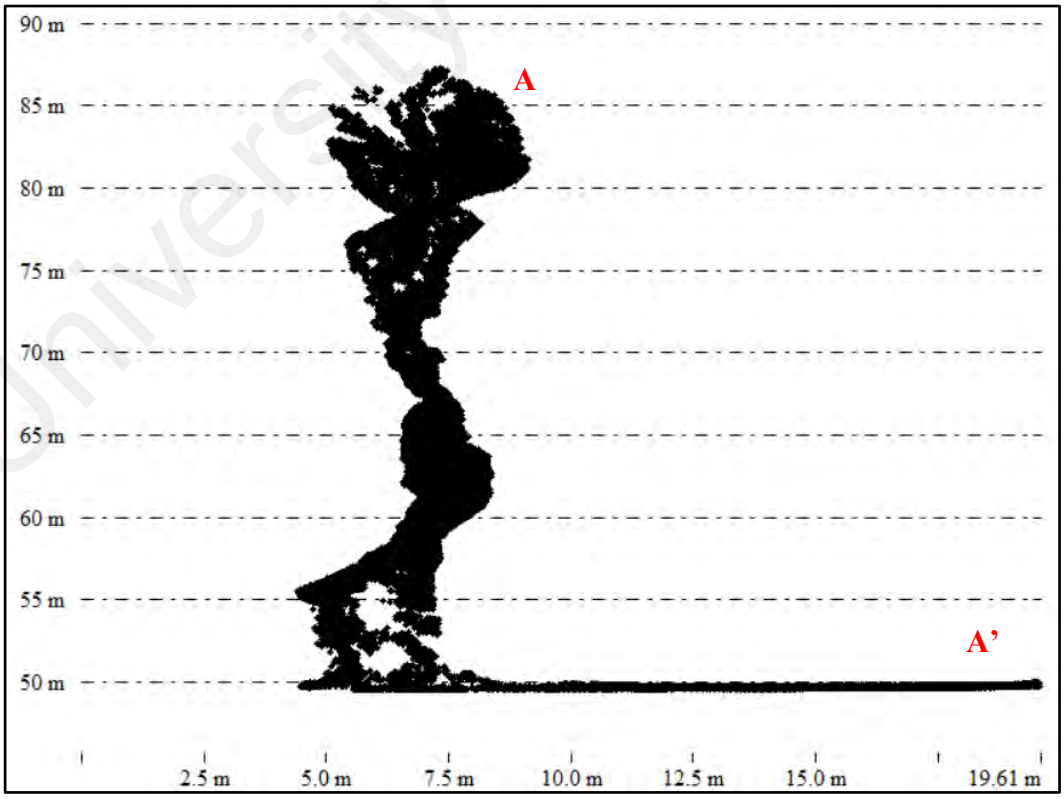

Figure 4.46: Profile A-A' of slope KLT 1 (a).

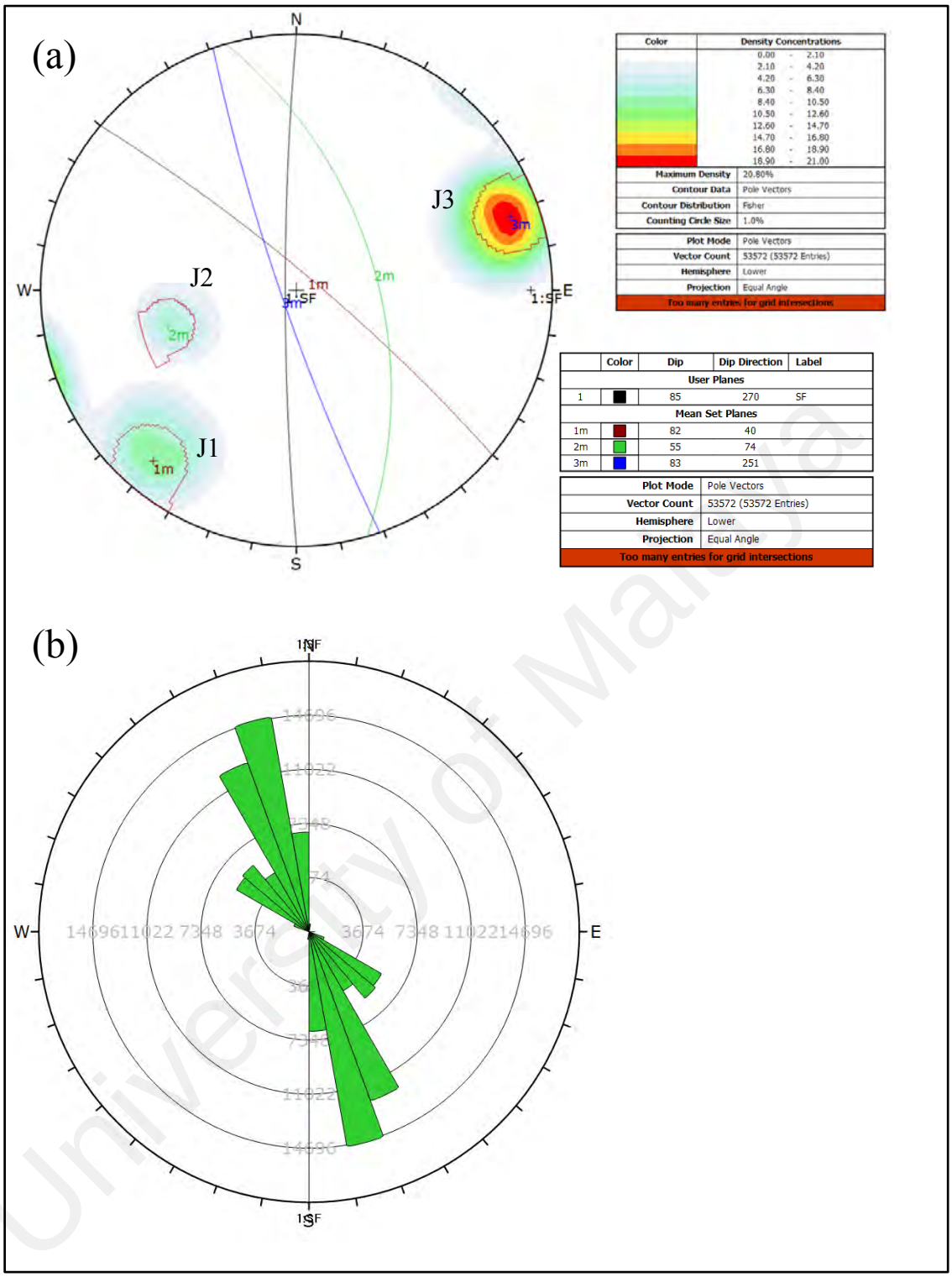

Figure 4.47: (a) Poles plot and major planes plot of all three joint sets in a stereonet (b) Rose plot showing the trend of all major joint sets and the slope face orientation in KLT 1 (a) slope. Based on the rose plot, most dominant joint sets orientation is trending northwest-southeast direction.

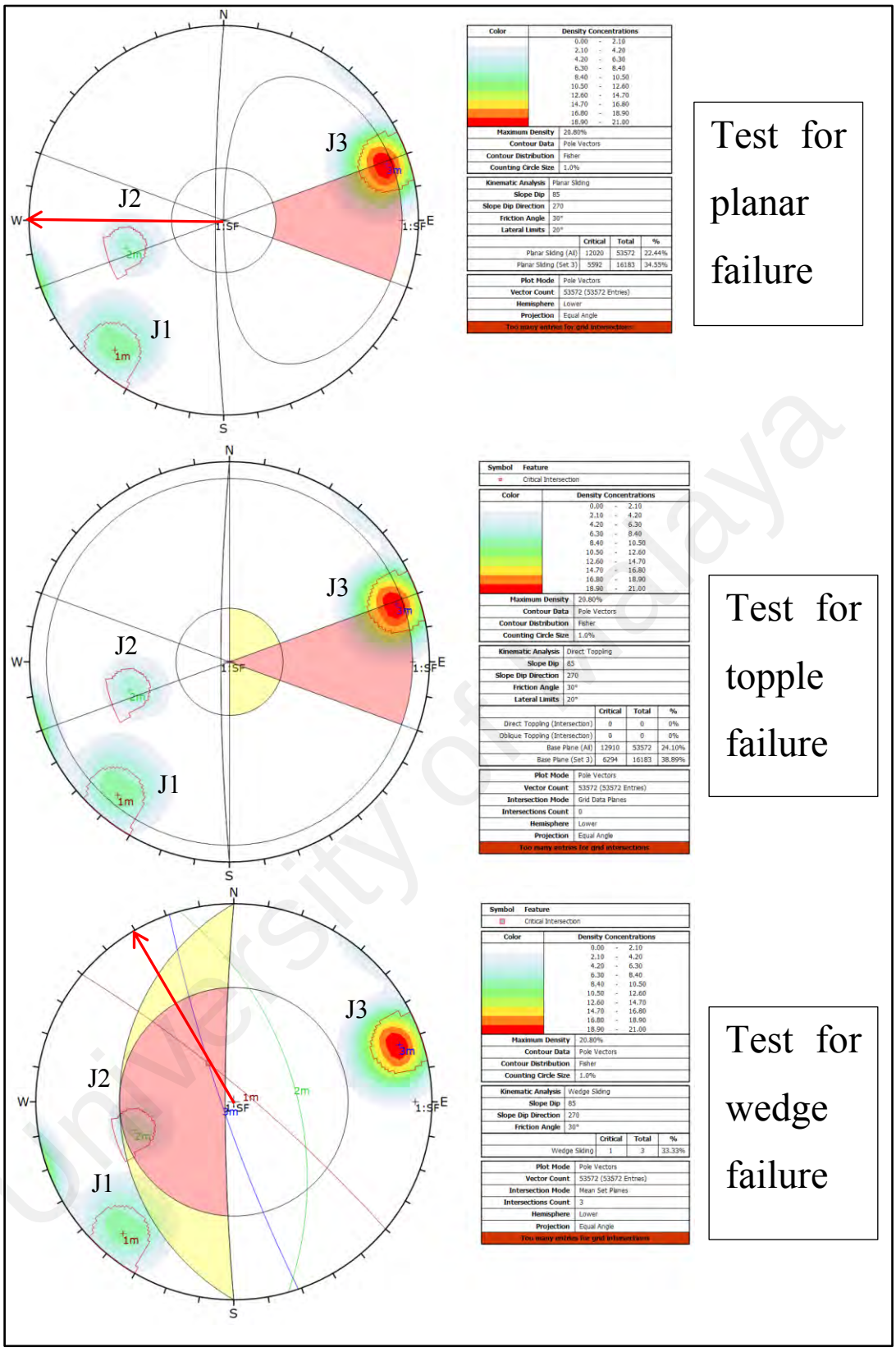

Figure 4.48: Kinematic analysis testing for planar failure, wedge failure, and topple failure in KLT 1 (a) slope. Red arrows represent the direction of possible failure.

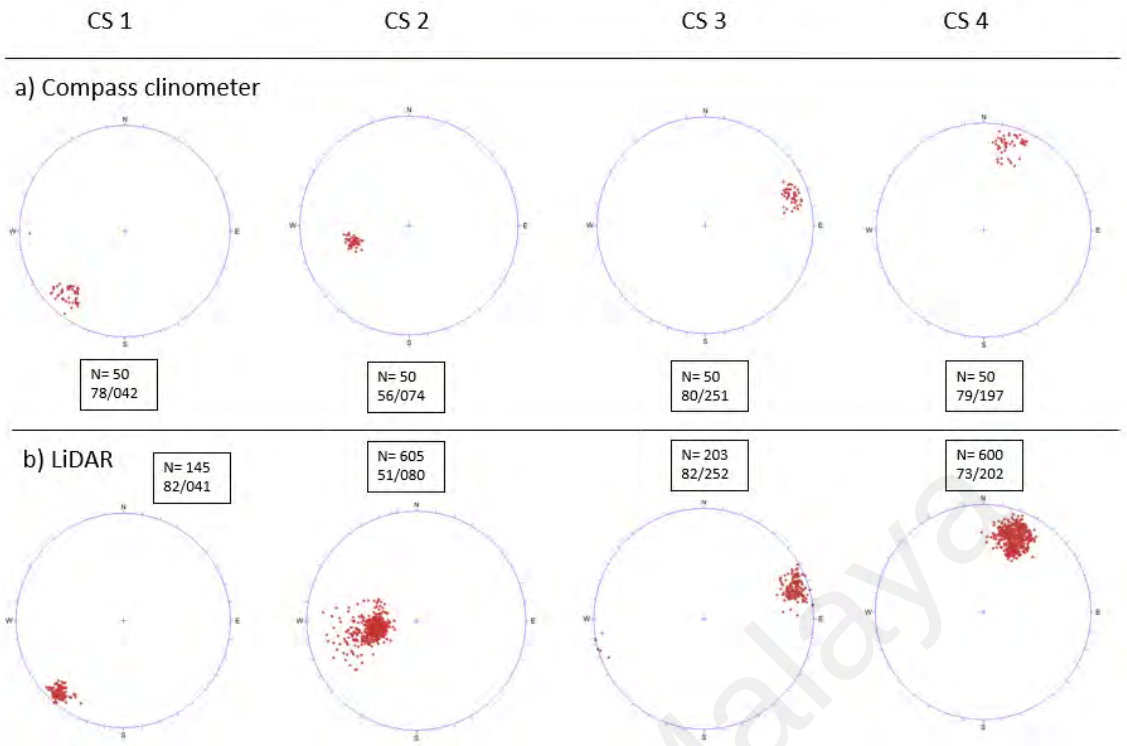

Figure 4.49: Lidar measurement validation with manual measurement at KLT 1 (a) slope. Four control surfaces CS1, CS2, CS3, and CS4 which represent the joint planes were selected on the slope for validation purposes.

Table 4.15: Validation at KLT 1 (a).

Control surfaces	Compass clinometer		Lidar measurements		Mean square error	
	Dip angle	Direction	Dip angle	Direction	Dip angle	Direction
CS 1	78	042	82	041	26.3	15.8
CS 2	58	074	51	080		
CS 3	80	251	82	252		
CS 4	79	197	73	202		

Figure 4.50: KLT 1 (a) slope.

Table 4.16: Manual measurements at KLT 1 (a).

Set	Dip Direction	Dip Angle	Joints Spacing (mm)	Trace length (m)	Seepage
J1	045	80	60-200	3-10	Dry
J2	076	57	60-200	3-10	Dry
J3	250	80	200-600	10-20	Dry

Table 4.17: Lidar measurements at KLT 1 (a).

Set	Dip Direction	Dip Angle	Joints Spacing (mm)	Trace length (m)	Seepage
J1	040	82	60-200	3-10	Dry
J2	074	55	60-200	3-10	Dry
J3	251	83	200-600	10-20	Dry

4.3.1.2 KLT 1 (b) Slope Stability Analysis

Based on the discontinuity selection from Coltop 3D software, three number of joint sets has been identified which are J1 (54/082), J2 (30/224), and J3 (67/122), and J4 (78/356) respectively in Figure 4.52b. Major plane of the joint sets is plotted in the stereonet and the trend of discontinuity orientation is presented in the rose plot such in Figure 4.55. Based on the plot, the major trend of discontinuity orientation is northeast-southwest direction with the slope face trend (75/280). Stability analysis test for planar, wedge, and topple failure are conducted and all of the possible failure are shown in Figure 4.56. For planar failure and wedge failure, there is no potential failure detected based on the kinematic analysis. For topple failure, no topple failure will occur, however joint plane J2 (30/224) will act as the base plane for topple failure. Highly weathered limestone at the base of the slope make it difficult to collect discontinuity data (Figure 4.51). Slope geometry and slope cross section profile are presented such as shown in Figure 4.53 and Figure 4.54. Validation of manual and Lidar measurements are also done (Figure 4.57). Based on the validation in Table 4.18, the mean square error for the dip angle is 14.3, while for the dip direction is 8.8. Discontinuity reading from manual and Lidar method are used for comparison such as shown in Table 4.19 and Table 4.20.

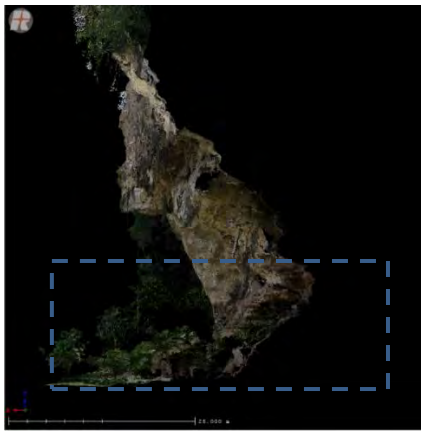

Figure 4.51: Cross section of view of the slope showing the highly weathered rock at the base of the slope (blue dotted box).

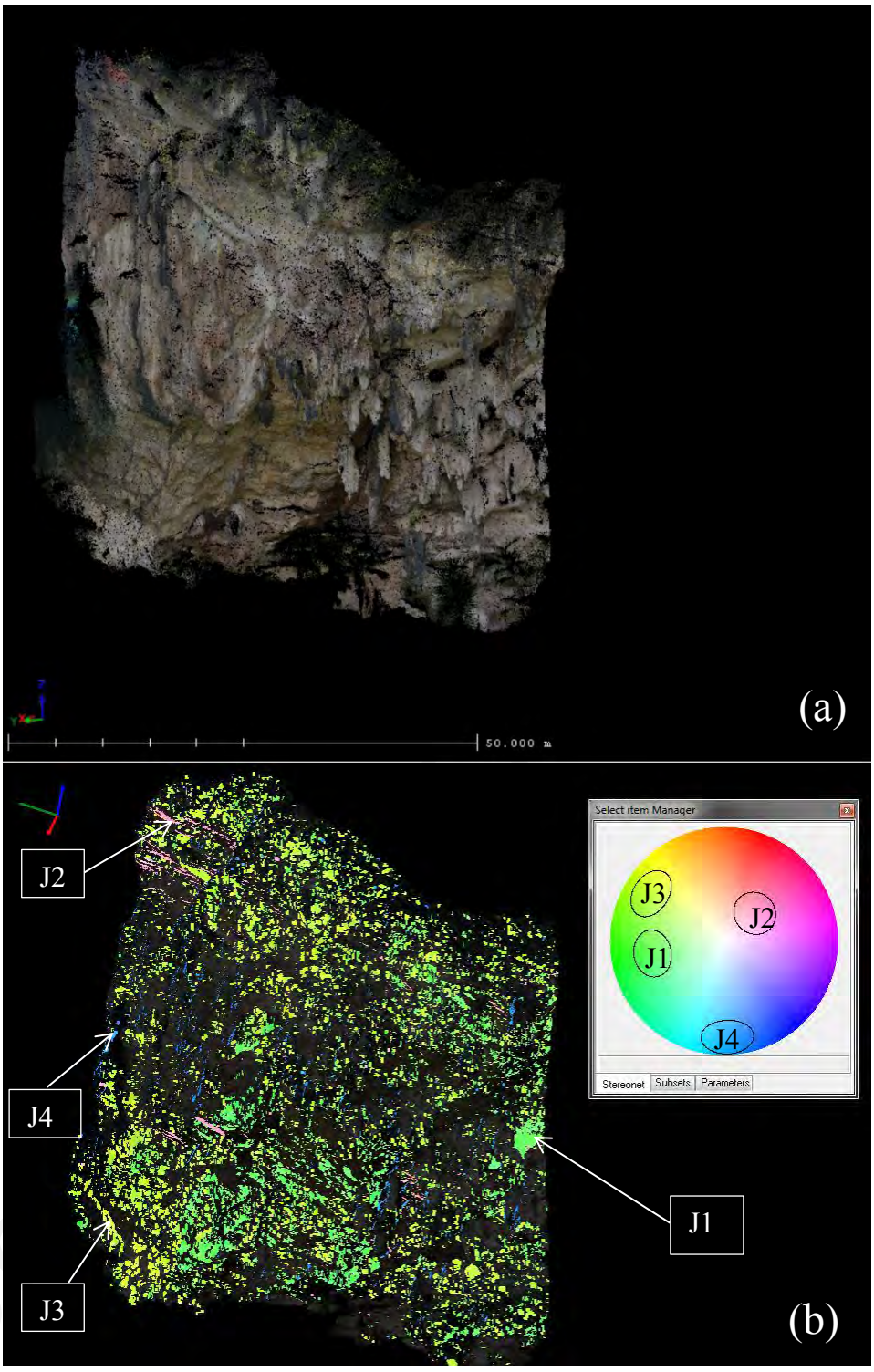

Figure 4.52: (a) True colour Digital Terrain Model (DTM) of KLT 1 (b) slope (b) 3D discontinuity model derived from Coltop 3D. Based on the model, four number of joint sets has been identified which are J1 (54/082), J2 (30/224), J3 (67/122), and J4 (78/356).

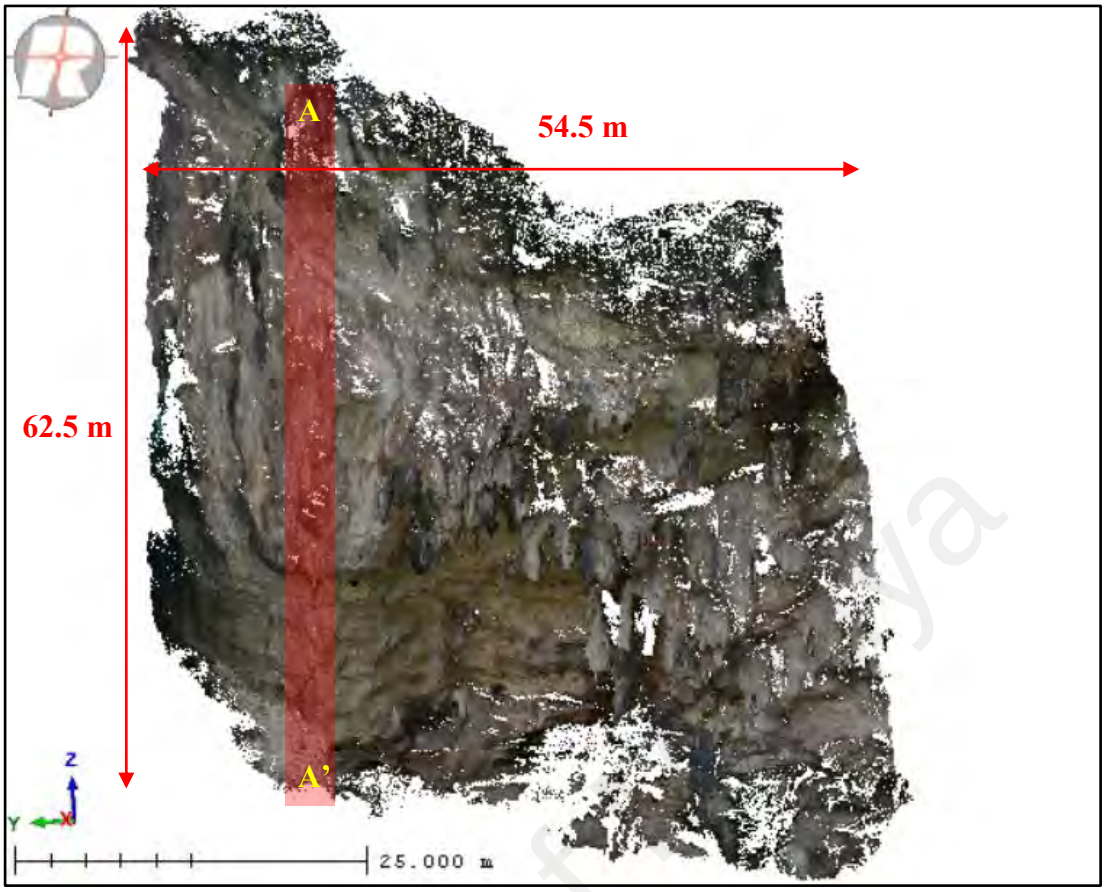

Figure 4.53: Slope geometry of KLT 1 (b). Figure shows the length, height, and the location of profile A-A' on the slope.

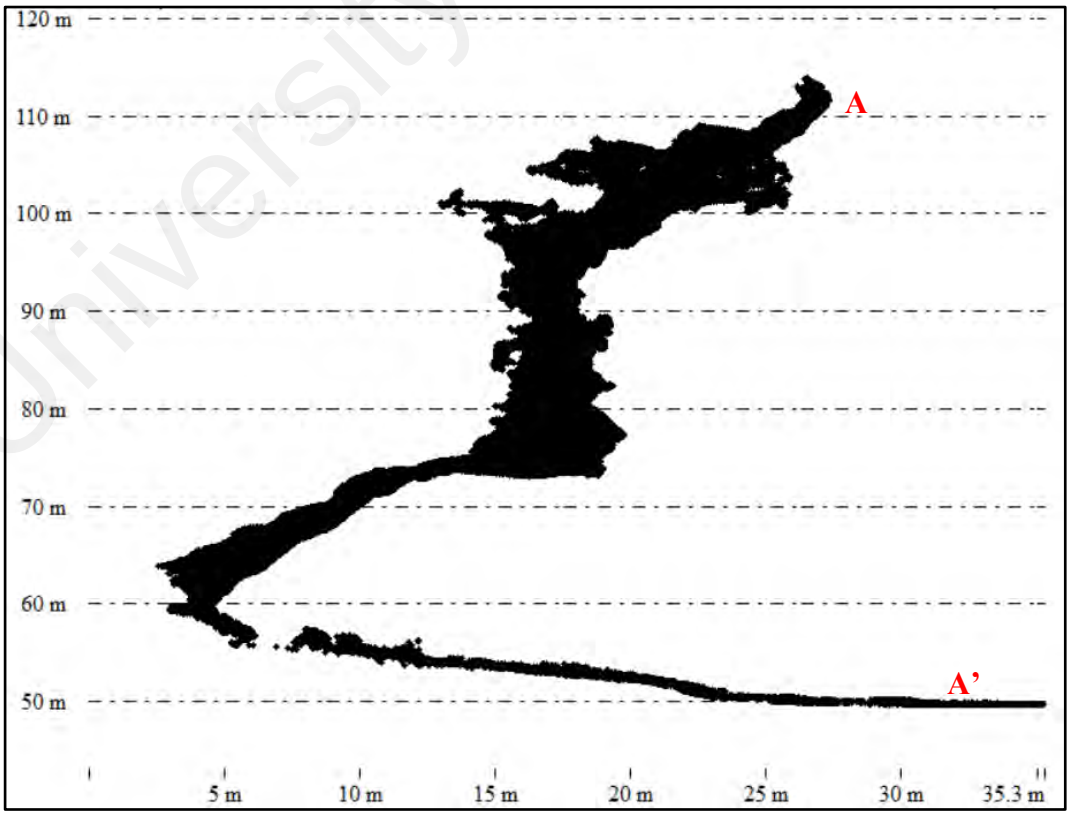

Figure 4.54: Profile A-A' of slope KLT 1 (b).

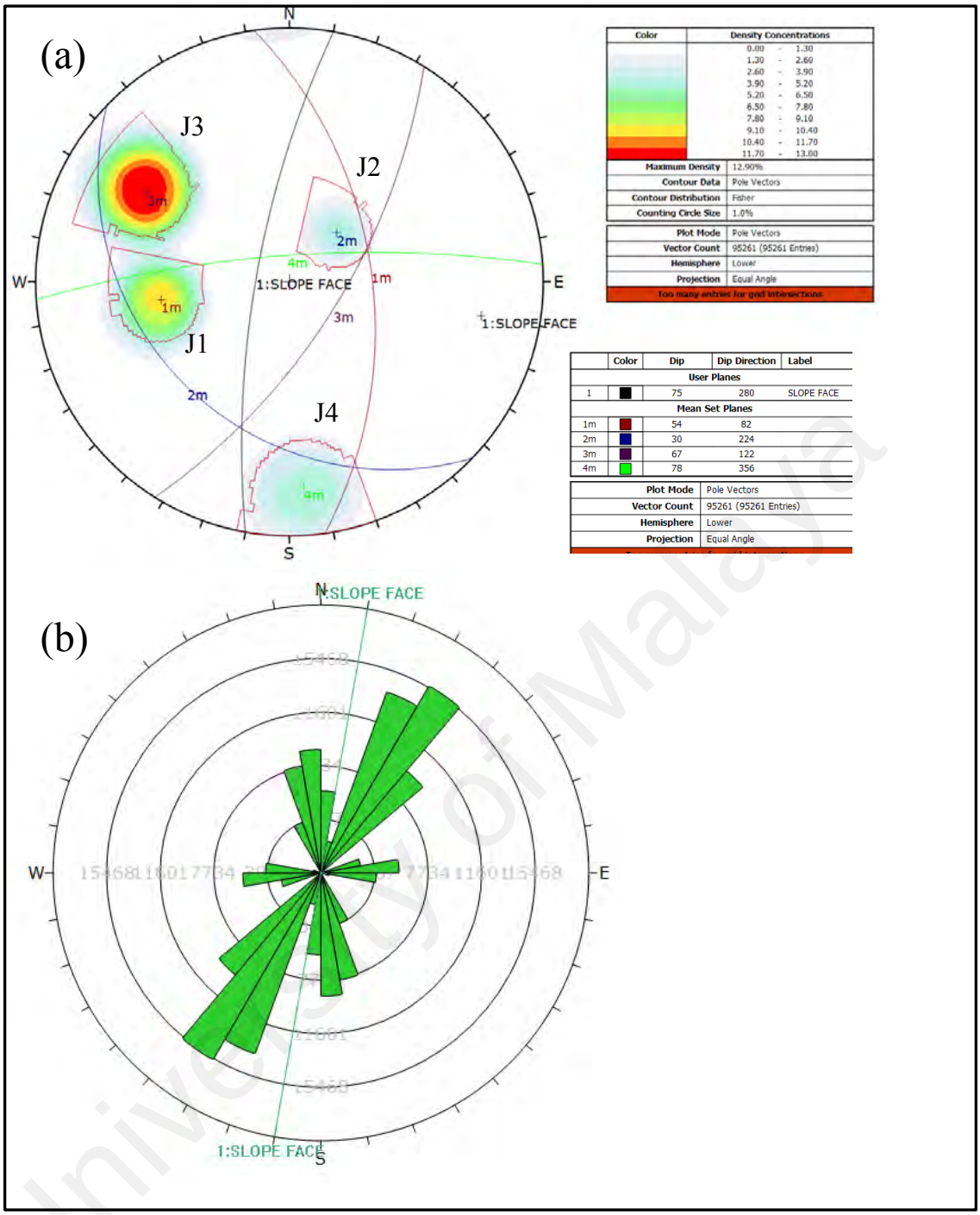

Figure 4.55: (a) Poles plot and major planes plot of all four joint sets in a stereonet (b) Rose plot showing the trend of all major joint sets and the slope face orientation in KLT 1 (b) slope. Based on the rose plot, most dominant joint sets orientation is trending northeast-southwest direction.

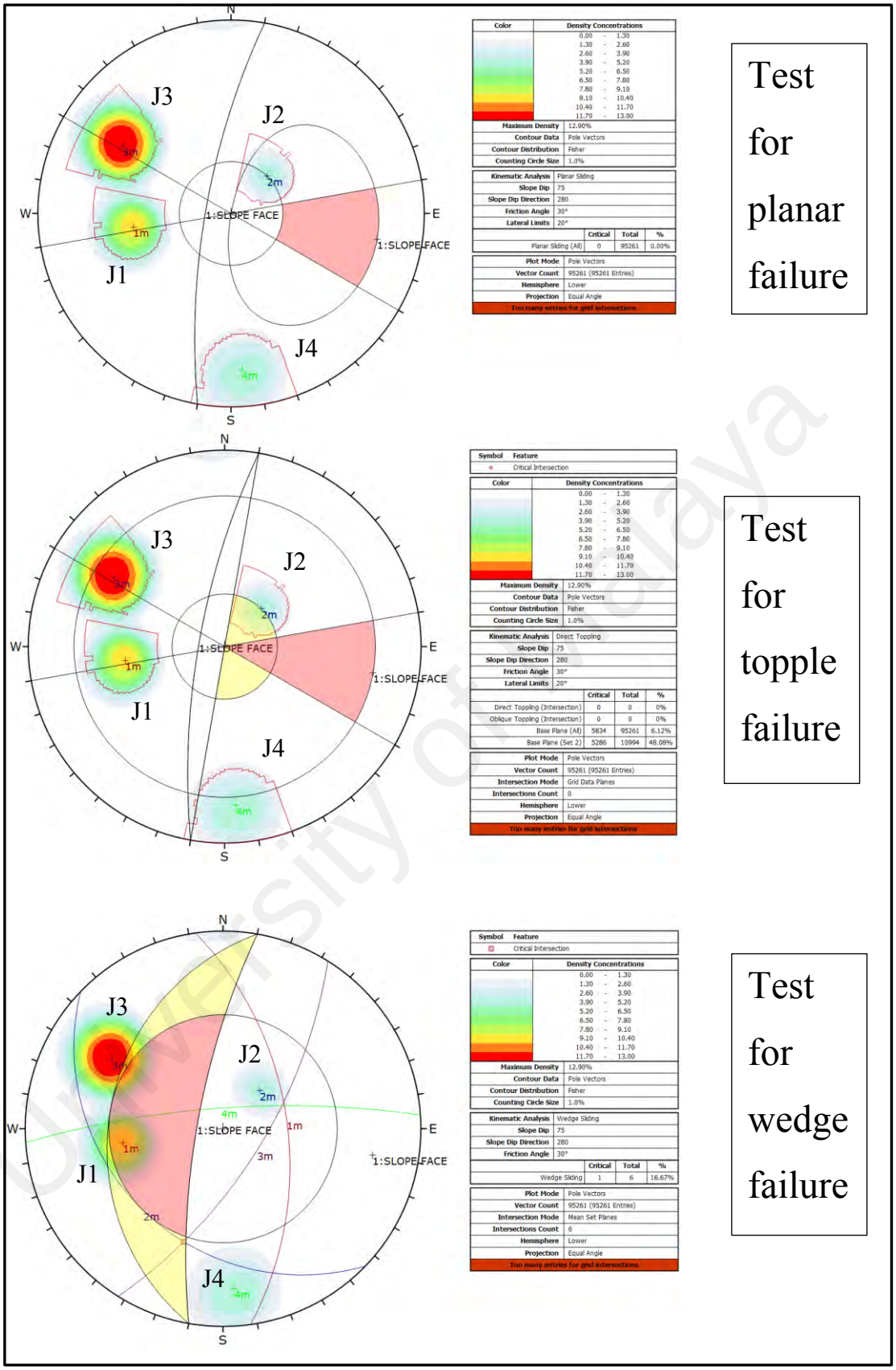

Figure 4.56: Kinematic analysis testing for planar failure, wedge failure, and topple failure in KLT 1 (b) slope. Red arrows represent the direction of possible failure.

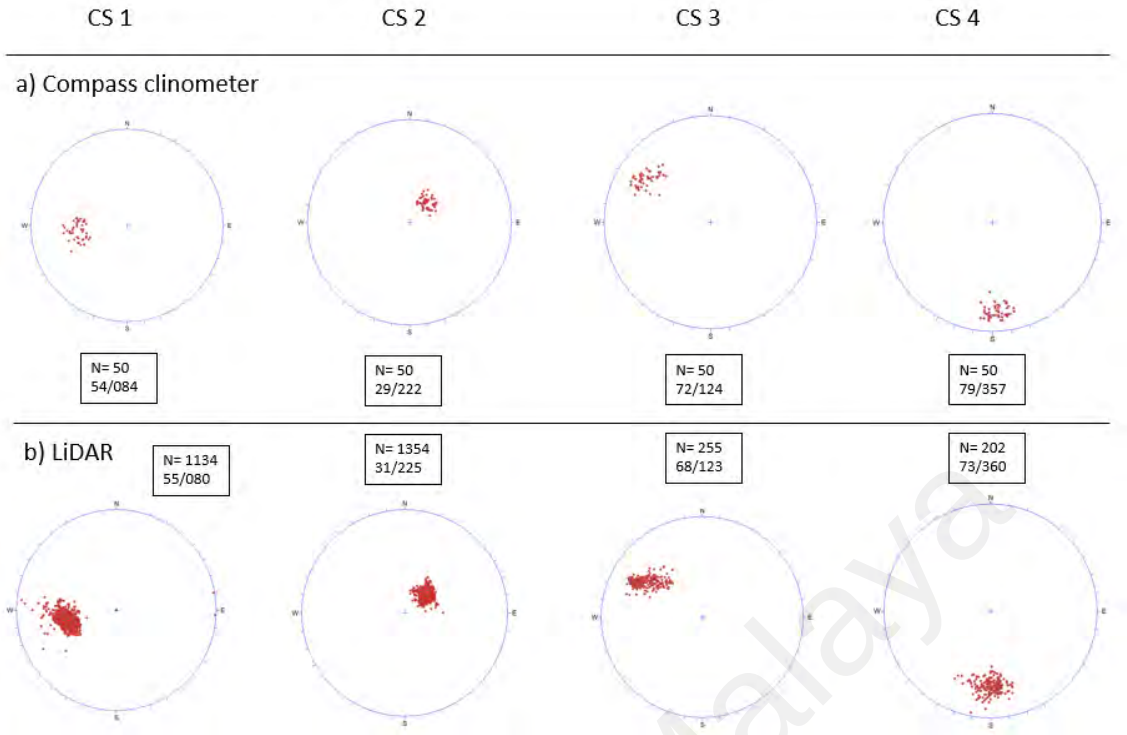

Figure 4.57: Lidar measurement validation with manual measurement at KLT 1 (b) slope. Four control surfaces CS1, CS2, CS3, and CS4 which represent the joint planes were selected on the slope for validation purposes.

Table 4.18: Validation at KLT 1 (b).

Control surfaces	Compass clinometer		Lidar measurements		Mean square error	
	Dip angle	Direction	Dip angle	Direction	Dip angle	Direction
CS 1	54	084	55	080	14.3	8.8
CS 2	29	222	31	225		
CS 3	72	124	68	123		
CS 4	79	357	73	360		

Figure 4.58: Slope KLT 1 (b).

Table 4.19: Manual measurements at KLT 1 (b).

Set	Dip Direction	Dip Angle	Joints Spacing (mm)	Trace length (m)	Seepage
J1	073	47	60-200	1-3	Dry
J2	119	40	60-200	1-3	Dry
J3	123	66	60-200	3-10	Dry
J4	350	80	60-200	1-3	Dry

Table 4.20: Lidar measurements at KLT 1 (b).

Set	Dip Direction	Dip Angle	Joints Spacing (mm)	Trace length (m)	Seepage
J1	082	54	60-200	1-3	Dry
J2	224	30	60-200	1-3	Dry
J3	122	67	60-200	3-10	Dry
J4	356	78	60-200	1-3	Dry

4.3.1.3 KLT 1 (c) Slope Stability Analysis

Based on the discontinuity selection and the kinematic analysis, four joint sets have been identified at the KLT 1 (c) slope which are J1 (79/299), J2 (70/163), J3 (75/108), and J4 (47/088) respectively in Figure 4.60b. Major plane of the joint sets is plotted in the stereonet and the trend of discontinuity orientation is presented in the rose plot such in Figure 4.63. Based on the plot, major trend of discontinuity orientation is northeast-southwest with the slope face trend (80/280). Stability analysis test are conducted and all of the possible failure are shown in Figure 4.64. For planar failure, some of the poles from joint sets J1 (79/299) satisfy the criteria for planar failure and the direction of possible planar failure is towards northwest direction (280^{o}). For topple failure, there is no topple failure detected however joint sets J1 (79/299) will act as the base plane for topple failure. For wedge failure, one possible wedge failure has been identified which involving the intersection between joint sets J1 and J2 respectively. The direction of possible wedge failure is towards southwest direction (220^{o}). No manual measurement collected in this slope because of the slope location which is above the cave entrance itself (Figure 4.59), and the joints surface is mostly highly weathered make it almost impossible to collect manual measurements. The slope geometry and slope cross section profile are presented such as in Figure 4.61 and Figure 4.62.

Figure 4.59: Location of KLT 1 (c) which located exactly above the cave entrance.

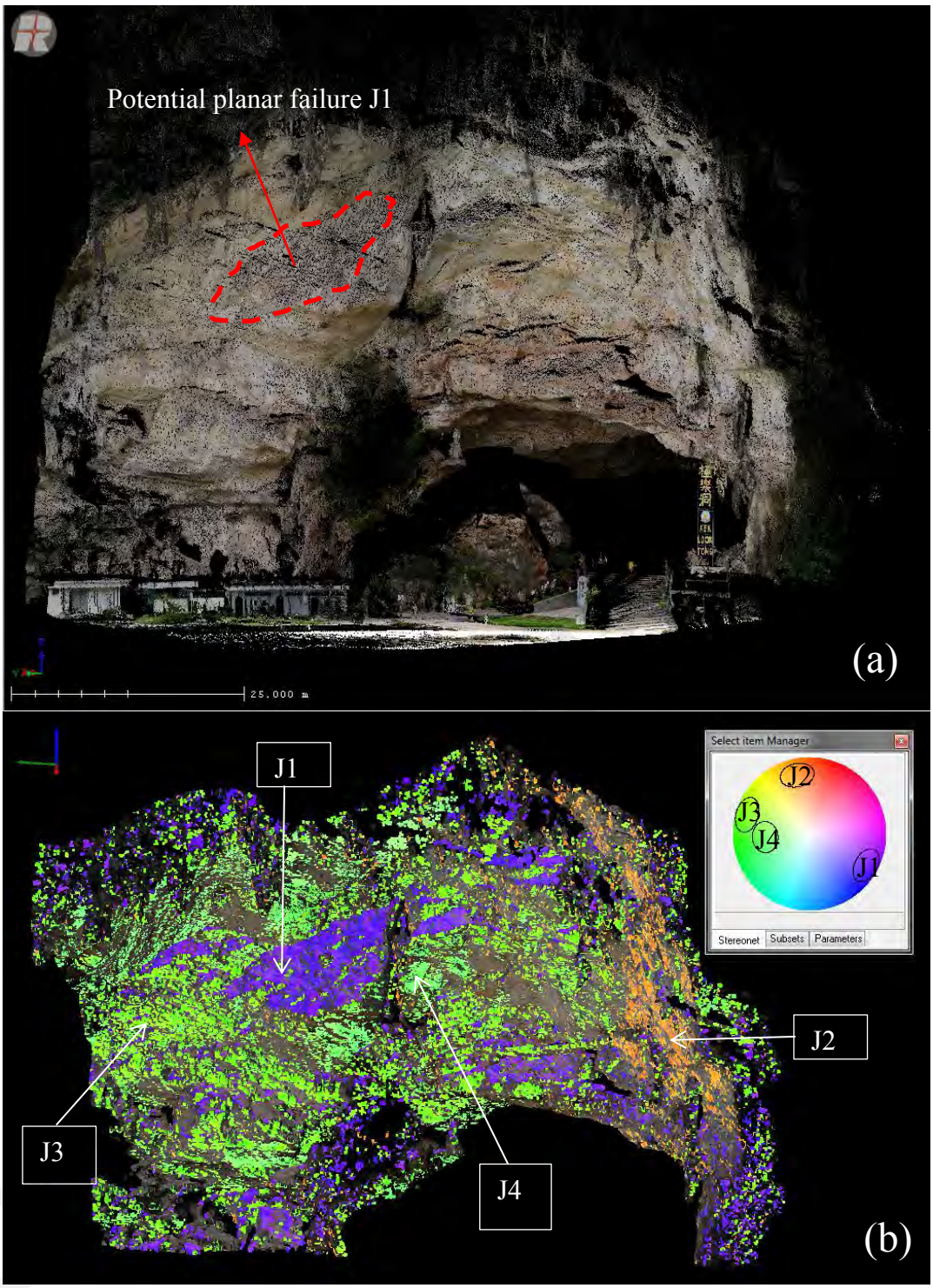

Figure 4.60: (a) Digital Terrain Model (DTM) of the slope (b) 3D discontinuity model derived from Coltop 3D, based on the model, four joint sets has been identified which are J1 (79/299), J2 (70/165), J3 (75/108), and J4 (47/088).

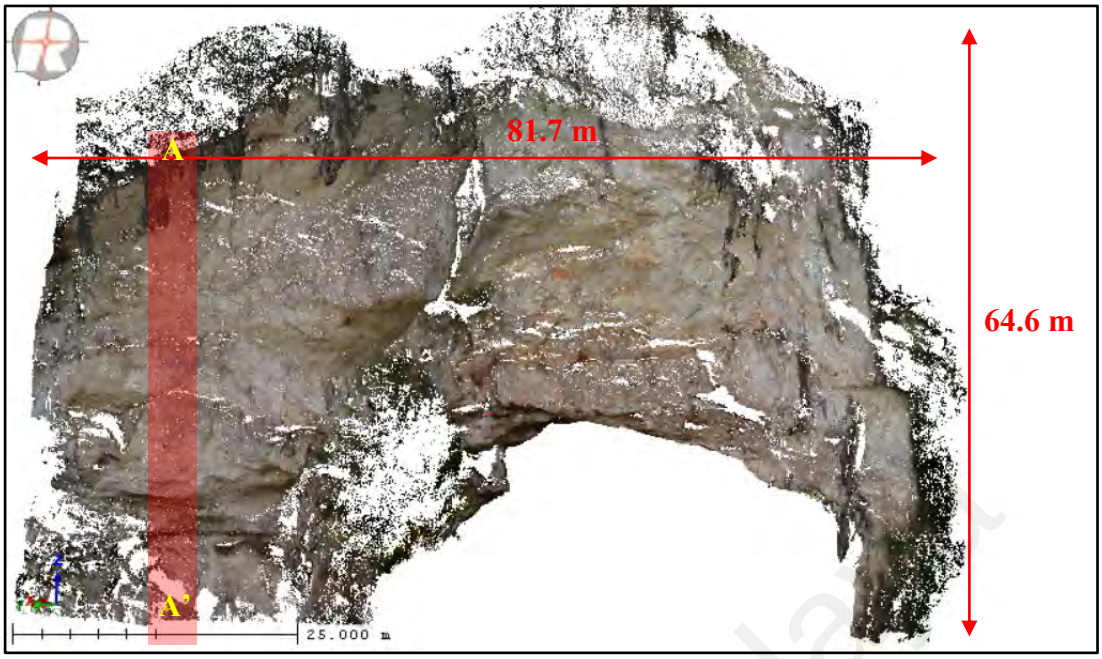

Figure 4.61: Slope geometry of KLT 1 (c). Figure shows the height, length, and the location of profile A-A' on the slope.

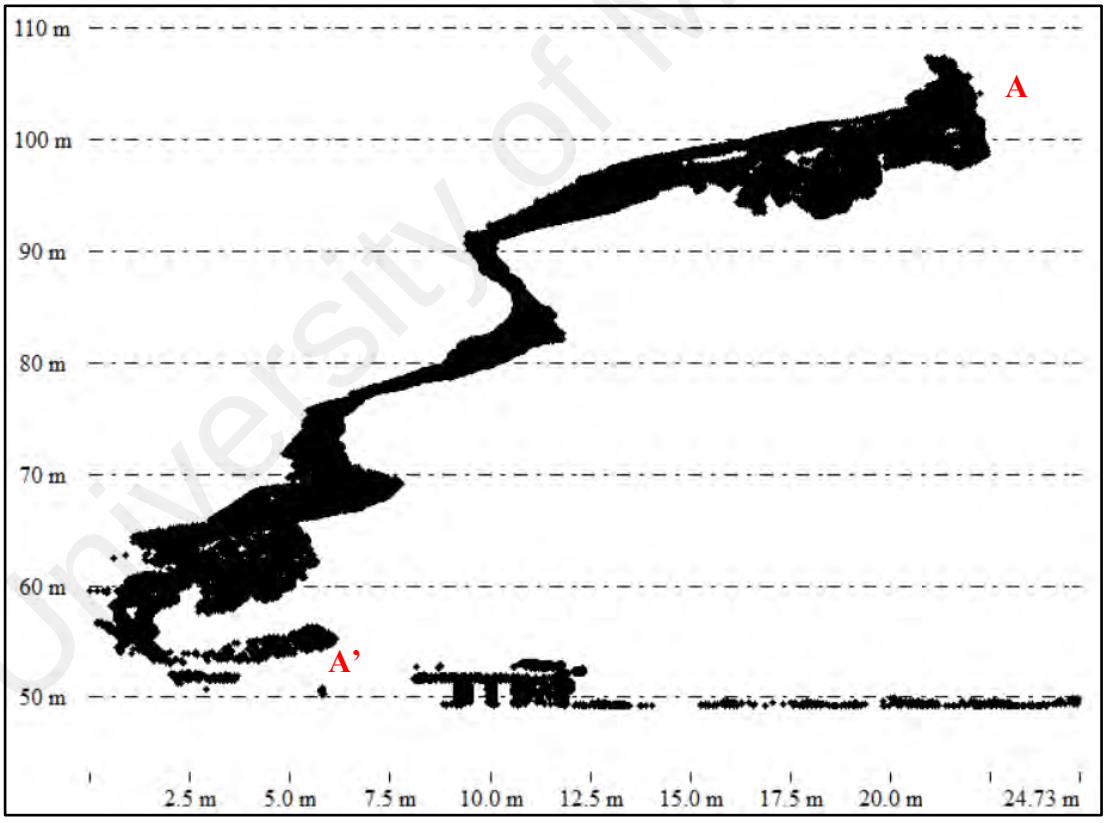

Figure 4.62: Profile A-A' of the slope KLT 1 (c).

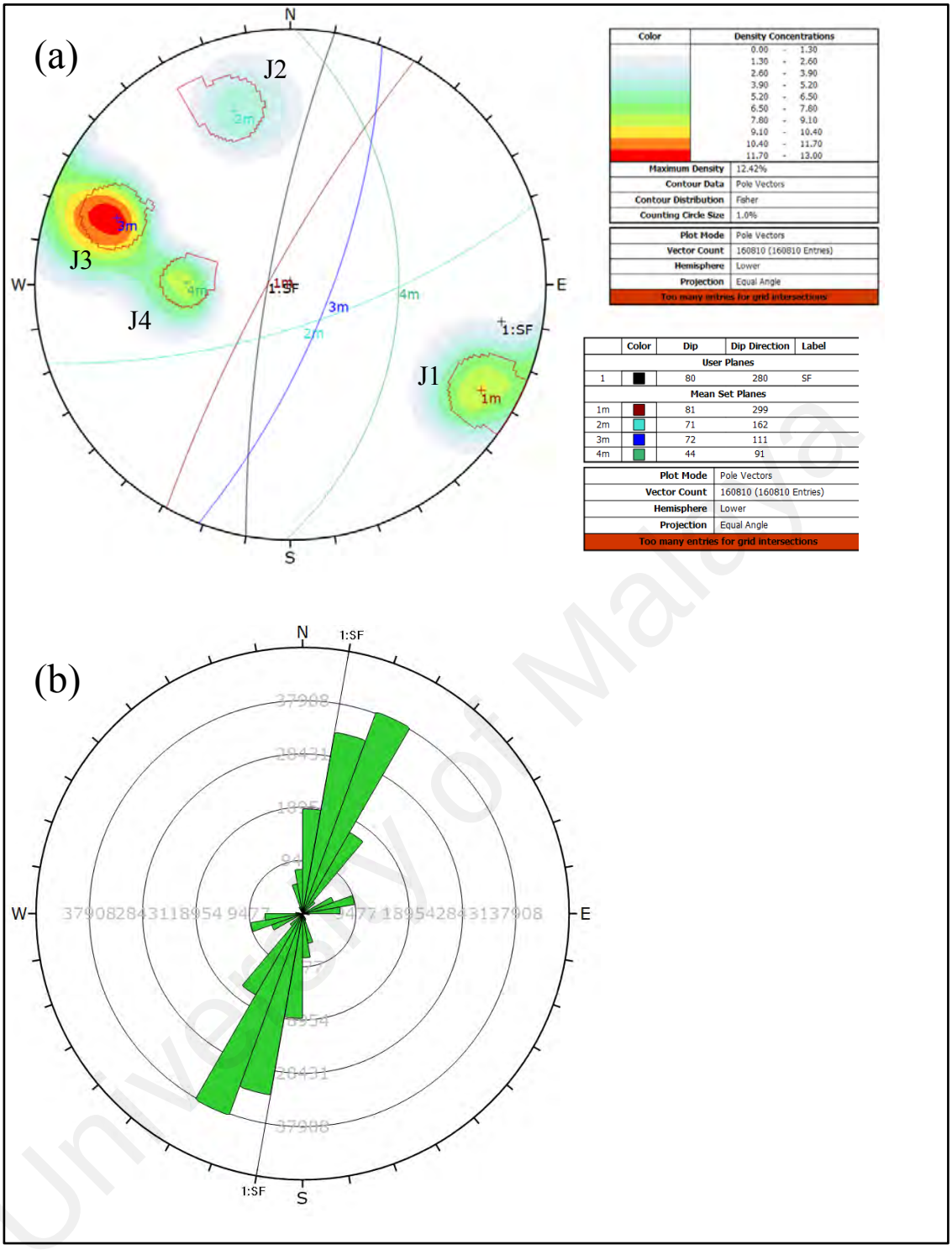

Figure 4.63: (a) Poles plot and major planes plot of all four joint sets in a stereonet (b) Rose plot showing the trend of all major joint sets and the slope face orientation in KLT 1 (c) slope. Based on the rose plot, most dominant joint sets orientation is trending northeast-southwest direction.

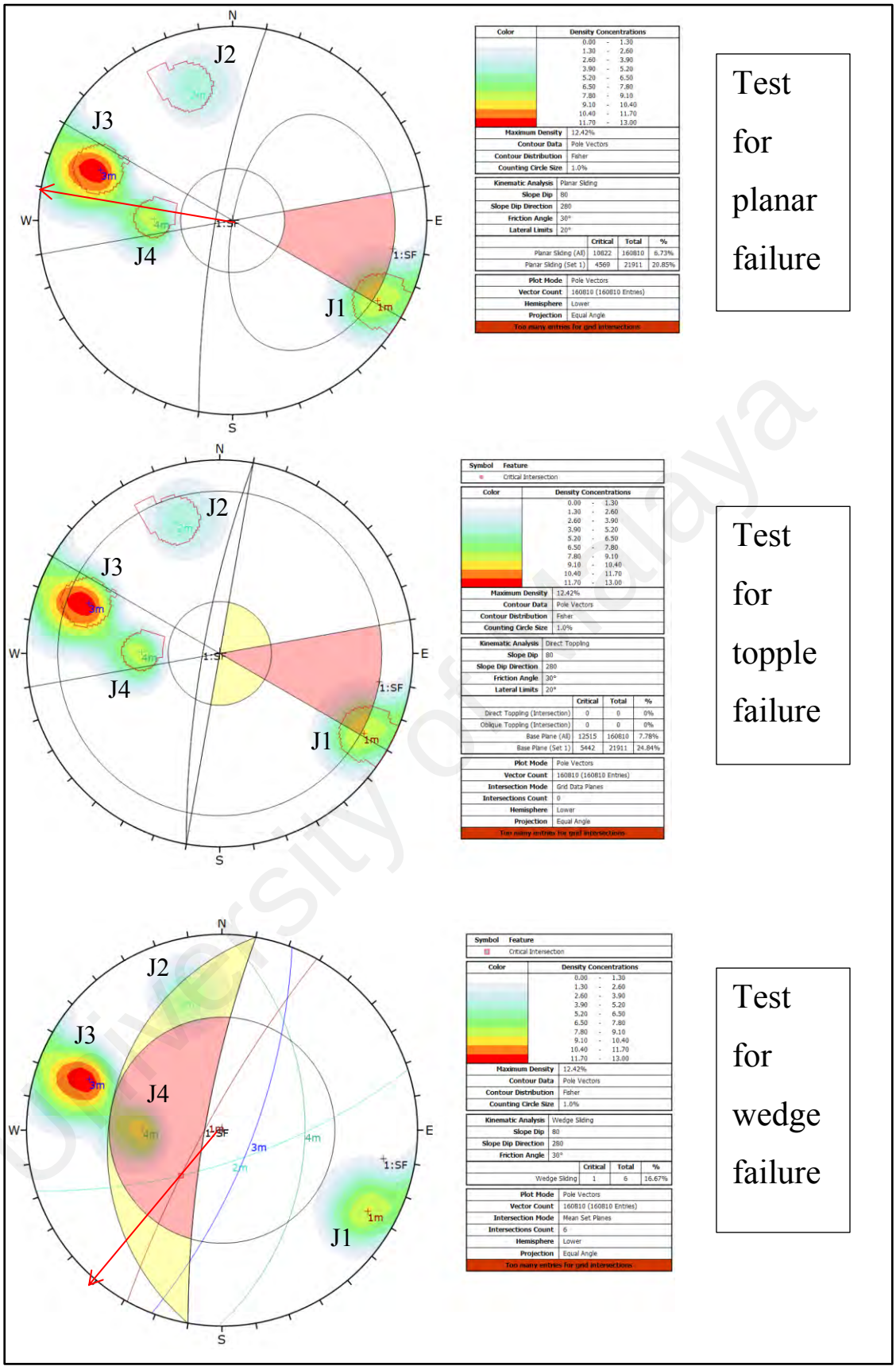

Figure 4.64: Kinematic analysis testing for planar failure, wedge failure, and topple failure in KLT 1 (c) slope. Red arrows represent the direction of possible failure.

4.3.1.4 KLT 2 Slope Stability Analysis

Based on the discontinuity selection from Coltop 3D, three number of joint sets has been identified which are J1 (64/279), J2 (80/108), and J3 (71/360) such as shown in Figure 4.66b. Major plane of the joint sets is plotted in the stereonet and the trend of discontinuity orientation is presented in the rose plot such in Figure 4.69. Based on the rose plot, major trend of discontinuity orientation is northeast-southwest direction with the slope face trend (85/100). Stability analysis test for planar, wedge, and topple failure are conducted and all of the possible failure are shown in Figure 4.70. For planar failure, one possible planar failure has been detected which involving joint sets from J2 (80/108) and the direction of failure is towards southeast direction (100^{o}). Figure 4.71 shows the example of potential planar failure on the slope. For topple failure, there is no failure detected, however, joint sets J2 (80/108) will act as the base plane for topple failure. For wedge failure, there is one possible wedge failure can be identified based on the kinematic analysis. The failure involving the intersection between joint sets J2 and J3 respectively. The direction of possible wedge failure is towards northeast direction (040^{o}). Slope geometry and slope cross section profile along A-A' are presented such as shown in Figure 4.67 and Figure 4.68. Manual and Lidar measurements are validated such as shown in Figure 4.72. Based on the validation in Table 4.21, the mean square error of the dip angle is 23.3, while for the dip direction is 14.8. Discontinuity reading from both manual and Lidar measurements are used for comparison such as shown in Table 4.22 and Table 4.23.

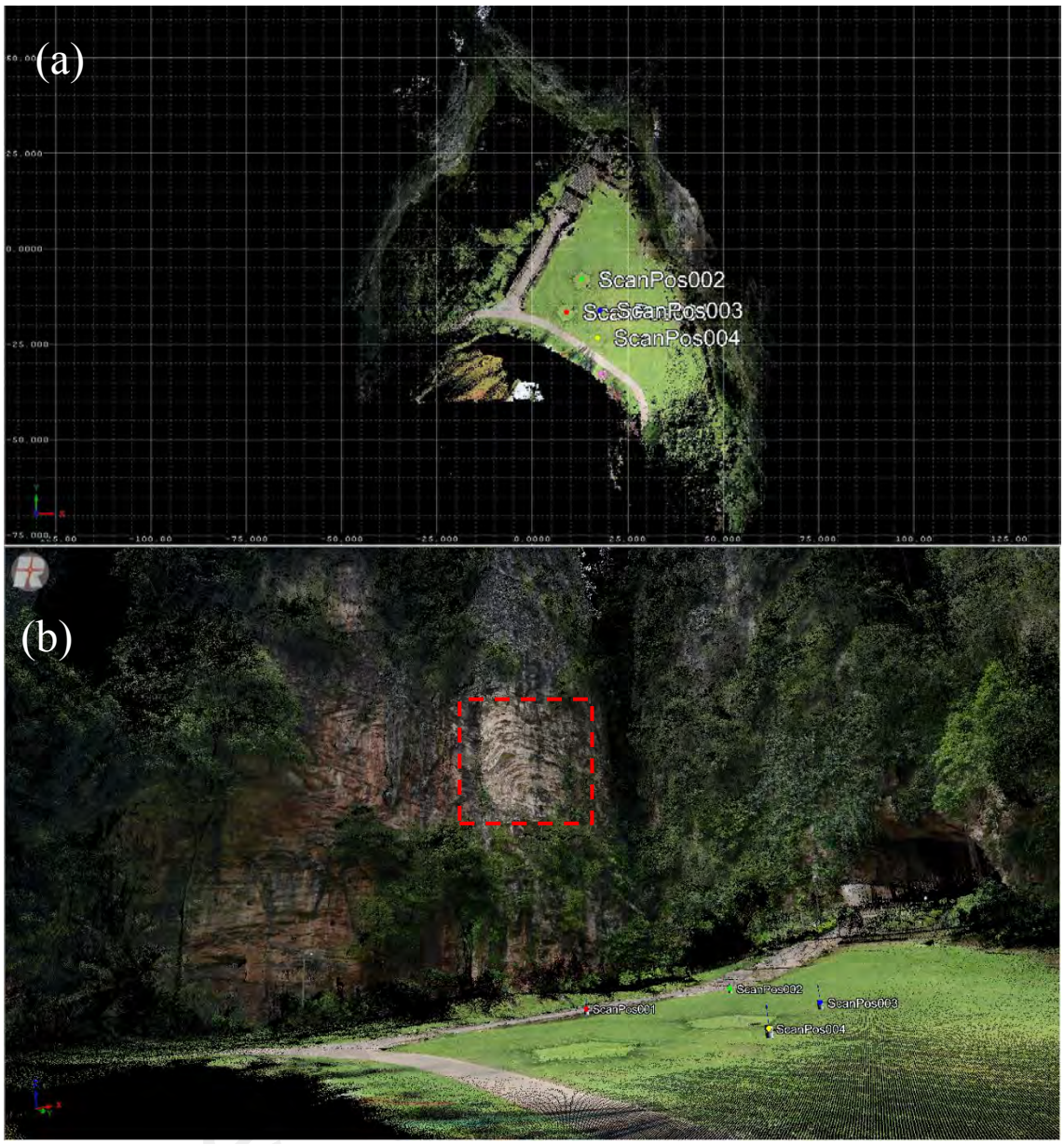

Figure 4.65: (a) Aerial view of 3D model of the KLT 2 slope together with the scanning position (b) The location of KLT 2 is exactly right after the cave exit. Red dotted box shows the area where the slope stability analysis was conducted.

A total number of four scanning positions were conducted in order to cover all side of the hills, however there is still some limitation that creates shadow zone and some occlusions on the data. Some of the thick vegetation presence on the slope face may also produce occlusions.

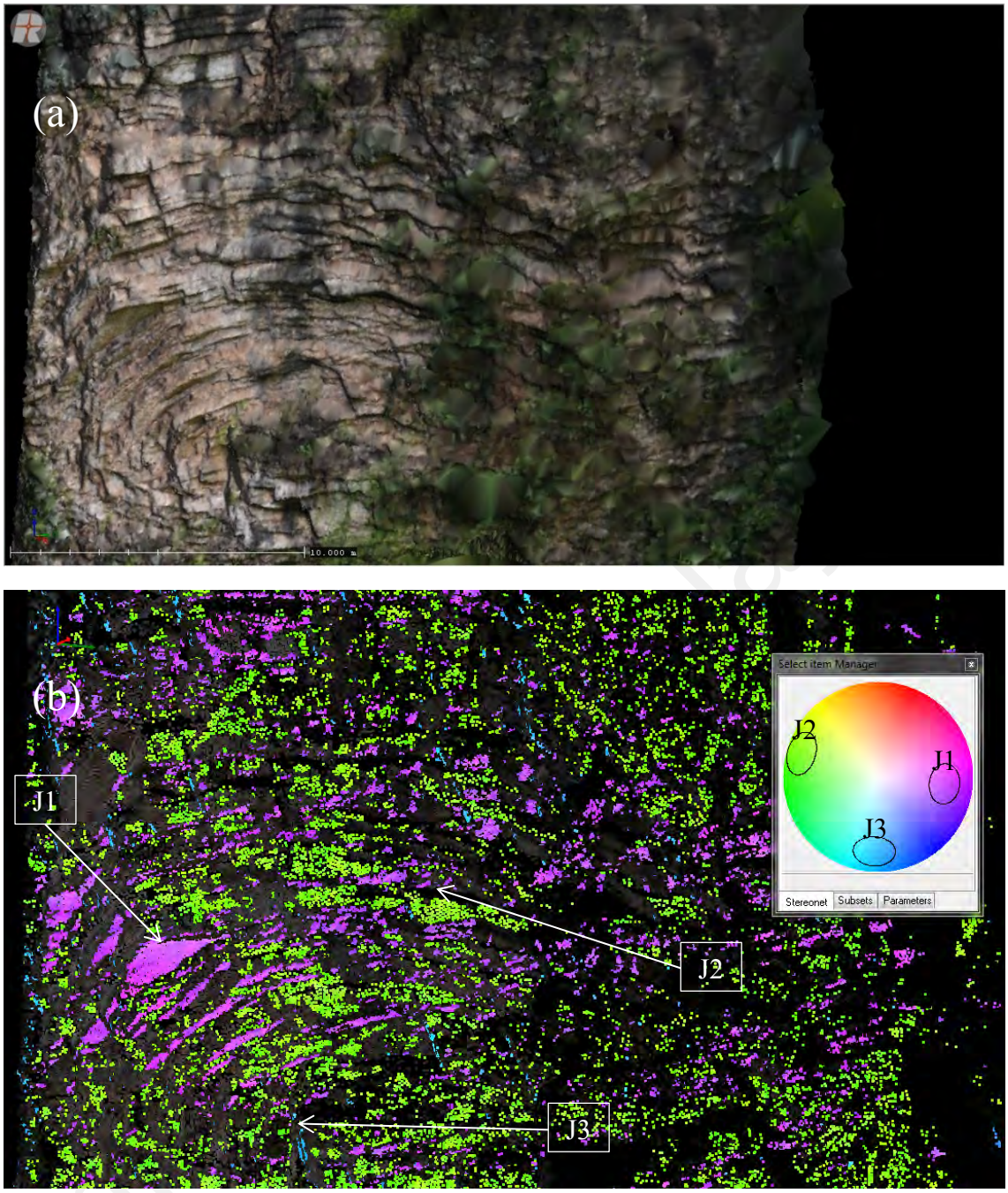

Figure 4.66: (a) Digital Terrain Model of KLT 2 slope (b) 3D discontinuity model derived from Coltop 3D, based on the model, three joint sets has been identified which are J1 (64/279), J2 (80/108), and J3 (71/360) respectively.

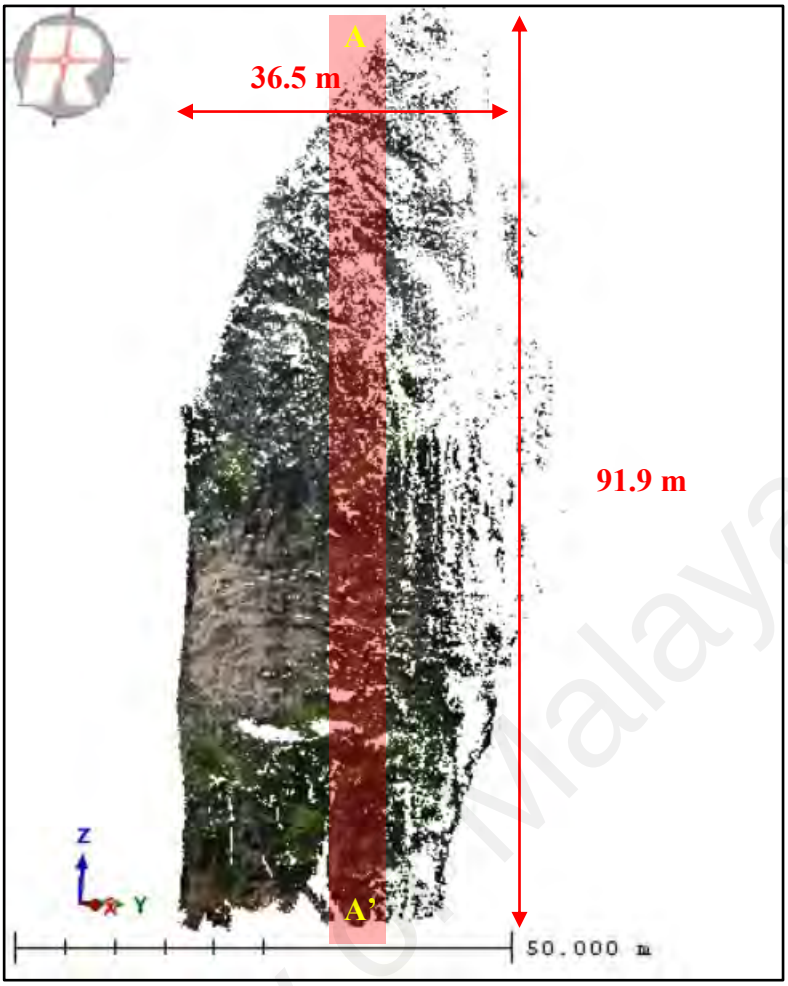

Figure 4.67: Slope geometry of KLT 2. Figure shows the height, length, and the location of profile A-A' on the slope.

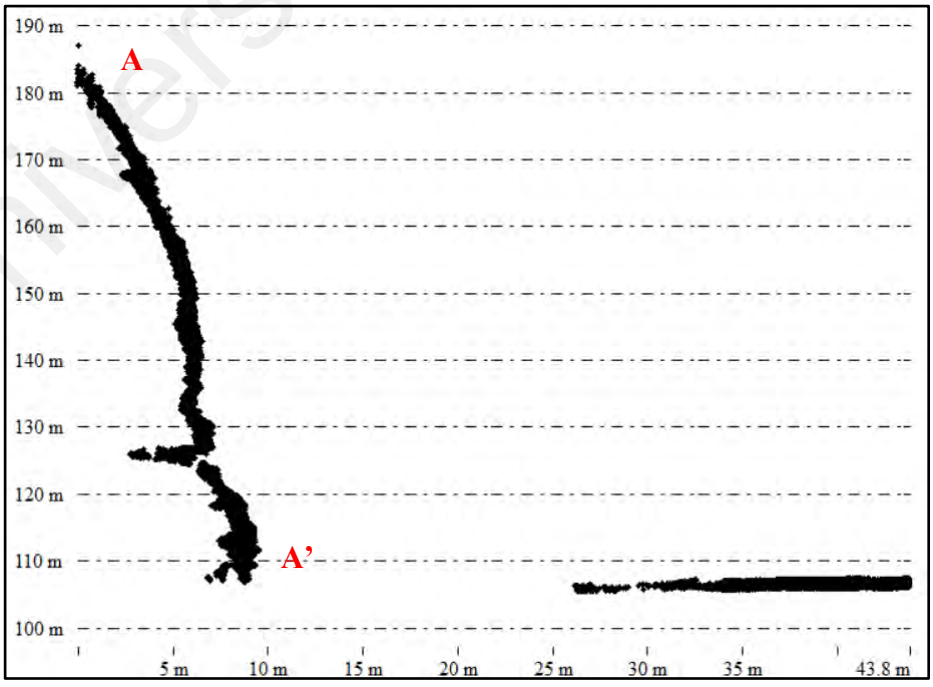

Figure 4.68: Profile A-A' of slope KLT 2.

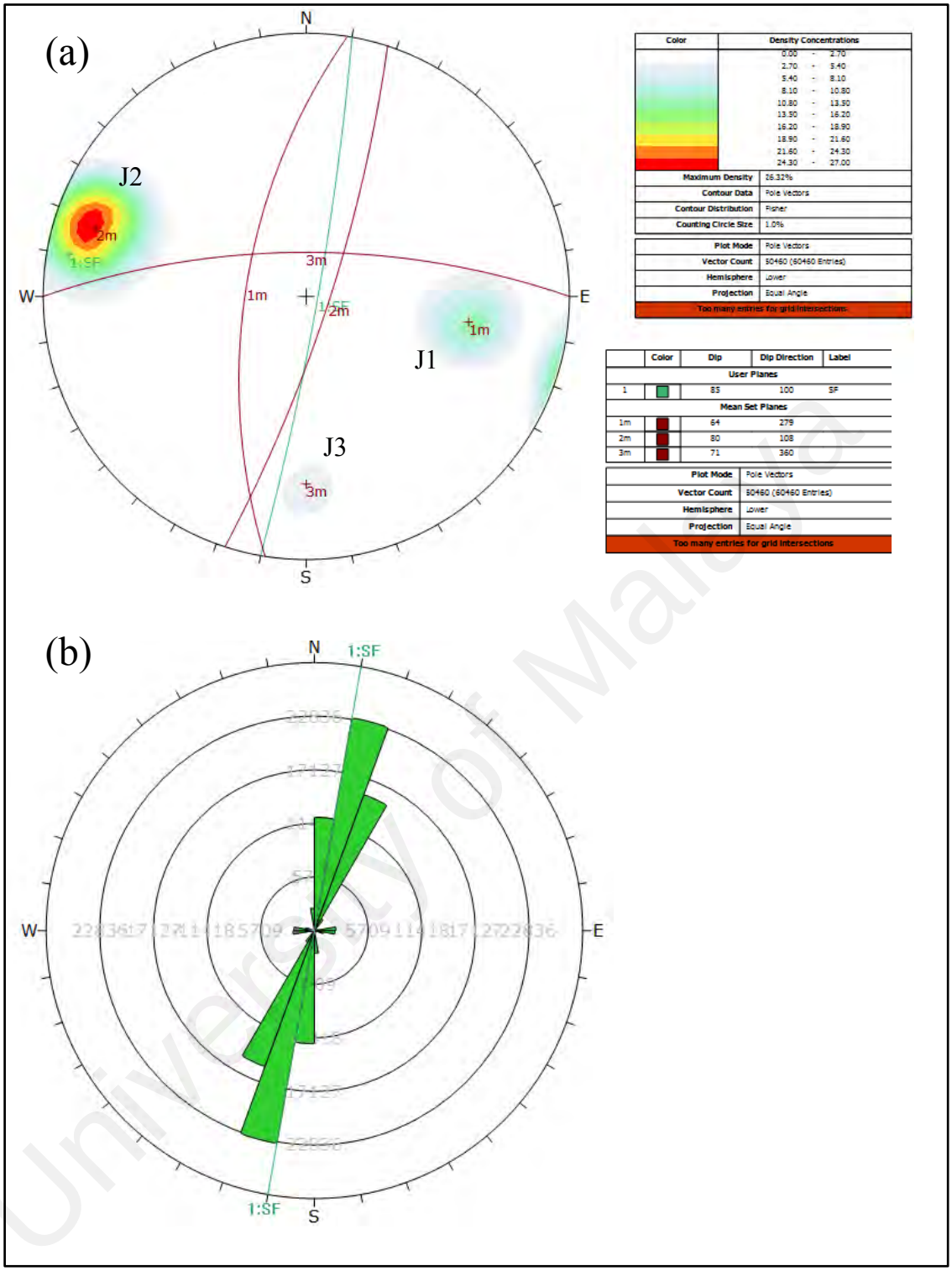

Figure 4.69: (a) Poles plot and major planes plot of all three joint sets in a stereonet (b) Rose plot showing the trend of all major joint sets and the slope face orientation in KLT 2 slope. Based on the rose plot, most dominant joint sets orientation is trending northeast-southwest direction.

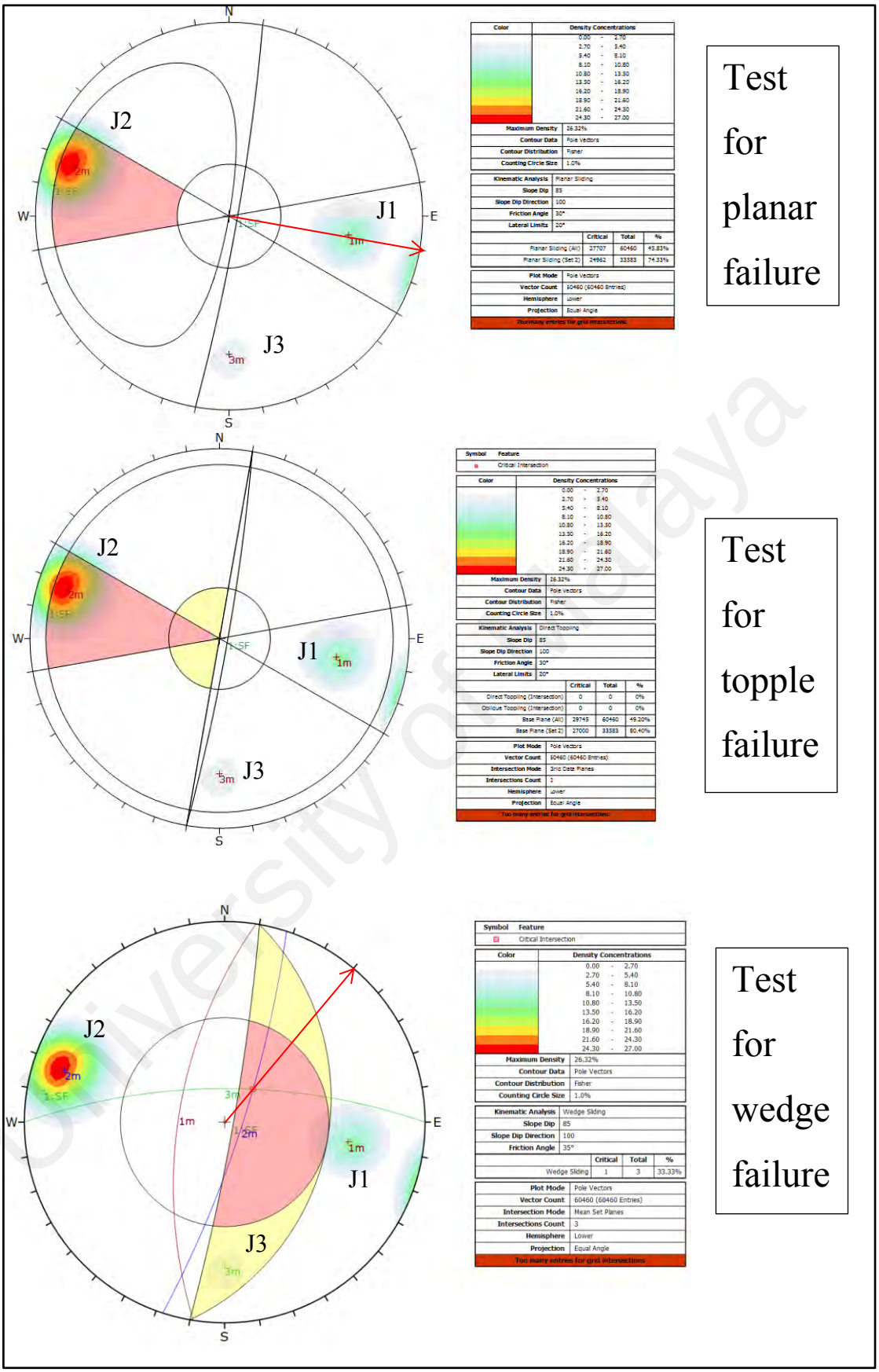

Figure 4.70: Kinematic analysis testing for planar failure, wedge failure, and topple failure in KLT 2 slope. Red arrows represent the direction of possible failure.

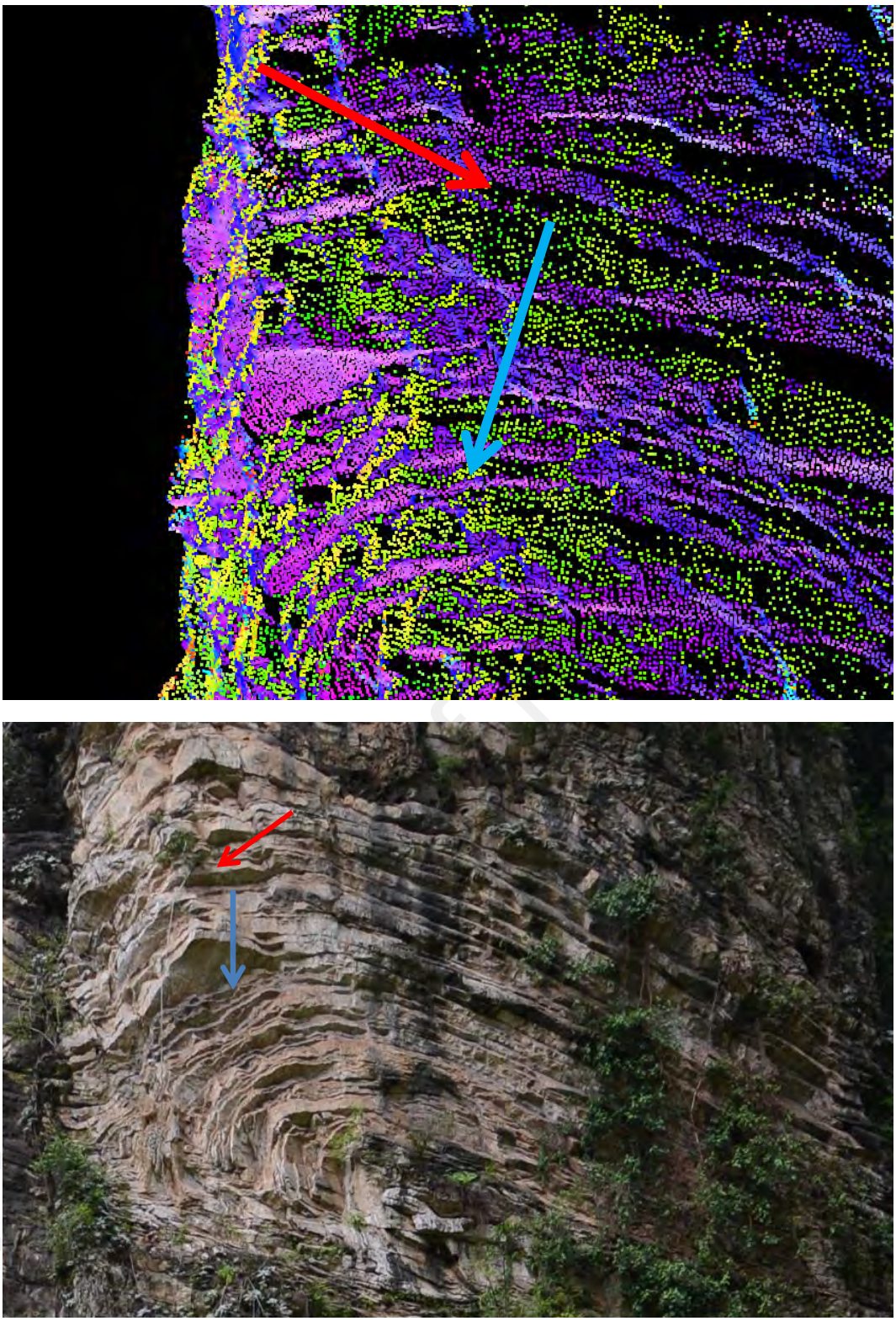

Figure 4.71: Example of possible planar failure involving J2 (80/100) in green point cloud view, Blue arrow represents the dip direction of J2 joints which is daylighting and is a potential for planar failure. Red arrow represents J1 (64/279) dipping direction which is dipping into the slope.

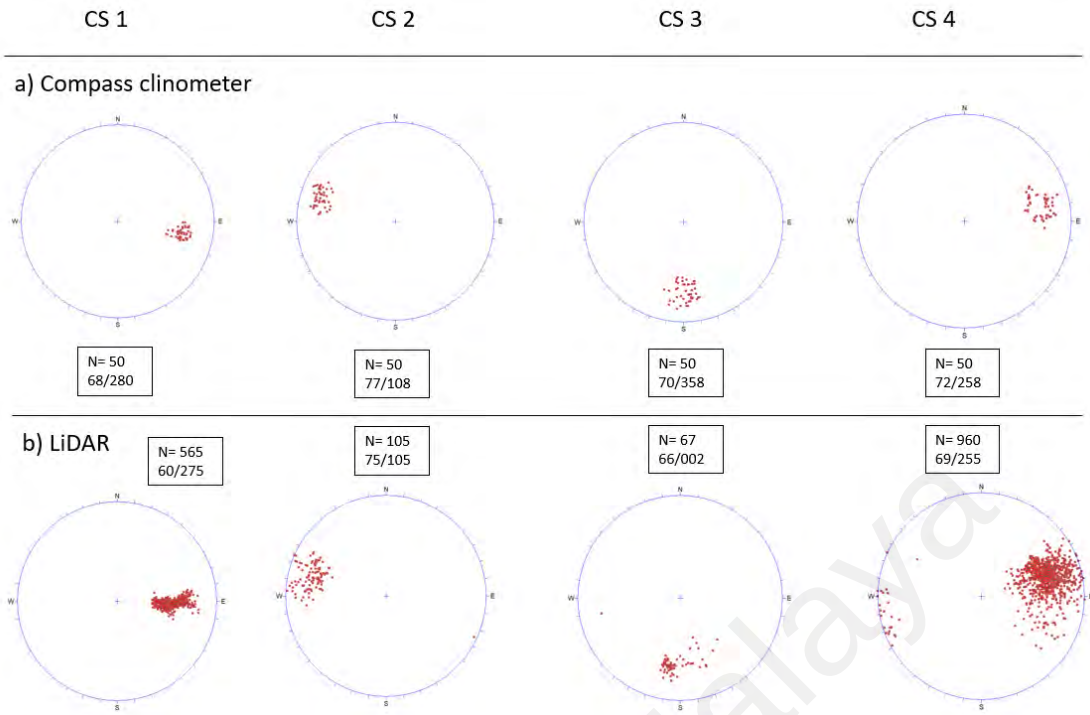

Figure 4.72: Lidar measurement validation with manual measurement at KLT 2 slope. Four control surfaces CS1, CS2, CS3, and CS4 which represent the joint planes were selected on the slope for validation purposes.

Table 4.21: Validation at KLT 2.

Control surfaces	Compass clinometer		Lidar measurements		Mean square error	
	Dip angle	Direction	Dip angle	Direction	Dip angle	Direction
CS 1	68	280	60	275	23.3	14.8
CS 2	77	108	75	105		
CS 3	70	358	66	002		
CS 4	72	258	69	255		

Figure 4.73: KLT 2 slope.

Table 4.22: Manual measurements KLT 2.

Set	Dip Direction	Dip Angle	Joints Spacing (mm)	Trace length (m)	Seepage
J1	270	70	60-200	1-3	Dry
J2	115	75	60-200	1-3	Dry

Table 4.23: Lidar measurements at KLT 2.

Set	Dip Direction	Dip Angle	Joints Spacing (mm)	Trace length (m)	Seepage
J1	279	64	60-200	1-3	Dry
J2	108	80	60-200	1-3	Dry
J3	360	71	60-200	3-10	Dry

4.3.1.5 KLT 3 Slope Stability Analysis

Based on the discontinuity selection from Coltop 3D, three number of joint sets has been identified which are J1 (36/276), J2 (74/095), and J3 (72/029) respectively in Figure 4.75b. Major planes of joint sets is plotted in the stereonet and the trend of discontinuity orientation is presented in the rose plot such as in Figure 4.78. Based on the rose plot, major trend of discontinuity orientation is towards slightly northeast-southwest direction with the slope face trend (80/090). Stability analysis test for planar, wedge, and topple failure are conducted and all of the possible failure are shown in Figure 4.79. For planar failure, some of poles from joints sets J2 (74/095) satisfy the criteria for planar failure and the direction of planar failure is towards east direction (090^{o}). For topple failure, there is no potential topple failure detected. However, joint sets J2 (74/095) will act as the base plane for topple failure. For wedge failure, there is one possible wedge detected which involving the intersection between joint sets J2 and J3 respectively. The direction of possible wedge failure is towards northeast direction (055^{o}). Slope geometry and cross section profile of the slope are presented in Figure 4.76 and Figure 4.77. Manual and Lidar measurements are validated such in Figure 4.80. Based on the validation in Table 4.24, the mean square error for the dip angle is 14.3, while for the dip direction is 9.5. Discontinuity reading from manual and Lidar method are used for comparison such as shown in Table 4.25 and Table 4.26.

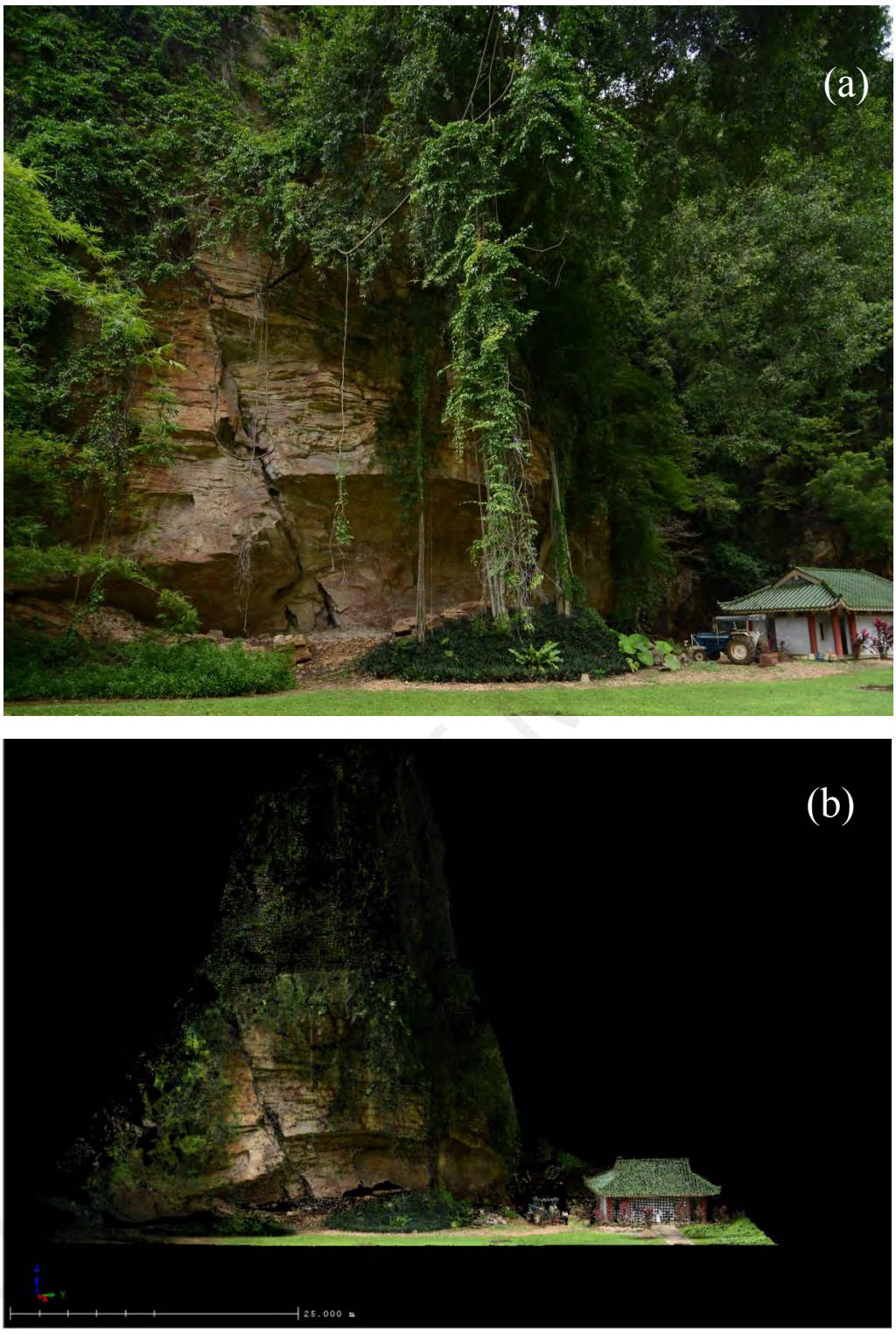

Figure 4.74: (a) Image taken by Nikon D800 camera showing the location of KLT 3 slope (b) Digital Terrain Model (DTM) of the slope with true color display.

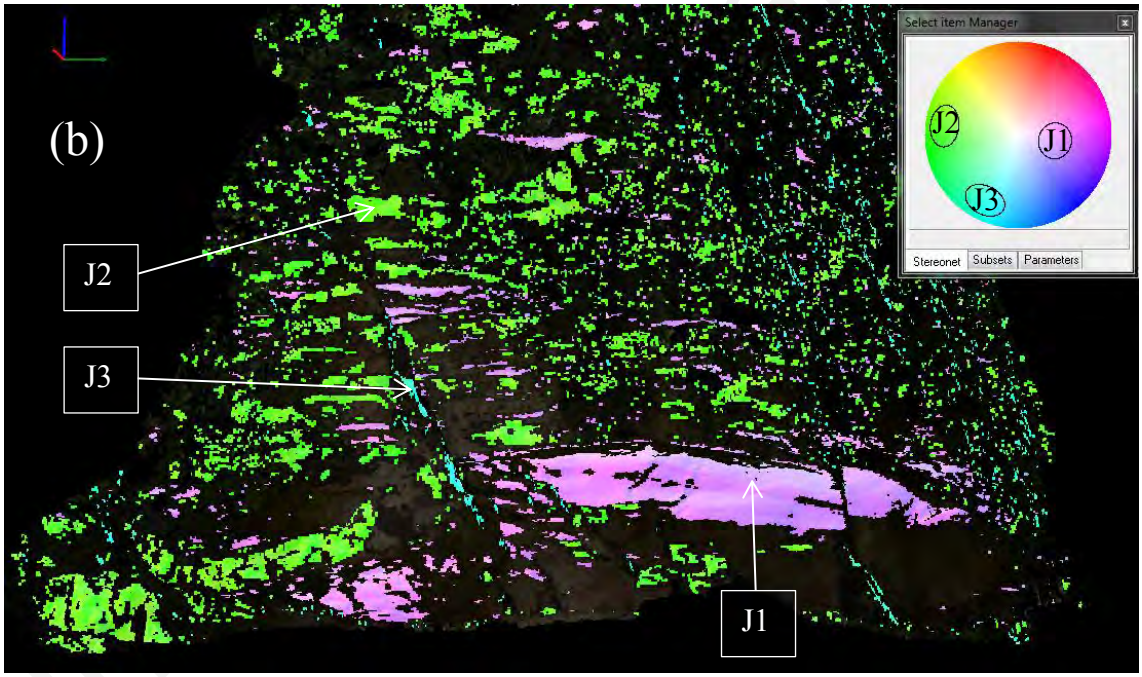

Figure 4.75: (a) True colour display of slope KLT 3 DTM (b) 3D discontinuity model derived from Coltop 3D, based on the model, three numbers of joint sets has been identified which are J1 (36/276), J2 (74/095), and J3 (72/029) respectively.

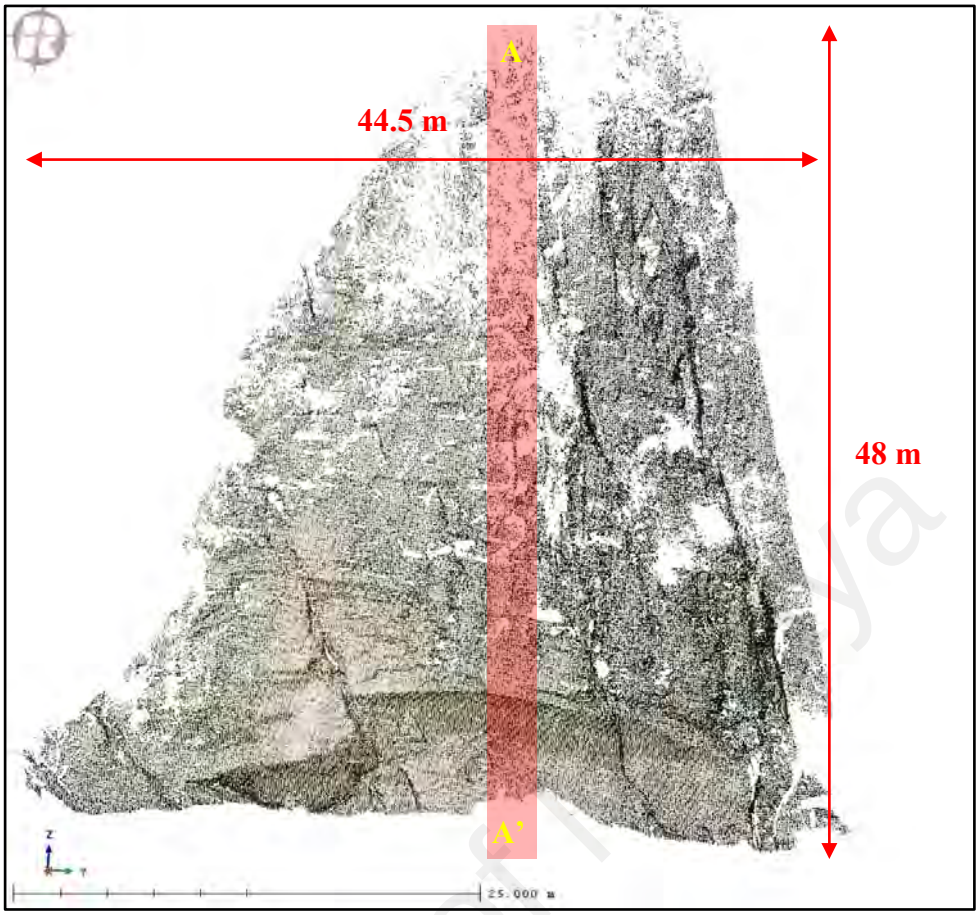

Figure 4.76: Slope geometry of KLT 3. Figure shows the height, length, and the location of profile A-A' on the slope.

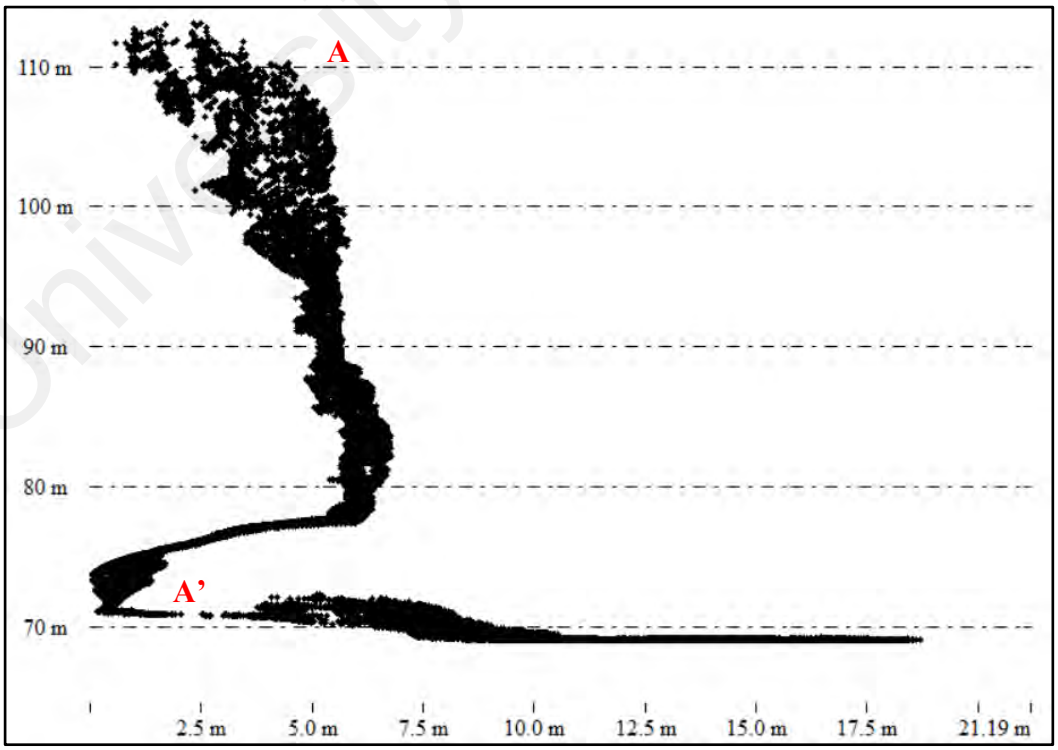

Figure 4.77: Profile A-A' of KLT 3.

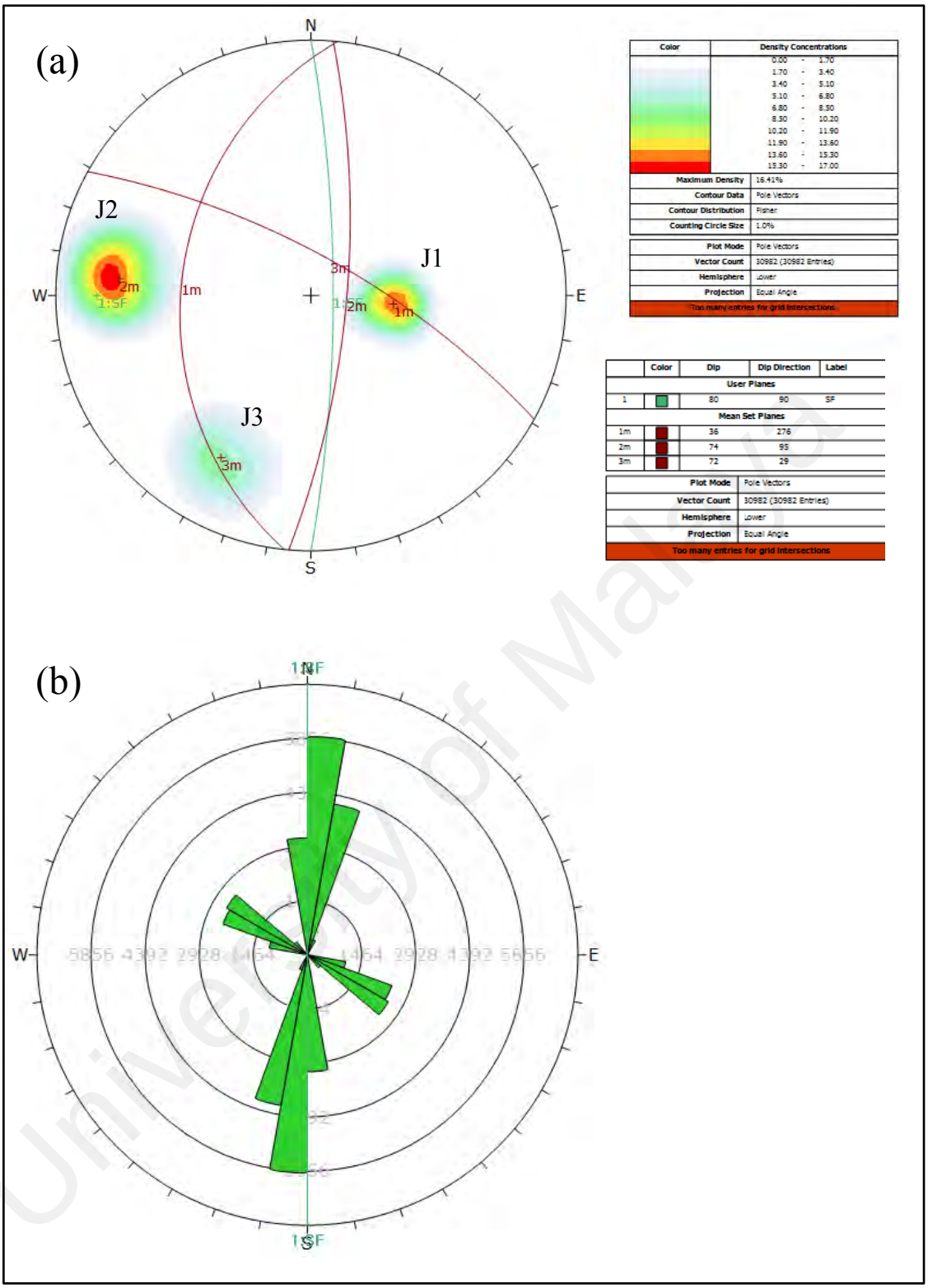

Figure 4.78: a) Poles plot and major planes plot of all three joint sets in a stereonet (b) Rose plot showing the trend of all major joint sets and the slope face orientation in KLT 3 slope. Based on the rose plot, most dominant joint sets orientation is trending slightly northeast-southwest direction.

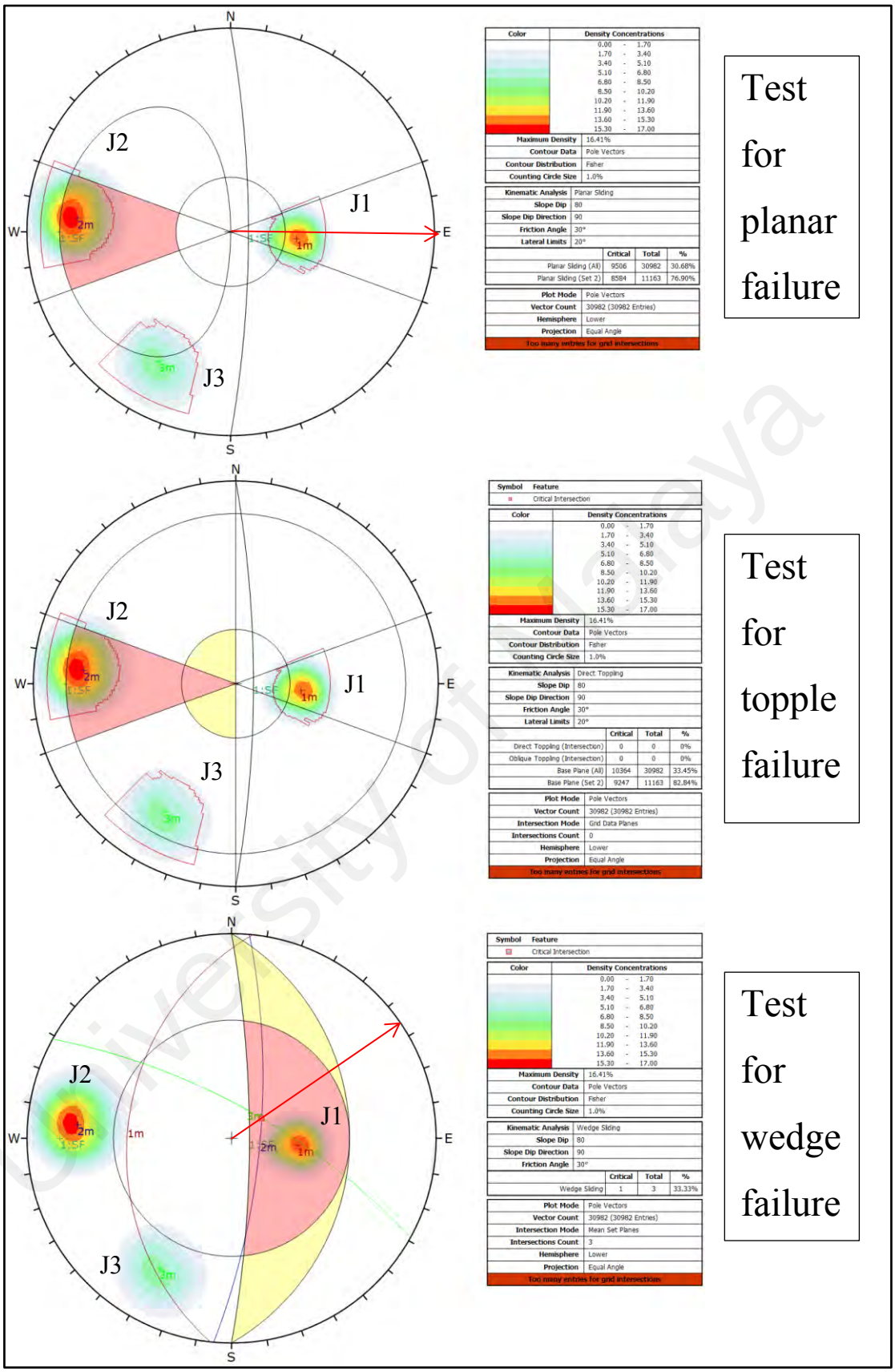

Figure 4.79: Kinematic analysis testing for planar failure, wedge failure, and topple failure in KLT 3 slope. Red arrows represent the direction of possible failure.

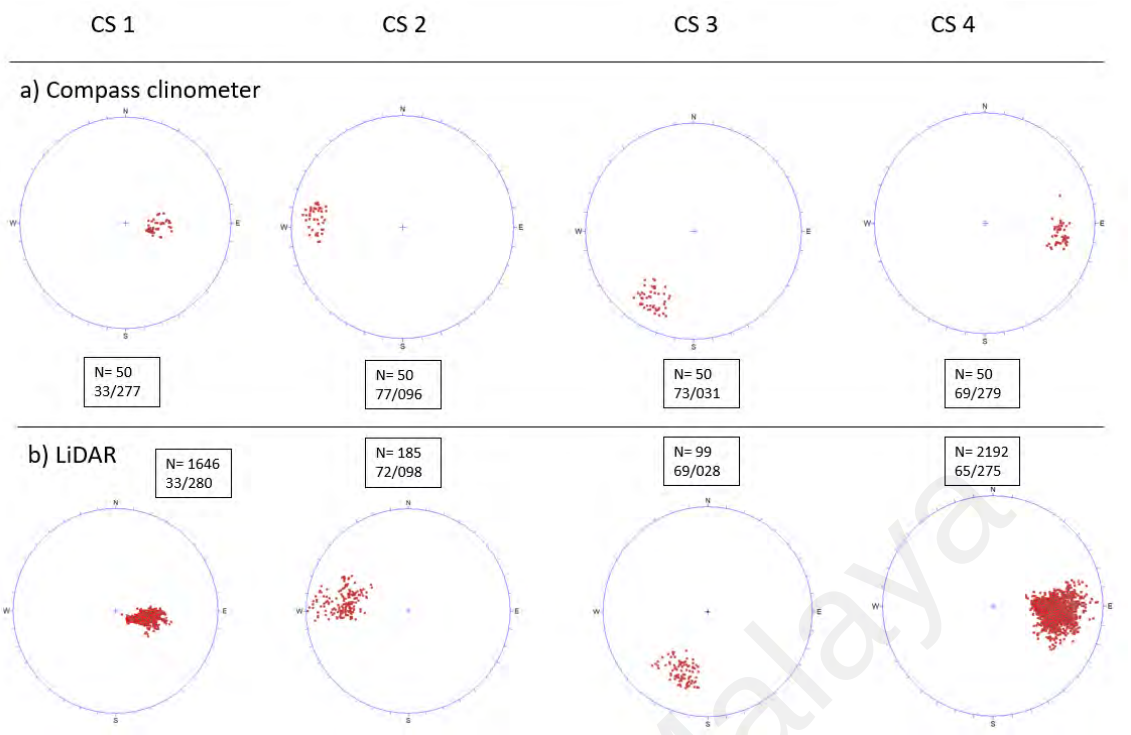

Figure 4.80: Lidar measurement validation with manual measurement at KLT 3 slope. Four control surfaces CS1, CS2, CS3, and CS4 which represent the joint planes were selected on the slope for validation purposes.

Table 4.24: Validation at KLT 3.

Control surfaces	Compass clinometer		Lidar measurements		Mean square error	
	Dip angle	Direction	Dip angle	Direction	Dip angle	Direction
CS 1	33	277	33	280	14.3	9.5
CS 2	77	096	72	098		
CS 3	73	031	69	028		
CS 4	69	279	65	275		

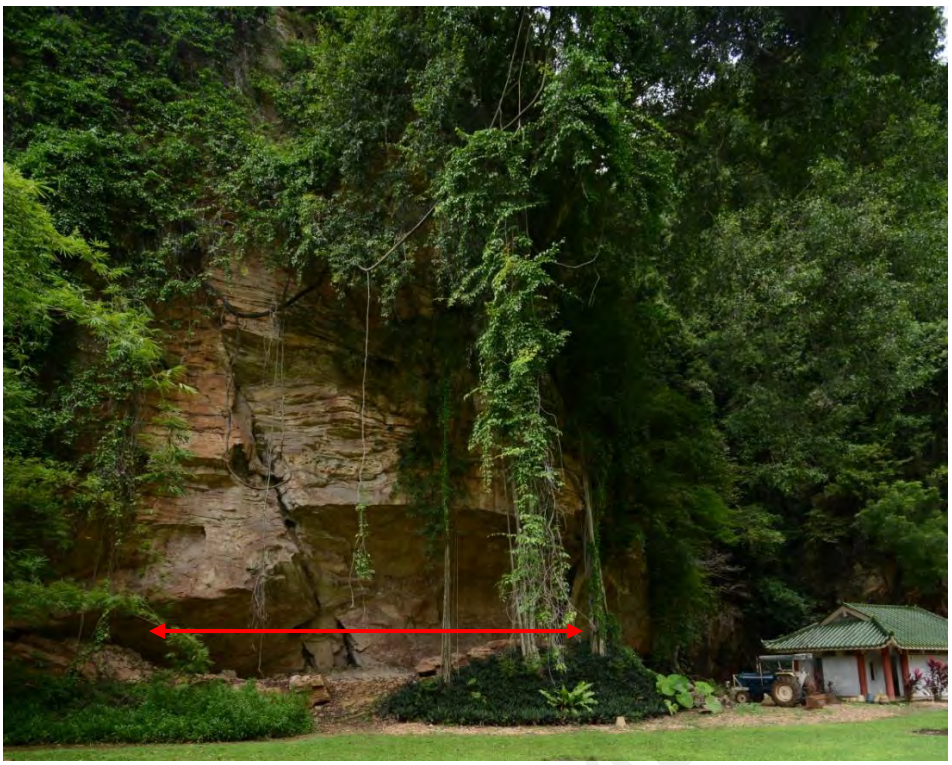

Figure 4.81: KLT 3 slope.

Table 4.25: Manual measurements at KLT 3.

Set	Dip Direction	Dip Angle	Joints Spacing (mm)	Trace length (m)	Seepage
J1	279	40	200-600	3-10	Dry
J2	100	70	200-600	3-10	Dry
J3	032	70	600-2000	>20	Dry

Table 4.26: Lidar measurements at KLT 3.

Set	Dip Direction	Dip Angle	Joints Spacing (mm)	Trace length (m)	Seepage
J1	276	36	200-600	3-10	Dry
J2	095	74	200-600	3-10	Dry
J3	029	72	600-2000	>20	Dry

4.3.2 Kwan Yin Tong Temple

Figure 4.82: Location map of Kwan Yin Tong temple (Google maps).

Kwan Yin Tong temple is located at Gunung Rapat limestone hills, which is two kilometre distance from Kek Lok Tong. The temple is located beside the main road of Jalan Raja Dr Nazrin Shah (Figure 4.82). The height of the slope is approximately 100 meter high from the ground level, while the length of the slope is 150 meter long. The reason why slope stability analysis is conducted on this slope is because the location of the temple which is based below the overhanging limestone block (Figure 4.83).

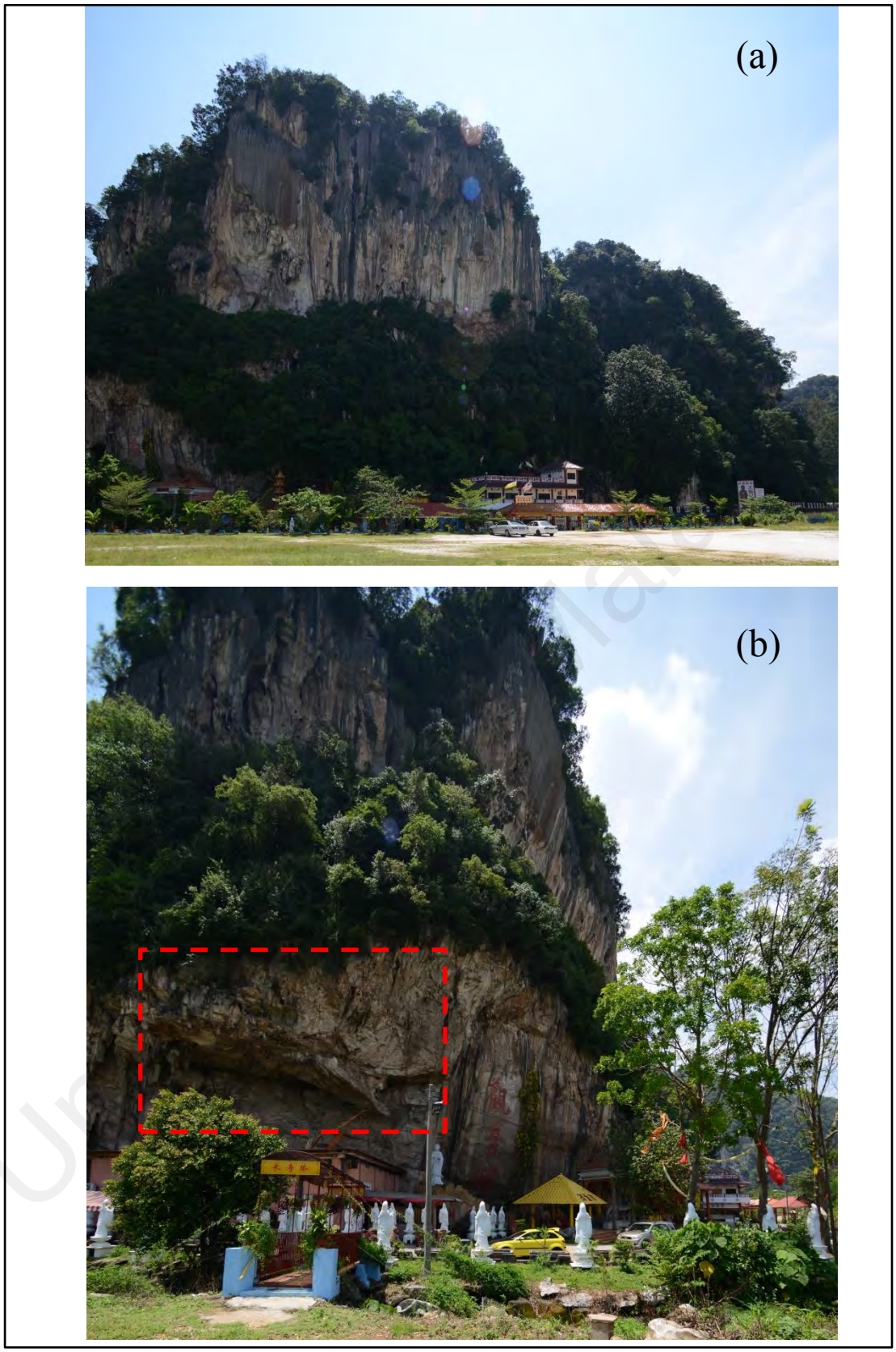

Figure 4.83: (a) Kwan Yin Tong temple location in the limestone hills (b) Location of temple below the overhanging limestone block (red dotted box).

3D terrestrial laser scanning was conducted in the area with a total number of 10 scanning position along the slope (Figure 4.84). The slope is divided into two parts which are KYT (a) and KYT (b) respectively as shown in Figure 4.85. Both of the slope are inaccessible because of its location at high elevation and position of the temple which is very close to the slope.

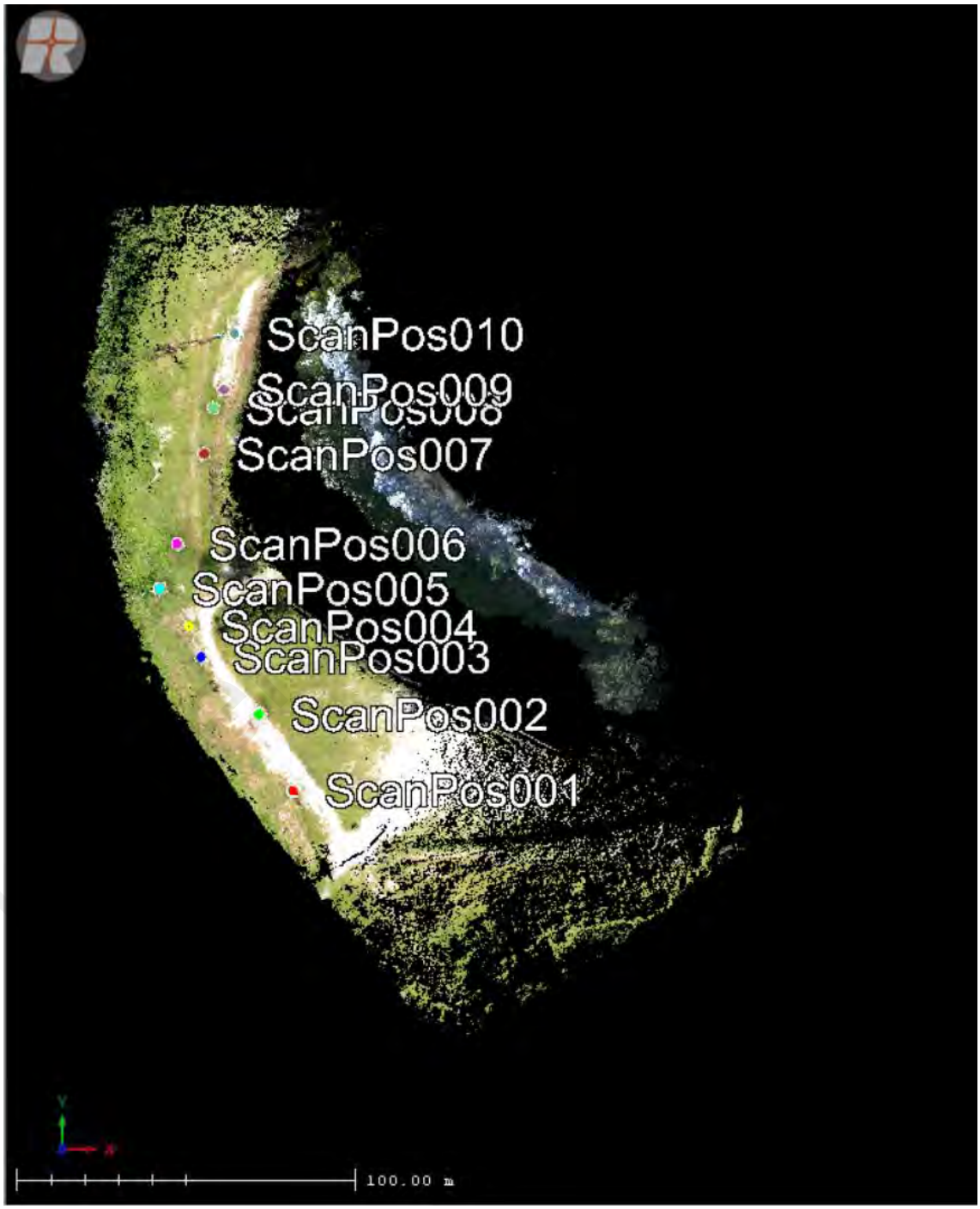

Figure 4.84: 10 number of scanning positions set up along the slope.

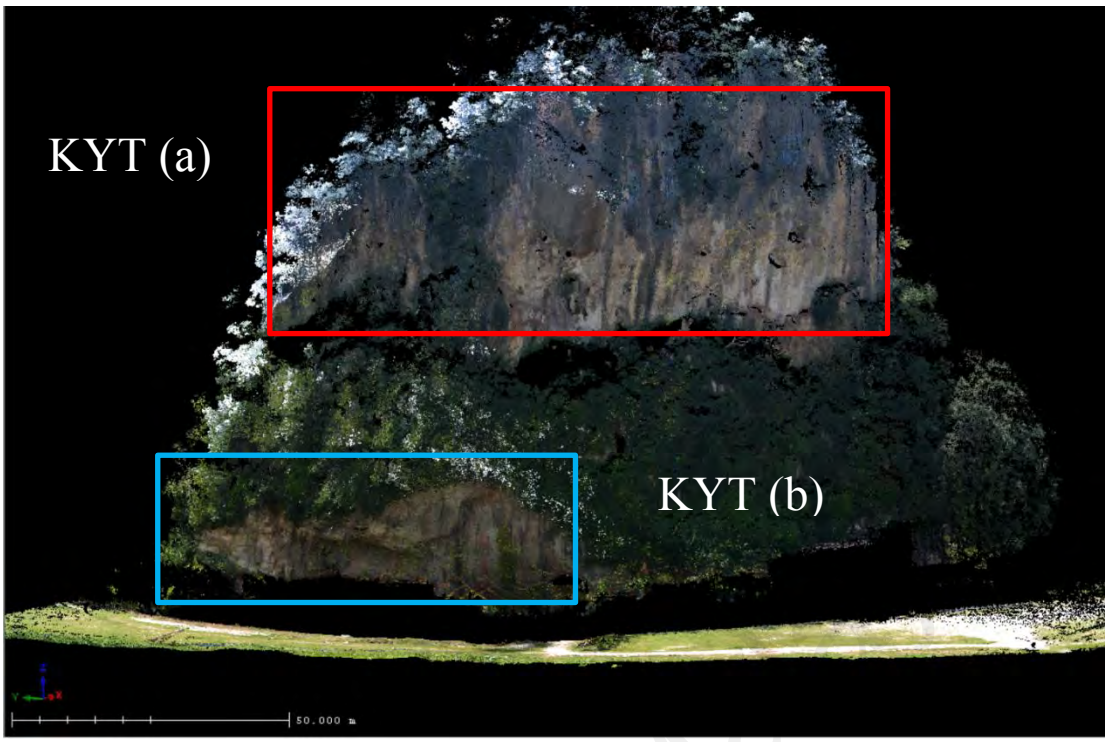

Figure 4.85: Slope division for stability analysis of KYT (a) in red box and KYT (b) in blue box.

4.3.2.1 KYT (a) Slope Stability Analysis

Based on the discontinuity selection from Coltop 3D software and the kinematic analysis, four joint sets have been identified at the KYT (a) slope which are J1 (80/349), J2 (81/224), J3 (83/247), and J4 (83/247) such as shown in Figure 4.87. Major plane of the joint sets is plotted in the stereonet and the trend of discontinuity orientation is presented in the rose plot (Figure 4.90). Based on the rose plot, trend of discontinuity orientation is towards northwest-southeast direction and with the slope face trend of (80/230). Stability analysis test for planar, wedge, and topple failure are conducted and all of the possible failure are shown in Figure 4.91. For planar failure, there are two possible planar failure which involving joint sets J2 (81/224) and J3 (83/247). The direction of planar failure is towards southwest direction (230^{o}). For topple failure, there is no potential topple failure detected. However joint sets J2 (81/224) and J3 (83/247) will act as the base plane for topple failure. For wedge failure, there are one potential

wedge failure recorded which involving the intersection between joint sets J2 (81/224) with J3 (83/247). The direction of wedge failure is towards northeast direction (290°). There is no manual scanline survey conducted in this slope because of inaccessible position of the slope and the location of the temple which is near to the slope.

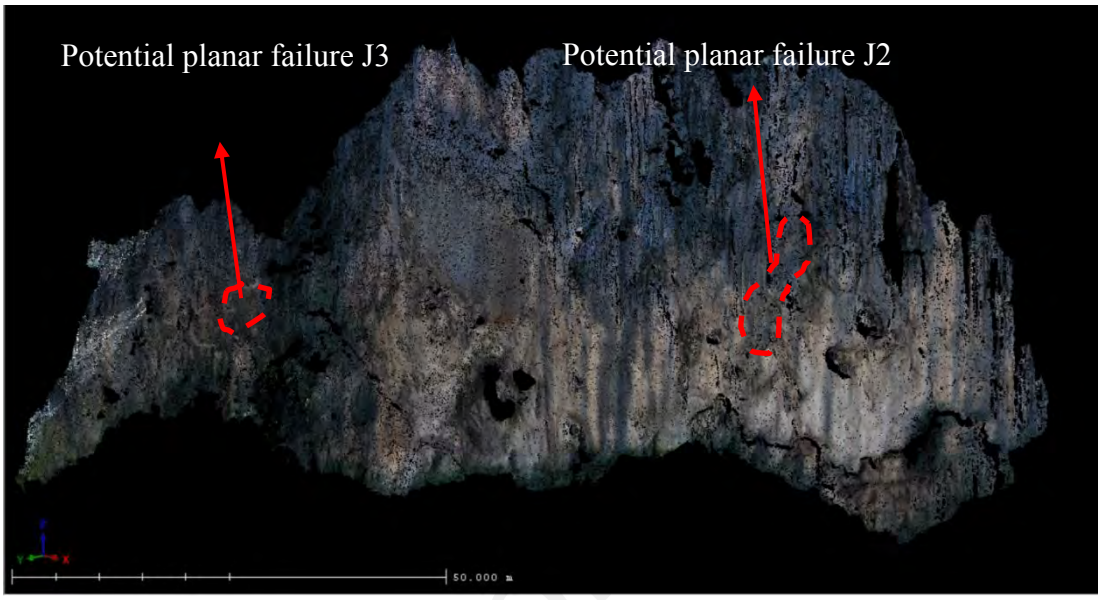

Figure 4.86: Overall view of Digital Terrain Model (DTM) of slope KYT (a) in true color display.

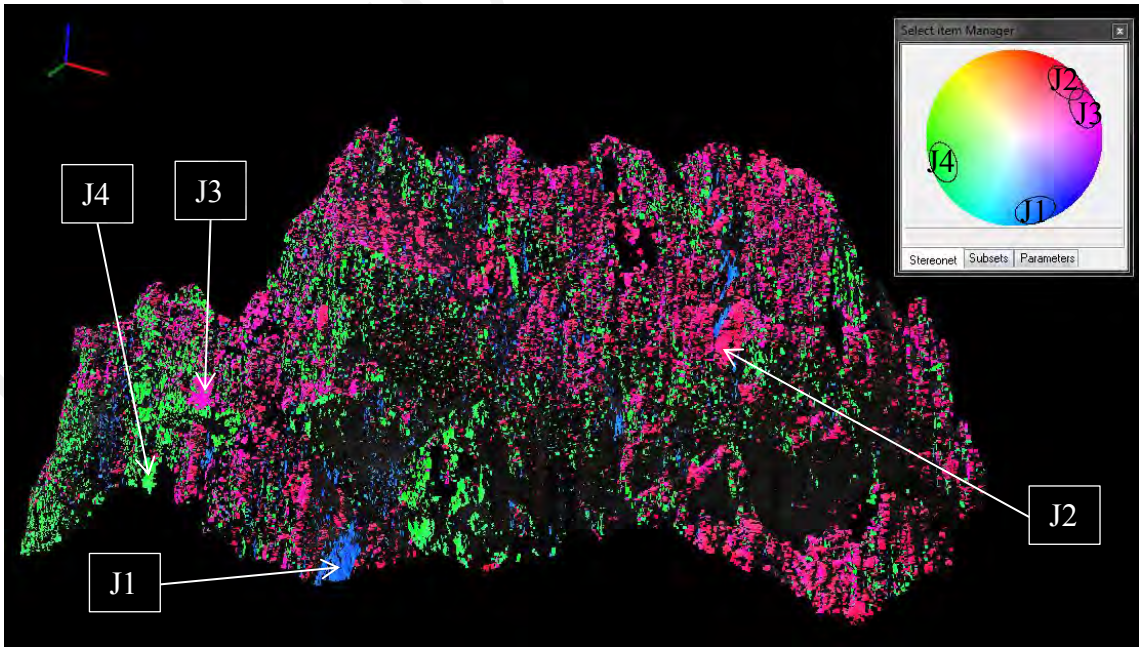

Figure 4.87: 3D discontinuity model derived from Coltop 3D software, based on the discontinuity selection, there are four joint sets that have been identified which are J1 (80/349), J2 (81/224), J3 (83/247), and J4 (76/068) respectively.

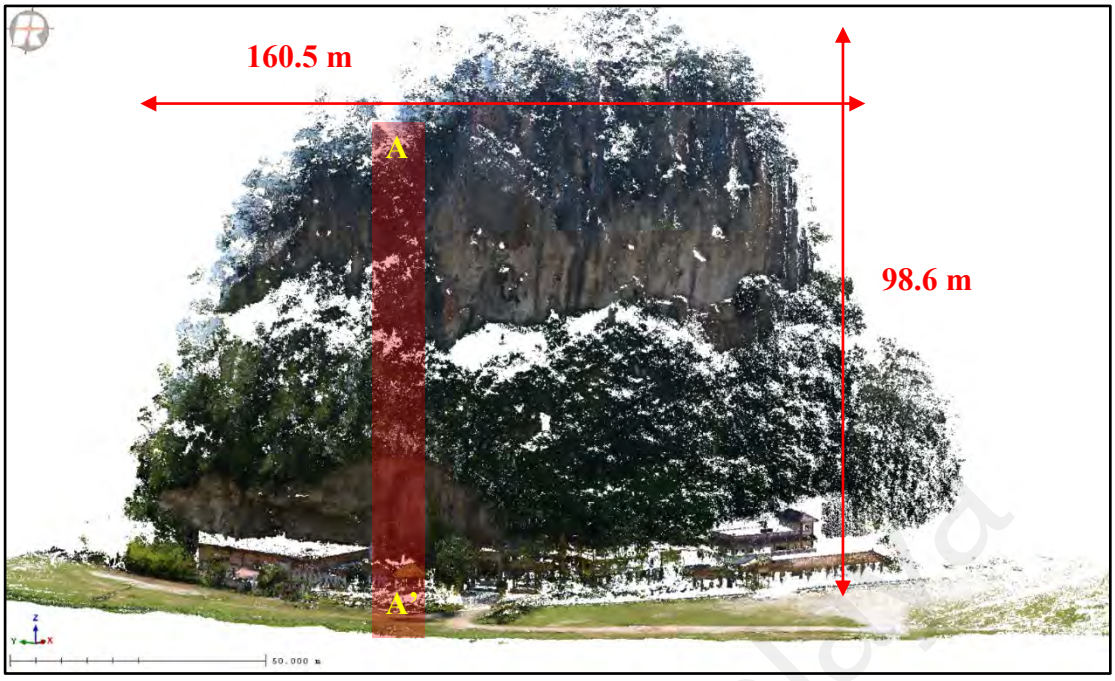

Figure 4.88: Slope geometry of KYT (a). Figure shows the height, length, and location of profile A-A' on the slope.

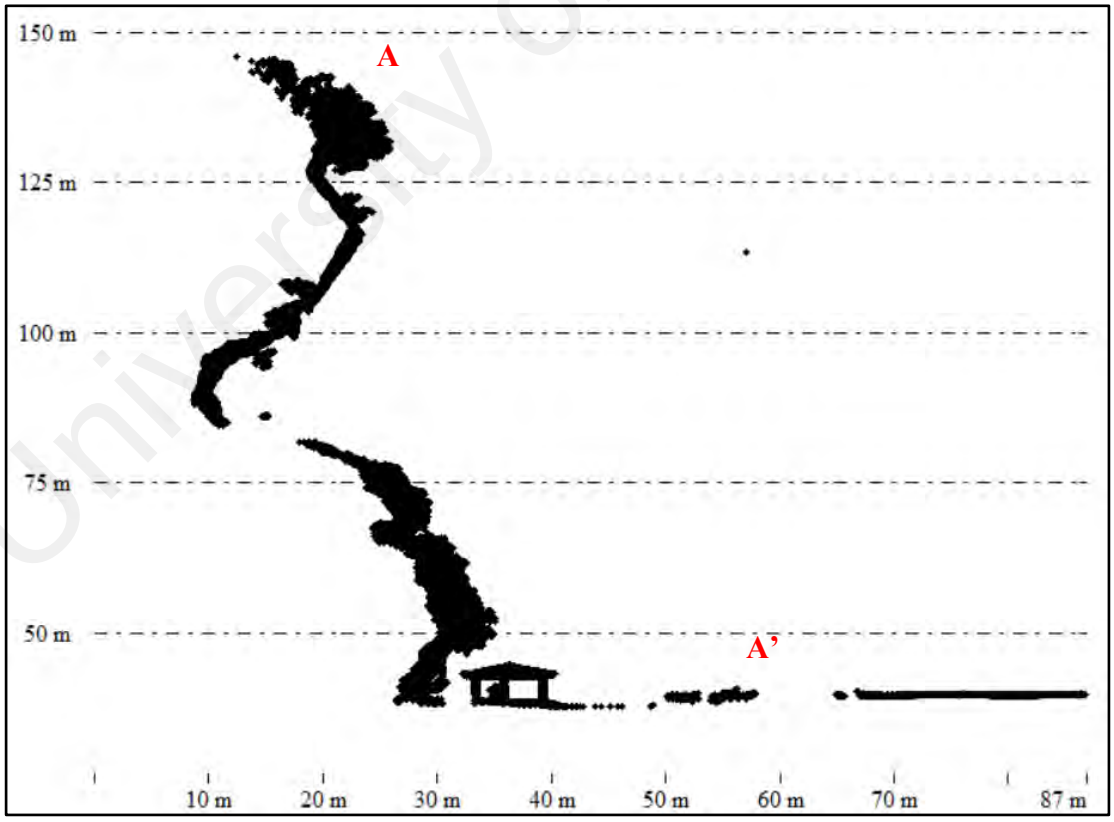

Figure 4.89: Profile A-A' of KYT (a).

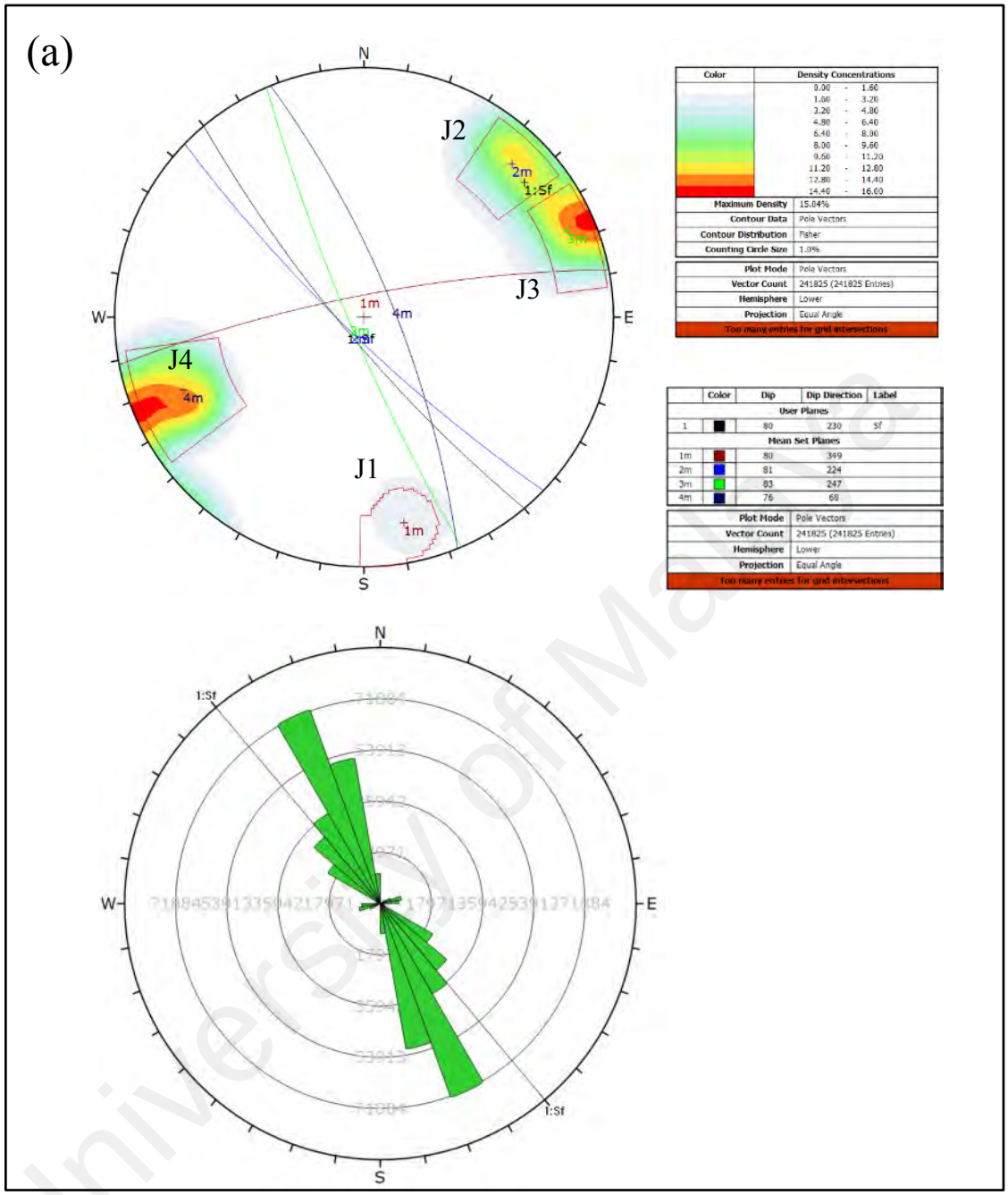

Figure 4.90: a) Poles plot and major planes plot of all four joint sets in a stereonet (b) Rose plot showing the trend of all major joint sets and the slope face orientation in KYT (a) slope. Based on the rose plot, most dominant joint sets orientation is trending slightly northwest-southeast direction.

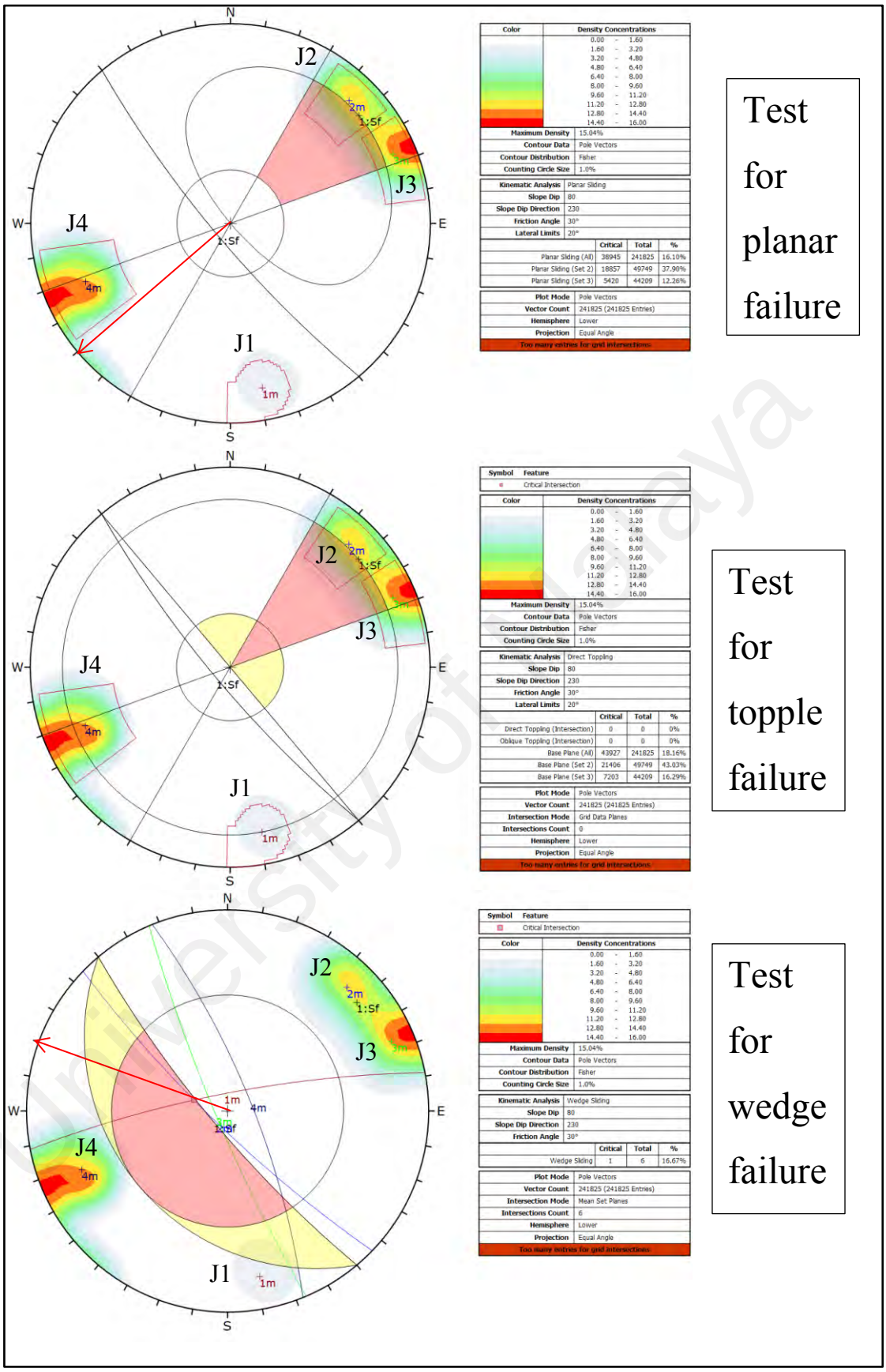

Figure 4.91: Kinematic analysis testing for planar failure, wedge failure, and topple failure in KYT (a) slope. Red arrows represent the direction of possible failure.

4.3.2.2 KYT (b) Slope Stability Analysis

Based on the discontinuity selection from Coltop 3D and kinematic analysis, four joint sets have been identified at KYT (b) slope which are J1 (37/112), J2 (84/244), J3 (77/212), and J4 (72/042) such as shown in Figure 4.92b. Major plane of the joint sets is plotted in the stereonet and the trend of discontinuity orientation is presented in the rose plot (Figure 4.93). Based on the rose plot, major trend of discontinuity orientation is towards northwest-southeast direction with the slope face trend of (80/260). Stability analysis test for planar, wedge, and topple failure are conducted and all of the possible failure are shown in Figure 4.94. For planar failure, poles from joint sets J2 (84/244) satisfy the criteria for planar failure and the direction of planar failure is towards southwest direction (260^{o}). For topple failure, there is no potential failure recorded. However, joint sets J2 (84/244) will act as the base plane for topple failure. For wedge failure, there is one possible wedge failure which involving the intersection between joint sets J2 (84/244) with joint sets J4 (72/042) and the direction of wedge failure is towards northwest direction (330^{o}). Slope geometry and slope cross section profile along A-A' are shown such in Figure 4.88 and Figure 4.89.

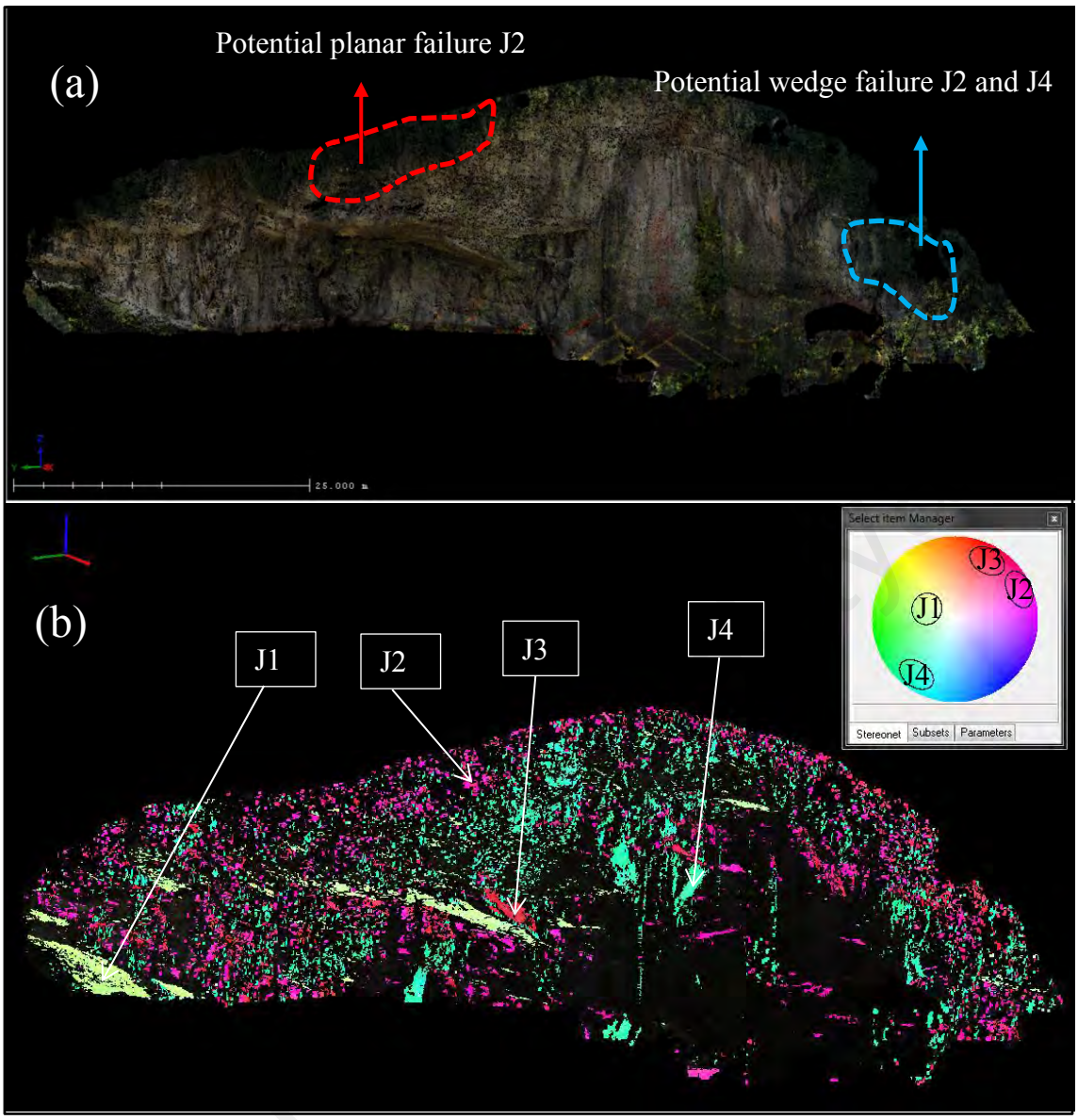

Figure 4.92: (a) Digital Terrain Model (DTM) of KYT (b) slope with true colour display (b) 3D discontinuity model derived from Coltop 3D, based on the discontinuity selection, four joint sets have been identified which are J1 (37/112), J2 (84/244), J3 (77/212), and J4 (72/042).

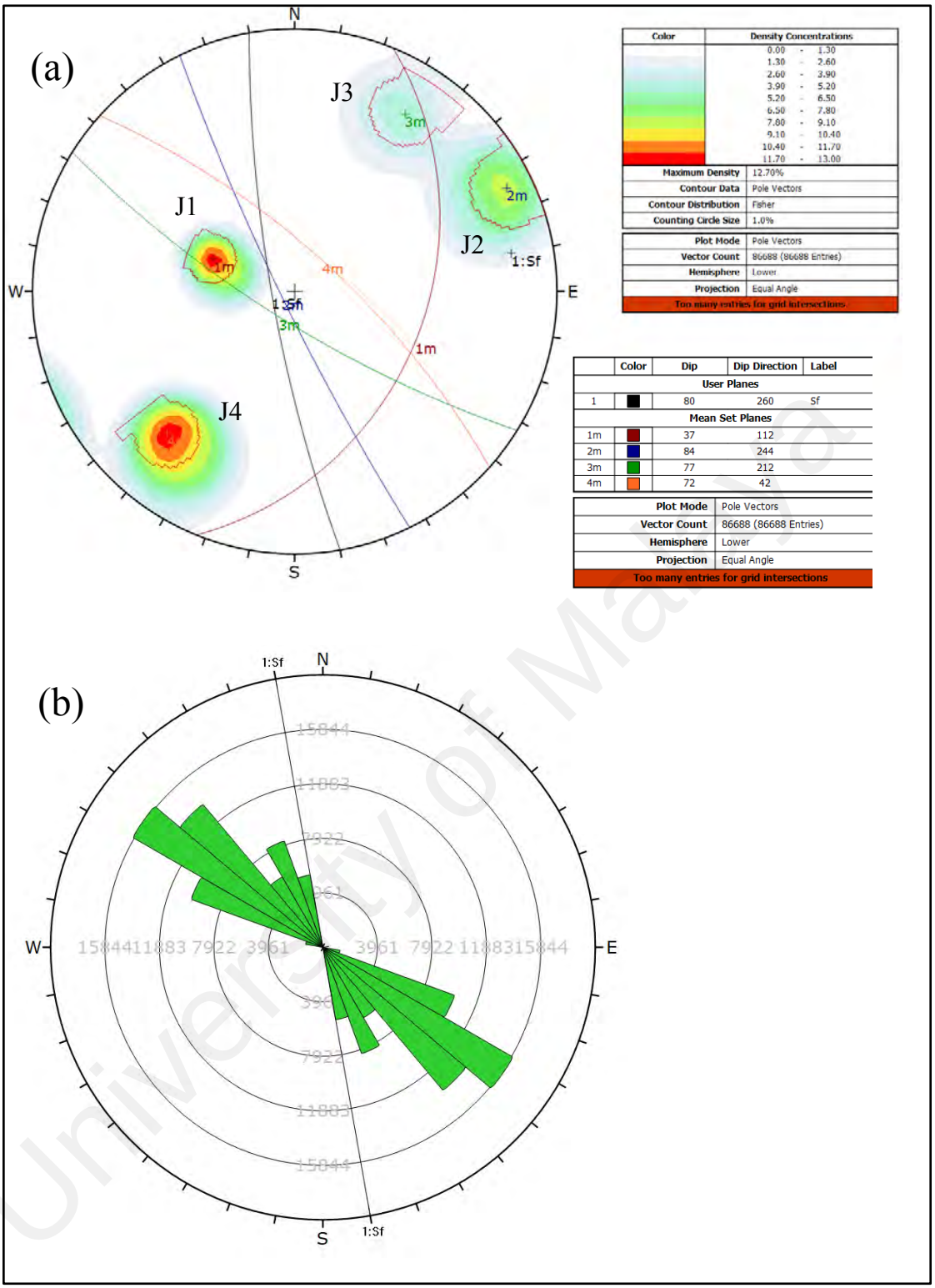

Figure 4.93: a) Poles plot and major planes plot of all four joint sets in a stereonet (b) Rose plot showing the trend of all major joint sets and the slope face orientation in KYT (b) slope. Based on the rose plot, most dominant joint sets orientation is trending slightly northwest-southeast direction.

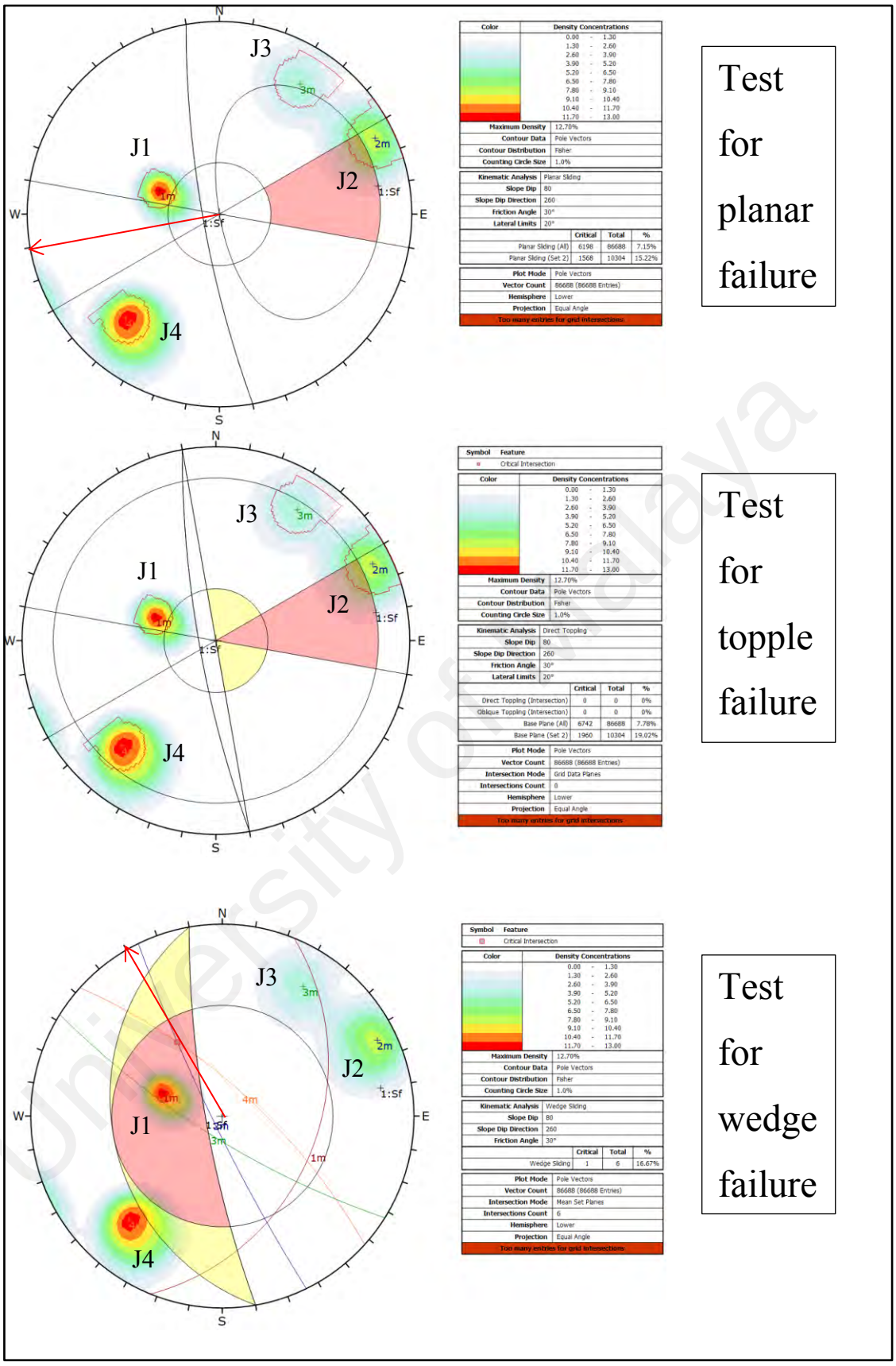

Figure 4.94: Kinematic analysis testing for planar failure, wedge failure, and topple failure in KYT (b) slope. Red arrows represent the direction of possible failure.

4.4 Gunung Cheroh Limestone Hills

Based on the discontinuity selection from Coltop 3D and kinematic analysis, five number of joint sets have been identified which are J1 (78/050), J2 (79/013), J3 (68/303), J4 (81/143), and J5 (83/198) respectively such in Figure 4.97b. Major planes of the joint sets are plotted in the stereonet and the trend of discontinuity orientation is presented in the rose plot (Figure 4.100). Based on the rose plot, major trend of discontinuity orientation is towards northwest-southeast direction with the slope face trend of (80/180). Stability analysis test for planar, wedge, and topple failure are conducted and all of the possible failure are shown in Figure 4.101. For planar failure, there is one possible planar failure detected which is involving joint sets J5 (83/198) and the direction of planar failure is towards south direction (180^{o}). For topple failure, there is no potential topple failure recorded, however, joint sets J5 (83/198) will act as the base plane for topple failure. For wedge failure, there are two possible failure detected which involving the intersection between joint sets J1 with J5 and J3 with J4 joint plane. The directions of wedge failure are towards southeast direction (120^{o}) and southwest direction (225^{o}).

Gunung Cheroh limestone hill is located beside the main road Jalan Raja Musa Aziz. Gunung Cheroh is also well known for its nearby temple which is Arulmigu Subramania Temple. There is also a previous rockfall occurrence in this area which kills a number of 40 people during 1973. A massive slab of rock which detached from Gunung Cheroh caused the demise of 40 people on 18th October 1973 (Shu & Lai, 1974). Most of the slope at this area is at high elevation and some of it are located behind the temple itself, thus make it almost impossible to conduct a manual scanline measurement in this area (Figure 4.95). Therefore, 3D TLS has being used to assess the Gunung Cheroh. Slope geometry and cross section profile along A-A' are shown such in Figure 4.98 and Figure 4.99.

Figure 4.95: Gunung Cheroh limestone hills, the presence of a shelter cave at the base of the limestone hills restricts the manual scanline survey measurement.

Figure 4.96: Location of scanning position at Gunung Cheroh.

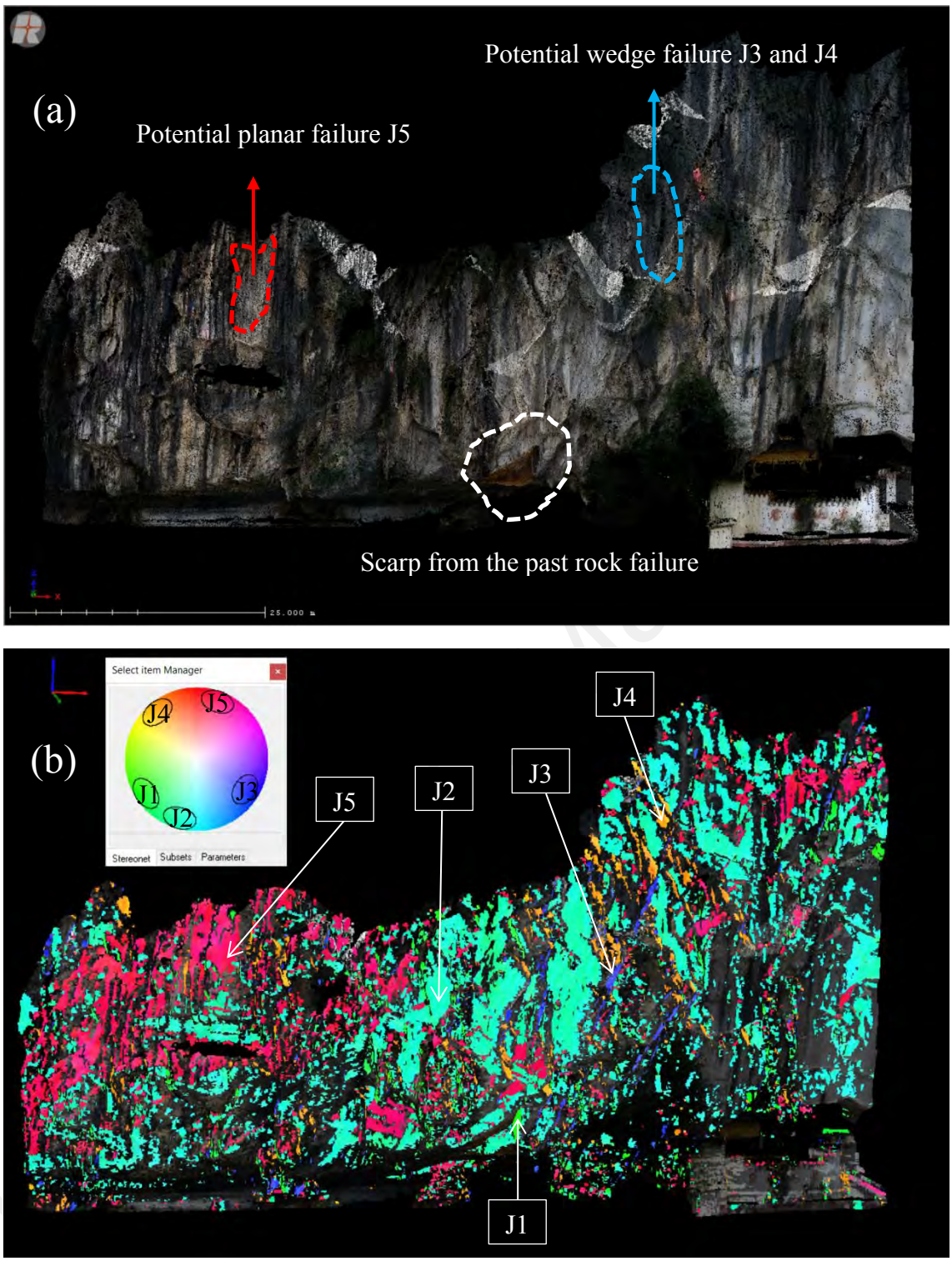

Figure 4.97: (a) 3D Digital Terrain Model (DTM) of Gunung Cheroh slope with true colour display (b) 3D discontinuity model derived from Coltop 3D, based on the discontinuity selection, there are five number of joint sets identified which are J1 (78/050), J2 (79/013), J3 (68/303), and J5 (83/198).

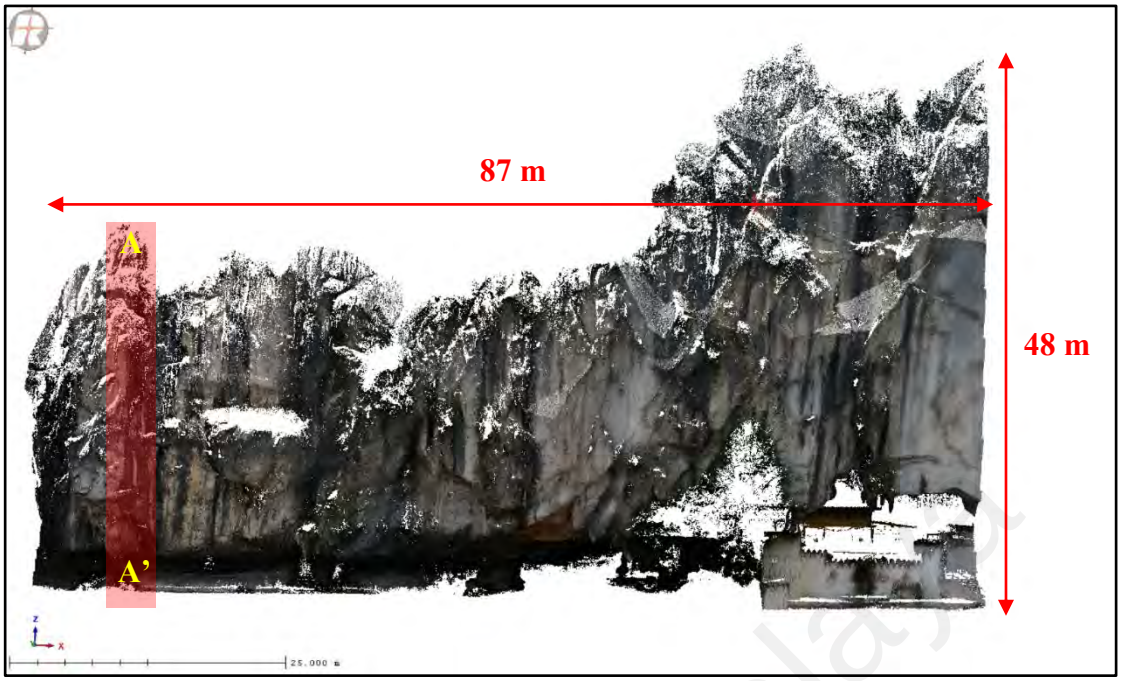

Figure 4.98: Slope geometry of Gunung Cheroh. Figure shows the length, height, and the location of profile A-A' on the slope.

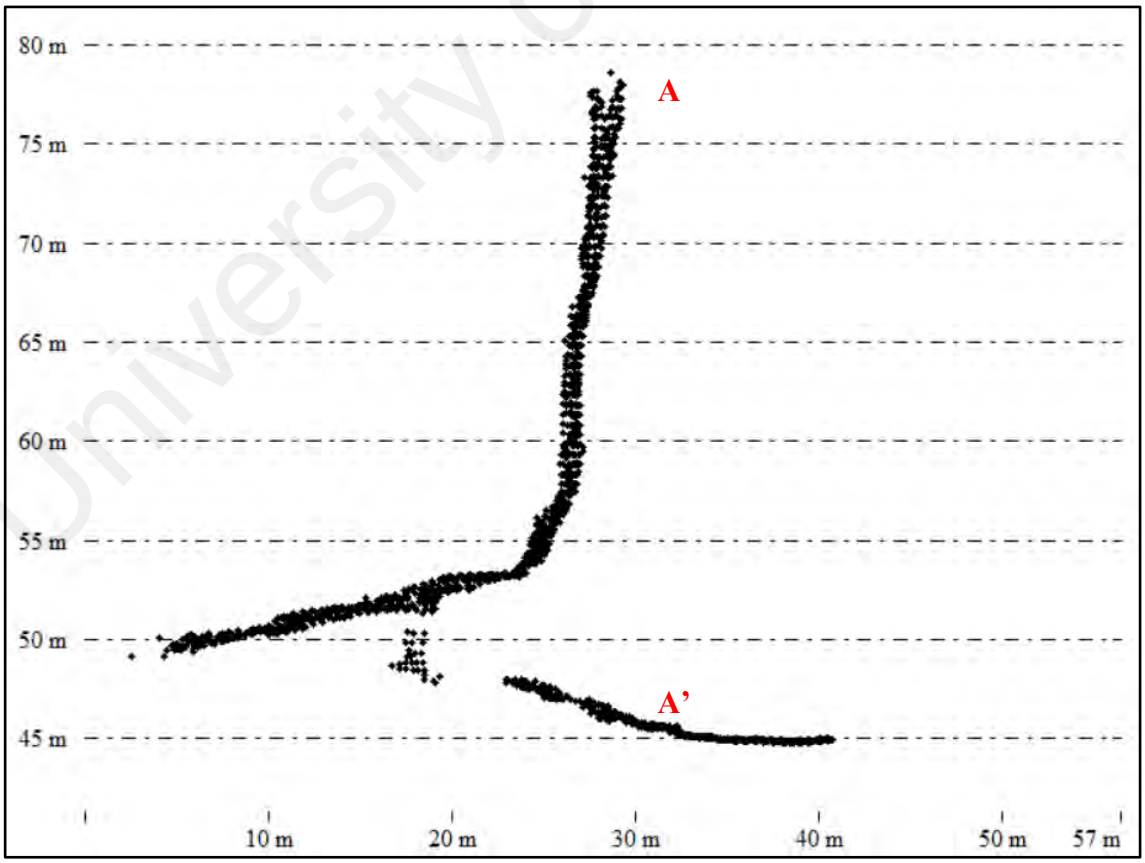

Figure 4.99: Profile A-A' of Gunung Cheroh.

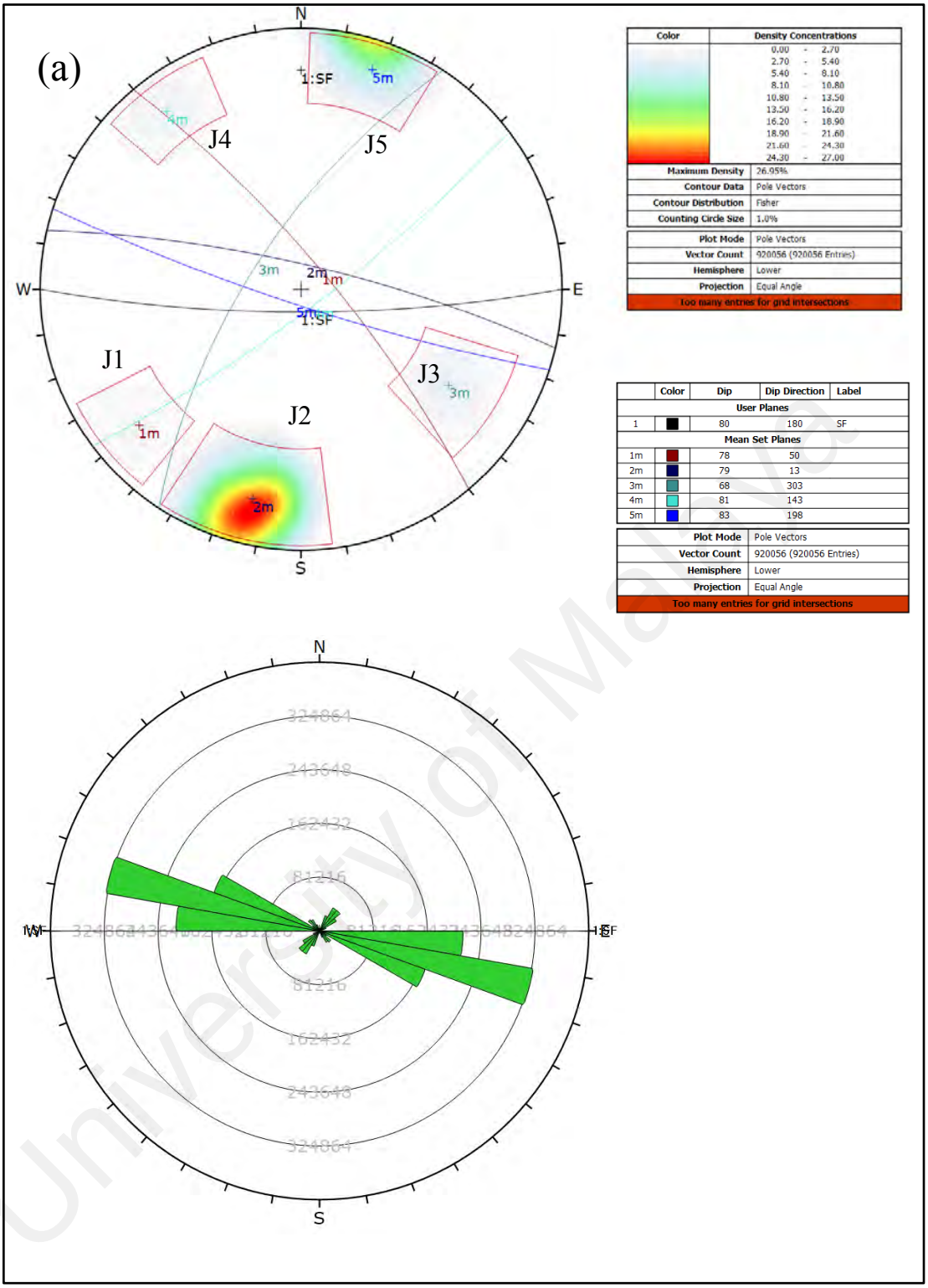

Figure 4.100: a) Poles plot and major planes plot of all five joint sets in a stereonet (b) Rose plot showing the trend of all major joint sets and the slope face orientation in Gunung Cheroh slope. Based on the rose plot, most dominant joint sets orientation is trending slightly northwest-southeast direction.

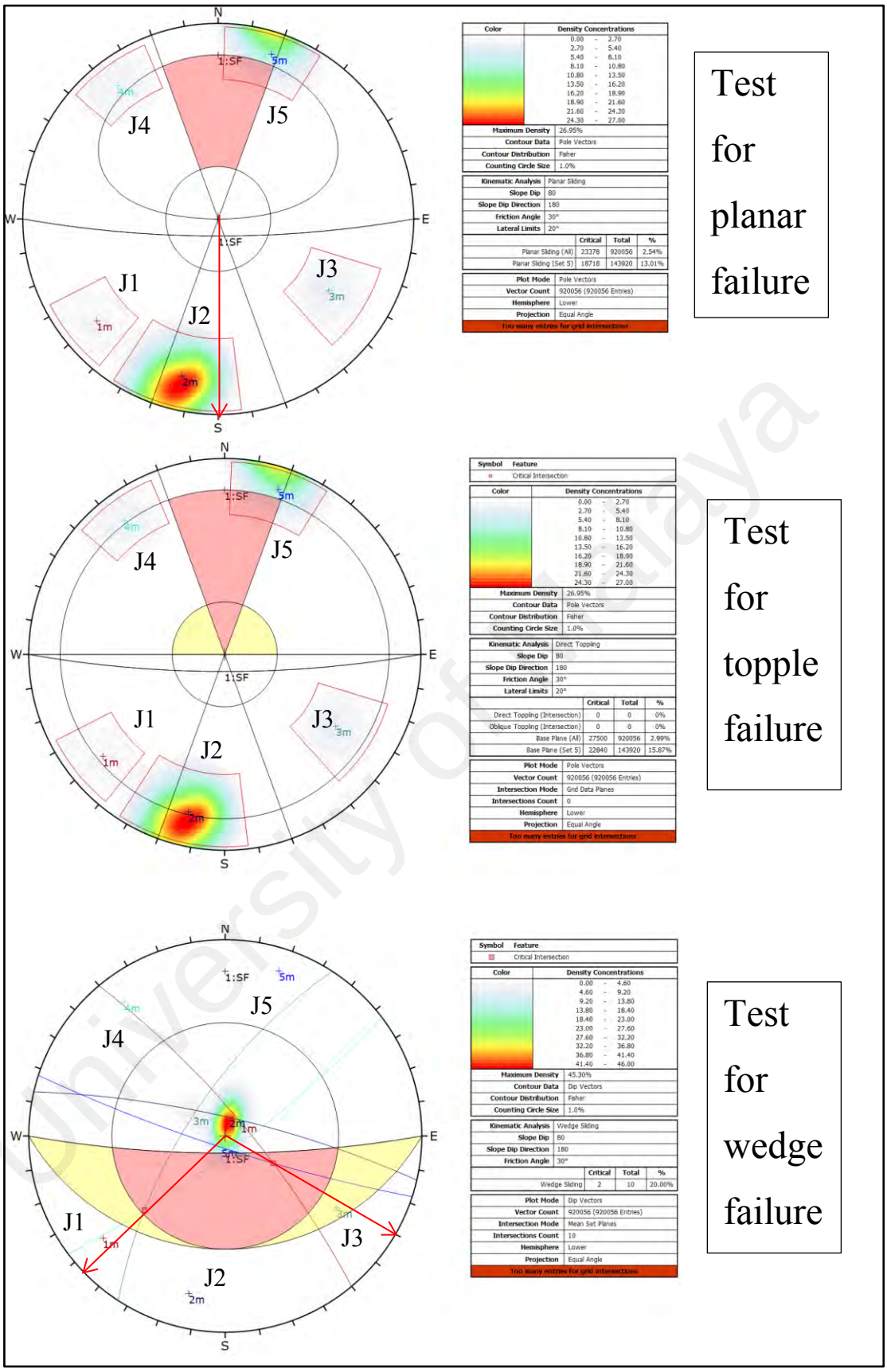

Figure 4.101: Kinematic analysis testing for planar failure, wedge failure, and topple failure in Gunung Cheroh slope. Red arrows represent the direction of possible failure.

4.5 Gunung Lanno Limestone Hills

Based on the discontinuity selection from Coltop 3D and kinematic analysis, four number of joint sets have been identified which are J1 (55/015), J2 (84/189), J3 (82/242), and J4 (78/062) such as shown in Figure 4.104b. Major planes plot of the joint sets is plotted in the stereonet and the trend of discontinuity orientation is presented in the rose plot (Figure 4.107). Based on the plot, major joint sets orientation is towards northwest-southeast direction with the slope face trend of (80/230). Stability analysis test for planar, wedge, and topple failure are conducted and all of the possible failure are shown in Figure 4.108. For planar failure, there is one possible planar failure detected which involving joint sets J3 (82/242) and the direction of planar failure is towards southwest direction (230^{o}). Based on the kinematic analysis, there is no potential for wedge failure and topple failure. However joint sets J3 (82/242) will act as the base plane for topple failure. No manual scanline survey conducted in this area because the slope is located behind the temple itself (Figure 4.102).

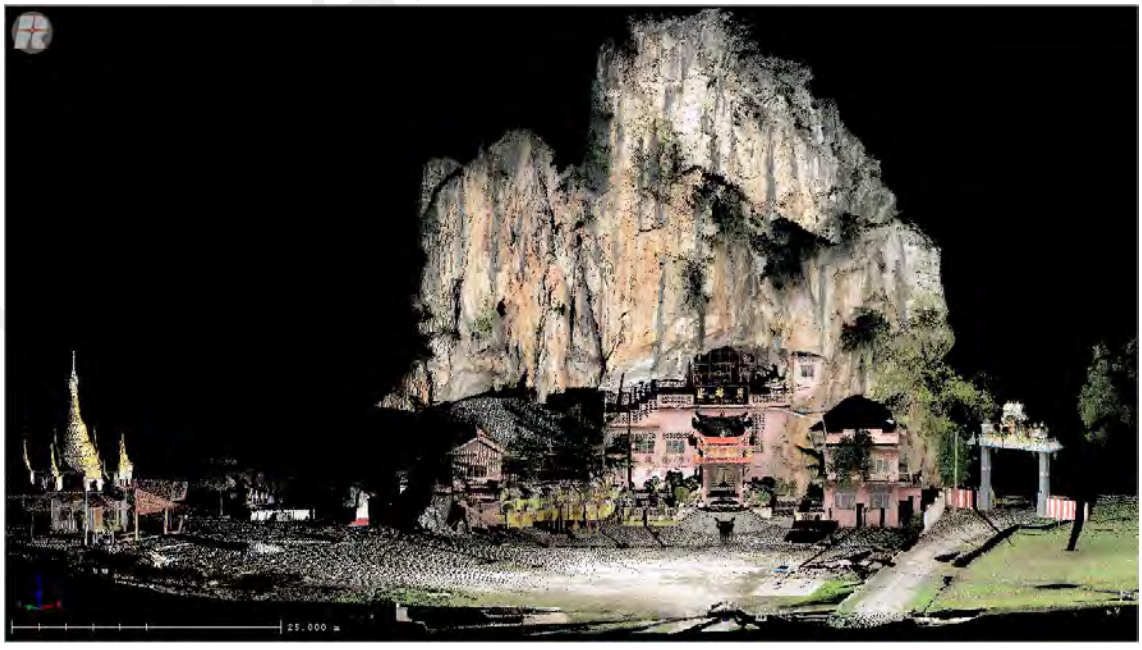

Figure 4.102: 3D model of Gunung Lanno slope showing the location of the temple at the base of the slope.

Gunung Lanno is located beside the north-south PLUS main highway (Figure 4.103), there are three number of temples located nearby the limestone hills which are the Sri Siva Subramaniam Temple, Kong Fook Ngam Temple, and Chinaraj Temple. Slope geometry and cross section profile along A-A' are presented such in Figure 4.105 and Figure 4.106.

Figure 4.103: (a) Location of Gunung Lanno limestone hills (b) Gunung Lanno rock slope for stability analysis.

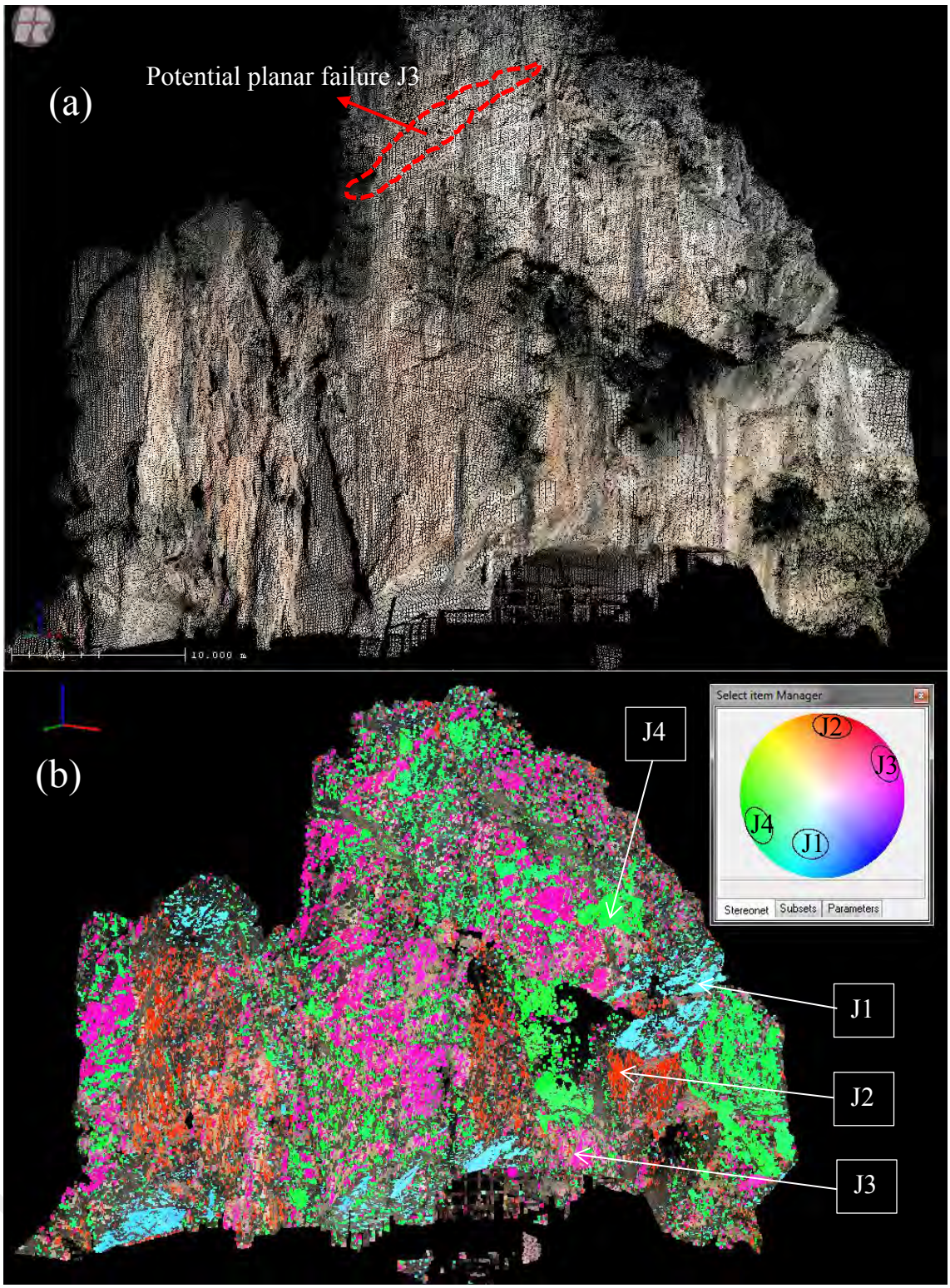

Figure 4.104: (a) Digital Terrain Model (DTM) of the slope with true colour display (b) 3D discontinuity model derived from Coltop 3D. Based on the discontinuity selection, four number of joint sets have been identified which are J1 (55/015), J2 (84/189), J3 (82/242), J4 (78/062).

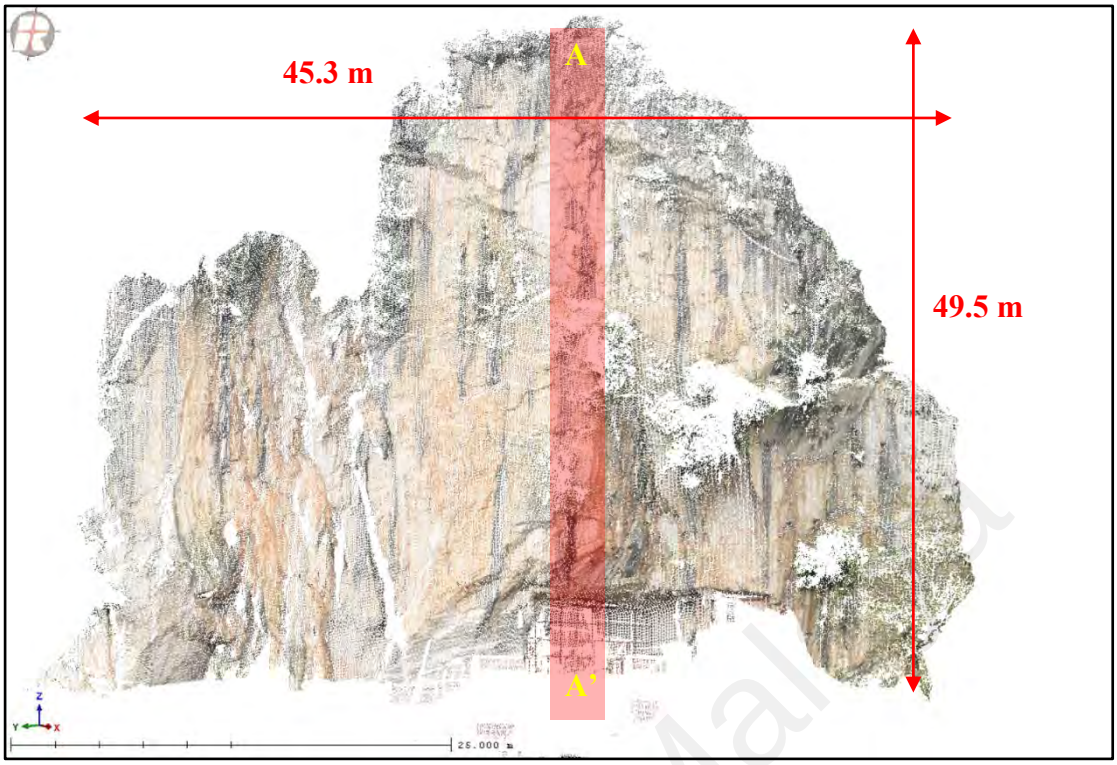

Figure 4.105: Slope geometry of Gunung Lanno. Figure shows the height, length, and location of profile A-A' on the slope.

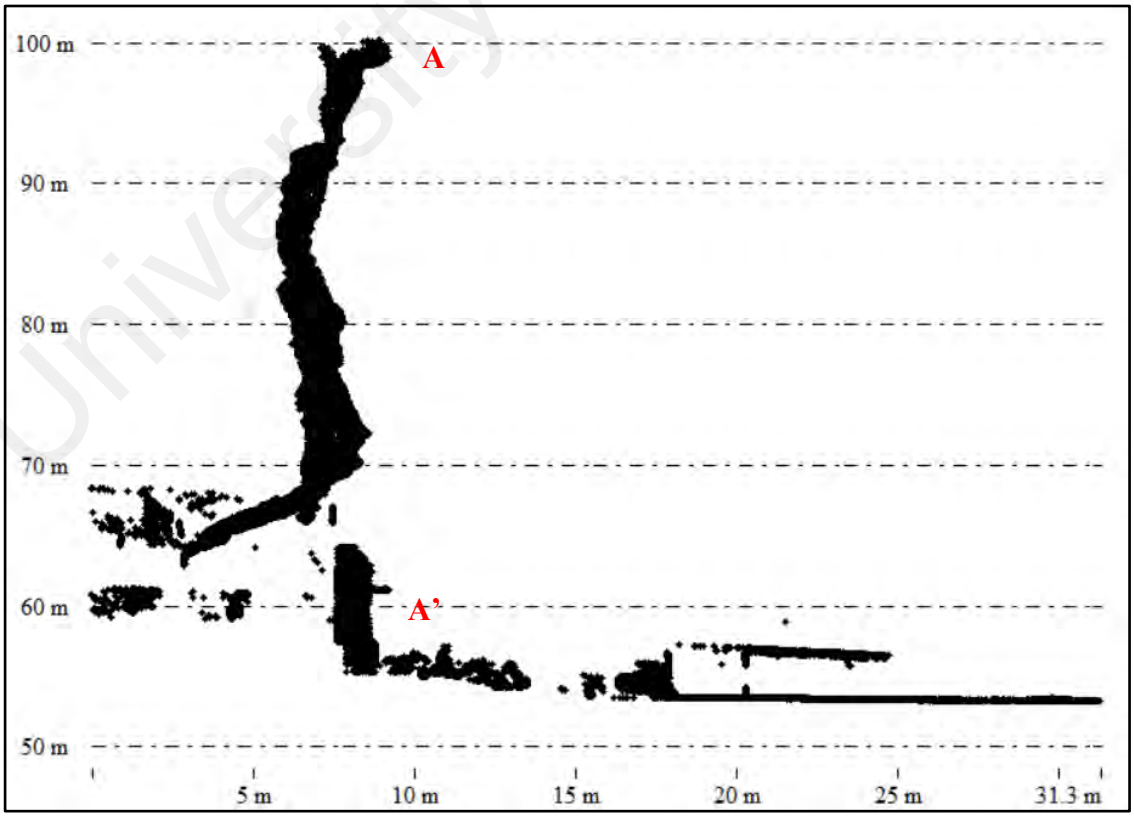

Figure 4.106: Profile A-A' of Gunung Lanno.

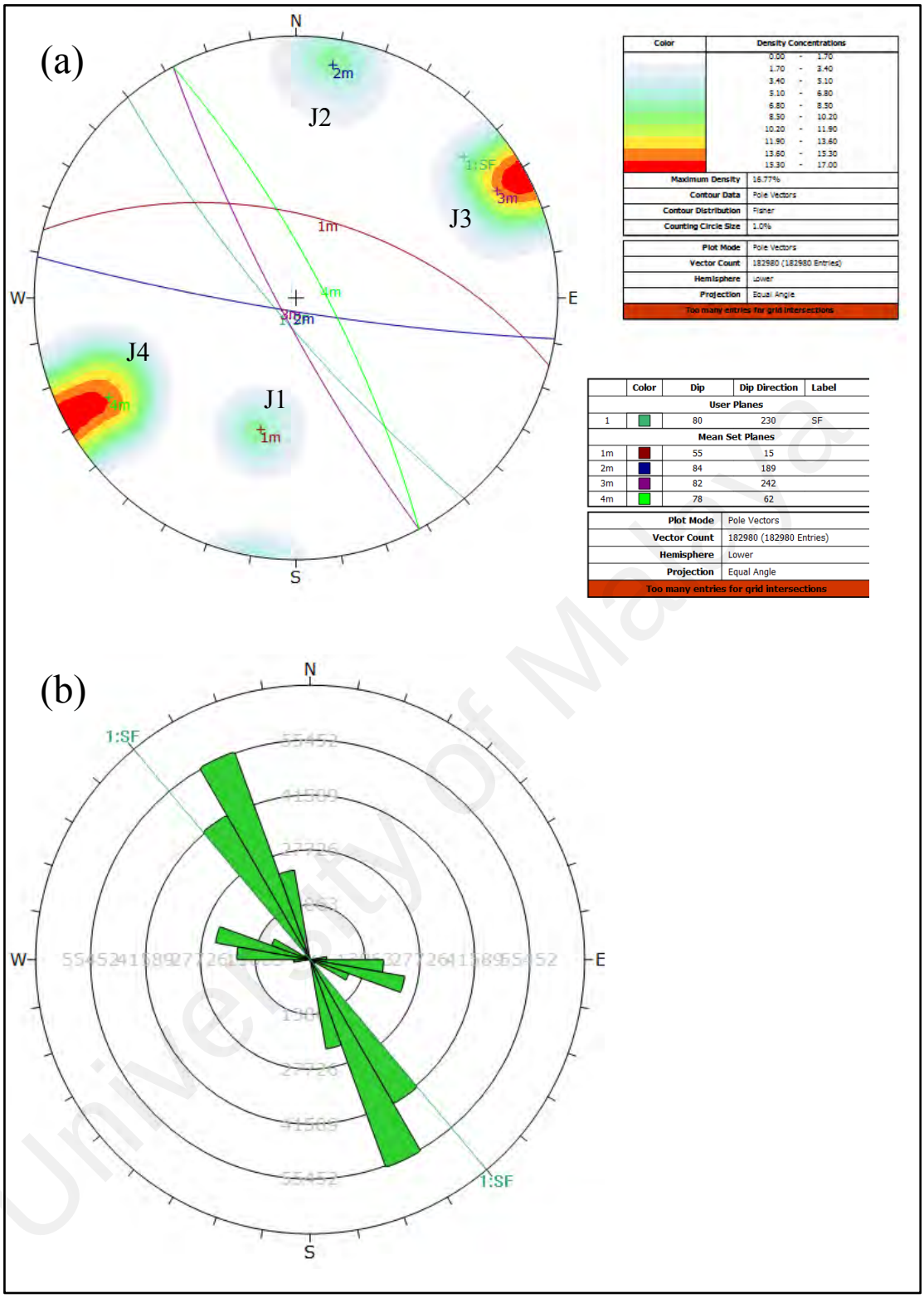

Figure 4.107: a) Poles plot and major planes plot of all four joint sets in a stereonet (b) Rose plot showing the trend of all major joint sets and the slope face orientation in Gunung Lanno slope. Based on the rose plot, most dominant joint sets orientation is trending slightly northwest-southeast direction.

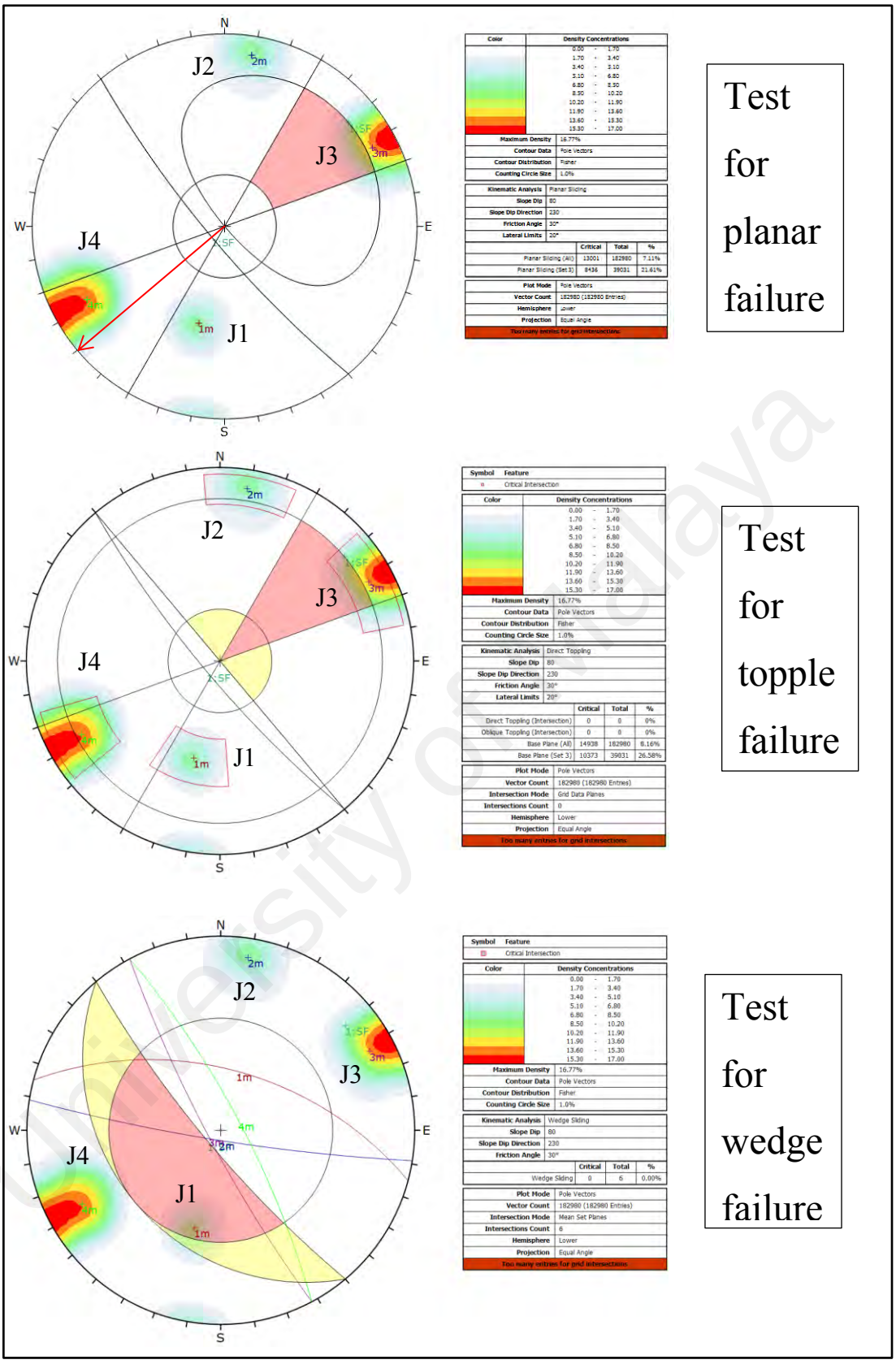

Figure 4.108: Kinematic analysis testing for planar failure, wedge failure, and topple failure in Gunung Lanno slope. Red arrows represent the direction of possible failure.

4.6 Relationship between Trends of Rockfall with Limestone Hills Structural Trends in Kinta Valley

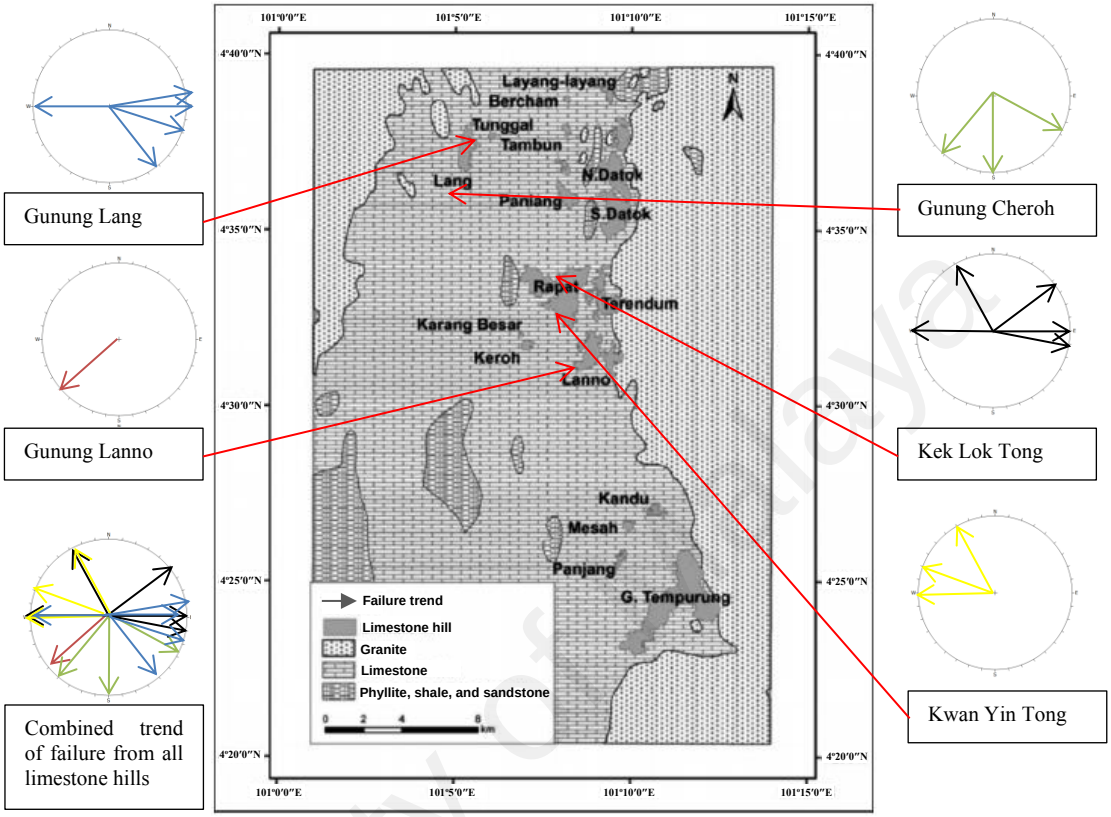

Figure 4.109: Trend of potential failure on the limestone hills based on the kinematic analysis. Arrows with multiple color represent different limestone hills trend of potential failure (Modified after Simon et al., 2015).

Morphology of the limestone hills in the Kinta Valley which is elongated towards north-south is generally controlled by many factors such as dissolution of the limestone hills and the structural trend of joint sets and faults that presence in the area. This research focus more on the effect of joint sets orientation and the trend of rock failure caused by it. Figure 4.109 shows the trend of failure of all limestone hills that has been studied. Based on the figure, most of the rock failures are trending generally towards west and east direction which is indeed perpendicular to the trend of limestone hills axes which is north-south direction. Generally, most of the joint sets presence on the limestone hills are trending slightly similar with the shape of the limestone hills axes

north-south. Based on the kinematic analysis done in overall limestone hills in this research, the orientation and intersection of joint sets creates failure which are perpendicular dipping out from the slope face (Table 4.27, Table 4.28, and Table 4.29). This trend thus shapes the morphology of the limestone hills. Figure 4.110, Figure 4.111, Figure 4.112, Figure 4.113, and Figure 4.114 shows example on the effect of the failure trends in controlling the morphology of the limestone hills in the study area generally. This statement is supported by Tan (1988), he stated that geological structures such as joints and fault together with the bedding planes of the limestones, these structures control the formation of karstic features and the morphology of the limestone hills in Kinta Valley. In Kek Lok Tong limestone hills, the formation of wangs is majorly controlled by the joints orientation presence on the area. Rock collapse and failure plays a major role in the formation of the wang in the area.

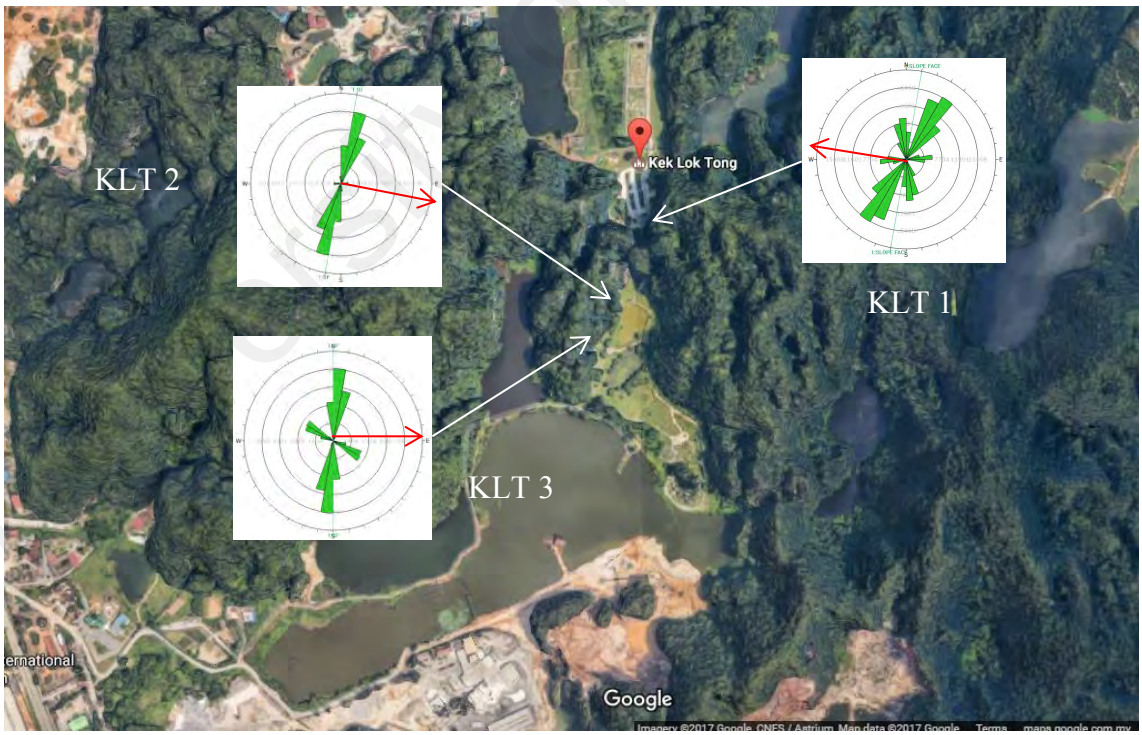

Figure 4.110: Figure shows the trend of major joint sets align with the morphology of the limestone hills, while the trend of failure occurs perpendicularly from the axes of the limestone hills. The direction of failure plays a major role in developing the wang at the area.

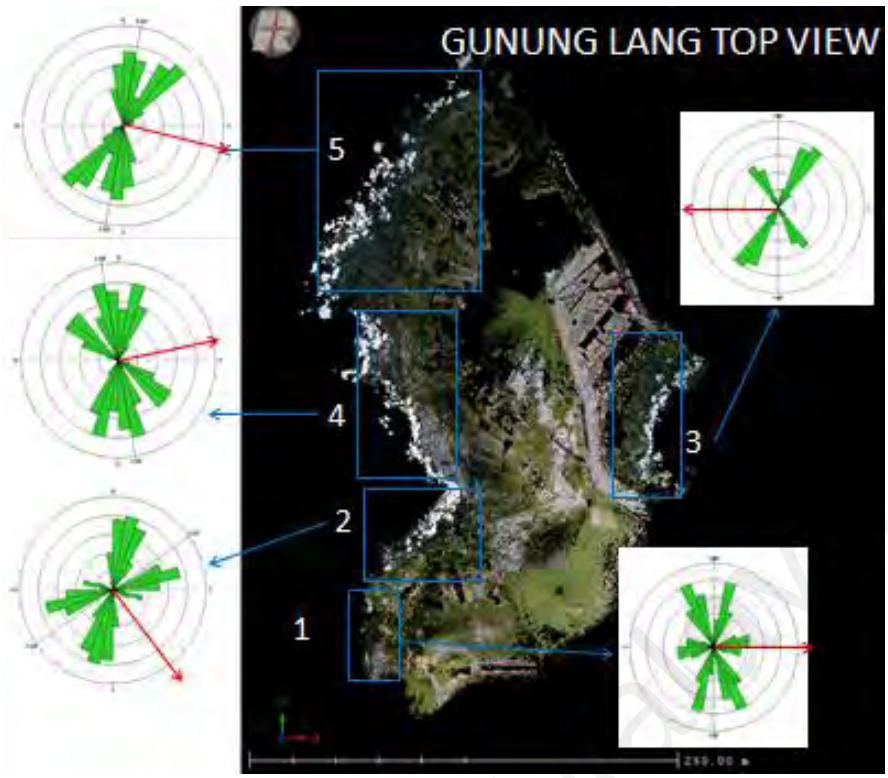

Figure 4.111: Figure shows the trend of major joint sets align with the morphology of the limestone hills, while the trend of failure occurs perpendicularly from the axes of the Gunung Lang limestone hills.

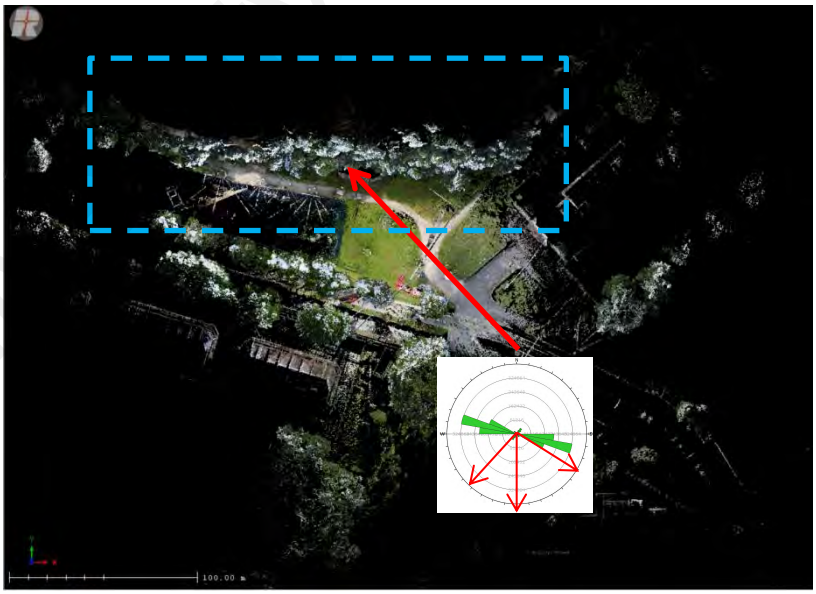

Figure 4.112: Aerial views showing the trend of major joint sets at Gunung Cheroh and the trend of potential failure.

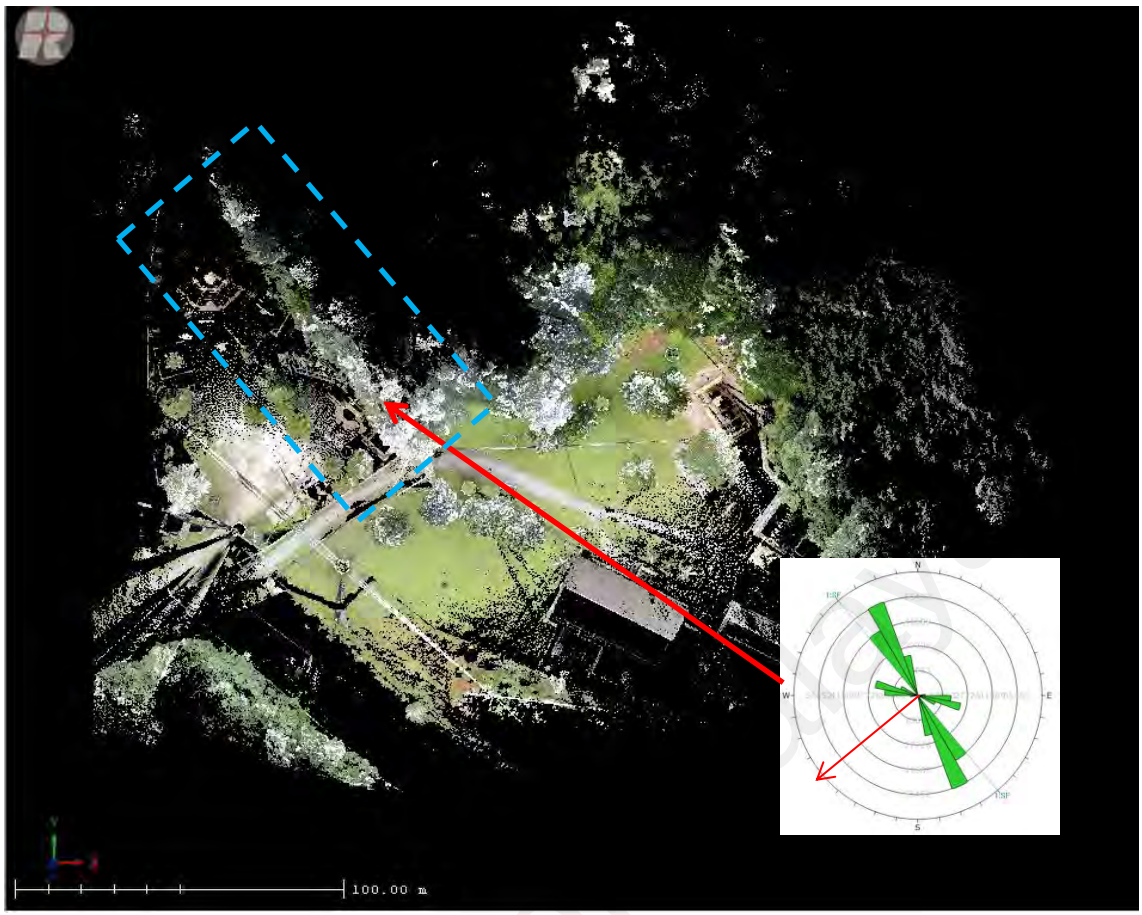

Figure 4.113: Aerial view of Gunung Lanno slope showing the trend of joint sets and the trend of potential failure.

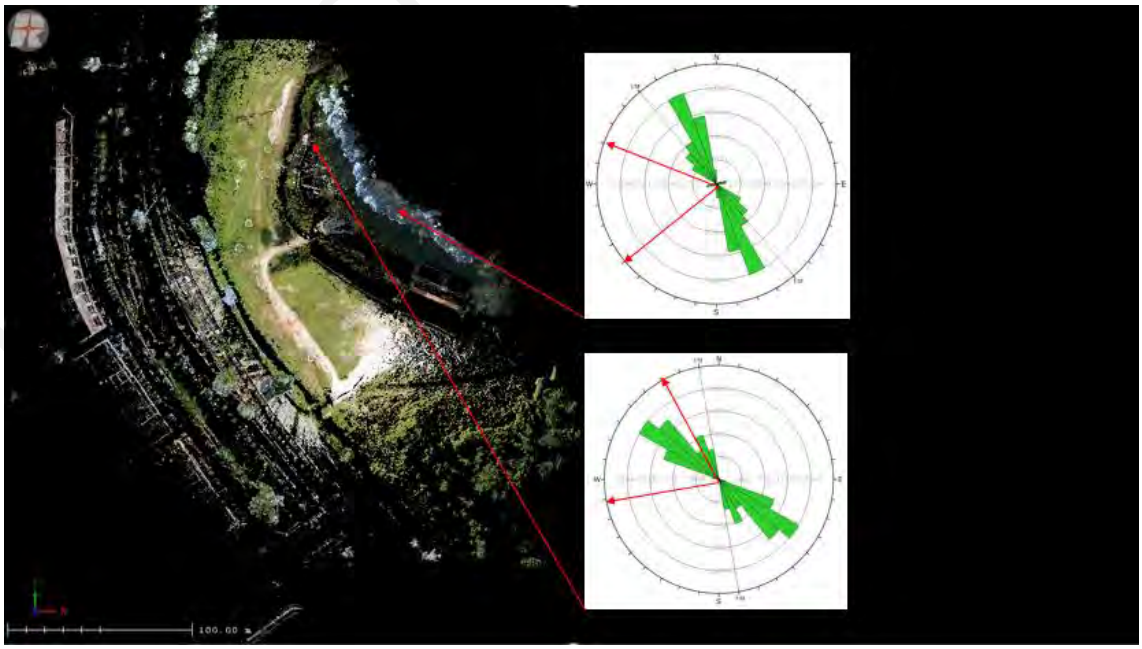

Figure 4.114: Aerial view of Kwan Yin Tong temple showing trend of joints sets and trend of potential failure.

4.7 Correlation of 3D TLS Data with Data from Previous Researchers

Discontinuity data of the rock slope such as joints dip angle and dip direction play a key role in determining the stability of the slope. Discontinuity survey such as scanline survey is done manually by compass clinometer directly on the outcrops. However, in massive rock masses such as limestone hills in Kinta Valley, only a limited number of manual measurements can be collected with this conventional method. This is because the surveys are usually concentrated in small areas where direct contact to the slope is accessible, which may not be representative of the entire rock mass. Traditional scanline mapping are affected by obvious drawbacks including sample representatives, accessibility and field safety (Ferrero et al., 2009). According to Sturzenegger and Stead (2009), discontinuities measured in small areas cannot be representative of the whole rock masses. Due to that, this research uses 3D TLS complemented with manual method to assess the slope and joints orientations.

Stability analysis has been conducted on four limestone hills in this research which includes Gunung Lang, Gunung Rapat, Gunung Lanno and Gunung Cheroh. Based on the survey data comparison between scanline and 3D TLS (Figure 4.115) on Gunung Lang, some of the discontinuities set from 3D TLS model correlated weakly with the manual measurements by Lai et al. (2016), while others have fair to strong correlation. An outcome from GL3 slope shows that both manual scanline survey and TLS survey managed to plot 4 sets of joint from the slope. 1 joint set from TLS survey shows strong correlation with joint set from the manual survey, 1 joint set shows fair to weak correlation and the other 2 joints show weak correlation. For the GL4 slope, the manual survey produced a plot with a number of 4 joint sets while TLS survey plotted 5 numbers of joint sets. TLS survey shows 1 number of joint sets with strong correlation with manual survey while the other 4 joint sets are weakly correlated. Data from Lai et al. (2016), in Figure 4.115 show results for manual scanline survey which focuses more

at the base of the slope while TLS concentrate on the upper part and overall slope which is not accessible for manual measurements.

Figure 4.115 also shows a pole plot of discontinuity trend collected on the same Gunung Lang slope; the only difference is the coverage of the data collection. However, there are also some biases in characterizing the discontinuity by using TLS. According to Sturzenegger and Stead (2009), the observation scale effect, the main function of the distance to the sensor (joint distance bias) and the size of the discontinuity (truncation bias) occurs when small traces are difficult to recognize from 3D point cloud data. Due to that, a cut off value located between 0.2 and 0.6 m was reported, which may result in over and under-characterizing of discontinuity on the slopes. Furthermore, this weak correlation between both methods may also occur mainly due to the joints surface roughness that varies along the joints plane itself. According to Li et al. (2016), generally the rock outcrop surfaces are rough and undulating, as well as they contain a great quantity of large-scale undulations and small-scale roughness. Manual measurements on rough exposed surfaces by compass are restricted to an accessible part of the joint surface without taking into account the whole surface variation (Kong et al., 2020). Thus, explained the differences in orientation measurements for lidar and manual method in this study.

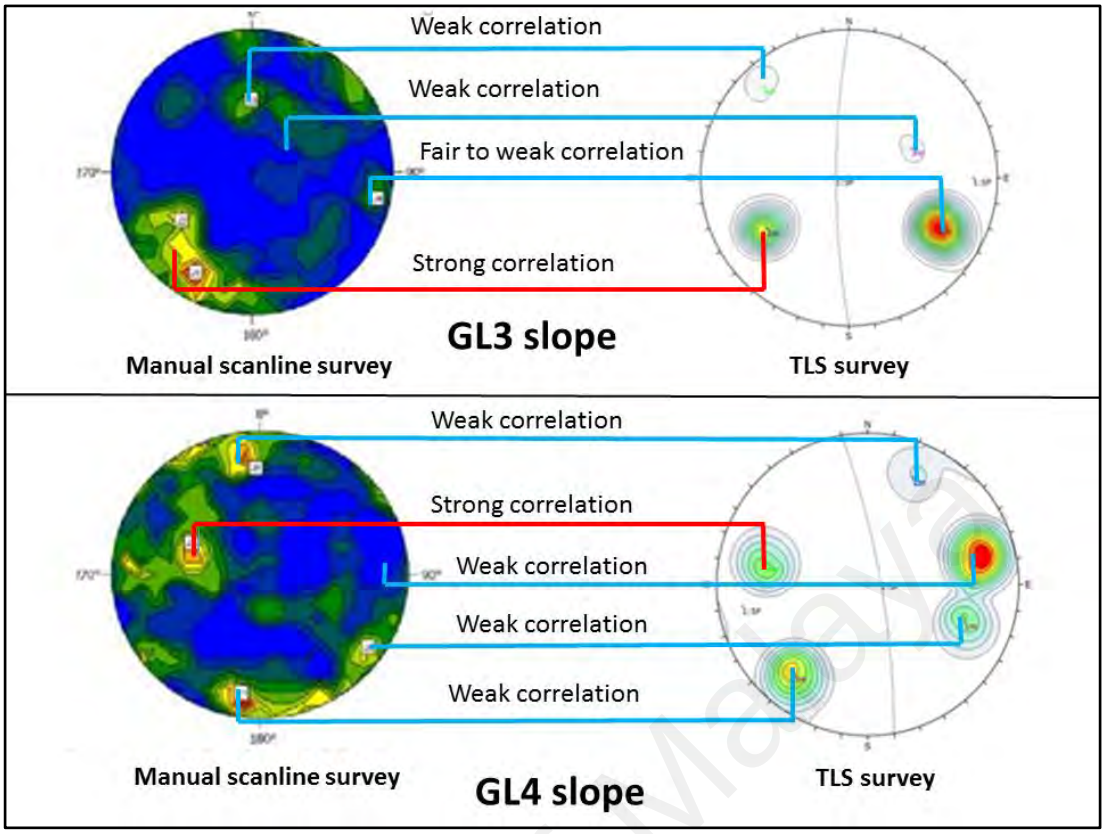

Figure 4.115: Comparison between 3D TLS poles plot data with scanline survey poles data.

Despite all of these limitations, TLS was able to provide a large number of discontinuity orientation data from the lower part to the upper part of the slope for stability analysis as compared to manual measurement. It is important for one to understand and acknowledge the limitations of 3D TLS survey before choosing it for analysis technique. Ignoring these limitations will produce false data and errors. This shows the importance of implementing both manual scanline method and 3D TLS as both compliments its own strengths and limitations in assessing slope from a different scale (Figure 4.116). According to Spreafico et al. (2015), the conventional survey techniques are more applicable at the outcrop scale, while when dealing with a large cliff or with an entire rock slab, the TLS technique is to be preferred.

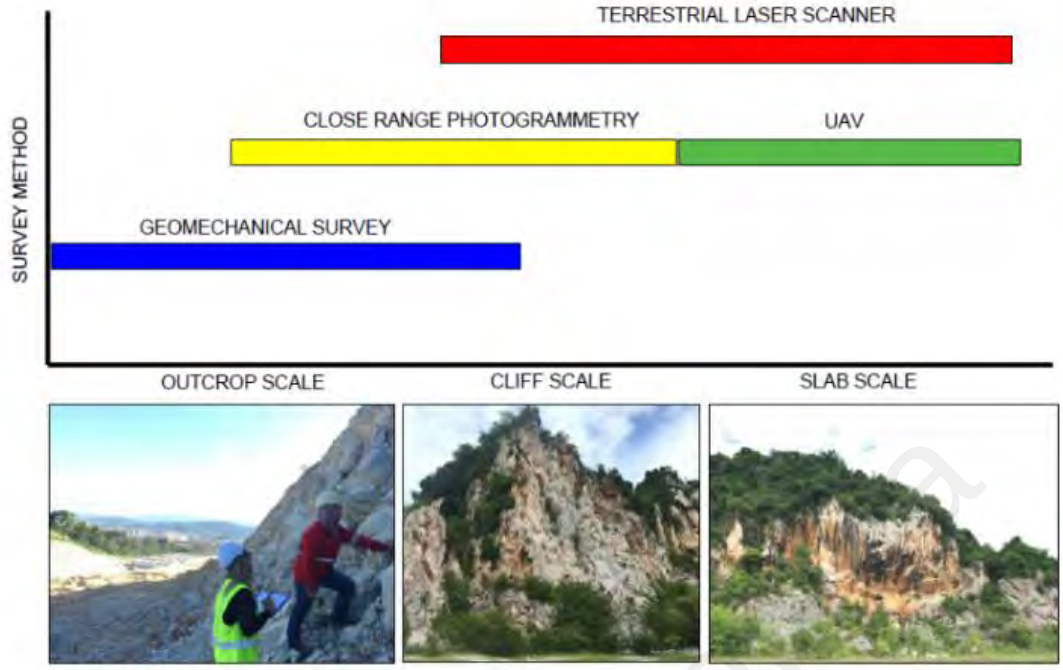

Figure 4.116: Indication of the scale at which the use of different technique is considered to be convenient.

4.8 Kinematic Analysis of the Selected Slope

The slope face, joints orientation and potential failure direction of the slopes are tabulated in Table 4.27, Table 4.28, and Table 4.29. All of the data presented in the table were derived from the TLS survey and extracted by using Coltop 3D software into the stereonet plot. There were limited manual scanline data collected due to site limitations such as thick vegetation covering the joints plane and the inaccessible location of the rock slope itself.

Based on the results, 13 out of 14 rock slope faces from Gunung Lang, Gunung Rapat, Gunung Cheroh, and Gunung Lanno have potential failure of planar and wedge which may occur by dipping perpendicularly away from the slope face. According to Hoek and Bray (1981), a planar failure is likely to occur when a discontinuity dips in the same direction (within 20^{o}) as the slope face at an angle gentler than the slope angle, but greater than the friction angle along the failure plane. A wedge failure may occur

when the line of intersection of two discontinuities, forming the wedge-shaped block plunges in the same direction as the slope face and the plunge angle is less than the slope angle but greater than the friction angle along the planes of failure (Hoek & Bray, 1981). The kinematic analysis assessment also revealed that slope KLT 1 (b) is considered to be safe from any potential failure.

The uses of lidar point clouds in slope characterization aims to not only make use of the advantages of modern computer techniques, but also allows the operators or researchers to apply their geological knowledge to monitor the output results. According to Feng and Röshoff (2015), a typical mapping procedure by lidar method is interactively performed between the computer and the operator: (1) select a part of rock surface from the whole 3D scanning model by the operator; (2) choose a fracture on the scanned rock surface, and mark the exposed fracture surface interactively by the operator; (3) automatically calculate the best fit fracture plane by the computer program, and then calculate the fracture orientation.

Table 4.27: Joints orientation and potential failure for Gunung Lang limestone hills.

Slope	Joints Orientation (°)		Potential Failure Direction (°)
GL1	SF	70/090	Planar (090/70)
	J1	67/286	Wedge (055/58, 115/47, 125/38)
	J2	68/197	
	J3	59/164	
	J4	69/004	
	J5	59/066	
GL2	SF	80/145	Planar (145/80)
	J1	54/291	Wedge (120/69, 130/65, 145/72)
	J2	74/164	
	J3	79/196	
	J4	73/085	
	J5	73/272	
GL3	SF	80/270	Planar (270/80)
	J1	69/299	Wedge (215/465, 220/29, 235/49)
	J2	66/058	
	J3	50/245	
	J4	80/137	
GL4	SF	80/080	Planar (080/80)
	J1	69/291	Wedge (085/67, 145/61)
	J2	75/203	
	J3	75/039	
	J4	68/101	
	J5	74/256	
GL5	SF	80/100	Planar (100/80)
	J1	73/310	Wedge (080/31, 120/73, 175/44
	J2	77/163	160/49)
	J3	51/141	
	J4	77/084	
	J5	66/280	
	J6	81/259	

Table 4.28: Joints orientation and potential failure for Gunung Rapat limestone hills.

Slope	Joints	Orientation (°)	Potential Failure Direction (°)
KLT 1 (a)	SF	85/270	Planar (270/85)
	J1	82/040	Wedge (330/63)
	J2	55/074	
	J3	83/251	
KLT 1 (b)	SF	75/280	No potential failure
	J1	54/082	
	J2	30/224	
	J3	67/122	
	J4	78/356	
KLT 1 (c)	SF	80/280	Planar (280/80)
	J1	81/299	Wedge (220/55)
	J2	71/162	
	J3	72/111	
	J4	44/091	
KLT 2	SF	83/100	Planar (100/83)
	J1	64/279	Wedge (040/65)
	J2	80/108	
	J3	71/360	
KLT 3	SF	80/090	Planar (090/80)
	J1	36/276	Wedge (055/70)
	J2	74/095	
	J3	72/029	
KYT (a)	SF	80/230	Planar (230/80)
	J1	80/349	Wedge (290/70)
	J2	81/224	
	J3	83/247	
	J4	76/068	
KYT (b)	SF	80/260	Planar (260/80)
	J1	37/112	Wedge (330/41)
	J2	84/244	
	J3	77/212	
	J4	72/042	

Table 4.29: Joints orientation and potential failure for Gunung Lanno and Gunung Cheroh.

Slope	Joints Orientation (°)		Potential Failure Direction (°)
G Cheroh	SF	80/180	Planar (180/80)
	J1	78/050	Wedge (225/30, 119/57)
	J2	79/013	
	J3	68/303	
	J4	81/143	
	J5	83/198	
G Lanno	SF	80/230	Planar (230/80)
	J1	55/015	
	J2	84/189	
	J3	82/242	
	J4	78/062	

CHAPTER 5: CONCLUSION AND RECOMMENDATION

5.1 Conclusion

Commonly, geotechnical survey such as scanline survey is done manually by compass clinometer directly on the outcrops. However, in massive rock masses such as limestone hills in Kinta Valley, only a limited number of manual measurements can be collected with this conventional method. This is because the surveys are usually concentrated in small areas where direct contact to the slope is accessible, which may not be representative of the entire rock mass. Therefore, this research combines both method of manual scanline survey with the 3D TLS survey. Data from both surveys are used in comparison which allows the main strength and limitations of each survey to be recorded. The integration of manual survey and 3D TLS survey will provide a more precise description of the joints properties in a rock mass. Interpretation of the stereonets showed that the TLS data more accurately described the joint structures of the tested site due to a higher number of measured points (Yiu & King, 2009). Based on the results presented in previous chapters and the objectives of the study, the following conclusions can be drawn:

5.1.1 Development and Extraction of Rock Mass Discontinuity Plane Model From 3D TLS Point Cloud Data for Kinematic Analysis

Rock mass discontinuity planes from 14 rock slope faces in the study area are created by using the point cloud data from the LiDAR scanning. Raw point clouds data undergone pre-processing and post-processing steps in order to produce a complete 3D rock mass model of the slope. RiSCAN Pro software were used to facilitate the processing workflow. A complete rock mass discontinuity model is essential in order to

fully understand the discontinuity properties for the rock mass. Discontinuity properties such as joint orientations are extracted from the plane model by using the COLTOP 3D software. COLTOP 3D software allow the automatic delimitation of a set of neighbourhood points characterized by the same normal vector and visualizes each of the discontinuity sets into a unique colour. All of the discontinuity selection is done manually by the author with geological background in order to monitor the output results. Joint orientations extracted from the COLTOP 3D are used for the kinematic analysis. High density point cloud data allow the author to calculate the spacing and trace length of the joints by using the tools provided by the RiSCAN Pro software.

5.1.2 Validation of 3D TLS Measurements with Manual Scanline Measurements in the Field

Validation of manual and Lidar measurements are done by selecting 4 control surfaces on the rock slope in the field. Joint orientation readings are collected on each of the control surfaces by using the compass clinometer and then being repeated by Coltop 3D selection on the same control surfaces. Joint orientation from manual and Lidar measurements are plotted on the stereonet for validation. Manual measurements are set to be the control for the validation. Mean square error analysis is used to evaluate the deviation of Lidar measurements from the manual measurements. Out of 14 rock slope faces, 5 rock slopes are not validated due to the site condition, thick vegetation and inaccessible rock slopes restrict the manual measurements. Based on the validation results, measurements from GL1 has the lowest mean square error (MSE) score which is 2.5 for the dip angle and 1.25 for the dip direction. On the other hand, KLT 1 (a) score the highest mean square error both for the dip angle and dip direction which are 26.3 and 15.8 respectively. This occur mainly due to the low exposure and highly

weathered joint plane surface on KLT 1 (a) which make it more challenging to collect consistent repetitive measurement on the same joint plane, thus producing more deviation. Generally, the deviation of Lidar measurements from the reference manual measurements are not more than 10^{o} degree both for dip angle and dip direction.

5.1.3 Relationship Between the Trend of Rockfall with Overall Kinta Valley Structural Trend

Kinematic and stability analysis have been conducted on four limestone hills in Kinta Valley; Gunung Lang, Gunung Rapat, Gunung Lanno, and Gunung Cheroh. All fourteen number of slopes assessed in this research shows 17 potential failures trends in various directions except for slope KLT 1 (b) which have no potential failure detected. The major trend of possible failure based on overall studied slopes is towards east direction (Figure 4.109). Based on the Figure 4.109, Gunung Lang shows major potential failure trend towards east direction, Gunung Lanno towards southwest, Kek Lok Tong shows trends towards east, Kwan Yin Tong towards west, and finally Gunung Cheroh with three direction of failure which are south, southwest and southeast direction. Based on the results, most of the rock failures are trending generally towards west and east direction which is indeed perpendicular to the trend of limestone hills axes which is north-south direction. Generally, most of the joint sets presence on the limestone hills are trending slightly similar with the shape of the limestone hills axes north-south. The orientation and intersection of joint sets creates failure which are perpendicular dipping out from the slope face (east and west). This trend thus shapes the morphology of the limestone hills in Kinta Valley.

5.1.4 Limitation and Recommendation

Limitation of the study

- For the purpose of comparison with Lidar measurements, only joint orientation, joint spacing, joint trace length, and water seepage are collected by manual measurements scanline survey.
- Some of the discontinuities measured by manual method are not detected by Lidar measurements due to small exposure of the joint plane that limits the point cloud spacing resolution by the Lidar scanner.
- Determination of cluster of poles of discontinuity are often uncertain and depending on user judgement, which may lead to error especially for users with less experience in rock characterization.
- Based on the survey data comparison between manual and Lidar measurements, there are differences in joint orientation reading recorded by the Lidar measurements. This occur mainly due to the joints surface roughness that varies along the joint plane itself.

Recommendation

- Other rock mass parameter should be considered as parameter for probabilistic slope analysis.
- TLS scanning positioning need to be revise if one encounter a rock slope with small exposure plane on site, scanner position should closer to the rock slope and the resolution of scanning should be increased.
- Rock mass characterization and discontinuity selection from the point cloud data should be done by the operator with geological background in order to monitor the output results.

REFERENCES

Abellán, A., Vilaplana, J., & Martínez, J. (2006). Application of a long-range Terrestrial Laser Scanner to a detailed rockfall study at Vall de Núria (Eastern Pyrenees, Spain). *Engineering Geology, 88*(3-4), 136-148.

Agliardi, F., & Crosta, G. (2003). High resolution three-dimensional numerical modelling of rockfalls. *International Journal of Rock Mechanics and Mining Sciences, 40*(4), 455-471.

Baltsavias, E. P. (1999). Airborne laser scanning: existing systems and firms and other resources. *ISPRS Journal of Photogrammetry and Remote Sensing, 54*(2-3), 164-198.

Barbarella, M., Fiani, M., & Lugli, A. (2015). Landslide monitoring using multitemporal terrestrial laser scanning for ground displacement analysis. *Geomatics, Natural Hazards and Risk, 6*(5-7), 398-418.

Barton, N. (1978). Suggested methods for the quantitative description of discontinuities in rock masses. *ISRM, International Journal of Rock Mechanics and Mining Sciences & Geomechanics Abstracts, 15*(6), 319-368.

Besl, P. J., & McKay, N. D. (1992). *Method for registration of 3-D shapes*. Paper presented at the Sensor fusion IV: Control paradigms and data structures. Boston, United States.

Bistacchi, A., Griffith, W. A., Smith, S. A., Di Toro, G., Jones, R., & Nielsen, S. (2011). Fault roughness at seismogenic depths from LIDAR and photogrammetric analysis. *Pure and Applied Geophysics, 168*(12), 2345-2363.

Buckley, S. J., Howell, J. A., Enge, H. D., & Kurz, T. H. (2008). Terrestrial laser scanning in geology: Data acquisition, processing and accuracy considerations. *Journal of the Geological Society, 165*(3), 625-638.

Bulut, F., & Tüdeş, Ş. (1996). Determination of discontinuity traces on inaccessible rock slopes using electronic tacheometer: An example from the Ikizdere (Rize) Region, Turkey. *Engineering Geology, 44*(1-4), 229-233.

Cawood, A. J., Bond, C. E., Howell, J. A., Butler, R. W., & Totake, Y. (2017). LiDAR, UAV or compass-clinometer? Accuracy, coverage and the effects on structural models. *Journal of Structural Geology, 98*, 67-82.

Chen, Y., & Medioni, G. G. (1992). Object modeling by registration of multiple range images. *Image Vision Comput., 10*(3), 145-155.

Coggan, J., Wetherelt, A., Gwynn, X., & Flynn, Z. (2007). *Comparison of hand-mapping with remote data capture systems for effective rock mass characterisation.* Paper presented at the 11th Congress of the International Society for Rock Mechanics. London, United Kingdom.

D'Amato, J., Guerin, A., Hantz, D., Rossetti, J.-P., & Jaboyedoff, M. (2015). Investigating rock fall frequency and failure configurations using terrestrial laser scanner. In *Engineering Geology for Society and Territory-Volume 2* (pp. 1919-1923): Springer.

De Souza, M. K., Veronez, M. R., Tognoli, F. M., & Da Silveira, L. G. (2013). Terrestrial laser scanning: Application for measuring of structures information in geological outcrops. *International Journal of Advanced Remote Sensing and GIS, 2*(1), 260-270.

Derron, M.-H., Jaboyedoff, M., Blikra, L., & Crosta, G. (2005). Preliminary assessment of rockslide and rockfall hazards using a DEM (Oppstadhornet, Norway). *Natural Hazards & Earth System Sciences, 5*(2), 285-292.

Dian, Z. (1996). A morphological analysis of Tibetan limestone pinnacles: Are they remnants of tropical karst towers and cones? *Geomorphology, 15*(1), 79-91.

Dunning, S., Massey, C., & Rosser, N. (2009). Structural and geomorphological features of landslides in the Bhutan Himalaya derived from terrestrial laser scanning. *Geomorphology, 103*(1), 17-29.

Eberhardt, E., Stead, D., & Morrison, T. (2007). *Rock Mechanics: Meeting Society's Challenges and Demands, Two Volume Set: Proceedings of the 1st Canada-US Rock Mechanics Symposium, Vancouver, Canada, 27-31 May 2007*: CRC Press.

Escher, B. (1931). *De Goenoeng Sewoe en het probleem van de Karst in de Tropen.* Paper presented at the Handelingen van het XXIII. Nederl. Natuur-en Geneeskundig Congres. Netherlands.

Ewan, V., & West, G. (1982). *Reproducibility of joint orientation measurements in rock, transport and road research laboratory supplementary report 702, 18P.* Paper presented at the International Journal of Rock Mechanics and Mining Science & Geomechanics Abstracts. Pergamon, Turkey.

Feng, Q., & Röshoff, K. (2015). A survey of 3D laser scanning techniques for application to rock mechanics and rock engineering. In *The ISRM Suggested Methods for Rock Characterization, Testing and Monitoring: 2007-2014* (pp. 265-293): Springer.

Feng, Q., Sjögren, P., Stephansson, O., & Jing, L. (2001). Measuring fracture orientation at exposed rock faces by using a non-reflector total station. *Engineering Geology, 59*(1-2), 133-146.

Feng, Q., Wang, G., & Röshoff, K. (2011). *Investigation of 3D terrestrial laser scanning techniques for potential application to rock mechanics.* Paper presented at the 12th ISRM Congress. Beijing, China.

Fernández, O. (2005). Obtaining a best fitting plane through 3D georeferenced data. *Journal of Structural Geology, 27*(5), 855-858.

Ferrero, A. M., Forlani, G., Roncella, R., & Voyat, H. (2009). Advanced geostructural survey methods applied to rock mass characterization. *Rock Mechanics and Rock Engineering, 42*(4), 631-665.

García-Sellés, D., Falivene, O., Arbués, P., Gratacos, O., Tavani, S., & Muñoz, J. A. (2011). Supervised identification and reconstruction of near-planar geological surfaces from terrestrial laser scanning. *Computers & Geosciences, 37*(10), 1584-1594.

Ghani, M. F. A., Simon, N., Lai, G. T., Mohamed, T. R. T., & Rafek, A. G. (2016). Study of lineament density in potential evaluation of rock fall in Kinta Valley. *Sains Malaysiana, 45*(12), 1887-1896.

Gigli, G., & Casagli, N. (2013). Extraction of rock mass structural data from high resolution laser scanning products. In C. Margottini, P. Canuti, & K. Sassa (Eds.), *Landslide science and practice: Volume 3: Spatial analysis and modelling* (pp. 89-94). Berlin, Heidelberg: Springer Berlin Heidelberg.

Gillespie, P., Monsen, E., Maerten, L., Hunt, D., Thurmond, J., Tuck, D., . . . Sullivan, M. (2011). Fractures in carbonates: From digital outcrops to mechanical models. *Outcrops revitalized—tools, techniques and applications: Tulsa, Oklahoma, SEPM Concepts in Sedimentology and Paleontology, 10*, 137-147.

Gobbett, D. (1973). Carboniferous and Permian correlation in Southeast Asia. *Geological Society of Malaysia, Bulletin 6*, 131-142.

Gold, P. O., Cowgill, E., Kreylos, O., & Gold, R. D. (2012). A terrestrial lidar-based workflow for determining three–dimensional slip vectors and associated uncertainties. *Geosphere, 8*(2), 431-442.

Guzzetti, F., Cardinali, M., Reichenbach, P., Cipolla, F., Sebastiani, C., Galli, M., & Salvati, P. (2004). Landslides triggered by the 23 November 2000 rainfall event in the Imperia Province, Western Liguria, Italy. *Engineering Geology, 73*(3-4), 229-245.

Harding, D., Abshire, J., Dabney, P., Seas, A., Shuman, C., Sun, X., . . . Huss, T. (2008). *The swath imaging multi-polarization photon-counting lidar (SIMPL): A spaceflight prototype.* Paper presented at the Proceedings of the 2008 IEEE International Geoscience & Remote Sensing Symposium. Boston, United States.

Herda, H. (1999). Strike standard deviation for shallow-dipping rock fracture sets. *Rock Mechanics and Rock Engineering, 32*(4), 241-255.

Hoek, E., & Bray, J. (1981). Rock slope engineering, institute of mining and metallurgy. *London, England, 358*.

Hutchison, C. S., & Tan, D. N. K. (2009). *Geology of peninsular Malaysia*: Published jointly by the University of Malaya [and] the Geological Society of Malaysia.

Ingham, F. T., & Bradford, E. F. (1960). *The geology and mineral resources of the Kinta Valley, Perak*: Federation of Malaya, Geological Survey.

Ismail, B., Kangsar, O., Rashidi, N. A., Darus, A. R., Roslan, H., Yazrol, A. M., & Bakar, K. (2017). Tapak Geologi Geopark Kebangsaan Lembah Kinta. *Jabatan Mineral dan Geosains Malaysia, Perak*.

ISRM, U. R., & Hudson, J. (2007). The complete ISRM suggested methods for rock characterization, testing and monitoring: 1974–2006. *Kozan, Ankara*.

Jaboyedoff, M., Metzger, R., Oppikofer, T., Couture, R., Derron, M., Locat, J., & Turmel, D. (2007). *New insight techniques to analyze rock-slope relief using DEM and 3D-imaging cloud points: COLTOP-3D software.* Paper presented at the Rock mechanics: Meeting Society's Challenges and demands. Vancouver, Canada.

Janeras, M., Navarro, M., Arnó, G., Ruiz, A., Kornus, W., Talaya, J., . . . López, F. (2004). *LIDAR applications to rock fall hazard assessment in Vall De Nuria.* Paper presented at the Proceedings, 4th ICA Mountain Cartography Workshop, Vall de Núria, Catalonia, Spain.

Jones, R., McCaffrey, K., Clegg, P., Wilson, R., Holliman, N. S., Holdsworth, R., . . . Waggott, S. (2009). Integration of regional to outcrop digital data: 3D visualisation of multi-scale geological models. *Computers & Geosciences, 35*(1), 4-18.

Kemeny, J., & Post, R. (2003). Estimating three-dimensional rock discontinuity orientation from digital images of fracture traces. *Computers & Geosciences, 29*(1), 65-77.

Kong, D., Wu, F., & Saroglou, C. (2020). Automatic identification and characterization of discontinuities in rock masses from 3D point clouds. *Engineering Geology, 265*, 105442.

Lai, G. T., Razib, A. M. M., Mazlan, N. A., Rafek, A. G., Ailie, N., Serasa, S., & Mohamed, T. R. (2016). Rock slope stability assessment using slope mass rating (SMR) method: Gunung Lang Ipoh Malaysia. *Scholars Journal of Engineering and Technology, 4*(4), 185-192.

Lato, M., Diederichs, M. S., Hutchinson, D. J., & Harrap, R. (2009). Optimization of LiDAR scanning and processing for automated structural evaluation of discontinuities in rockmasses. *International Journal of Rock Mechanics and Mining Sciences (1997), 46*(1), 194-199.

Lato, M. J., & Vöge, M. (2012). Automated mapping of rock discontinuities in 3D lidar and photogrammetry models. *International Journal of Rock Mechanics and Mining Sciences (1997), 54*, 150-158.

Leman, M. S. (2013). *Proposed Kinta Valley Geopark-utilizing geological resources for environmental quality improvement and society well being enhancement. Keynote address.* Paper presented at the Proceeding of the National Geosience Conference. Ipoh, Perak.

Li, X., Chen, J., & Zhu, H. (2016). A new method for automated discontinuity trace mapping on rock mass 3D surface model. *Computers & Geosciences, 89*, 118-131.

Lim, M., Petley, D. N., Rosser, N. J., Allison, R. J., Long, A. J., & Pybus, D. (2005). Combined digital photogrammetry and time-of-flight laser scanning for monitoring cliff evolution. *The Photogrammetric Record, 20*(110), 109-129.

Marquinez, J., Duarte, R. M., Farias, P., & Sanchez, M. J. (2003). Predictive GIS-based model of rockfall activity in mountain cliffs. *Natural Hazards, 30*(3), 341-360.

Martín, S., Uzkeda, H., Poblet, J., Bulnes, M., & Rubio, R. (2013). Construction of accurate geological cross-sections along trenches, cliffs and mountain slopes using photogrammetry. *Computers & Geosciences, 51*, 90-100.

Mazlan, N. A., Lai, G. T., Razib, A. M. M., Rafek, A. G., Serasa, A. S., Simon, N., . . . Mohamed, T. R. (2018). The geomechanical strength of carbonate rock in Kinta Valley, Ipoh, Perak Malaysia. *AIP Conference Proceedings, 1940*(1), 020046.

Monserrat, O., & Crosetto, M. (2008). Deformation measurement using terrestrial laser scanning data and least squares 3D surface matching. *ISPRS Journal of Photogrammetry and Remote Sensing, 63*(1), 142-154.

Muhammad, R. F., & Djin, T. H. (2003). The morphostructures of Kinta Valley karst. *Geological Society of Malaysia, Bulletin 46*, 319-328.

Muhammad, R. F., & Komoo, I. (2003). Lanskap kars Lembah Kinta warisan kebangsaan yang perlu dipelihara (IN MALAY), The Kinta Valley karst landscape—A national heritage to be preserved. *Geological Society of Malaysia, Bulletin 46*, 447-453.

Oppikofer, T., Jaboyedoff, M., Blikra, L., & Metzger, R. (2009). Characterization and monitoring of the Åknes rockslide using terrestrial laser scanning. *Natural Hazards and Earth System Sciences, 9*(3), 1003-1019.

Post, R. M., Kemeny, J. M., & Murphy, R. (2001). *Image processing for automatic extraction of rock joint orientation data from digital images.* Paper presented at the DC Rocks 2001, The 38th US Symposium on Rock Mechanics (USRMS). Washington, United States.

Priest, S., & Hudson, J. (1981). *Estimation of discontinuity spacing and trace length using scanline surveys*. Paper presented at the International Journal of Rock Mechanics and Mining Sciences & Geomechanics Abstracts. Pergamon, Turkey.

Priest, S. D. (1993). The collection and analysis of discontinuity orientation data for engineering design, with examples. In *Rock Testing and Site Characterization* (pp. 167-192): Elsevier.

Rabatel, A., Deline, P., Jaillet, S., & Ravanel, L. (2008). Rock falls in high-alpine rock walls quantified by terrestrial lidar measurements: A case study in the Mont Blanc area. *Geophysical Research Letters, 35*(10), 1-5.

Romana, M. (1985). *New adjustment ratings for application of Bieniawski classification to slopes.* Paper presented at the Proceedings of the international symposium on role of rock mechanics, Zacatecas, Mexico.

Rowe, E., Hutchinson, D. J., & Kromer, R. A. (2018). An analysis of failure mechanism constraints on pre-failure rock block deformation using TLS and roto-translation methods. *Landslides, 15*(3), 409-421.

Shu, Y. K., & Lai, K. H. (1974). Rockfall at Gunung Cheroh, Ipoh. *Geological Survey Report Ipoh: Minerals & Geoscience Department, Malaysia*.

Simon, N., Ghani, M. F. A., Hussin, A., Goh, T. L., Rafek, A. G., Surip, N., . . . Lee, K. E. (2015). Assessment of rockfall potential of limestone hills in the Kinta Valley. *Journal of Sustainability Science and Management, 10*(2), 24-34.

Slob, S., Hack, R., & Turner, A. K. (2002). *An approach to automate discontinuity measurements of rock faces using laser scanning techniques.* Paper presented at the ISRM International Symposium-EUROCK 2002. Funchal, Portugal.

Slob, S., Van Knapen, B., Hack, R., Turner, K., & Kemeny, J. (2005). Method for automated discontinuity analysis of rock slopes with three-dimensional laser scanning. *Transportation Research Record, 1913*(1), 187-194.

Song, L. (1983). *Geological structure: An important factor controlling karst development.* Paper presented at the New Direction in Karst. Proceedings of the Anglo-French Symposium. Norwich, United Kingdom.

Spreafico, M. C., Perotti, L., Cervi, F., Bacenetti, M., Bitelli, G., Girelli, V. A., . . . Borgatti, L. (2015). Terrestrial Remote Sensing techniques to complement conventional geomechanical surveys for the assessment of landslide hazard: The San Leo case study (Italy). *European Journal of Remote Sensing, 48*(1), 639-660.

Sturzenegger, M., & Stead, D. (2009). Close-range terrestrial digital photogrammetry and terrestrial laser scanning for discontinuity characterization on rock cuts. *Engineering Geology, 106*(3-4), 163-182.

Sturzenegger, M., Yan, M., Stead, D., & Elmo, D. (2007). *Application and limitations of ground-based laser scanning in rock slope characterization.* Paper presented at the Proceedings of the first Canadian US rock mechanics symposium. British Columbia, Canada.

Suntharalingam, T. (1968). Upper Palaeozoic stratigraphy of the area west of Kampar, Perak. *Geological Society of Malaysia, Bulletin 1*, 1-15.

Tan, B. (1988). Engineering geology of the Ipoh area, Perak. *Final Report, Research Project No. 7, 86*.

Tan, B. (1998). *Engineering geological survey of limestone cliffs in the Tambun area, Perak, Malaysia.* Paper presented at the Engineering Geology: A global view from the Pacific Rim. Rotterdam, Netherlands.

Tavani, S., Granado, P., Corradetti, A., Girundo, M., Iannace, A., Arbués, P., . . . Mazzoli, S. (2014). Building a virtual outcrop, extracting geological information from it, and sharing the results in Google Earth via OpenPlot and Photoscan: An example from the Khaviz Anticline (Iran). *Computers & Geosciences, 63*, 44-53.

Teza, G., Galgaro, A., Zaltron, N., & Genevois, R. (2007). Terrestrial laser scanner to detect landslide displacement fields: A new approach. *International Journal of Remote Sensing, 28*(16), 3425-3446.

Tjia, H. D. (1969). Slope development in tropical karst. *Zeitschrift fuer Geomorphologie, 13*(3), 260-266.

Voyat, I., Roncella, R., Forlani, G., & Ferrero, A. M. (2006). *Advanced techniques for geo structural surveys in modelling fractured rock masses: Application to two Alpine sites.* Paper presented at the Golden Rocks 2006, The 41st US Symposium on Rock Mechanics (USRMS). Colorado, United States.

Yiu, K., & King, B. (2009). Stereonet data from terrestrial laser scanner point clouds. *Survey Review, 41*(314), 324-338.

LIST OF PUBLICATION AND PAPER PRESENTED

1. **Hellmy, M. A. A**., Muhammad, R. F., Shuib, M. K., Fatt, N. T., Abdullah, W. H., Abu Bakar, A., & Kugler, R. (2019). Rock slope stability analysis based on terrestrial LiDAR on karst hills in Kinta Valley Geopark, Perak, Peninsular Malaysia. *Sains Malaysiana*, *48*(11), 2595-2604.